Simulation of Elastic-Plastic Material Behaviour with Uncertain Material Parameters

A Spectral Stochastic Finite Element Approach

Von der Fakultät für
Bauingenieurwesen und Geodäsie der
Gottfried Wilhelm Leibniz Universität Hannover
zur Erlangung des Grades eines
Doktor–Ingenieurs
genehmigte

Dissertation

Vorgelegt von
Dipl.-Ing (FH) Sebastian Fink

Hauptreferent: Prof. Dr.-Ing. U. Nackenhorst
Korreferent: Prof. Dr. H. G. Matthies

Tag der mündlichen Prüfung: 26. Februar 2015

Institut für Baumechanik und Numerische Mechanik
Gottfried Wilhelm Leibniz Universität Hannover
2015

The only thing certain is nothing is certain
MICHEL DE MONTAIGNE

Abstract

In this PhD thesis, an approach for the simulation of non-linear elastic-plastic three-dimensional structures, including random material parameters, is presented. The material parameters, which are assumed to be uncertain are the Young's modulus, yield stress and the hardening parameters. These parameters are represented by independent random fields, which are realized with the KARHUNEN-LOÈVE Expansion as well as the Spectral Representation Method. The former approach is coupled with the Polynomial Chaos (PC), which leads to the well known Spectral Stochastic Finite Element Method. The Spectral Representation Method on the other hand is coupled with a simple Monte Carlo Sampling (SPRM-MCS).

First, the basic theories are presented. In particular, these are: the continuum mechanics, the finite element method, the numerical realization of elastic-plastic material behaviour and the probability theory. Afterwards, some remarks on the characterization of uncertainties and its stochastic realization by random fields/processes are discussed. With the introduction of the Polynomial Chaos, the *linear* Spectral Stochastic Finite Element Method (SSFEM) is presented in the next step. First of all, the stochastic counterpart of the deterministic weak form of equilibrium is derived. This is realized by transferring the deterministic weak form into the so-called spectral form. To be more specific, a stochastic discretization of the deterministic weak form is applied and projecting it via the GALERKIN method onto an orthogonal expansion basis. Such a basis is spanned by polynomials, for instance, HERMITE polynomials when a GAUSSIAN distribution is applied.

Afterwards, the extension of the linear SSFEM for solving non-linear problems is presented. The developed approach is an extension of the deterministic radial return mapping. To allocate the random variables, in the subsequent solution process with each other, some special mathematically algebraic rules and methods are necessary, which are presented first. In particular, these are the PC-algebra as well as the collocation method. Then, the coupling of the developments of the previous sections (resp. chapters) are presented for the solution of stochastic non-linear problems by applying the SSFEM. The developed approach, for the stochastic radial return mapping, is an intrusive purely algebraic formulation, which are evaluated with the introduced methods in this thesis. Finally, the presented formulation is tested with two numerical examples and the results are compared with those obtained from the coupled SPRM-MCS as well as a Latin Hypercube Sampling.

Keywords   Finite Element Method, Stochastic Theory, Characterization of Uncertainties, Random Fields/Processes, Polynomial Chaos, Linear Stochastic Finite Elements, Polynomial Chaos Algebra, non-linear Stochastic Finite Elements

iv

Kurzfassung

In der vorliegenden Arbeit wird ein Ansatz zur Berechnung von nichtlinearem Materialverhalten vorgestellt. Mit diesem Ansatz können nicht lineare elastisch-plastische dreidimensionale Strukturen, unter Berücksichtigung von stochastischen Materialparametern, simuliert werden können. Als zufällige Materialparameter werden der E-Modul, die Fließgrenze sowie die isotrope und kinematische Verfestigung gewählt, wobei die Materialparameter durch Zufallsfelder charakterisiert werden. Die Erzeugung dieser Zufallsfelder erfolgt mit Hilfe von zwei Methoden, der KARHUNEN-LOÈVE Expansion (KLE) sowie der Spektralen Representation Methode (SPRM). Die KLE wird mit dem Polynom-Chaos (PC) kombiniert, was auf die bekannte Spektrale Stochastische Finite Elemente Methode führt. Die SPRM auf der anderen Seite wird mit dem Monte-Carlo Sampling (SPRM-MCS) gekoppelt.

Zuerst werden die Grundlagen der Kontinuumsmechanik, der finiten Elemente Methode sowie der Wahscheinlichkeitstheorie behandelt. Ebenfalls wird die numerische Umsetzung von elastisch-plastischem Materialverhalten präsentiert, welche im weiteren Verlauf dieser Arbeit auf elastisch-plastisches Materialverhalten, mit zufälligen Parametern erweitert wird. Im Anschluss an die theoretischen Grundlagen wird sich der Charakterisierung von zufällig verteilten Materialparametern sowie deren Beschreibung durch Zufallsfelder/-prozesse zugewendet. Nachdem auf das Polynom-Chaos eingegangen wurde, wird im nächsten Schritt die Spektrale Stochastische Finite Elemente Methode (SSFEM) detailliert beschrieben. Zuerst wird das stochastische Equivalent der deterministischen schwachen Form des Gleichgewichts hergeleitet. Hierzu wird die deterministische schwache Form in die spektrale Form überführt. Im Einzelnen bedeutet das, dass die deterministische Form zuerst im stochastischen Raum diskretisiert wird und anschließend mit der GALERKIN-Methode auf eine orthogonale Basis projiziiert wird. Eine solche Basis wird z.B., bei der Verwendung der Normalverteilung, durch HERMITE-Polynome aufgespannt.

Nachdem die lineare Formulierung an einem numerischen Beispiel diskutiert wurde, wird ein neuer Ansatz der stochastischen SSFEM vorgestellt, in welchem elasto-plastisches Materialverhalten berücksichtigt werden kann. Der Ansatz basiert auf dem deterministischen Radial-Return Mapping, welches um einen stochastischen Teil, zum stochastischen Radial-Return Mapping, erweitert wird. Um im späteren Lösungsprozess die Zufallsvariablen miteinander verrechnen zu können, sind einige spezielle, mathematisch algebraische Regeln und Methoden notwendig, welche zuerst vorgestellt werden. Weiterhin wird die Kollokationsmethode eingeführt, welche ebenfalls zur Lösung der entsprechenden Gleichungen verwendet wird. Bei dem präsentierten Ansatz für das stochastische Radial-Return Mapping handelt es sich um eine intrusive Formulierung, welche mit den vorgestellten Methoden gelöst wird. Abschließened wird die entwickelte Methode an zwei Bespielen getestet und die Ergebnisse werden mit der gekoppelten SPRM-MCS sowie mit dem Latin Hypercube Sampling verglichen.

Stichworte Finite Elemente Methode, Stochastik, Charakterisierung von Unsicherheiten, Zufallsfelder/-prozesse, Polynom-Chaos, Lineare Stochastische Finite Elemente Methode, Polynom-Chaos Algebra, nicht-lineare Stochastische Finite Elemente

Table of Contents

1. Introduction

The modelling of engineering problems often leads to non-linear ordinary and partial differential equations. These non-linear *solid mechanics* problems are often solved by numerical methods such as the well-established Finite Element Method (FEM), which has been developed over the last five decades. The non-linear constitutive equations have been formulated in order to characterize the underlying material behaviour, e.g., elastic-plastic theories, where its basis formulations goes back to Tresca about 150 years ago, where a detailed historical overview can be found in Horstemeyer and Bammann [2010]. Based on TRESCAS formulation, SAINT-VENANT and LEVY proposed the foundation for the modern plasticity. In the next decades, a large number of well-known scientists (e.g., VON MISES, HENCKY and PRANDTL) made important contributions to the theory of plasticity. After the second world war, a unified theory of plasticity has been presented, based on the continuum formulations proposed by PRAGER and DRUCKER. Probably, one of the first textbooks that gives an established theoretical background on plasticity was published by Hill [1950]. In the early days of the plasticity theory, the solution of non-linear problems is limited to relatively simple cases. Nowadays, due to the continuous development of the theories of solid mechanics, as well as the development of powerful computers, *computational plasticity* is widely used in computational engineering, both in academic researches and industrial applications. Some examples for applications are: standard stress analysis, soil or rock mechanics up to the simulation of manufacturing processes such as metal forming. A general stress analysis with inelastic material behaviour can include different non-linear effects, as listed below.

- *Material Non-Linearity*: Small deformations with only small displacements and small strains (only a few percent).

- *Large Deformations*: This formulation is characterized by small strains and large displacements.

- *Geometrically Non-Linear*: In this formulation the strains and the displacements are large.

In this work only material non-linearities are considered and the proposed constitutive equations are derived with respect to this assumption. The state-of-the-art of the general formulation on small- and large-strain plasticity as well as the numerical treatment is documented in a large number of textbooks, for instance, Lemaitre and Chaboche [1990]; Simo and Hughes [1998]; Kojic and Bathe [2005]; Ibrahimbegovic [2006]; Chen and Han [2007]; Lubliner [2008]; Besson et al. [2010]; de Borst et al. [2012].

In addition to the ongoing developments of solid mechanics and computer resources, the design of modern structures to very complex ones has also continuously evolved. In most cases, the input parameters of the structural models are assumed to be of deterministic nature, which is accurate enough for the analysis of the structural response and the design by small fluctuations. In most structural systems, the uncertainties are not so small that they can be neglected. In this case, a stochastic formulation is needed in order to overcome this drawback. There are a large number of probabilistic methods available. However, most of structural systems are designed by idealizing
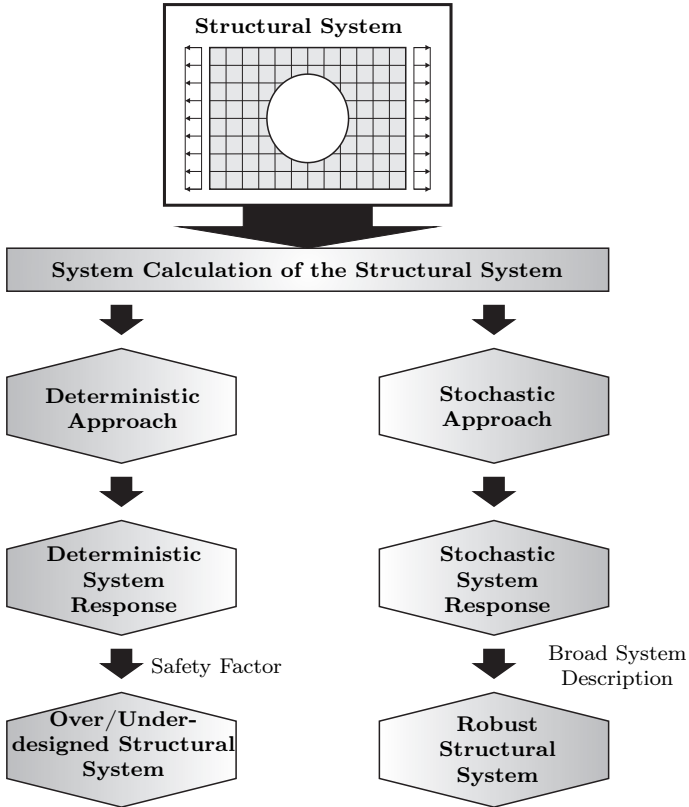
Figure 1.1.: Schematic illustration of the system calculation of a structural system by using a deterministic approach or a stochastic approach (inspired by Choi et al. [2007]).

the deterministic methods, e.g., by using a safety factor. Figure 1.1 illustrates the two major branches of a system calculation, the *deterministic* approach on the left side and *stochastic* approach on the right side. The application of the deterministic approach using a safety factor often results in overly expensive designs, because the safety factor is often too conservative. This fact stands in conflict with the major challenge to get an optimal design involving the proper material at the right place of the structure. Moreover, an optimal design gives an improvement in security but, e.g., the use of a larger amount of matter can results in negative structural effects. For example, a increasing wall thickness of a pressure vessel can indeed decrease purely mechanical stresses, cf. Besson et al. [2010]. The application of the stochastic approach has a number of advantages: So, statistical results, such as the expected value, the variance and further statistical moments allows a detailed (comprehensive) analysis of the system response. To ensure that the mechanical structure fulfils

the system requirements, it is necessary to take into account the fluctuations of the relevant system parameters, e.g., the material parameters. In this PhD thesis the classical three-dimensional elastic-plastic formulation is extended by an approach to taking into account uncertainties of various material parameters.

1.1. The Objectives and Scope of the Thesis

The design of engineering structures can become very complex, e.g., due to the fabrication of the materials, construction and/or localization of stresses. The design process often consists of two parts:

1. Defining the internal force field that acting on the materials and

2. evaluating the structure response of the material with respect to this force field.

The focus of the former part lies on the analysis of the stresses acting on structural elements, the finite elements, while for the second part the knowledge of the structural material properties is necessary. However, as already discussed in the previous section, such properties are not percisely known. There are different approaches available to overcome this problem. A stochastic approach is a reasonable choice to deal with the material uncertainties without making too many simplifying assumptions. In stochastic mechanics, especially in stochastic finite element analysis, only linear-elastic material behaviour is often considered, see e.g., Geistefeldt [2003]; Stefanou and Papadrakakis [2007]; Xiu [2010] and only a few studies have taken into account non-linear material phenomena. Here, Anders [2000]; Sett [2007]; Rosić [2013] should be named.[1] An extension of standard finite element procedure to cope with the stochastic plasticity requires an extension of the theory of deterministic plasticity. In this context, it provides more realistic estimates of load-carrying capacities of structures in terms of mean values, variances and confidence intervals. In addition, it leads to a better understanding of the structural response due to the internal forces in the material. In summary: A better understanding of the role of the relevant mechanical variables which represents the characteristic response of the material to the applied forces is essential for an optimal design of the structure and the more comprehensive the knowledge, the more exact will be the structural design.

With respect to these summary, the main goal of this PhD thesis is formulated as follows:

The development of a fully descriptive[2] Spectral Stochastic Finite Element Method for elastic-plastic material behaviour including stochastic material properties

The proposed stochastic formulation has been implemented into an in-house finite element program based on MATLAB and its applicability has been verified in various numerical examples.

Scope of the Thesis

The focus lies on the formulation of a stochastic three-dimensional elastic plastic material model. The formulation of the stochastic elastic-plastic problem is done

---

[1]See section 1.2 for more details.

[2]A fully descriptive stochastic method provides the complete stochastic information about the system response.

in a convex setting, which is similar to the deterministic case. In the deterministic elastic-plastic formulation, variational inequalities (VIs) are applied to separate the purely elastic material behaviour from the post-yield inelastic behaviour. However, as already mentioned, all materials have fluctuations. Therefore, these uncertainties should be included in the mathematical formulation. This could be done, for example, by extending the deterministic VIs to stochastic variational inequalities (SVIs). The solution of the SVIs is realized by solving the corresponding stochastic convex-optimization problem. According to this, a new approach for the well-known predictor-corrector method the *stochastic radial return mapping* is proposed. For the sake of simplicity, the classical J_2 flow theory (Simo and Hughes [1998]) with linear isotropic and kinematic hardening is applied.

The random material parameters, which have a influence to the constitutive relation and the evolution path are modelled by random fields. The evaluation of the corresponding equations is realized by using the stochastic Galerkin method, which is similar to the method applied in the deterministic finite element method, see e.g., Braess [1992]; Oden and Reddy [2011]. This stochastic projection method has been proved to be very effective for solving many kinds of engineering problems including uncertainties. Here, the solution of the governing equations is characterized by variational inequalities and subsequently projected onto a truncated polynomial chaos basis, which can be computed with appropriate computational methods. A major advance of stochastic projection approaches is the computationally efficiency, which is often more efficient than sampling-based methods, such as the Monte-Carlo Simulation (MCS).

The fluctuations of the material parameters are represented by the Karhunen-Loève Expansion (KLE) (Ghanem and Spanos [2003]; Adler and Taylor [2007]) and the system response is evaluated with the Polynomial Chaos Expansion (PCE), proposed by Ghanem and Spanos [2003].

In general, the stochastic Galerkin method can be divided into the following two classes:

- The intrusive method and
- the non-intrusive method.

The former method based on the reformulation of the governing system equations of the original model by projecting it onto a polynomial chaos. With this approach, a direct solution through linear and non-linear operations of polynomial chaos algebra is achieved, cf. Debusschere et al. [2005]; Le Maître and Knio [2010]. This method is essentially algebraic and requires only one program-run, which makes them computationally very efficient. However, for the computational realization of this methodology, it is necessary to have an access to the program code, which is in commercial program codes not possible.

The latter method, for instance, collocation methods (Najm [2009]; Xiu [2010]) or MCS (Lemieux [2009]), approximates the structural response in a sampling manner. This procedure has the major advantage that the program code can be considered as a "black-box", because no particular modification of existing codes is necessary. However, to get a satisfactory approximation of the system response many resolutions of the deterministic model are necessary, which leads to drastically increasing computational costs. In this thesis, the regression method as proposed, e.g., in Sudret et al. [2003] is applied for selected mathematical operations and not as complete "standalone" numerical method. For the purpose of verification, the MCS is used to com-

pare the achieved results from the sampling with those obtained from the proposed new stochastic approach. By this, the MCS is coupled with the Spectral Representation Method (SPRM) (Shinozuka and Deodatis [1991, 1996]) where, similar to the KLE, the random material parameters are represented by random fields, which are generated by the SPRM. The resolution of the mechanical system is performed by applying the MCS. The random field generation as well as the subsequent calculation of the repeating model calculation can be performed in parallel, which significantly reduces the computation time.

1.2. Related Works on Stochastic Elastic-Plastic Mechanics

Already in his publication in 2003, Oden (Oden et al. [2003]) has recognized that the probabilistic modelling of mechanical problems will be a topic of great importance and interest in the next decade. Nowadays, the field of stochastic mechanics has received an increasing amount of attention and being quickly and constantly evolving. Therefore, this section will not show an attempt to present an intensive review of all available methods, their applications nor results. The aim of this section is to give an overview of the recent developments of numerical methods for stochastic non-linear computations with a special focus on stochastic elastic-plastic material behaviour. In addition to the distinction between the deterministic and stochastic approach, which was illustrated in Fig. 1.1, shows Fig. 1.2 the difference in the nature of uncertainties. In the probabilistic approach it is assumed that the probability density function of
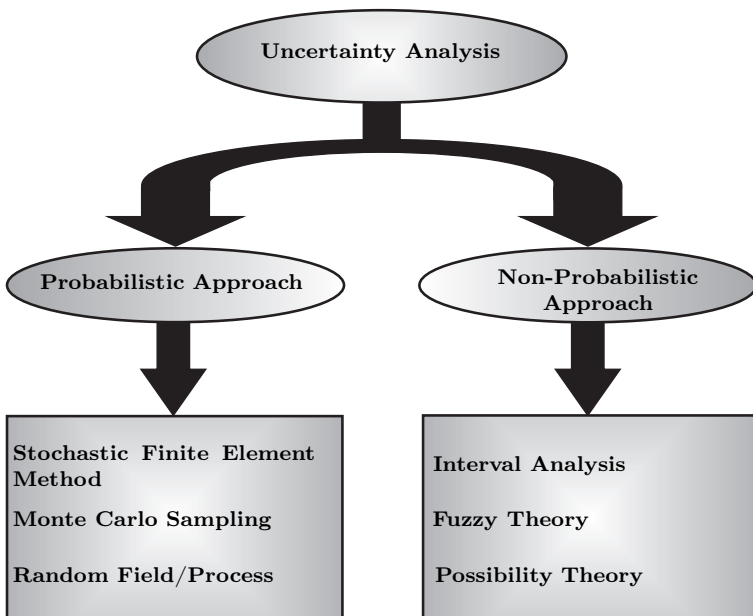
Figure 1.2.: Categories of stochastic analysis.

the parameters of interest are known. By this approach the uncertainties of the parameters are characterized by random variables, random processes and/or fields. On the other hand, the non-probabilistic approach is primarily used when the parameters are not precisely known. In the present work, the focus lies on the application of the Stochastic Finite Element Method where the input parameters are represented by random fields. This combination is well known as Spectral Stochastic Finite Element Method (SSFEM). For the remaining methods in Fig. 1.2, the interested reader is referred to Sudret and der Kiureghian [2000]; Hanss [2005]; Sudret [2007]; Choi et al. [2007]; Kriegesmann [2012] and the references therein. In what follows, the recently published works on non-linear stochastic mechanics with elastic-plastic material behaviour will be briefly outlined.

The first approach for the analysis of elastic-plastic material behaviour with random material parameters was proposed by Anders and Hori [1999]; Anders [2000]; Anders and Hori [2001]. They approximated the stochastic elastic-plastic constitutive equations by applying a bounding body analysis. The presented approach has been tested with various two- and three-dimensional examples, whereas only one input parameter, the Young's modulus, was assumed to be uncertain. The fluctuation of the random variable was represented by the KLE and the stochastic field variables were evaluated by the PCE. This approach makes it necessary to approximate the joint PDF of the governing variables (Young's modulus, stress, strain and displacements) by approximating the yield function via a perturbation expansion. Indeed, the authors have presented that the approximation with only one term in the perturbation expansion results in accurate results, see Anders and Hori [1999]. But, especially strongly non-linear problems require more than one term. Another disadvantage is the manageability of large variances when applying the perturbation method. In recently published textbooks (Le Maître and Knio [2010]; Xiu [2010]) the coefficient of variation is specified to 10%. The next disadvantage could be due to the complexity of numerical approximation, which does not allow more than one random parameter (in this particular case, the Young's modulus) to be considered. An additional remark is the limitation to only one random variable due to the mathematical treatment, which is a further simplification and not optimal when the objective is to describe "realistic" material behaviour as well as the structural response of the system.

A further treatment of uncertain material behaviour in an elastic-plastic framework has been presented by Jeremić et al. [2007]; Sett [2007]; Sett et al. [2007b,a]; Jeremić and Sett [2009]; Sett and Jeremić [2010]; Sett et al. [2011]. In these works, a special form of the Fokker-Planck-Kolmogorov (FPK) equation, derived by Kavvas [2003], was applied to represent the random system response of a physical system with stochastic input parameters. After these citations lies the advantage of the FPK equation on probabilistic elasto-plasticity is that it transforms the non-linear stochastic elastic-plastic constitutive rate equation in the real space into a linear deterministic partial differential equation in the probability density space. This leads to a simplification of the corresponding numerical solution process of the probabilistic constitutive equations, cf. Sett et al. [2011]. In addition, the Fokker-Planck-Kolmogorov approach for probabilistic elastic-plastic material behaviour leads to a second-order accurate probabilistic constitutive solution. The authors have also pointed out that the proposed method did not suffer from a closure problem associated with perturbation technique or high computational cost associated with a MCS. However, the presented stochastic framework was only applied to a one-dimensional numerical example. It should be remarked that the computational effort increases drastically when the FPK equation is applied to higher-dimensional problems, as often found in engineering applications.

Another concept has been proposed by Arnst and R.Ghanem [2012] where the mathematical treatment of the stochastic boundary value problem involves inequality constraints. The authors define a set of stochastic variational inequalities to characterize the solution of specified inequality-constrained stochastic boundary value problems. The discretization of this problems is done via a projection onto a polynomial chaos expansion and collocation of the inequality constraints. In the numerical test only one input parameter was assumed to be random, namely the linear isotropic hardening modulus. Furthermore, the presented approach has been tested only on a two-dimensional example.

The last reviewed methodology in this section is proposed by Rosić and Matthies [2008]; Rosić et al. [2010]; Rosić and Matthies [2012]; Rosić [2013]. In these recent presented works, similar to the approach presented by Arnst and R.Ghanem [2012], a class of stochastic variational inequalities is defined to represent the elastic-plastic material behaviour with random material parameters. The standard return-mapping for J_2 elastic-plastic material behaviour has been extended to calculate mechanical problems in both small and large displacements with uncertain material properties. The algebraic characteristics of this formulation allow the calculation of the material response in each iteration step with the NEWTON-RAPHSON method and the solution of the material response is given in a form of polynomial chaos expansion. Beside the intrusive GALERKIN approach, a non-intrusive collocation approach has also been presented. Both approaches were validated on various two-dimensional examples in plain strain conditions whose reference solution is computed via direct integration methods. The fluctuations of the material parameters (the bulk modulus, the shear modulus and the isotropic hardening modulus) were represented by random fields, discretized by the KLE.

1.3. Outline of the Thesis

This thesis consists of ten chapters and comprises of three main parts. The first part (Chaps. 2−4) discusses about the basic theories of continuum mechanics, the Finite Element Method and the bases of the probability theory. It also provides a detailed discussion of the numerical realization of elastic-plastic material behaviour. The second part (Chaps. 5−6) discusses about the characterization of uncertainties and its stochastic realization by random fields/processes. Moreover, a brief review of the applied methods in this work is given. In the third part (Chaps. 7−9), the previously presented techniques are combined to a new approach for the calculation of elastic-plastic material behaviour including material uncertainties. In detail, these are the realization of the material properties by random fields and the subsequent calculation of the non-linear problem by using a novel numerical approach, consisting of the stochastic GALERKIN method and the regression method. The thesis ends with a brief discussion of open questions for further developments and improvements of the methods/concepts and some aspects for further research. Specifically, some specifications are outlined where, based on those discussed in the individual chapters in this work, may be possible. An illustration of the framework of a stochastic analysis in terms of the individual chapters is given in Fig. 1.3. A more detailed outline of each chapter is given below.

**Representation of the Structural Model
via Continuum Mechanics and the FEM**

Uncertainty Representation

**Spectral Stochastic
Analysis**

**Stochastic System
Application**

Statistical Response

Sampling Methods
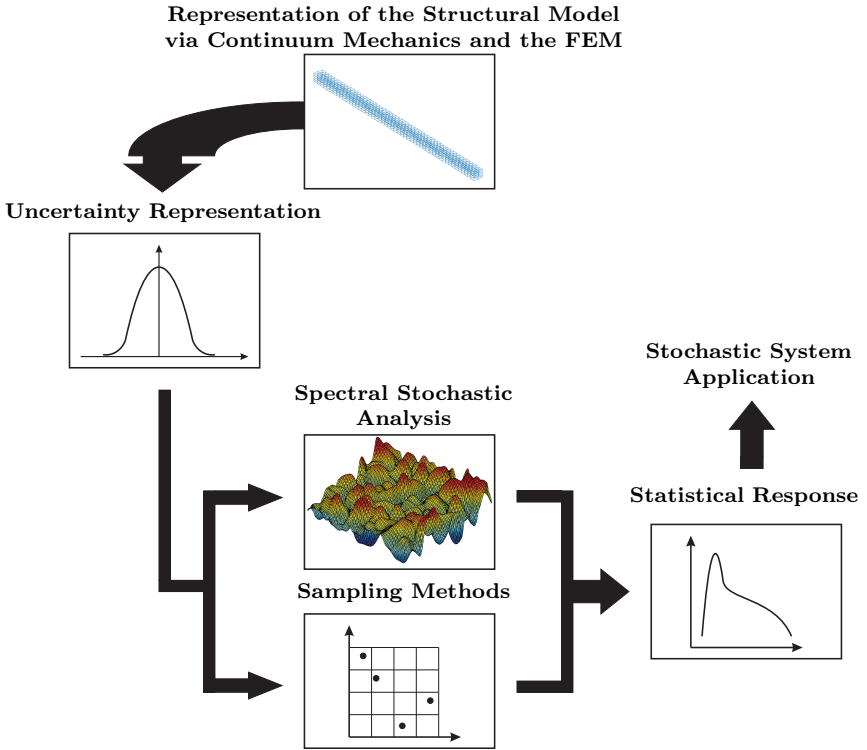
Figure 1.3.: Schematic illustration of the interaction of the contents of this thesis.

Chapter 2 presents the basics of continuum mechanics, which are needed for the formulation of the FEM for solid mechanics and structural problems. The kinematics, the balance laws and the constitutive relations are briefly presented. The constitutive equations are confined to the standard J_2 elastic-plasticity as it is applied in this work. In **Chapter 3**, the Finite Element Method is discussed. Starting from the strong formulation of equilibrium, the weak form is derived by using variational principles. Afterwards, the linearization of the previously derived weak form is presented and subsequently the discretization of the weak form is discussed. After a brief summary of the Newton-Raphson scheme, the computational implementation of deterministic plasticity is presented in detail. This formulation will be extended during this thesis to be able to handle non-linear structural problems with stochastic input parameters. An introduction to stochastic input parameters is presented in **Chapter 4**. The focus of this chapter lies on the necessary background on probability theory. It contains the properties of single variables as well as the properties of multiple random variables. Particular emphasis is placed on different sampling techniques including the Monte-Carlo methods and some more efficient strategies, such as the Latin Hypercube Sampling (LHS) and the Quasi Monte Carlo (QMC) Sampling. Hereby, the first part, the theoretical framework, is complete.

The second part of this thesis starts with **Chapter 5**, where the general characterization and quantification of uncertainties of various properties and their stochastic description are presented. Afterwards, the two basic types of uncertainties, namely *epistemic* and *aleatory*, are introduced. For the consideration of these uncertainties, different mathematical frameworks are listed, whereas the scope of the present thesis lies solely on the *probability methods*. In static analysis the parameter *time* is neglected, whereas it is irrelevant whether a deterministic or stochastic simulation is performed. On the other hand, dynamic analysis (e.g., structural, fluid or fatigue) makes the consideration of the time explicitly necessary. In conjunction with time-dependent random parameters the theory of the *stochastic process* is necessary. For the simulation of such processes, many different mathematical concepts are available, where in this work, the following methods are applied:

- the Spectral Representation Method,
- the KARHUNEN-LOÈVE Expansion and
- the Polynomial Chaos Expansion.

A brief review of the respective level of development of each representation method is given. For parameters of material strength as well as for the cross section, a negative value is in particular not physical and therefore the assumption of a normal (GAUSSIAN) distribution is not well suited. In view of this fact, the subsection about Non-GAUSSIAN Models gives a brief overview about some techniques to handle with non-GAUSSIAN distributions. Two methods are mainly referred to this context; the memoryless transformation of the GAUSSIAN distribution and the *Askey*-scheme (Xiu and Karniadakis [2002, 2003]; Xiu [2009, 2010]). The chapter completes with a general introduction of random fields. This methodology is later adopted to represent the fluctuations of the material parameters. After the brief introduction on the quantification of uncertainties and the subsequent overview of the methods applied in this thesis, **Chapter 6** is dedicated to the charaterization of material uncertainties by the theory of random fields. Then, different discretization techniques are briefly discussed. This includes the point and the averaging discretization techniques as well as the series expansion methods, where special emphasis is placed on the latter methods. To be more specific, these methods are the KLE and SPRM. First, the KLE is presented in detail. Once, the basics are introduced, the analytical solution of the KLE is presented and afterwards its numerical formulation is proposed. This formulation is then applied in a numerical example and the results are discussed subsequently. Then the SPRM is presented, where the formulation for the two-dimensional as well as for the three-dimensional case are given. Afterwards, different investigations are performed, especially on two-dimensional random fields. With the presentation of the random field theory, the second part is complete.

The third and last part of this thesis starts with the introduction of the Polynomial Chaos Expansion in **Chapter 7**. First of all, basic definitions and necessary functional spaces are introduced. Afterwards, the general construction of a PCE with the order p and dimension M is discussed. Based on these definitions, a formal expansion of a second-order random variable in terms of the PCE is given. The construction of a PCE system is examined for the case of GAUSSIAN random variables, where the HERMITE-Polynomials are the optimal choice to approximate the stochastic basis. In one-dimensional systems, the HERMITE polynomials are applied directly. In multi-dimensional systems, the basis of the PCE is defined in terms of a partial tensorization of the one-dimensional HERMITE polynomials. The truncation of the PCE at a finite order p is discussed as also the generalized PCE decompositions, the al-

ready mentioned *Askey* scheme. The chapter ends with some remarks in terms of the implementation of the PCE. After introducing the PCE, **Chapter 8** is addressed to the linear Stochastic Finite Element Method. The chapter starts with a brief review of four different methods for the representation of the fluctuating part of the SFEM. Namely, these are the *perturbation method*, the *weighted integral method*, the Neumann expansion method and the *improved* Neumann method. At the end of this section, a brief discussion of the intrusive and non-intrusive approach is given. After this short overview, the linear Spectral Stochastic Finite Element Method (SSFEM) is discussed in detail. First, the stochastic counterpart of the deterministic weak form of equilibrium is derived. This is realized by transferring the deterministic weak form into the "so-called" spectral form. To be more specific, this is done by performing a stochastic discretization of the deterministic weak form and projecting it via the Galerkin method onto an orthogonal expansion basis, which is spanned by polynomials. Then, some remarks on the computational realization of the SSFEM are given. The evaluation of the statistical response is outlined for the first four statistical moments, namely the mean value, the standard deviation, the skewness and the kurtosis and some extensions of the SSFEM are discussed. In particular, these are the extension to *log-normal random variables*, to *log-normal random fields* and to *multiple input random fields*. The extension to multiple input random fields is discussed in some details, because in this thesis, four different random quantities are included in the formulation of the governing equations. The chapter ends with a numerical example with an analysis of the computed results. After presenting the SFEM with a focus on the linear SSFEM, **Chapter 9** provides the extension of the linear SSFEM to a new SSFEM formulation for solving non-linear problems. Details on the PC-algebra as well as some details on the applied regression method are discussed. Then, the coupling of the developments of the previous sections (resp. chapters) are proposed for the solution of stochastic non-linear problems by using the non-linear SSFEM. The presented approach is tested on two numerical examples and the results are compared with those obtained from the coupled SPRM-MCS and a simple Latin Hypercube sampling. The thesis ends with **Chapter 10**, where the major findings, achieved from the theoretical and numerical realization of the proposed method, are summarized. Open questions and possible future research work are also discussed in this chapter.

In **Appendix A**, some additional mathematical remarks are summarized. An overview of frequently used probability density functions in engineering applications is given in **Appendix B**. **Appendix C** specifies the detailed derivation of the tangent modulus which is needed to evaluate the constitutive equation, presented in section 3.4. Finally, **Appendix D** is devoted to some additional results of the SPRM.

2. Continuum Mechanical Framework

The physically correct description of a material body and its deformation is based on interactions of the atomic scale. Material behaviour, such as plasticity can be described on this length scale by a movement of imperfections in the atomic lattice. This detailed modelling is quiet difficult and also unnecessary for engineering applications on the macroscopic length scale due to the high effort for modeling and computational time. Furthermore, the behaviour at the atomic level is often not of interest and the description of the macroscopic behaviour is sufficient for engineering applications in many cases. According to this, the microscopic structure of the material is described macroscopically in the continuum mechanics as a continuous medium. Most of the materials are, for example, inhomogeneous on smaller length scale. However, the discrete structures of matter are often neglected, i.e their macroscopic behaviour is assumed to be homogeneous. Therefore, the continuum mechanic framework will be used for describing the microscopic behaviour of materials throughout this thesis.

The theoretical framework of the continuum mechanics, which is presented in this chapter, is mainly inspired by the standard textbook by Holzapfel [2000]. Besides this textbook, a detailed treatment of continuum mechanics as well as on constitutive theory can be found in Gurtin [1981]; Chadwick [1999]; Haupt [2000]; Betten [2001]; Ibrahimbegovic [2006]; Altenbach [2012]. For additional information on non-linear mechanics, the reader is referred to the textbooks by Wriggers [2008] and de Borst et al. [2012]. In addition to the literature mentioned above, the books by de Boer [1982]; Schade and Neemann [2009] and Itskov [2009] should be listed here, where the tensor calculus is treated in detail.

This chapter gives an overview to the necessary continuum mechanical subdivisions and is structured as follows: The kinematics and deformations of a continuum are covered in section 2.1. In section 2.2 the mechanical stress concept is introduced. The physical processes considered here are described by balance laws and the two laws of thermodynamics, which are discussed in sections 2.3 and 2.4. The constitutive theory of materials under consideration is presented in section 2.5. In this thesis, the plasticity theory are the basis for the stochastic approach, which will be presented in the later chapters. Therefore, section 2.6 provides the preliminaries to the generalized plasticity with the subsequent extension to materials with hardening behaviour.

2.1. Kinematics

In continuum mechanics, a material body $\mathcal{B}$ is a continuous description of matter in space and time. The material body is imagined as being a composition of a continuous set of material points, described by $P \in \mathcal{B}$. Let Φ be the motion of the body which can be expressed by the mapping χ of the body $\mathcal{B}$ in the three-dimensional EUCLIDEAN space $\mathbb{R}^3$. This mapping is called *configuration* of the body $\mathcal{B}$ and can be mathematically written as

$$\chi : \mathcal{B} \longrightarrow \mathbb{R}^3 \tag{2.1}$$
$$P \longmapsto \chi(P) = \{x_1, x_2, x_3\} \, , \tag{2.2}$$

see also the illustration in Fig. 2.1. A set of three real numbers describes a material
point P and can be identified by the vector $\mathbf{x} = \chi(\text{P})$.
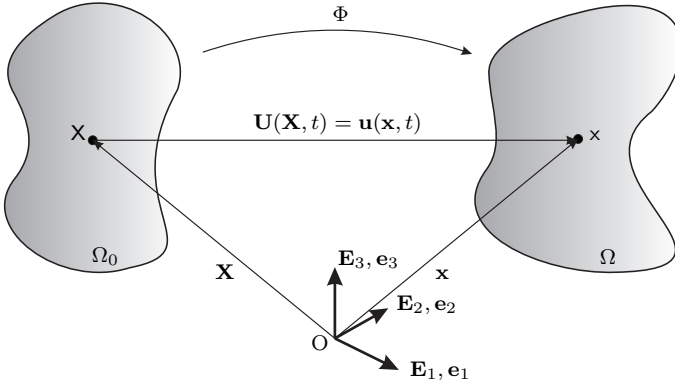
Figure 2.1.: Reference configuration Ω_0 and current configuration Ω of a continuum
body in $\mathbb{R}^3$.

To characterize a deformation process, one configuration has to be chosen as a basis
configuration, denoted as the *reference configuration* Ω_0, as shown in Fig. 2.1. Based
on this figure, each material point P at the initial time instant $t = 0$ (in the following
labelled as t_0) corresponds to a geometrical point X embedded in the initial region Ω_0.
Now, P can be identified by the position vector $\mathbf{X} = X_A \mathbf{E}_A$, where $\mathbf{E}_A$, $A = 1, 2, 3$,
defines an orthogonal base system in the reference configuration relative to the fixed
origin O. If the body transforms from Ω_0 to a new configuration Ω at a subsequent
time $t > 0$, the new configuration of $\mathcal{B}$ is denoted as the *current configuration*. The
corresponding position vector $\mathbf{x} = x_a \mathbf{e}_a$ represents the associated geometrical point x
in the current configuration. The one-to-one mapping of the continuum body $\mathcal{B}$ from
the reference configuration Ω_0 to the current configuration Ω is described by

$$\mathbf{x} = \Phi(\mathbf{X}, t) \ . \tag{2.3}$$

Because of the assumption that Φ is uniquely invertible, it exists a unique inverse
motion Φ^{-1} at any time t and the relation between $\mathbf{X}$ and $\mathbf{x}$ can be expressed by

$$\mathbf{X} = \Phi^{-1}(\mathbf{x}, t) \ . \tag{2.4}$$

After these primarily remarks, a clear distinction between variables and mathematical
operators, related to each domain, has to be made. The notation employed here is
pointed out below.

- Vector and tensor variables defined in the reference configuration Ω_0 are written
  with bold face capital letters, like $\mathbf{X}$. Scalar variables defined in this configu-
  ration are written with capital letters, like X. The operators defined in this
  configuration starts with a capital letter, e.g., Div or Grad.

- For those variables related to the current configuration $\Phi(\Omega_0)$, the bold face lower-case letters are used, for example, $\mathbf{x}$. The scalar variables and operators are denoted by using only lower-case letters, e.g, x, grad or div.

The *displacement field* $\mathbf{U}$ links the position of a material point in the reference configuration with its corresponding position in the deformed configuration (current configuration) by

$$\mathbf{U}(\mathbf{X},t) = \mathbf{x}(\mathbf{X},t) - \mathbf{X} , \qquad (2.5)$$

which holds for all material points and is also illustrated in Fig. 2.1. The formulation
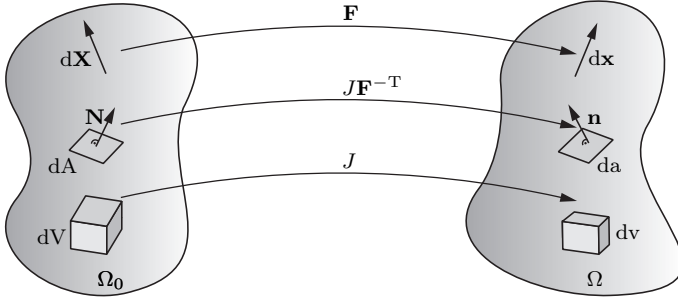
Figure 2.2.: Transformation of line, area and volume elements from the reference configuration Ω_0 to the current configuration Ω.

of the displacement field in equation (2.5) is denoted as the material description (Lagrangian form). The corresponding representation in the spatial description (Eulerian form) is defined by

$$\mathbf{u}(\mathbf{x},t) = \mathbf{x} - \mathbf{X}(\mathbf{x},t) . \qquad (2.6)$$

The velocity field $\mathbf{V}$ in the material description are expressed by

$$\mathbf{V}(\mathbf{X},t) = \frac{\partial\Phi(\mathbf{X},t)}{\partial t} , \qquad (2.7)$$

and the corresponding acceleration field $\mathbf{A}$ is given by

$$\mathbf{A}(\mathbf{X},t) = \frac{\partial\mathbf{V}(\mathbf{X},t)}{\partial t} . \qquad (2.8)$$

By applying the motion Φ, the velocity $\mathbf{V}$ and acceleration $\mathbf{A}$ can be transformed into the spatial coordinates $\mathbf{v}(\mathbf{x},t)$ and $\mathbf{a}(\mathbf{x},t)$ as follows:

$$\mathbf{V}(\mathbf{X},t) = \mathbf{V}\left[\Phi^{-1}(\mathbf{x},t)\right] = \mathbf{v}(\mathbf{x},t) , \qquad (2.9)$$

and accordingly for the acceleration by

$$\mathbf{A}(\mathbf{X},t) = \mathbf{A}\left[\Phi^{-1}(\mathbf{x},t)\right] = \mathbf{a}(\mathbf{x},t) . \qquad (2.10)$$

In order to map an infinitesimal small line element $d\mathbf{X}$ placed in the reference con-

figuration to the corresponding element d$\mathbf{x}$ placed in the current configuration, the deformation gradient $\mathbf{F}$ is introduced. Such a transformation of a line element d$\mathbf{X}$ to the equivalent element d$\mathbf{x}$ is given by

$$d\mathbf{x} = \mathbf{F}(\mathbf{X}, t)d\mathbf{X} . \tag{2.11}$$

Here, $\mathbf{F}$ is defined by

$$\mathbf{F}(\mathbf{X}, t) = \frac{\partial \Phi(\mathbf{X}, t)}{\partial \mathbf{X}} \quad = \quad \text{Grad}\,\mathbf{x}(\mathbf{X}, t) , \tag{2.12}$$

or in index notation by

$$\mathrm{F}_{aA} = \frac{\partial \Phi_a}{\partial X_A} \quad = \quad \text{Grad}_{X_A}\, x_a . \tag{2.13}$$

The deformation gradient is a two-point tensor, which connects points in two different configurations, indicated by the two different indices A and a in equation (2.13). To fulfil the condition of the inverse transformation $\mathbf{F}^{-1}$, $\mathbf{F}$ may not be singular, which is equivalent to the following condition

$$J(\mathbf{F}, t) = \det\mathbf{F}(\mathbf{X}, t) \neq 0 .$$

A further constraint is given through the impenetrability of matter. Mathematically, that would be possible but in reality negative volumes are not physical. Therefore, the Jacobian determinant J must always be greater than zero, thus

$$J(\mathbf{F}, t) > 0 , \tag{2.14}$$

and all other volume ratios are excluded. The area and volume elements can also be transformed from the reference configuration Ω_0 into the current configuration Ω (and vice versa) by applying the deformation gradient $\mathbf{F}$. For a graphical illustration see Fig. 2.2. The transformation of an infinitesimal small area element d$\mathbf{A}$ to the corresponding area element d$\mathbf{a}$ is given by

$$d\mathbf{a} = J\mathbf{F}^{-T}d\mathbf{A} , \tag{2.15}$$

with d$\mathbf{A} = \mathbf{N}dA$ and d$\mathbf{a} = \mathbf{n}da$, where $\mathbf{N}$ is the normal vector on d$\mathbf{A}$ and $\mathbf{n}$ is the normal vector on d$\mathbf{a}$. The relation (2.15) is also known as Nanson's formula. By the Jacobian determinant, the relation for the transformation of an infinitesimal small volume element can be expressed as

$$dv = JdV . \tag{2.16}$$

In non-linear continuum mechanics, different strain measures have been introduced for specific purposes. The deformation gradient $\mathbf{F}$ can also be considered as one of them. One basic characteristic of $\mathbf{F}$ is the description of the entire motion including the rigid body motion. This means, that $\mathbf{F}$ is not objective and depends on the reference coordinate system. In the case, that only deformations are described $\mathbf{F}$ is not suitable and other strain measures are needed, where in table 2.1 the most common strain measures are listed. For a detailed mathematical description and further explanations reference is made to the given literature at the beginning of this chapter.

Table 2.1.: Commonly used strain tensors.

	reference configuration	current configuration
strain tensors	Green-Lagrange strain tensor $\mathbf{E} = \frac{1}{2}(\mathbf{C} - \mathbf{1})$ with right Cauchy-Green tensor $\mathbf{C} = \mathbf{F}^{\mathrm{T}}\mathbf{F}$	Euler-Almansi strain tensor $\mathbf{e} = \frac{1}{2}(\mathbf{1} - \mathbf{b}^{-1})$ with left Cauchy-Green tensor $\mathbf{b} = \mathbf{F}\mathbf{F}^{\mathrm{T}}$
push-forward/ pull-back for strain tensors	$\mathbf{E} = \mathbf{F}^{\mathrm{T}}\mathbf{e}\mathbf{F}$	$\mathbf{e} = \mathbf{F}^{-\mathrm{T}}\mathbf{E}\mathbf{F}^{-1}$

The tensor $\mathbf{1}$, introduced in Tab. 2.1, is the second order identity tensor and the push-forward operation transforms material tensors (tensors defined in the reference configuration) into spatial tensors (tensors defined in the current configuration) or vice versa for the pull-back operation.

2.2. The Definition of Stress

Besides different measures for the strains, there also exists various measures of stresses. Physically, stress has the dimension of force per unit of area. To define the concept of stress, the continuous body $\mathcal{B}$ in its reference configuration Ω_0 and current configuration Ω is considered here. Based on Newton's third law (action equals reaction) it is stated that the applied forces and the resulting reaction forces on the body surface $\partial\Omega_0$ and $\partial\Omega$ must be in equilibrium. A cut through the body provides an insight into the resulting internal forces. An infinitesimal area element $\mathrm{d}a$ and the infinitesimal acting force vector $\mathrm{d}\mathbf{f}$ are defined in the current configuration. The corresponding area element in the reference configuration is characterized by $\mathrm{d}A$. The value and direction of the infinitesimal acting force $\mathrm{d}\mathbf{f}$ in both configurations is assumed to be equal. Thus, the surface tractions are defined by

$$\mathbf{T} = \frac{\mathrm{d}\mathbf{f}}{\mathrm{d}A} \quad \text{and} \quad \mathbf{t} = \frac{\mathrm{d}\mathbf{f}}{\mathrm{d}a}\,, \tag{2.17}$$

$$\mathbf{T} = \mathbf{T}(\mathbf{X}, t, \mathbf{N})\,, \quad \mathbf{t} = \mathbf{t}(\mathbf{x}, t, \mathbf{n})\,, \tag{2.18}$$

where $\mathbf{T}$ is referred to as the first Piola-Kirchhoff or nominal traction vector and $\mathbf{t}$ is the Cauchy or true traction vector. Further important (second-order) tensors are defined by Cauchy's stress theorem:

$$\mathbf{t}(\mathbf{x}, t, \mathbf{n}) = \boldsymbol{\sigma}(\mathbf{x}, t)\mathbf{n}\,,$$
$$\mathbf{T}(\mathbf{X}, t, \mathbf{N}) = \mathbf{P}(\mathbf{X}, t)\mathbf{N} \quad \text{or} \quad T_a = P_{aA}N_A\,, \tag{2.19}$$

where $\boldsymbol{\sigma}$ dentoes the Cauchy stress tensor and $\mathbf{P}$ is referred to the first Piola-Kirchhoff stress tensor. The index notation given in equation (2.19) illustrates that $\mathbf{P}$, similar to $\mathbf{F}$, is a two-field tensor. Two further characteristics of $\mathbf{P}$ are that it is usually not symmetric and not objective. Therefore, alternative stress measures are defined. They are often used for practical non-linear analyses, with the remark that most of their components do not have a direct physical interpretation. Two of them, the second Piola-Kirchhoff stress tensor $\mathbf{S}$ and the Kirchhoff stress tensor $\boldsymbol{\tau}$

should be named here, which are listed together with the introduced stress measures in Table 2.2 on the next page.

Table 2.2.: Commonly used stress tensors.

	reference configuration	two field tensors	current configuration
stress definitions		1. Piola-Kirchhoff stress tensor $\mathbf{P}$ $\mathbf{PN} = \mathbf{T}$	Cauchy stress tensor $\boldsymbol{\sigma}$ $\boldsymbol{\sigma}\mathbf{n} = \mathbf{t}$
stress tensors	2. Piola-Kirchhoff stress tensor $\mathbf{S}$ $\mathbf{S} = \mathbf{F}^{-1}\mathbf{P} \ (\Longrightarrow \mathbf{P} = \mathbf{FS})$	1. Piola-Kirchhoff stress tensor $\mathbf{P}$ $\mathbf{P} = J\boldsymbol{\sigma}\mathbf{F}^{-\mathrm{T}}$	Cauchy stress tensor $\boldsymbol{\sigma}$ and Kirchhoff stress tensor $\boldsymbol{\tau}$ $\boldsymbol{\tau} = J\boldsymbol{\sigma}$
push-forward/ pull-back for stress tensors	$\mathbf{S} = J\mathbf{F}^{-1}\boldsymbol{\sigma}\mathbf{F}^{-\mathrm{T}} = \mathbf{F}^{-1}\mathbf{P} = \mathbf{S}^{\mathrm{T}}$		$\boldsymbol{\sigma} = J^{-1}\mathbf{FSF}^{\mathrm{T}}$

2.3. Balance Laws

Balance laws represent generally accepted laws of nature. It is important to distinguish between the global form of the balance laws (refers to the entire continuum body) and the local form (refers to each material point of the continuum body). In this section the fundamental balance principles, i.e. the conservation of mass, linear and angular momentum and the balance of mechanical energy are presented.

2.3.1. Conservation of Mass

In what follows, only closed systems are considered, i.e. that the mass of a system is conserved and

$$m(\Omega_0) = m(\Omega) > 0 \tag{2.20}$$

holds for all times t. The differential form of equation (2.20) is given by

$$dm(\mathbf{X}) = dm(\mathbf{x}, t) > 0 . \tag{2.21}$$

The equation above shows an infinitesimal mass element dm in the reference configuration and in the current configuration, which has to be equal. With the relation

$$dm(\mathbf{X}) = \rho_0(\mathbf{X}) \, dV \quad \text{and} \quad dm(\mathbf{x}, t) = \rho(\mathbf{x}, t) \, dv , \tag{2.22}$$

where dV is an infinitesimal volume element in the reference configuration and dv is the corresponding one in the current configuration, the following expression is obtained

$$\rho_0(\mathbf{X}) \, dV = \rho(\mathbf{x}, t) \, dv > 0 . \tag{2.23}$$

Here, ρ_0 denotes the density in the reference configuration and ρ is the corresponding one in the current configuration. Integration of the infinitesimal mass dm over the entire region leads to the total mass m of that region and equation (2.23) can be rewritten as

$$m = \int_{\Omega_0} \rho_0(\mathbf{X}) \, dV = \int_{\Omega} \rho(\mathbf{x}, t) \, dv = \text{const} > 0 , \tag{2.24}$$

for all times t. The rate of mass is calculated by

$$\dot{m} = \frac{Dm}{Dt} = \frac{D}{Dt} \int_{\Omega} \rho(\mathbf{x}, t) \, dv = 0 . \tag{2.25}$$

Using the transformation in equation (2.16), the mass densities in the material and spatial description are related to each other via

$$\rho_0 = J\rho = \rho \det \mathbf{F} , \tag{2.26}$$

$$\frac{\rho_0}{\rho} = \det \mathbf{F} . \tag{2.27}$$

From the previous equation it is obvious that the determinant of $\mathbf{F}$ can be written in terms of the density by $\frac{\rho_0}{\rho}$. For the global rate of mass continuity (2.25), the following

identity[1] is obtained

$$\int\limits_{\Omega} \left[\dot{\rho}(\mathbf{x}, t) + \rho(\mathbf{x}, t) \operatorname{div} \mathbf{v}(\mathbf{x}, t) \right] \mathrm{d}v = 0 \; , \tag{2.28}$$

where $\mathbf{v}$ describes the velocity of a mass particle. The equation above states, that the change of mass density with respect to time equals the flow of mass density over the boundaries.

2.3.2. Balance of Linear Momentum

The linear momentum of a continuum body $\mathcal{B}$, at an arbitrary region Ω_0 (Ω) and covered by the boundary surface $\partial\Omega_0$ $(\partial\Omega)$ at time t, can be written as follows:

$$\mathbf{L}(t) = \int\limits_{\Omega} \rho \, \mathbf{v} \, \mathrm{d}v = \int\limits_{\Omega_0} \rho_0 \, \mathbf{V} \, \mathrm{d}V \; , \tag{2.29}$$

where the quantities ρ, $\mathbf{v}$ and $\mathrm{d}v$ are measured with respect to the current configuration and ρ_0, $\mathbf{V}$ and $\mathrm{d}V$ are the ones with respect to the reference configuration. The total time derivative of equation (2.29) corresponds to the resulting force $\mathbf{F}(t)$ acting on the continuum, i.e.

$$\dot{\mathbf{L}}(t) = \frac{\mathrm{D}}{\mathrm{D}t} \int\limits_{\Omega} \rho \, \mathbf{v} \, \mathrm{d}v = \frac{\mathrm{D}}{\mathrm{D}t} \int\limits_{\Omega_0} \rho_0 \, \mathbf{V} \, \mathrm{d}V = \mathbf{F}(t) \; , \tag{2.30}$$

$$\dot{\mathbf{L}}(t) = \int\limits_{\Omega} \rho \, \dot{\mathbf{v}} \, \mathrm{d}v = \int\limits_{\Omega_0} \rho_0 \, \dot{\mathbf{V}} \, \mathrm{d}V = \mathbf{F}(t) \; . \tag{2.31}$$
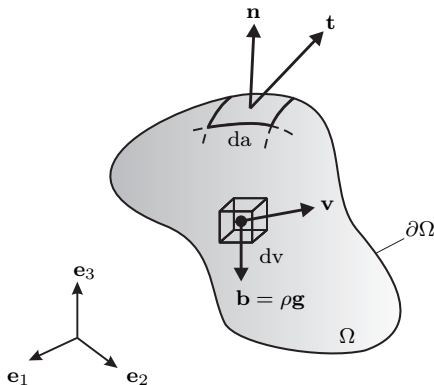
Figure 2.3.: Mechanical forces acting on the current configuration Ω.

---

[1] Evaluated with the transport theorem: $\frac{\mathrm{D}}{\mathrm{D}t} \int\limits_{\Omega} \rho(\mathbf{x}, t) \, \mathrm{d}v = \int\limits_{\Omega} \left[\dot{\rho}(\mathbf{x}, t) + \rho(\mathbf{x}, t) \operatorname{div} \mathbf{v}(\mathbf{x}, t) \right] \mathrm{d}v.$

This external force $\mathbf{F}(t)$ can be decomposed into a body force $\mathbf{b}$ in Ω and a surface load $\mathbf{t}$ acting on the boundary surface $\partial\Omega$, as illustrated in Fig. 2.3. Hence, with the decomposition of $\mathbf{F}$, the balance of linear momentum can be written as

$$\mathbf{F}(t) = \int_{\Omega} \mathbf{b} \, dv + \int_{\partial\Omega} \mathbf{t} \, da \, . \tag{2.32}$$

A typical body force is the gravity loading per unit volume of an arbitrary body. Finally, with regard to equation (2.31), the global form of balance of linear momentum can be written in spatial coordinates as

$$\int_{\Omega} \rho \, \mathbf{a} \, dv = \int_{\Omega} \mathbf{b} \, dv + \int_{\partial\Omega} \mathbf{t} \, da \, , \tag{2.33}$$

with $\mathbf{a} = \dot{\mathbf{v}}$ being the acceleration. With equation $(2.19)_1$ and by use of the divergence theorem[2] the global formulation of the balance of linear momentum becomes

$$\int_{\Omega} (\operatorname{div} \boldsymbol{\sigma} + \mathbf{b} - \rho \, \mathbf{a}) \, dv = \mathbf{0} \, , \tag{2.34}$$

which is also known as Cauchy's first equation of motion. Under the assumption that this relation holds for any volume dv, the local form is obtained as follows:

$$\operatorname{div} \boldsymbol{\sigma} + \mathbf{b} = \rho \, \mathbf{a} \, , \tag{2.35}$$

and in purely static systems, where the acceleration vanishes, equation (2.35) becomes

$$\operatorname{div} \boldsymbol{\sigma} + \mathbf{b} = \mathbf{0} \, . \tag{2.36}$$

The last equation is often referred to as Cauchy's equation of equilibrium.

2.3.3. Balance of Angular Momentum

For a continuous body $\mathcal{B}$ the angular momentum $\mathbf{J}$ is defined as

$$\mathbf{J}(t) = \int_{\Omega} \mathbf{r} \times \rho \, \mathbf{v} \, dv = \int_{\Omega_0} \mathbf{r} \times \rho_0 \, \mathbf{V} \, dV \, , \tag{2.37}$$

with the position vector $\mathbf{r}(\mathbf{x}) = \mathbf{x} - \mathbf{x}_0$ and the operator $\times$ denotes the mathematical cross product. The quantities ρ, $\mathbf{v}$ and dv are formulated with respect to the current configuration and ρ_0, $\mathbf{V}$ and dV are measured with respect to the reference configuration. It states that the temporal change of angular momentum is equal to the sum of all external momentums $\dot{\mathbf{J}} = \mathbf{M}(t)$ acting on $\mathcal{B}$, which can be written as

$$\dot{\mathbf{J}}(t) = \frac{\mathrm{D}}{\mathrm{D}t} \int_{\Omega} \mathbf{r} \times \rho \, \mathbf{v} \, dv = \frac{\mathrm{D}}{\mathrm{D}t} \int_{\Omega_0} \mathbf{r} \times \rho_0 \mathbf{V} \, dV = \mathbf{M}(t) \, . \tag{2.38}$$

---

[2] Divergence theorem: $\int_a \mathbf{u} \cdot \mathbf{n} \, da = \int_v \operatorname{div} \mathbf{u} \, dv$.

M and **F** can be additively split into

$$\mathbf{M}(t) = \int_{\partial\Omega} \mathbf{r} \times \mathbf{t} \, da + \int_{\Omega} \mathbf{r} \times \mathbf{b} \, dv \,. \tag{2.39}$$

Inserting this split into equation (2.38) the global form of balance of angular momentum is obtained as

$$\dot{\mathbf{J}}(t) = \frac{\mathrm{D}}{\mathrm{D}t} \int_{\Omega} \mathbf{r} \times \rho \, \mathbf{v} \, dv = \int_{\partial\Omega} \mathbf{r} \times \mathbf{t} \, da + \int_{\Omega} \mathbf{r} \times \mathbf{b} \, dv \,. \tag{2.40}$$

2.3.4. Balance of Mechanical Energy

The mechanical energy results from three various parts. These are the *external mechanical power* $\mathcal{P}_{\text{ext}}(t)$

$$\mathcal{P}_{\text{ext}}(t) = \int_{\Omega} \mathbf{b} \cdot \mathbf{v} \, dv + \int_{\partial\Omega} \mathbf{t} \cdot \mathbf{v} \, da \,, \tag{2.41}$$

the *kinetic energy* $\mathcal{K}(t)$

$$\mathcal{K}(t) = \int_{\Omega} \frac{1}{2} \rho \, \mathbf{v} \cdot \mathbf{v} \, dv \,, \tag{2.42}$$

and the *rate of internal mechanical work* $\mathcal{P}_{\text{int}}(t)$

$$\mathcal{P}_{\text{int}}(t) = \int_{\Omega} \boldsymbol{\sigma} : \mathbf{d} \, dv \,, \tag{2.43}$$

where $\mathbf{d} = \frac{1}{2}\left(\operatorname{grad} \mathbf{v} + \operatorname{grad}^{\mathrm{T}} \mathbf{v}\right)$ denotes the deformation rate tensor. With these parts in hand, the *balance of mechanical energy*, in the global form in spatial description, can be written as

$$\frac{\mathrm{D}}{\mathrm{D}t} \int_{\Omega} \frac{1}{2} \rho \, \mathbf{v} \cdot \mathbf{v} \, dv + \int_{\Omega} \boldsymbol{\sigma} : \mathbf{d} \, dv = \int_{\Omega} \mathbf{b} \cdot \mathbf{v} \, dv + \int_{\partial\Omega} \mathbf{t} \cdot \mathbf{v} \, da \,, \tag{2.44}$$

or in short form, written only in terms of $\mathcal{K}$, $\mathcal{P}_{\text{int}}$ and $\mathcal{P}_{\text{ext}}$ as

$$\frac{\mathrm{D}}{\mathrm{D}t} \mathcal{K}(t) + \mathcal{P}_{\text{int}}(t) = \mathcal{P}_{\text{ext}}(t) \,. \tag{2.45}$$

The interpretation of equation (2.45) is as follows:

The rate of change of kinetic energy $\mathcal{K}$ of a system in combination with the rate of internal mechanical work $\mathcal{P}_{\text{int}}$, occurred by internal stresses, is equal to the rate of external mechanical power $\mathcal{P}_{\text{ext}}$ acting on the system by surface tractions $\mathbf{t}$ and body forces $\mathbf{b}$.

With the *balance of thermal energy*

$$\frac{D}{Dt}\mathcal{E}(t) = \mathcal{P}_{\text{int}}(t) + \mathcal{Q}(t) \,, \tag{2.46}$$

where $\mathcal{Q}$ denotes the *thermal power*

$$\mathcal{Q}(t) = \int_{\Omega} r \, \mathrm{d}v + \int_{\partial\Omega} q_{\text{n}} \, \mathrm{d}a \,. \tag{2.47}$$

Substituting equation (2.46) into equation (2.45) leads to the *first law of thermodynamics*, i.e.

$$\frac{D}{Dt}\mathcal{K}(t) + \frac{D}{Dt}\mathcal{E}(t) = \mathcal{P}_{\text{ext}}(t) + \mathcal{Q}(t) \,, \tag{2.48}$$

with the relation

$$\mathcal{E}(t) = \int_{\Omega} e_{\text{c}}(\mathbf{x}, t) \, \mathrm{d}v \,. \tag{2.49}$$

Here, e_{c} is the specific internal energy defined per unit current volume. The variables r and q_{n} in equation (2.47) are illustrated in Fig. 2.4 and denotes the heat source and the normal heat flux, which is defined (in spatial description) as

$$q_{\text{n}}(\mathbf{x}, t, \mathbf{n}) = -\mathbf{q}(\mathbf{x}, t) \cdot \mathbf{n} \,, \tag{2.50}$$

where $\mathbf{q} = \mathbf{q}(\mathbf{x}, t)$ is the Cauchy heat flux. The negative sign in equation (2.50) is needed in order to get a positive thermal flux when heat flows into the body, because $\mathbf{n}$ is an outward normal. Formulated in an explicit expression, equation (2.48) can be written as

$$\frac{D}{Dt} \int_{\Omega} \left(\frac{1}{2} \rho \, \mathbf{v}^2 + e_{\text{c}} \right) \mathrm{d}v = \int_{\Omega} (\mathbf{b} \cdot \mathbf{v} + r) \, \mathrm{d}v + \int_{\partial\Omega} (\mathbf{t} \cdot \mathbf{v} + q_{\text{n}}) \, \mathrm{d}a \,. \tag{2.51}$$

From equation (2.51), it is obvious that the total energy, on the left hand side of this equation, is equal to the external mechanical power $\mathcal{P}_{\text{ext}}$ and heat supply $\mathcal{Q}$, which stands on the right hand side. A more explicit expression of equation (2.51) are obtained by first rewriting equation (2.47) by using of equation (2.50) and the divergence theorem, which leads to

$$\mathcal{Q}(t) = \int_{\Omega} (r - \operatorname{div} \mathbf{q}) \, \mathrm{d}v \,. \tag{2.52}$$

After inserting the equations (2.43), (2.49) and (2.52) into equation (2.46) results in the reduced global form of balance energy in spatial description, i.e.

$$\frac{D}{Dt} \int_{\Omega} e_{\text{c}} \, \mathrm{d}v = \int_{\Omega} (\boldsymbol{\sigma} : \mathbf{d} - \operatorname{div} \mathbf{q} + r) \, \mathrm{d}v \,. \tag{2.53}$$
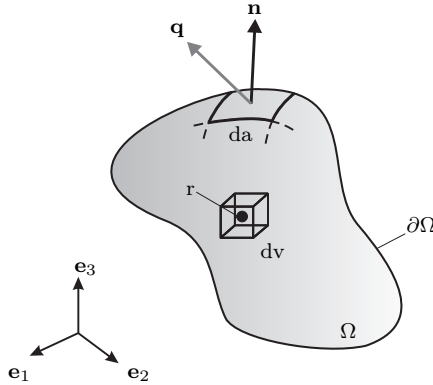
Figure 2.4.: Heat source r and the Cauchy heat flux $\mathbf{q}$ in the current configuration Ω.

2.4. Entropy Inequality

Through the conservation of total energy, an energy form can be transformed into another energy form. However, the first law of thermodynamics contains no detail about the direction of such an energy transformation. Furthermore, there is no information if the process is reversible or irreversible. Therefore, the second law of thermodynamics is introduced, which gives an information of the process direction. This formulation is based on the concept of entropy.[3]

Let $\mathcal{B}$ be a continuous body, occupying a certain region (Ω_0 or Ω) with the entropy

$$\mathcal{S}(t) = \int_{\Omega} \eta_c(\mathbf{x}, t) \, \mathrm{d}v = \int_{\Omega_0} \eta(\mathbf{X}, t) \, \mathrm{d}V \,, \tag{2.54}$$

inside this system. Here η_c and η are the specific entropy per unit volume in the current and reference configuration. The rate of the entropy input

$$\tilde{\mathcal{Q}}(t) = \int_{\Omega} \tilde{r} \, \mathrm{d}v - \int_{\partial\Omega} \mathbf{h} \cdot \mathbf{n} \, \mathrm{d}a \,, \tag{2.55}$$

is a total product of the entropy transferred across the boundary surface of the body and the entropy generated (or dissipated) inside the considered region. In this formula denotes $\tilde{r}$ the time-dependent entropy sources (defined per unit time and unit volume) and $\mathbf{h}$ is the also time-dependent Cauchy entropy flux. The negative sign in equation (2.55) results from the definition of the unit vector $\mathbf{n}$, which is outward to $\partial\Omega$, see Fig. 2.4. With these two relations, the total production of entropy per unit time can

---

[3]The entropy can be viewed as a quantitative measure of microscopic disorder and randomness, cf. Holzapfel [2000]. Here, the entropy is considered as a measure of how much free energy is transformed into heat.

be written as follows:

$$\Gamma(t) \equiv \frac{\mathrm{D}}{\mathrm{D}t} \mathcal{S}(t) - \tilde{\mathcal{Q}}(t) \geq 0 , \tag{2.56}$$

which is known as the second law of thermodynamics or entropy inequality principle and states that the total entropy production of all thermodynamic processes is never negative. With the use of equations (2.54) and (2.55), a more common expression of equation (2.56) is obtained, which leads to the global spatial form of the second law of thermodynamics

$$\Gamma(t) \equiv \frac{\mathrm{D}}{\mathrm{D}t} \int \eta_{\mathrm{c}}(\mathbf{x},t) \, \mathrm{d}v + \int_{\partial\Omega} \mathbf{h} \cdot \mathbf{n} \, \mathrm{d}a - \int_{\Omega} \tilde{r} \, \mathrm{d}v \geq 0 . \tag{2.57}$$

In reality, the inequalities in equations (2.56) and (2.57) hold, i.e. real processes are irreversible. The equal sign is applied only for idealized process, i.e. reversible processes.

By inserting the proportional factor $1/\Theta$, where $\Theta = \Theta(\mathbf{x},t)$ describes the absolute temperature in Kelvin, the entropy flux $\mathbf{h}$ and the entropy sources $\tilde{r}$ can be redefined by

$$\mathbf{h} = \frac{\mathbf{q}}{\Theta} \qquad \text{and} \qquad \tilde{r} = \frac{r}{\Theta} . \tag{2.58}$$

Substituting these two identities in equation (2.57) leads to the Clausius-Duhem inequality

$$\mathcal{D}(t) \equiv \frac{\mathrm{D}}{\mathrm{D}t} \int_{\Omega} \eta_{\mathrm{c}} \, \mathrm{d}v + \int_{\partial\Omega} \frac{\mathbf{q}}{\Theta} \cdot \mathbf{n} \, \mathrm{d}a - \int_{\Omega} \frac{r}{\Theta} \, \mathrm{d}v \geq 0 , \tag{2.59}$$

which is written here in the spatial description. To obtain the local form of the Clausius-Duhem inequality, the surface integral in equation (2.59) needs to be covered into a volume integral via the divergence theorem, thus

$$\int_{\partial\Omega} \frac{\mathbf{q}}{\Theta} \cdot \mathbf{n} \, \mathrm{d}a = \int_{\Omega} \frac{1}{\Theta} \, \mathrm{div} \, \mathbf{q} \, \mathrm{d}v . \tag{2.60}$$

Afterwards, the product rule is applied on equation (2.60) and substitute it into equation (2.59) leads to the local spatial form

$$\dot{\eta}_{\mathrm{c}} + \frac{1}{\Theta} \, \mathrm{div} \, \mathbf{q} - \frac{1}{\Theta^2} \, \mathbf{q} \cdot \mathrm{grad} \, \Theta - \frac{r}{\Theta} \geq 0 , \tag{2.61}$$

where $\mathrm{grad} \, \Theta$ denotes the spatial gradient of the temperature field Θ . The local form of the inequality stated above can be coupled with the reduced local form of the first law of thermodynamics, derived from equation (2.53), as

$$\dot{e}_{\mathrm{c}} = \boldsymbol{\sigma} : \mathbf{d} - \mathrm{div} \, \mathbf{q} + r , \tag{2.62}$$

which finally results i

$$\dot{\eta}_{\mathrm{c}} + \frac{1}{\Theta} \, \mathrm{div} \, \mathbf{q} - \frac{1}{\Theta^2} \, \mathbf{q} \cdot \mathrm{grad} \, \Theta - \frac{1}{\Theta} \left(\dot{e}_{\mathrm{c}} + \mathrm{div} \, \mathbf{q} - \boldsymbol{\sigma} : \mathbf{d} \right) \geq 0 . \tag{2.63}$$

With the introduction of the Helmholtz free-energy function ψ, in the current configuration,

$$\psi = e_c - \Theta \eta_c \,, \tag{2.64}$$

and the material time derivative of ψ

$$\dot{\psi} = \dot{e}_c - \left(\dot{\Theta} \eta_c + \Theta \dot{\eta}_c \right) \,, \tag{2.65}$$

and when substituting (2.65) into equation (2.63) leads to the reduced form of the second law of thermodynamics:

$$\boldsymbol{\sigma} : \mathbf{d} - \left(\dot{\psi} + \dot{\Theta} \, \eta_c \right) - \frac{1}{\Theta} \mathbf{q} \cdot \operatorname{grad} \Theta \geq 0 \,. \tag{2.66}$$

The Helmholtz free-energy function is essential for the construction of constitutive relations (see also the following section 2.5) of material behaviour. Some special cases of the thermodynamic processes can be defined, for example, an isothermal process, where the temperature in the body is constant ($\Theta = \text{const.}$), where equation (2.66) reduces to

$$\boldsymbol{\sigma} : \mathbf{d} - \dot{\psi} \geq 0 \,. \tag{2.67}$$

2.5. Constitutive Theory

With the balance laws, introduced in subsections 2.3.2 to 2.3.4, eight equations (without thermal energy) are available for the solution of a mechanical process. However, there are fourteen variables, namely the density ρ, velocity $\mathbf{v}$, stress $\boldsymbol{\sigma}$ as well as the internal energy $\mathcal{E}$, to be determined. When considering a thermomechanical process, the number of variables to be determined increases to nineteen. These are, additionally, the entropy η, temperature Θ and the heat flux $\mathbf{q}$. As already pointed out in section 2.4, the second law of thermodynamics defines only the direction of the process but gives no additional equation. The missing six equations of a mechanical process and the eleven equations of a thermomechanical process can be formulated with respect to the so-called *constitutive equations*. The systematic derivation of constitutive equations based on fundamental principles, which guarantee the mathematical and physical consistency. In the following these principles are briefly summarized.

- *Principle of Causality*: By this principle the dependent and independent variables, with respect to cause and effect, will be selected. For example, if the motion and the temperature are investigated in a thermomechanical analysis, the heat fluxes, free energy and the entropy are the dependent variables, because they change their values relative to the investigated ones.

- *Principle of Determinism*: The current state of a continuum is determined by the actual loading condition as well as the entire history. This means that the reaction of the considered material point depends on the reactions of all other material points inside the continuum body.

- *Principle of Equipresence*: A set of independent variables, which specifies the thermodynamic state of the material, must be included for the considered continuum model in all other constitutive equations.

- *Principle of Material Frame Indifference*: The constitutive equations must be independent from the choice of the reference system, which describes the deformation of the body.

- *Principle of Local Agency*: The conditions in the material points only depend on the close surrounding of the material point. Long-distance effects are neglected, which is sufficient for "simple" materials.

- *Principle of Fading Memory*: A Material has a "memory" and reflects effects of the past in different ways. This axiom enables simplifications regarding to the temporal description. In the case of a fading memory it is assumed that past effects have less influence than recent effects.

- *Principle of Physical Consistence*: Constitutive equations may not contradict the balance laws.

2.5.1. Thermodynamics with Internal Variables

The previously formulated principles are far too general to have practical utility in modelling real materials. Therefore, it is necessary to formulate constitutive relationships to describe the specific properties of a material. For example, the thermodynamic state of a material can be described by the movement $\mathbf{x} = \Phi(\mathbf{X}, t)$ and the temperature $\Theta(\mathbf{X}, t)$ of the material points P at time t. If $\mathbf{x}$ and Θ are selected as independent variables the Cauchy stress tensor $\boldsymbol{\sigma}$, free energy ψ, heat flux vector $\mathbf{q}$ and the specific entropy η_c are the dependent variables. Using the axioms listed at the beginning of this section, the constitutive equations, formulated in the current configuration, have the following functional dependencies:

$$
\begin{aligned}
\psi &= \psi\left(\mathbf{x}, \Theta, \dot{\Theta}, \operatorname{grad}\Theta, \operatorname{grad}\dot{\Theta}, \mathbf{F}, \dot{\mathbf{F}}, \rho, \dot{\rho}\right) , \\
\eta_c &= \eta_c\left(\mathbf{x}, \Theta, \dot{\Theta}, \operatorname{grad}\Theta, \operatorname{grad}\dot{\Theta}, \mathbf{F}, \dot{\mathbf{F}}, \rho, \dot{\rho}\right) , \\
\boldsymbol{\sigma} &= \boldsymbol{\sigma}\left(\mathbf{x}, \Theta, \dot{\Theta}, \operatorname{grad}\Theta, \operatorname{grad}\dot{\Theta}, \mathbf{F}, \dot{\mathbf{F}}, \rho, \dot{\rho}\right) , \\
\mathbf{q} &= \mathbf{q}\left(\mathbf{x}, \Theta, \dot{\Theta}, \operatorname{grad}\Theta, \operatorname{grad}\dot{\Theta}, \mathbf{F}, \dot{\mathbf{F}}, \rho, \dot{\rho}\right) .
\end{aligned}
\tag{2.68}
$$

If the material is assumed to be thermoelastic homogeneous, the material time derivatives can be neglected, because no time dependent effects occur. In this case, the material properties at all points are the same and the constitutive equations do not depend on the position vector $\mathbf{x}$ as well as the mass density ρ and the set of functional dependencies in equation (2.68) simplifies to

$$
\begin{aligned}
\psi &= \psi\left(\Theta, \operatorname{grad}\Theta, \mathbf{F}\right) \\
\eta_c &= \eta_c\left(\Theta, \operatorname{grad}\Theta, \mathbf{F}\right) \\
\boldsymbol{\sigma} &= \boldsymbol{\sigma}\left(\Theta, \operatorname{grad}\Theta, \mathbf{F}\right) \\
\mathbf{q} &= \mathbf{q}\left(\Theta, \operatorname{grad}\Theta, \mathbf{F}\right) .
\end{aligned}
\tag{2.69}
$$

Following the functional dependencies listed above, the rate of change of the specific free energy reads

$$
\dot{\psi} = \frac{\partial\psi}{\partial\mathbf{F}} : \dot{\mathbf{F}} + \frac{\partial\psi}{\partial\Theta}\dot{\Theta} + \frac{\partial\psi}{\partial\operatorname{grad}\Theta}\operatorname{grad}\dot{\Theta} .
\tag{2.70}
$$

Substituting this equation into the Clausius-Duhem inequality (2.66) gives

$$\boldsymbol{\sigma} : \mathbf{d} - \left(\frac{\partial \psi}{\partial \mathbf{F}} : \dot{\mathbf{F}} + \frac{\partial \psi}{\partial \Theta} \dot{\Theta} + \frac{\partial \psi}{\partial \mathrm{grad}\,\Theta} \mathrm{grad}\,\dot{\Theta} + \dot{\Theta} \eta_\mathrm{c} \right) - \frac{1}{\Theta}\,\mathbf{q}\,\mathrm{grad}\,\Theta \geq 0 , \quad (2.71)$$

and with

$$\boldsymbol{\sigma} : \mathbf{d} = \boldsymbol{\sigma}\mathbf{F}^{-\mathrm{T}} : \dot{\mathbf{F}} , \qquad (2.72)$$

the inequality (2.71) becomes

$$\left(\boldsymbol{\sigma}\mathbf{F}^{-\mathrm{T}} - \frac{\partial \psi}{\partial \mathbf{F}} \right) : \dot{\mathbf{F}} - \left(\frac{\partial \psi}{\partial \Theta} + \eta \right) \dot{\Theta} - \frac{\partial \psi}{\partial \mathrm{grad}\,\Theta} \cdot \mathrm{grad}\dot{\Theta} - \frac{1}{\Theta}\,\mathbf{q} \cdot \mathrm{grad}\,\Theta \geq 0 . \quad (2.73)$$

The last term of equation (2.73) can be interpret as a restriction, which states that the heat flux must act against the direction of the temperature gradient. To follow the principle of physical consistence, the inequality in (2.73) must hold for any pair of functions $\{\dot{\mathbf{F}}(t), \dot{\Theta}(t)\}$, which implies

$$\boldsymbol{\sigma} = \frac{\partial \psi}{\partial \mathbf{F}}\mathbf{F}^{\mathrm{T}} , \quad \eta_\mathrm{c} = -\frac{\partial \psi}{\partial \Theta} \quad \text{and} \quad \frac{\partial \psi}{\partial \mathrm{grad}(\Theta)} = 0 , \qquad (2.74)$$

for the constitutive equations.

2.5.2. Material Symmetries

The incorporation of material symmetries can lead to a significant simplification of the constitutive equations. Basis for the consideration of symmetries is the experimental experience, that a large number of continua have a dependence of direction (anisotropy). The application of statements on the material symmetry have a practical benefit, because it results in a simplification of the mathematical equations.

At the beginning of this subsection, some expressions are listed, which are used during this subsection. The first Piola-Kirchhoff stress tensor $\mathbf{P}$ can be expressed in terms of the free energy function ψ as

$$\mathbf{P} = \frac{\partial \psi(\mathbf{F})}{\partial \mathbf{F}} . \qquad (2.75)$$

With the push-forward operation, see Tab. 2.2, the Cauchy stress $\boldsymbol{\sigma}$ reads

$$\boldsymbol{\sigma} = J^{-1}\mathbf{P}\mathbf{F}^{\mathrm{T}} , \qquad (2.76)$$

which, when taking into account equation (2.75) gives

$$\boldsymbol{\sigma} = J^{-1}\mathbf{F}\left(\frac{\partial \psi}{\partial \mathbf{F}} \right)^{\mathrm{T}} = 2J^{-1}\mathbf{F}\frac{\partial \psi}{\partial \mathbf{C}}\mathbf{F}^{\mathrm{T}} . \qquad (2.77)$$

This equation implies that

$$\left(\frac{\partial \psi}{\partial \mathbf{F}} \right)^{\mathrm{T}} = 2\frac{\partial \psi}{\partial \mathbf{C}}\mathbf{F}^{\mathrm{T}} . \qquad (2.78)$$

The first and second Piola-Kirchhoff stress tensor can be also derived with equation

(2.78) as follows:

$$\mathbf{P} = 2\mathbf{F}\frac{\partial\psi}{\partial\mathbf{C}} \quad \text{or} \quad P_{aA} = 2F_{aB}\frac{\partial\psi}{\partial C_{AB}} \,, \tag{2.79}$$

and

$$\mathbf{S} = 2\frac{\partial\psi}{\partial\mathbf{C}} = \frac{\partial\psi}{\partial\mathbf{E}} \quad \text{or} \quad S_{AB} = 2\frac{\partial\psi}{\partial C_{AB}} = \frac{\partial\psi}{\partial E_{AB}} \,, \tag{2.80}$$

where $\mathbf{E}$ denotes the Green-Lagrange strain tensor.

The derivation of the stress tensor by the strain tensor gives the fourth-order tensor, denoted as material tensor $\mathbb{C}$, where below the derivations of $\mathbb{C}$ with respect to $\mathbf{E}$ or $\mathbf{S}$ are listed:

$$\mathbb{C} = \frac{\partial\mathbf{S}}{\partial\mathbf{E}} \quad \text{or} \quad C_{ABCD} = \frac{\partial S_{AB}}{\partial E_{CD}} \,, \tag{2.81}$$

$$\mathbb{C} = 2\frac{\partial\mathbf{S}}{\partial\mathbf{C}} \quad \text{or} \quad C_{ABCD} = 2\frac{\partial S_{AB}}{\partial C_{CD}} \,. \tag{2.82}$$

In the special case, where elastic behaviour and small deformations are assumed, i.e. $\mathbf{E} \to \boldsymbol{\epsilon}$, with the linear strain tensor $\boldsymbol{\epsilon}$, $\mathbb{C}$ equals the elasticity tensor. In this case, $\mathbb{C}$ is represented by the generalized Hooke's law, which can be either isotropic or anisotropic, which postulates the linear dependency between the small strains and the stresses and reads

$$\boldsymbol{\sigma} = \mathbb{C} : \boldsymbol{\epsilon} \,. \tag{2.83}$$

The fourth-order material tensor has 81 independent components and is always symmetric in the first two slots and in the second two, i.e.

$$C_{ABCD} = C_{BACD} = C_{ABDC} \,, \tag{2.84}$$

which leads to a reduction to 36 independent components in $\mathbb{C}$. This symmetry condition is independent of ψ and holds for any isotropic elastic material. With respect to equation $(2.80)_3$ and $(2.82)_2$, $\mathbb{C}$ can be also expressed as

$$\mathbb{C} = 4\frac{\partial^2\psi}{\partial\mathbf{C}\partial\mathbf{C}} \quad \text{or} \quad C_{ABCD} = 4\frac{\partial^2\psi}{\partial C_{AB}\partial C_{CD}} \,, \tag{2.85}$$

with the symmetries

$$C_{ABCD} = C_{CDAB} \,. \tag{2.86}$$

Considering these characteristics the tensor $\mathbb{C}$ has only 21 independent components and can be expressed in matrix formulation as

$$\mathbb{C} = \begin{pmatrix} \mathbb{C}_{1111} & \mathbb{C}_{1122} & \mathbb{C}_{1133} & \mathbb{C}_{1112} & \mathbb{C}_{1113} & \mathbb{C}_{1123} \\ & \mathbb{C}_{2222} & \mathbb{C}_{2233} & \mathbb{C}_{2212} & \mathbb{C}_{2213} & \mathbb{C}_{2223} \\ & & \mathbb{C}_{3333} & \mathbb{C}_{3312} & \mathbb{C}_{3313} & \mathbb{C}_{3323} \\ & s & & \mathbb{C}_{1212} & \mathbb{C}_{1213} & \mathbb{C}_{1223} \\ & & y & & \mathbb{C}_{1313} & \mathbb{C}_{1323} \\ & & & m & & \mathbb{C}_{2323} \end{pmatrix} \,. \tag{2.87}$$

Further reductions of the independent components of $\mathbb{C}$ are possible by the consideration of material symmetries, based on the structure of the crystal lattice. By anisotropic elasticity a distinction can be made between:

- Monotropy: 13 independent components, one symmetry plane in the material.

- Orthotropy: 9 independent components, at least two orthogonal symmetry planes in the material.

- Transversal isotropy: 5 independent components, there is a symmetry in the material with respect to the assumption that all properties are equal.

- If there are at least two axes of symmetry in the material and the elastic properties are the same for these axes, the material is denoted as isotropic, where a common isotropic expression for $\mathbb{C}$, in terms of the Young's modulus E and the Poisson's ratio ν, is as follows:

$$\mathbb{C}_{\text{iso}} = \frac{E}{(1+\nu)(1-2\nu)} \begin{pmatrix} 1-\nu & \nu & \nu & 0 & 0 & 0 \\ \nu & 1-\nu & \nu & 0 & 0 & 0 \\ \nu & \nu & 1-\nu & 0 & 0 & 0 \\ 0 & 0 & 0 & \frac{1-\nu}{2} & 0 & 0 \\ 0 & 0 & 0 & 0 & \frac{1-\nu}{2} & 0 \\ 0 & 0 & 0 & 0 & 0 & \frac{1-\nu}{2} \end{pmatrix} , \quad (2.88)$$

where $\mathbb{C}_{\text{iso}}$ is introduced to distinguish between the general material tensor and the isotropic counterpart.

2.6. Theory of Plasticity

In this work only ductile metals with only small deformations are considered. In this case, the current configuration can be considered as a small perturbation around the reference configuration and an additive decomposition of the linear strain tensor in an elastic $\boldsymbol{\epsilon}^{\text{el}}$ and an inelastic (plastic) part $\boldsymbol{\epsilon}^{\text{pl}}$ can be made as follows:

$$\boldsymbol{\epsilon} = \boldsymbol{\epsilon}^{\text{el}} + \boldsymbol{\epsilon}^{\text{pl}} \quad \text{or} \quad \epsilon_{ij} = \epsilon_{ij}^{\text{el}} + \epsilon_{ij}^{\text{pl}} , \tag{2.89}$$

where the elastic strain $\boldsymbol{\epsilon}^{\text{el}}$ is given by

$$\boldsymbol{\epsilon}^{\text{el}} = \boldsymbol{\epsilon} - \boldsymbol{\epsilon}^{\text{pl}} \quad \text{or} \quad \epsilon_{ij}^{\text{el}} = \epsilon_{ij} - \epsilon_{ij}^{\text{pl}} , \tag{2.90}$$

and with equation (2.83) $\boldsymbol{\epsilon}^{\text{el}}$ can also be expressed as

$$\boldsymbol{\epsilon}^{\text{el}} = \mathbb{C}^{-1} : \boldsymbol{\sigma} \quad \text{or} \quad \epsilon_{ij}^{\text{el}} = C_{ijkl}^{-1} \sigma_{kl} . \tag{2.91}$$

Within this framework, the previously introduced continuum basics are applied to formulate a general elastic-plastic constitutive model. The basic definitions for the yield function and the yield criteria are introduced in the one-dimensional case and extended then to the generalized three-dimensional case. The evolution of the plastic strain is described with a plastic flow rule, whereas the general formulation is given for materials with distinct work-hardening properties. Here the kinematic and the isotropic hardening are in focus, and for simplification reasons, thermal effects are ignored in the formulation of the constitutive equations.

Apart from the textbook by Neto et al. [2008], the book by Lubliner [2008] mainly inspires for the formulation of the classical theory in this section. Further theoretical background of plasticity can be found in Lemaitre and Chaboche [1990]; Chen and Han [2007] and Besson et al. [2010].

2.6.1. Plasticity at Small Deformations

First of all, some basic concepts of plasticity in one-dimensional problems are summarized. Afterwards, the extension on the generalization to three-dimensional problems is presented.

A yield function of the form

$$f(\sigma, \sigma_y) = |\sigma| - \sigma_y , \qquad (2.92)$$

is chosen, which is controlled by the given yield stress σ_y in the elastic domain $\mathcal{D}_{el}$ as follows:

$$\mathcal{D}_{el} = \{\sigma \mid f(\sigma, \sigma_y) < 0\} , \qquad (2.93)$$

which states that the elastic domain covers all stresses which satisfy

$$|\sigma| < \sigma_y . \qquad (2.94)$$

By definition, the stress is not allowed to be above the current yield region. More precisely, the plastic yielding occurs either in the elastic domain or at the elastic boundary of it, i.e.

$$f(\sigma, \sigma_y) \leq 0 , \qquad (2.95)$$

which is also known as yield limit. For the yield function f, it is necessary to distinguish between the followoing three states:

$$\begin{aligned}
f(\sigma, \sigma_y) &< 0 \quad \text{elastic, } \sigma \text{ lies in the elastic domain } \mathcal{D}_{el} \\
f(\sigma, \sigma_y) &= 0 \quad \text{plastic, } \sigma \text{ lies at the boundary } \partial\mathcal{D}_{el} \qquad (2.96) \\
f(\sigma, \sigma_y) &> 0 \quad \text{inadmissible, } \sigma \text{ lies outside of } \mathcal{D}_{el} .
\end{aligned}$$

The yield criterion is defined as

$$\begin{aligned}
&\text{If } f(\sigma, \sigma_y) < 0 \Longrightarrow \dot{\epsilon}^{pl} = 0, \\
&\text{If } f(\sigma, \sigma_y) = 0 \Longrightarrow \begin{cases} \dot{\epsilon}^{pl} = 0 & \text{for elastic unloading } , \\ \dot{\epsilon}^{pl} \neq 0 & \text{for plastic loading } , \end{cases} \qquad (2.97)
\end{aligned}$$

where $\dot{\epsilon}^{pl}$ denotes the plastic strain rate, which will be described in more detail later.

As previously mentioned, the formulation of the plasticity should be now extended to three-dimensional problems. For the three-dimensional generalization, the free energy function ψ

$$\psi = \psi(\boldsymbol{\epsilon}, \boldsymbol{\epsilon}^{pl}, \boldsymbol{\alpha}) , \qquad (2.98)$$

is considered. Here, $\boldsymbol{\epsilon}$ is the total strain, $\boldsymbol{\epsilon}^{pl}$ is the plastic strain (considered as

internal variable) and $\boldsymbol{\alpha}$ is an additional set of internal variables used for describing the hardening. Furthermore, is ψ additively split as follows:

$$
\begin{aligned}
\psi(\boldsymbol{\epsilon}, \boldsymbol{\epsilon}^{\mathrm{pl}}, \boldsymbol{\alpha}) &= \psi^{\mathrm{el}}(\boldsymbol{\epsilon} - \boldsymbol{\epsilon}^{\mathrm{pl}}) + \psi^{\mathrm{pl}}(\boldsymbol{\alpha}) \,, \\
&= \psi^{\mathrm{el}}(\boldsymbol{\epsilon}^{\mathrm{el}}) + \psi^{\mathrm{pl}}(\boldsymbol{\alpha}) \,,
\end{aligned}
\tag{2.99}
$$

where the elastic contribution ψ^{el} depends only on the elastic strain and the plastic contribution ψ^{pl} depends on the internal variable $\boldsymbol{\alpha}$. With the free energy function (equation (2.99)) the Clausius-Duhem inequality can be rewritten as

$$
\left(\boldsymbol{\sigma} - \frac{\partial \psi^{\mathrm{el}}}{\partial \boldsymbol{\epsilon}^{\mathrm{el}}} \right) : \dot{\boldsymbol{\epsilon}}^{\mathrm{el}} + \boldsymbol{\sigma} : \dot{\boldsymbol{\epsilon}}^{\mathrm{pl}} - \frac{\partial \psi^{\mathrm{pl}}}{\partial \boldsymbol{\alpha}} * \dot{\boldsymbol{\alpha}} \geq 0 \,,
\tag{2.100}
$$

where $*$ denotes an appropriate product operation between $\mathbf{A}$ and $\dot{\boldsymbol{\alpha}}$. After introducing the thermodynamical force

$$
\mathbf{A} \equiv \frac{\partial \psi^{\mathrm{pl}}}{\partial \boldsymbol{\alpha}} \,,
\tag{2.101}
$$

equation (2.100) can be rewritten as

$$
\left(\boldsymbol{\sigma} - \frac{\partial \psi^{\mathrm{el}}}{\partial \boldsymbol{\epsilon}^{\mathrm{el}}} \right) : \dot{\boldsymbol{\epsilon}}^{\mathrm{el}} + \boldsymbol{\sigma} : \dot{\boldsymbol{\epsilon}}^{\mathrm{pl}} - \mathbf{A} * \dot{\boldsymbol{\alpha}} \geq 0 \,,
\tag{2.102}
$$

From equation (2.100) and (2.102), the stress tensor $\boldsymbol{\sigma}$ can be directly derived from

$$
\boldsymbol{\sigma} = \frac{\partial \psi^{\mathrm{el}}}{\partial \boldsymbol{\epsilon}^{\mathrm{el}}} \,.
\tag{2.103}
$$

When taking into account that the plastic dissipation function, referred as D^{pl}, cannot be negative, the formulation of D^{pl} can be written as

$$
D^{\mathrm{pl}}(\boldsymbol{\sigma}, \mathbf{A}; \dot{\boldsymbol{\epsilon}}^{\mathrm{pl}}, \dot{\boldsymbol{\alpha}}) \equiv \boldsymbol{\sigma} : \dot{\boldsymbol{\epsilon}}^{\mathrm{pl}} - \mathbf{A} * \dot{\boldsymbol{\alpha}} \geq 0 \,.
\tag{2.104}
$$

In the generalized three-dimensional case, plastic flow occurs when

$$
f(\boldsymbol{\sigma}, \mathbf{A}) = 0 \,,
\tag{2.105}
$$

and the corresponding elastic domain is defined as the set

$$
\mathcal{D}_{\mathrm{el}} = \{ \boldsymbol{\sigma} \,|\, f(\boldsymbol{\sigma}, \mathbf{A}) < 0 \} \,,
\tag{2.106}
$$

of stresses where plastic yielding is not possible. This set is analogous to the expression in equation (2.93) for the uni-axial case. The stresses, which lie in the elastic domain or on the boundary of it, are defined by the set

$$
\bar{\mathcal{D}}_{\mathrm{el}} = \{ \boldsymbol{\sigma} \,|\, f(\boldsymbol{\sigma}, \mathbf{A}) \leq 0 \} \,.
\tag{2.107}
$$

The set in which the plastic yielding may occur is defined by the hyper-surface

$$
\mathcal{Y} = \{ \boldsymbol{\sigma} \,|\, f(\boldsymbol{\sigma}, \mathbf{A}) = 0 \} \,,
\tag{2.108}
$$

which is understood as the yield surface. The complete characterization of the general constitutive model for plasticity requires an explicit definition of the evolution laws

for the internal variables, i.e. the variables associated with the dissipative phenomena. In the present formulation, these are the plastic strain $\boldsymbol{\epsilon}^{\mathrm{pl}}$ and the set of hardening variables $\boldsymbol{\alpha}$. The plastic flow rule and hardening law are defined by, cf. Neto et al. [2008],

$$\dot{\boldsymbol{\epsilon}}^{\mathrm{pl}} = \dot{\lambda} \mathbf{N}(\boldsymbol{\sigma}, \mathbf{A}) \,, \tag{2.109}$$

$$\dot{\boldsymbol{\alpha}} = \dot{\lambda} \mathbf{H}(\boldsymbol{\sigma}, \mathbf{A}) \,. \tag{2.110}$$

Here, $\mathbf{N}(\boldsymbol{\sigma}, \mathbf{A})$ is the flow vector, $\mathbf{H}(\boldsymbol{\sigma}, \mathbf{A})$ describes the evolution of the hardening variables and $\dot{\lambda}$ denotes the so-called plastic multiplier, which is a non-negative value by definition. These two equations are completed by the Kuhn-Tucker (also known as Karush-Kuhn-Tucker or loading/unloading) conditions

$$f(\boldsymbol{\sigma}, \mathbf{A}) \leq 0 \,, \quad \dot{\lambda} \geq 0 \,, \quad \dot{\lambda} f(\boldsymbol{\sigma}, \mathbf{A}) = 0 \,. \tag{2.111}$$

The flow vector $\mathbf{N}(\boldsymbol{\sigma}, \mathbf{A})$ is derived from

$$\mathbf{N}(\boldsymbol{\sigma}, \mathbf{A}) \equiv \frac{\partial \Psi}{\partial \boldsymbol{\sigma}} \quad \text{with the flow potential } \Psi = \Psi(\boldsymbol{\sigma}, \mathbf{A}) \,. \tag{2.112}$$

The hardening law can be derived by using the same potential,

$$\mathbf{H}(\boldsymbol{\sigma}, \mathbf{A}) \equiv -\frac{\partial \Psi}{\partial \mathbf{A}} \,. \tag{2.113}$$

For the determination of the plastic multiplier $\dot{\lambda}$ the consistency condition

$$\dot{f} \lambda = 0 \,, \tag{2.114}$$

is used, which implies that $\dot{f} = 0$ under plastic yielding ($\lambda \neq 0$). The differentiation of f with respect to time reads

$$\dot{f} = \frac{\partial f}{\partial \boldsymbol{\sigma}} : \dot{\boldsymbol{\sigma}} + \frac{\partial f}{\partial \mathbf{A}} * \dot{\mathbf{A}} \,. \tag{2.115}$$

With respect to equation (2.83) the rate of the stress tensor can be written as

$$\dot{\boldsymbol{\sigma}} = \mathbb{C}^{\mathrm{el}} : \dot{\boldsymbol{\epsilon}} \,, \tag{2.116}$$

where the superscript $\bullet^{\mathrm{el}}$ denotes that $\mathbb{C}^{\mathrm{el}}$ is the elasticity tensor with respect to Hooke's law. With the expression $(2.90)_1$ and the plastic flow rule given in equation (2.109), equation (2.116) can be reformulated as

$$\dot{\boldsymbol{\sigma}} = \mathbb{C}^{\mathrm{el}} : (\dot{\boldsymbol{\epsilon}} - \dot{\lambda} \mathbf{N}(\boldsymbol{\sigma}, \mathbf{A})) \,. \tag{2.117}$$

Using the definition of $\mathbf{A}$ in terms of ψ, see equation (2.101), the evolution law (2.110) and the rate of the stress tensor (2.117), equation (2.115) becomes

$$\dot{f} = \frac{\partial f}{\partial \boldsymbol{\sigma}} : \mathbb{C}^{\mathrm{el}} : (\dot{\boldsymbol{\epsilon}} - \dot{\lambda} \mathbf{N}(\boldsymbol{\sigma}, \mathbf{A})) + \dot{\lambda} \frac{\partial f}{\partial \mathbf{A}} * \frac{\partial^2 \psi^{\mathrm{pl}}}{\partial \boldsymbol{\alpha}^2} * \mathbf{H}(\boldsymbol{\sigma}, \mathbf{A}) \,. \tag{2.118}$$

When $\dot{f} = 0$, the plastic multiplier $\dot{\lambda}$ can be determined from equation (2.118) as

$$\dot{\lambda} = \frac{\frac{\partial f}{\partial \boldsymbol{\sigma}} : \mathbb{C}^{\mathrm{el}} : \dot{\boldsymbol{\epsilon}}}{\frac{\partial f}{\partial \boldsymbol{\sigma}} : \mathbb{C}^{\mathrm{el}} : \mathbf{N}(\boldsymbol{\sigma}, \mathbf{A}) - \frac{\partial f}{\partial \mathbf{A}} * \frac{\partial^2 \psi^{\mathrm{pl}}}{\partial \boldsymbol{\alpha}^2} * \mathbf{H}(\boldsymbol{\sigma}, \mathbf{A})} \ . \tag{2.119}$$

For the elastic region, the constitutive equation for the stress are given by equation (2.116). When plastic flow occurs, the corresponding rate equation are defined by

$$\dot{\boldsymbol{\sigma}} = \mathbb{C}^{\mathrm{ep}} : \dot{\boldsymbol{\epsilon}} \ , \tag{2.120}$$

where the fourth-order tensor $\mathbb{C}^{\mathrm{ep}}$ is the elastic-plastic tangent modulus and by substituting equation (2.119) into equation (2.117) gives

$$\mathbb{C}^{\mathrm{ep}} \equiv \mathbb{C}^{\mathrm{el}} - \frac{(\mathbb{C}^{\mathrm{el}} : \mathbf{N}(\boldsymbol{\sigma}, \mathbf{A})) \otimes (\frac{\partial f}{\partial \boldsymbol{\alpha}} : \mathbb{C}^{\mathrm{el}})}{\frac{\partial f}{\partial \boldsymbol{\sigma}} : \mathbb{C}^{\mathrm{el}} : \mathbf{N}(\boldsymbol{\sigma}, \mathbf{A}) - \frac{\partial f}{\partial \mathbf{A}} * \frac{\partial^2 \psi^{\mathrm{pl}}}{\partial \boldsymbol{\alpha}^2} * \mathbf{H}(\boldsymbol{\sigma}, \mathbf{A})} \ , \tag{2.121}$$

where $\otimes$ denotes the tensor product operator.

2.6.2. Yield Criteria

In the previous subsection, the generalized elastic-plastic constitutive model has been established, whereas the yield criteria are introduced without referring to any specific one. In engineering applications, different yield criteria, such as the Tresca, von Mises, Mohr-Coulomb or the Drucker-Prager criteria are available. The selection of each criterion, depends primarily on the material to be applied. For metals, as considered in this work, pressure-insensitve criteria, like Tresca or von Mises are adequate. For materials like soil, rock or concrete which are compressible, a pressure-sensitive criteria are necessary. Examples of this are the Mohr-Coulomb or the Drucker-Prager criteria. This work focuses on the von Mises criteria, proposed by Mises [1913]. Informations about the other yield criteria are available in the cited literature in this section. Detailed phenomenological aspects can be found, e.g., in the textbook by Rösler et al. [2008].

By assuming that the material behaviour is isotropic as well as the knowledge that metals are plastically incompressible, the yield function can be formulated in terms of the invariants of the stress tensor or the principal stresses captured by the assumption of von Mises. This assumption states that *plastic yielding occurs when the J_2 stress-deviator invariant reaches a critical value*, cf. Neto et al. [2008]. According to this, the yield function can only be formulated in terms of the second invariant J_2 of the deviatoric stresses $\mathbf{s}$ as follows:

$$f(\boldsymbol{\sigma}) = f(J_2) \ , \tag{2.122}$$

with

$$J_2 = \frac{1}{2} \mathbf{s} : \mathbf{s} = \frac{1}{2} \parallel \mathbf{s} \parallel^2 \tag{2.123}$$

where the deviatoric stresses $\mathbf{s}$ are defined by

$$\mathbf{s} = \boldsymbol{\sigma} - \frac{1}{3} \operatorname{tr}(\boldsymbol{\sigma}) \mathbf{1} \ , \tag{2.124}$$

with the second-order identity tensor **1** and tr ($\bullet$) is the trace of $\bullet$. With these relations, the von Mises yield criterion can be expressed by the yield function as

$$f(\boldsymbol{\sigma}) = \sqrt{3\,J_2(\mathbf{s}(\boldsymbol{\sigma}))} - \sigma_y \,, \tag{2.125}$$

$$f(\mathbf{s}) = \sqrt{\frac{3}{2}\mathbf{s} : \mathbf{s}} - \sigma_y \,. \tag{2.126}$$

A classical representation of the von Mises criterion is to characterize it by a circular cylinder in the space of principal stresses with the hydrostatic axis as the axis of rotation as illustrated in Fig. 2.5. In view of the relation between J_2 and the octahedral
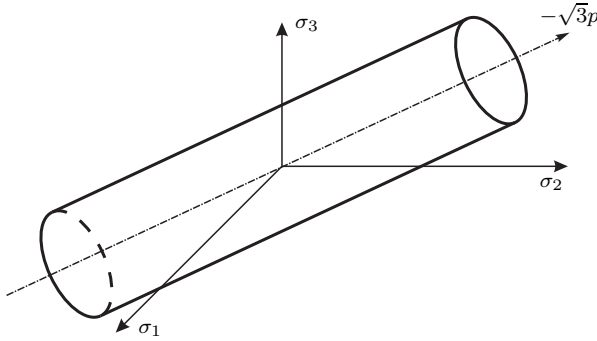
Figure 2.5.: von Mises yield surface in principal stress space.

shear stress, the von Mises criterion is also known as *maximum-octahedral-shear-stress* criterion, cf. Lubliner [2008].

2.6.3. Plastic Flow Rule

Until now, the formulation of the plasticity based on the definition of the flow rule in terms of a potential function Ψ. For metals, the associated plasticity are often assumed and, therefore, the constitutive equations are usually formulated in terms of their yield function f instead of a potential function Ψ, thus

$$\Psi \equiv f \,, \tag{2.127}$$

In that case, the rate equation of plastic strain can be expressed by

$$\dot{\boldsymbol{\epsilon}}^{\mathrm{pl}} = \dot{\lambda}\frac{\partial f}{\partial \boldsymbol{\sigma}} \,, \tag{2.128}$$

and the evolution equation of the hardening variables is given by

$$\dot{\boldsymbol{\alpha}} = -\dot{\lambda}\frac{\partial f}{\partial \mathbf{A}} \,. \tag{2.129}$$

The expression in equation (2.127) implies that $\mathbf{N}(\boldsymbol{\sigma}, \mathbf{A}) = \partial f/\partial \boldsymbol{\sigma}$ and the plastic strain rate is a tensor in the direction normal to the yield surface in the space of

stresses.

Another possibility to determine the rate equations (2.128) and (2.129), is the application of the *principle of maximum dissipation*, proposed among others by Hill [1948]. An explanation of this formulation is here omitted and the reader is referred to the cited literature in this section.

The use of the Prantl-Reuss plasticity law, in conjunction with the von Mises yield function (2.126) as the flow potential, makes it possible to express the flow vector (2.112) as

$$\mathbf{N}(\boldsymbol{\sigma}, \mathbf{A}) \equiv \frac{\partial f}{\partial \boldsymbol{\sigma}} = \frac{\partial}{\partial \boldsymbol{\sigma}} \left(\sqrt{3\, J_2(\mathbf{s})} \right) = \sqrt{\frac{3}{2}} \frac{\mathbf{s}}{\| \mathbf{s} \|} \,, \tag{2.130}$$

and accordingly, the flow rule (2.128) can be rewritten as

$$\dot{\boldsymbol{\epsilon}}^{\mathrm{pl}} = \dot{\lambda} \sqrt{\frac{3}{2}} \frac{\mathbf{s}}{\| \mathbf{s} \|} \,. \tag{2.131}$$

The flow direction of the associative yield condition, based on the von Mises model is shown in Fig. 2.6. The principal directions of $\mathbf{N}(\boldsymbol{\sigma}, \mathbf{A})$ and $\mathbf{s}$ are identical, so the it is obvious that the flow vector is normal to the yield surface and perpendicular to the hydrostatic axis. Furthermore, based on the von Mises hypothesis, $\mathbf{N}(\boldsymbol{\sigma}, \mathbf{A})$, is a deviatoric tensor.
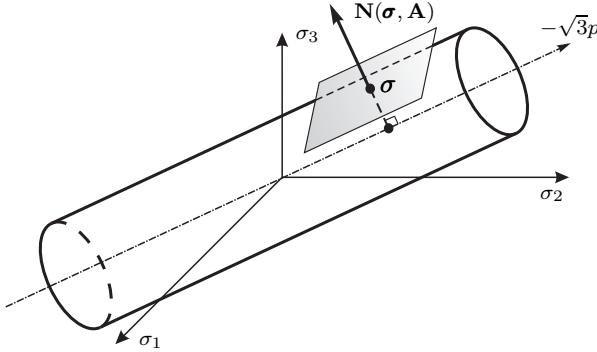
Figure 2.6.: Illustration of the Prantl-Reuss flow vector in the principal stress space.

2.6.4. Hardening Laws

Hardening is represented by changes in the hardening thermodynamical force, $\mathbf{A}$, during plastic yielding. The yield surface may be changed in the shape, size and position in the stress space. Mathematically, this fact is taken into account by additional terms in the yield function, which describes the change of the yielding surface. In this subsection, three different types of hardening behaviour are presented, namely, the *perfect plasticity*, *isotropic* and the *kinematic* hardening.

Perfect Plasticity

A material is referred as perfectly plastic if no hardening occurs during plastic defor-
mation. This means that the yield surface f remains constant and the yield stress σ_y
remains unchanged during the entire deformation process. Such a material behaviour
is illustrated in Fig. 2.7. In reality, there is no perfect plastic material. However, these
material models are often employed in the metal forming technology. Further areas
of application are the determination of limit loads and safety factors, cf. Neto et al.
[2008].
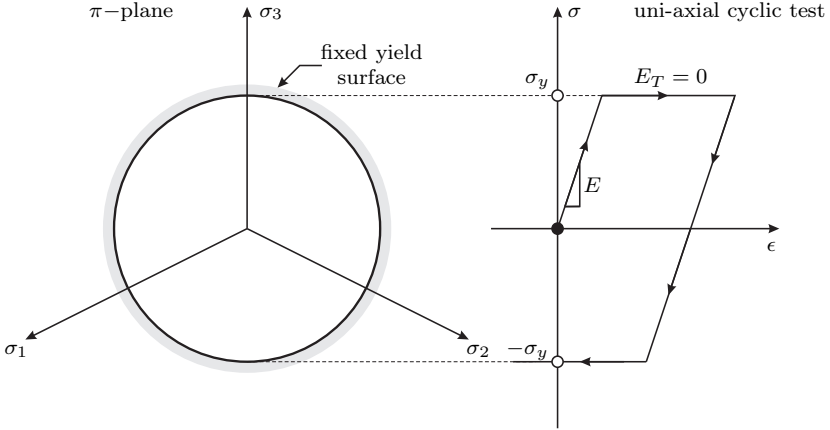
Figure 2.7.: Illustration of perfect plasticity.

Isotropic Hardening

A plasticity model an isotropic hardening behaviour if the yield surface evolves in such
a way that it isotropically expands with respect to the initial yield surface, without
translation, as shown in Fig. 2.8. In the case of a multiaxial plasticity model, the von
Mises yield surface grows symmetrically in a cylinder shape around the hydrostatic
axis. For the characterization of isotropic hardening, the tensor $\boldsymbol{\alpha}$ is reduced to a
single scalar variable, which determines the size of the yield surface.

Consider the typical case of the von Mises accumulated plastic strain

$$\bar{\epsilon}^{\mathrm{pl}} = \int\limits_0^t \sqrt{\frac{2}{3}\dot{\boldsymbol{\epsilon}}^{\mathrm{pl}} : \dot{\boldsymbol{\epsilon}}^{\mathrm{pl}}} \ \mathrm{d}t = \sqrt{\frac{2}{3}} \int\limits_0^t \parallel \dot{\boldsymbol{\epsilon}}^{\mathrm{pl}} \parallel \ \mathrm{d}t \,, \tag{2.132}$$

where the corresponding rate equation of $\bar{\epsilon}^{\mathrm{pl}}$ can be expressed by

$$\dot{\bar{\epsilon}}^{\mathrm{pl}} = \sqrt{\frac{2}{3}\dot{\boldsymbol{\epsilon}}^{\mathrm{pl}} : \dot{\boldsymbol{\epsilon}}^{\mathrm{pl}}} = \sqrt{\frac{2}{3}} \parallel \dot{\boldsymbol{\epsilon}}^{\mathrm{pl}} \parallel \ . \tag{2.133}$$

By taking the flow rule $\dot{\boldsymbol{\epsilon}}$ of equation (2.131) into account, leads to

$$\dot{\bar{\epsilon}}^{\mathrm{pl}} = \dot{\lambda} \ . \tag{2.134}$$

The function which describes the strain hardening is defined by

$$\sigma_y = \sigma_y(\bar{\epsilon}^{\mathrm{pl}}) \ , \tag{2.135}$$

with the initial condition $\sigma_y(\bar{\epsilon}^{\mathrm{pl}} = 0) = \sigma_{y_0}$. The growth of the yield surface according to the accumulated increasing plastic strain determined by a hardening law. In the present work, the hardening modulus is assumed to be a linear function in $\bar{\epsilon}^{\mathrm{pl}}$, which is often used in conjunction with metals. Formulated as a rate equation, the hardening in equation (2.135) law reads

$$\dot{\sigma}_y = \mathrm{H}_{\mathrm{iso}} \dot{\bar{\epsilon}}^{\mathrm{pl}} \ , \tag{2.136}$$

where $\mathrm{H}_{\mathrm{iso}}$ is the constant isotropic hardening modulus. Integrating this rate equation gives

$$\sigma_y(\bar{\epsilon}^{\mathrm{pl}}) = \sigma_{y_0} + \mathrm{H}_{\mathrm{iso}} \bar{\epsilon}^{\mathrm{pl}} \ , \tag{2.137}$$

with σ_{y_0} being the constant initial yield stress.
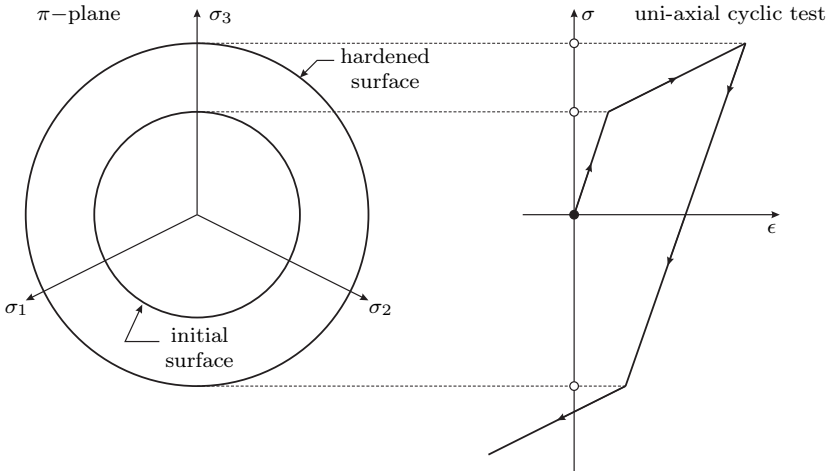
Figure 2.8.: Illustration of isotropic hardening.

Kinematic Hardening

If kinematic hardening occurs, the yield surface changes neither its shape nor size, but the center of the yield surface translates in the stress space. A further phenomenon which can be characterized by means of kinematic hardening is the reduction of the yield stress in the opposite direction after being loaded in one direction. This effect

is denoted as Bauschinger effect. These phenomena are both exemplary illustrated in Fig. 2.9.

The yield function of a model with kinematic hardening is given by

$$f(\boldsymbol{\sigma}, \boldsymbol{\beta}) = \sqrt{3\,J_2(\boldsymbol{\eta}(\boldsymbol{\sigma}, \boldsymbol{\beta}))} - \sigma_y \;, \tag{2.138}$$

where $\boldsymbol{\eta}(\boldsymbol{\sigma}, \boldsymbol{\beta})$

$$\boldsymbol{\eta}(\boldsymbol{\sigma}, \boldsymbol{\beta}) \equiv \mathbf{s}(\boldsymbol{\sigma}) - \boldsymbol{\beta} \;, \tag{2.139}$$

describes the difference between the stress deviator $\mathbf{s}(\boldsymbol{\sigma})$ and the symmetric deviatoric tensor $\boldsymbol{\beta}$, denoted as back-stress tensor. The associated plastic flow rule in the case of kinematic hardening is given by

$$\mathbf{N}(\boldsymbol{\sigma}, \mathbf{A}) \equiv \frac{\partial f}{\partial \boldsymbol{\sigma}} = \sqrt{\frac{3}{2}} \frac{\boldsymbol{\eta}}{\|\boldsymbol{\eta}\|} \;, \tag{2.140}$$

with the plastic strain rate equation

$$\dot{\boldsymbol{\epsilon}}^{\mathrm{pl}} = \dot{\lambda}\mathbf{N}(\boldsymbol{\sigma}, \mathbf{A}) = \dot{\lambda}\sqrt{\frac{3}{2}} \frac{\boldsymbol{\eta}}{\|\boldsymbol{\eta}\|} \;. \tag{2.141}$$

To complete the definition of the kinematic hardening, an evolution equation for the tensor $\boldsymbol{\beta}$ is needed. Therefore, Prager's linear kinematic hardening rule is applied and the rate form of $\boldsymbol{\beta}$ reads

$$\dot{\boldsymbol{\beta}} = \frac{2}{3}\mathrm{H}_{\mathrm{kin}}\dot{\boldsymbol{\epsilon}}^{\mathrm{pl}} = \dot{\lambda}\mathrm{H}_{\mathrm{kin}}\sqrt{\frac{2}{3}} \frac{\boldsymbol{\eta}}{\|\boldsymbol{\eta}\|} \;, \tag{2.142}$$

where $\mathrm{H}_{\mathrm{kin}}$ is the constant linear kinematic hardening modulus.
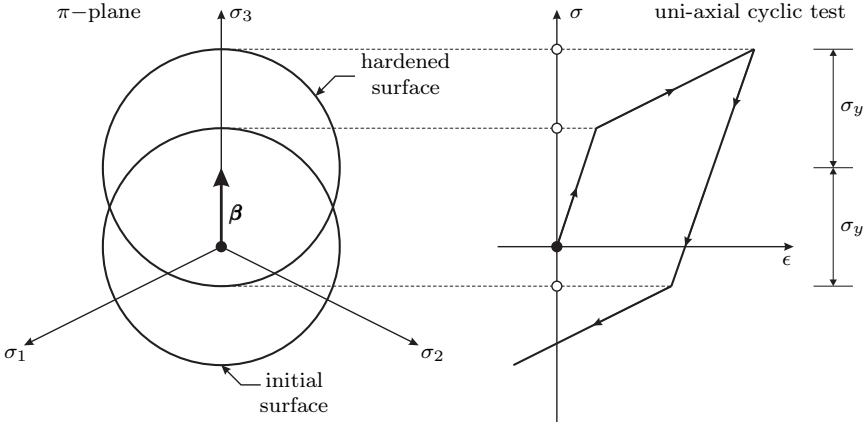
Figure 2.9.: Illustration of kinematic hardening.

3. Finite Element Method

Many physical processes can be described by differential equations. If the investigated problems are simple, the corresponding differential equations can be solved analytically. However, in many engineering applications this is not the case and a numerical approach is often applied as an alternative technique to solve these equations. In this regard, the finite element method (FEM) is a widely applied numerical technique to get an approximate solution of the underlying partial differential equations, which has been applied to a wide range of problems, such as structural mechanics, structural dynamics, fluid dynamics or heat transfer.

When considering boundary value problems for static or quasi-static processes, elliptical partial differential equations have to be solved. In this work, elastic-plastic problems (neglecting inertia effects) are considered, where this kind of equations occurs. Furthermore, only small deformations ($\mathbf{F} \approx 1$) are assumed, where a distinction between the initial and the current configuration is not required. This means, that all kinematic quantities as well as the related constitutive equations are written in the current configuration.

This chapter is organized as follows: It starts with the well known (standard) variational formulation of the FEM in section 3.1. The linearisation of the governing equations, within an iterative solution scheme will be subsequently discussed in section 3.2. The discretization procedure is addressed in section 3.3, where a brief summary about the computation of non-linear equation systems is given in addition. Afterwards, the incremental predictor-corrector method for the integration of the constitutive laws of the elastic-plastic material, proposed in the previous chapter, is presented in section 3.4.

This chapter gives only a brief overview on the finite element method. For a detailed treatment of the finite element method the reader is referred to the standard textbooks, for example, the ones by Crisfield [1991]; Zienkiewicz and Taylor [2000]; Hughes [2000]; Bathe [2002]; Wriggers [2008]; de Borst et al. [2012].

3.1. Weak Form of Equilibrium

The finite element method requires the formulation of the balance laws in form of variational principles. The first one to be mentioned here is the balance of linear momentum

$$\operatorname{div} \boldsymbol{\sigma} + \mathbf{b} = \mathbf{0} \,, \tag{3.1}$$

which has been already introduced in equation (2.36). Together with the prescribed displacements on the boundary (also known as DIRICHLET boundary conditions)

$$\mathbf{u} = \bar{\mathbf{u}} \quad \text{on } \partial\Omega_{\mathrm{u}} \,, \tag{3.2}$$

and the surface tractions (also known as Neumann boundary conditions)

$$\bar{\mathbf{t}} = \boldsymbol{\sigma} \cdot \mathbf{n} \quad \text{on } \partial\Omega_\sigma \,, \tag{3.3}$$

where $\partial\Omega = \partial\Omega_u \bigcup \partial\Omega_\sigma$ and $\partial\Omega_u \bigcap \partial\Omega_\sigma = \emptyset$ are disjoint parts, the quasi-static boundary value problem is completely defined. The $\bar{\bullet}$ denotes the prescribed functions on the boundaries. The set of equations to derive the weak form of mechanical equilibrium is summarized in the following:

$$\begin{cases} \operatorname{div} \boldsymbol{\sigma} + \mathbf{b} &= \mathbf{0} \,, \\ \mathbf{u} &= \bar{\mathbf{u}} \qquad \text{on} \quad \partial\Omega_u \,, \\ \bar{\mathbf{t}} &= \boldsymbol{\sigma} \cdot \mathbf{n} \qquad \text{on} \quad \partial\Omega_\sigma \,. \end{cases} \tag{3.4}$$

For the FE-formulation of the boundary value problem, a variational formulation is applied to equation $(3.4)_1$. Multiplying this equation by a vector-valued function $\boldsymbol{\delta}_u = \{\boldsymbol{\delta}_u \,|\, \boldsymbol{\delta}_u = \mathbf{0} \text{ on } \partial\Omega_u\}$, known as the virtual displacement or test function, and integrating over the region Ω yields

$$g(\mathbf{u}) = \int_\Omega (\operatorname{div} \boldsymbol{\sigma} + \mathbf{b}) \cdot \boldsymbol{\delta}_u \, dv = 0 \,. \tag{3.5}$$

Applying the product rule on the term $\operatorname{div} \boldsymbol{\sigma} \cdot \boldsymbol{\delta}_u$, i.e.

$$\operatorname{div} \boldsymbol{\sigma} \cdot \boldsymbol{\delta}_u = \operatorname{div}(\boldsymbol{\sigma}\boldsymbol{\delta}_u) - \boldsymbol{\sigma} : \operatorname{grad} \boldsymbol{\delta}_u \,,$$

gives

$$g(\mathbf{u}) = \int_\Omega \operatorname{div}(\boldsymbol{\sigma}\boldsymbol{\delta}_u) \, dv - \int_\Omega \boldsymbol{\sigma} : \operatorname{grad} \boldsymbol{\delta}_u \, dv + \int_\Omega \mathbf{b} \cdot \boldsymbol{\delta}_u \, dv = 0 \,, \tag{3.6}$$

and applying the divergence theorem on equation (3.6) leads to

$$g(\mathbf{u}) = \int_{\partial\Omega} \boldsymbol{\sigma}\boldsymbol{\delta}_u \cdot \mathbf{n} \, da - \int_\Omega \boldsymbol{\sigma} : \operatorname{grad} \boldsymbol{\delta}_u \, dv + \int_\Omega \mathbf{b} \cdot \boldsymbol{\delta}_u \, dv = 0 \,. \tag{3.7}$$

Substituting the traction boundary condition, given in equation $(3.4)_3$, into equation (3.7) and rearranging the terms, the weak form of equilibrium is obtained as

$$g(\mathbf{u}) = \int_\Omega \boldsymbol{\sigma} : \operatorname{grad} \boldsymbol{\delta}_u \, dv - \int_\Omega \mathbf{b} \cdot \boldsymbol{\delta}_u \, dv - \int_{\partial\Omega} \bar{\mathbf{t}} \cdot \boldsymbol{\delta}_u \, da \,. \tag{3.8}$$

Due to the symmetry of the Cauchy stress $\boldsymbol{\sigma} = \boldsymbol{\sigma}^T$, equation (3.8) can be rewritten as

$$g = \int_\Omega \boldsymbol{\sigma} : \nabla^{\text{sym}\cdot}\boldsymbol{\delta}_u \, dv - \int_\Omega \mathbf{b} \cdot \boldsymbol{\delta}_u \, dv - \int_{\partial\Omega} \bar{\mathbf{t}} \cdot \boldsymbol{\delta}_u \, da \,, \tag{3.9}$$

where

$$\nabla^{\text{sym}\cdot}\boldsymbol{\delta}_u = \frac{1}{2}\left(\operatorname{grad} \boldsymbol{\delta}_u + \operatorname{grad}^T \boldsymbol{\delta}_u\right) \,. \tag{3.10}$$

The first part of equation (3.9)

$$\delta W_{\text{int}} = \int_{\Omega} \boldsymbol{\sigma} : \nabla^{\text{sym.}} \boldsymbol{\delta}_{\text{u}} \, \mathrm{d}v \,,$$

is referred to as the *virtual internal work* δW_{int}, and the second part

$$\delta W_{\text{ext}} = -\int_{\Omega} \mathbf{b} \cdot \boldsymbol{\delta}_{\text{u}} \, \mathrm{d}v - \int_{\partial\Omega} \bar{\mathbf{t}} \cdot \boldsymbol{\delta}_{\text{u}} \, \mathrm{d}a \,,$$

is related as the *external virtual work* δW_{ext}. For a vanishing acceleration, equation (3.9) implies that the virtual internal work equals the external virtual work

$$\delta W_{\text{int}} = \delta W_{\text{ext}} \,. \tag{3.11}$$

The weakness of the variational formulation arises from the fact that the balance of linear momentum is not fulfilled locally in each material point, but rather in the integral average. It has to be fulfilled for any arbitrary test function $\boldsymbol{\delta}_{\text{u}}$ satisfying the boundary conditions.

3.2. Linearization

One of the main goals in structural analysis is to find the unknown displacement field, which is a solution of the associated non-linear boundary value problem. As already mentioned at the beginning of this thesis, it can be distinguished between *geometrical* non-linearities, for example, non-linear strain measures described by the Green-Lagrange strain tensor and *material* non-linearities like plasticity, as considered in this work. In view of these non-linearities, it is in general not possible to get direct (analytical) solutions for the non-linear boundary value problem(s). Such problems are often solved by applying an iterative procedure as the widely used Newton-Raphson scheme. By this, linearizations of the underlying differential equations are necessary, where it is quite convenient to linearise the governing equations by applying the first-order Taylor series expansion. In view of the previous section, the linearization of the weak form in equation (3.9) reads

$$g\left(\mathbf{u} + \Delta\mathbf{u}\right) = g\left(\mathbf{u}\right) + \Delta g(\mathbf{u}, \Delta\mathbf{u}) + \mathcal{R} \,, \tag{3.12}$$

where $\Delta g(\mathbf{u}, \Delta\mathbf{u})$ denotes the linear increment of g at $\mathbf{u}$, $\Delta\mathbf{u}$ is the increment of the displacement field and $\mathcal{R}$ defines the residual of the Taylor series expansion. The term $\Delta g(\mathbf{u}, \Delta\mathbf{u})$ is solved by the Gâteaux derivative

$$\Delta g(\mathbf{u}, \Delta\mathbf{u}) = \frac{\mathrm{d}}{\mathrm{d}\epsilon} g(\mathbf{u} + \epsilon\Delta\mathbf{u})\bigg|_{\epsilon=0} = \frac{\partial g}{\partial \mathbf{u}} \cdot \Delta\mathbf{u} \,, \tag{3.13}$$

where ϵ is a scalar parameter. Under the assumption that the body forces $\mathbf{b}$ and the surface traction $\mathbf{t}$ are independent of the displacement field $\mathbf{u}$, the linearization of the weak form can be expressed by

$$g\left(\mathbf{u} + \Delta\mathbf{u}\right) = \int_{\Omega} \boldsymbol{\sigma} : \nabla^{\text{sym}} \boldsymbol{\delta}_{\text{u}} \, \mathrm{d}v + \int_{\Omega} \Delta\boldsymbol{\sigma} : \nabla^{\text{sym}} \boldsymbol{\delta}_{\text{u}} \, \mathrm{d}v - \int_{\Omega} \mathbf{b} \cdot \boldsymbol{\delta}_{\text{u}} \, \mathrm{d}v - \int_{\partial\Omega} \bar{\mathbf{t}} \cdot \boldsymbol{\delta}_{\text{u}} \, \mathrm{d}a \,. \tag{3.14}$$

The incremental stress tensor $\Delta\boldsymbol{\sigma}$, appearing in the second integral, has also be calculated by a Gâteaux derivative as follows:

$$\Delta\boldsymbol{\sigma}(\mathbf{u},\Delta\mathbf{u}) = \frac{\mathrm{d}}{\mathrm{d}\epsilon}\boldsymbol{\sigma}(\mathbf{u}+\epsilon\Delta\mathbf{u})\bigg|_{\epsilon=0} = \frac{\partial\sigma_{ij}}{\partial\epsilon_{kl}}\Delta\epsilon_{kl} = \mathbb{C}:\boldsymbol{\epsilon}. \tag{3.15}$$

3.3. Discretization of the Weak Form

The weak form as well as its linearization are functions that are continuous in space and time. In this section the approximation of these functions are presented. A common way to solve the weak form numerically is to discretize the continuous body $\mathcal{B}$ using the finite element method. To be more specific, the geometry of the considered domain is subdivided into n_e finite elements, which have to fulfil the following two requirements, cf. Wriggers [2008]:

- They are not allowed to overlap each other and

- there should be no gap between them.

The approximation of the geometry of $\mathcal{B}$, as illustrated in Fig. 3.1, can be expressed as the union of all elements Ω_e, cf. Wriggers [2008],

$$\mathcal{B} \approx \mathcal{B}^h = \bigcup_{e=1}^{n_e} \Omega_e\,, \tag{3.16}$$

where $\bigcup$ denotes the assembly process.
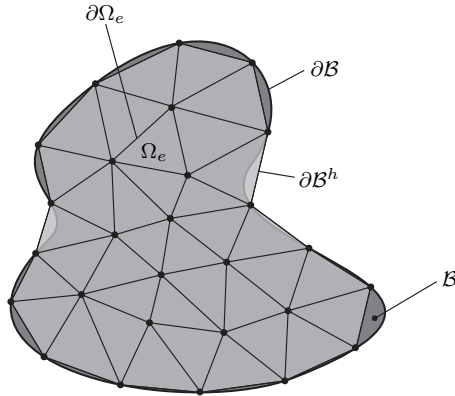
Figure 3.1.: Discretization of a physical body $\mathcal{B}$ where $\partial\mathcal{B}$ defines the associated boundary and Ω_e and $\partial\Omega_e$ are, respectively, an element and the corresponding boundaries of the discretized body.

The approximation of the nodal displacement field $\mathbf{u}$ within element e are realized with the shape functions N, where the approximation of the displacements $\mathbf{u}$ within

each element can be done as follows:

$$\mathbf{u}(\mathbf{x}) \approx \hat{\mathbf{u}}(\mathbf{x}) = \sum_{I=1}^{n_n} N_I(\boldsymbol{\eta})\mathbf{u}_I \, , \tag{3.17}$$

where, $\hat{\bullet}$ denotes the approximation of the variable, n_n is the number of nodes per element, $\mathbf{x}$ is the position vector with respect to Ω_e, $N_I(\boldsymbol{\eta})$, $\boldsymbol{\eta} = [\xi, \eta, \zeta]^{\mathrm{T}}$, represents the shape functions which are defined in Ω_e and $\mathbf{u}_I$ are the nodal displacements. In general, the shape functions are polynomials defined on a reference element $\Omega_\square$ and expressed in terms of the isoparametric coordinates (specified here for the 3-dimensional case) ξ, η and ζ.

The idea of the isoparametric concepts is to interpolate the geometry of a structural system and the displacement of an element e with the same shape functions in the following way:

$$\hat{\mathbf{u}}^e(\boldsymbol{\eta}) = \sum_{I=1}^{n_n} N_I(\boldsymbol{\eta})\mathbf{u}_I = \mathbf{H}(\boldsymbol{\eta})\mathbf{u}^e \, , \tag{3.18}$$

$$\hat{\mathbf{x}}^e(\boldsymbol{\eta}) = \sum_{I=1}^{n_n} N_I(\boldsymbol{\eta})\mathbf{x}_I = \mathbf{H}(\boldsymbol{\eta})\mathbf{x}^e \, . \tag{3.19}$$

In this work, only 8-node brick elements are used, where the shape functions are defined by

$$N_I(\xi, \eta, \zeta) = \frac{1}{8} \left(1 + \xi_I \xi\right) \left(1 + \eta_I \eta\right) \left(1 + \zeta_I \zeta\right) \, , \tag{3.20}$$

with the local coordinates ξ, η and $\zeta \in [-1, 1]^3$ and the index $\bullet_I$ denotes the field variables at node I, for example, $\mathbf{u}_I = \{u_x, u_y, u_z\}_I^{\mathrm{T}}$. The vector $\bullet^e$ includes the values of the primal variables at all nodes associated with element e and the matrix $\mathbf{H}(\boldsymbol{\eta})$ gathers the corresponding interpolation functions N_I. In view of the linearized weak form in equation (3.14), the shape functions, which are defined in the local coordinates, must be differentiated with respect to the global coordinates x, y, z. This can be done by using the chain rule, for instance, the first derivative of N_I, with respect to ξ reads

$$\frac{\partial N_I}{\partial \xi} = \frac{\partial N_I}{\partial \mathrm{x}} \frac{\partial \mathrm{x}}{\partial \xi} + \frac{\partial N_I}{\partial \mathrm{y}} \frac{\partial \mathrm{y}}{\partial \xi} + \frac{\partial N_I}{\partial \mathrm{z}} \frac{\partial \mathrm{z}}{\partial \xi} \, . \tag{3.21}$$

Performing the differentiations of N_I with respect to η and ζ in the same way and writing the resulting derivatives in a matrix form gives

$$\begin{bmatrix} \dfrac{\partial N_I}{\partial \xi} \\ \dfrac{\partial N_I}{\partial \eta} \\ \dfrac{\partial N_I}{\partial \zeta} \end{bmatrix} = \underbrace{\begin{bmatrix} \dfrac{\partial \mathrm{x}}{\partial \xi} & \dfrac{\partial \mathrm{y}}{\partial \xi} & \dfrac{\partial \mathrm{z}}{\partial \xi} \\ \dfrac{\partial \mathrm{x}}{\partial \eta} & \dfrac{\partial \mathrm{y}}{\partial \eta} & \dfrac{\partial \mathrm{z}}{\partial \eta} \\ \dfrac{\partial \mathrm{x}}{\partial \zeta} & \dfrac{\partial \mathrm{y}}{\partial \zeta} & \dfrac{\partial \mathrm{z}}{\partial \zeta} \end{bmatrix}}_{J} \begin{bmatrix} \dfrac{\partial N_I}{\partial \mathrm{x}} \\ \dfrac{\partial N_I}{\partial \mathrm{y}} \\ \dfrac{\partial N_I}{\partial \mathrm{z}} \end{bmatrix} \, . \tag{3.22}$$

Here J is known as Jacobian matrix or simply as Jacobian, which was already introduced in the previous chapter. By using the interpolation in equation (3.19), the

components of the JACOBIAN can be calculated explicitly and the derivatives of the global coordinates are obtained from

$$
\begin{bmatrix} \dfrac{\partial N_I}{\partial x} \\ \dfrac{\partial N_I}{\partial y} \\ \dfrac{\partial N_I}{\partial z} \end{bmatrix} = J^{-1} \begin{bmatrix} \dfrac{\partial N_I}{\partial \xi} \\ \dfrac{\partial N_I}{\partial \eta} \\ \dfrac{\partial N_I}{\partial \zeta} \end{bmatrix} .
\tag{3.23}
$$

Calculating the derivatives $\frac{\partial u_x}{\partial x}$, $\frac{\partial u_x}{\partial y}$, $\frac{\partial u_x}{\partial z}$, $\frac{\partial u_y}{\partial x}$, $\frac{\partial u_y}{\partial y}$ ... $\frac{\partial u_z}{\partial z}$ and gather them into a matrix leads to the strain-displacement interpolation matrix, simply denoted as the **B**-matrix. By use of this matrix, the approximation of the strains $\boldsymbol{\epsilon}^e$ of element e can be expressed as

$$
\boldsymbol{\epsilon}^e = \mathbf{B}\mathbf{u}^e .
\tag{3.24}
$$

With the approximations $\mathbf{u}^e = \hat{\mathbf{u}}^e$, $\boldsymbol{\delta}_\mathrm{u} = \boldsymbol{\delta}_{\hat{\mathrm{u}}}$, $\Delta\mathbf{u}^e = \Delta\hat{\mathbf{u}}^e$ and $\boldsymbol{\epsilon}^e$ as well as with the incremental constitutive law (3.15) and HOOKE's law (2.83) the discretized linearized form of equation (3.14) can be expressed as:

$$
\boldsymbol{\delta}_{\hat{\mathrm{u}}} \underbrace{\int_\Omega \mathbf{B}^\mathrm{T} \boldsymbol{\sigma} \, \mathrm{d}v}_{\mathbf{f}^{e\,\mathrm{int}}} + \boldsymbol{\delta}_{\hat{\mathrm{u}}} \underbrace{\int_\Omega \mathbf{B}^\mathrm{T} \, \mathbb{C} \, \mathbf{B} \, \mathrm{d}v}_{\mathbf{k}^e} \, \Delta\hat{\mathbf{u}}^e
$$
$$
- \boldsymbol{\delta}_{\hat{\mathrm{u}}} \underbrace{\left(\int_\Omega \mathbf{H}^\mathrm{T} \, \mathbf{b} \, \mathrm{d}v - \int_{\partial\Omega} \mathbf{H}^\mathrm{T} \, \bar{\mathbf{t}} \, \mathrm{d}a \right)}_{\mathbf{f}^{e\,\mathrm{ext}}} = 0 ,
\tag{3.25}
$$

where $\mathbf{f}^{e\,\mathrm{int}}$ are the internal forces, $\mathbf{f}^{e\,\mathrm{ext}}$ are the external forces and $\mathbf{k}^e$ denotes the element stiffness matrix, all with respect to element e. Note, that this equation is valid within each element of the FE-mesh, indicated by $\bullet^e$. Since the (approximated) test function $\boldsymbol{\delta}_{\hat{\mathrm{u}}}$ is arbitrary, the remaining parts must be zero, which leads to

$$
\mathbf{f}^{e\,\mathrm{int}} - \mathbf{f}^{e\,\mathrm{ext}} + \mathbf{k}^e \Delta\mathbf{u} = 0 .
\tag{3.26}
$$

All entries in the **B**-matrix are given in terms of the local coordinates, but the integration in equation (3.25) is done over the global coordinates, which makes it necessary to transform these volume integrals into local coordinates, i.e.

$$
\mathrm{d}x \, \mathrm{d}y \, \mathrm{d}z = \mathrm{d}v = \det J \, \mathrm{d}\xi \, \mathrm{d}\eta \, \mathrm{d}\zeta .
\tag{3.27}
$$

Using this transformation, the element stiffness matrix, for example, can be rewritten as

$$
\mathbf{k}^e = \int_\Omega \mathbf{B}^\mathrm{T} \, \mathbb{C} \, \mathbf{B} \det J \, \mathrm{d}\xi \, \mathrm{d}\eta \, \mathrm{d}\zeta .
\tag{3.28}
$$

Finally, the global system are obtained by assembling the element systems presented above, which results in the following equation:

$$\bigcup_{e=1}^{n_e} \left[\boldsymbol{\delta}_{\hat{u}} \int\limits_{\Omega} \mathbf{B}^{\mathrm{T}} \boldsymbol{\sigma} \, \mathrm{d}v + \boldsymbol{\delta}_{\hat{u}} \int\limits_{\Omega} \mathbf{B}^{\mathrm{T}} \mathbb{C} \, \mathbf{B} \, \mathrm{d}v \, \Delta\hat{\mathbf{U}} \right.$$
$$\left. - \boldsymbol{\delta}_{\hat{u}} \left(\int\limits_{\Omega} \mathbf{H}^{\mathrm{T}} \mathbf{b} \, \mathrm{d}v - \int\limits_{\partial\Omega} \mathbf{H}^{\mathrm{T}} \bar{\mathbf{t}} \, \mathrm{d}a \right) \right] = 0 \, . \tag{3.29}$$

Since $\boldsymbol{\delta}_{\hat{u}}$ is arbitrary and with respect to the local form given in equation (3.26), the discrete global boundary value reads

$$\mathbf{F}^{\mathrm{int}} - \mathbf{F}^{\mathrm{ext}} + \mathbf{K}\Delta\mathbf{U} = 0 \, . \tag{3.30}$$

Here, $\mathbf{F}^{\mathrm{int}}$ are the global internal forces, $\mathbf{F}^{\mathrm{ext}}$ are the global external ones and $\mathbf{K}$ denotes the global stiffness matrix.

Because some functions in the discretized weak form, e.g., the first two integrals in equation (3.29), are usually rational functions and the analytical integration is not always applicable. A convenient solution is to apply a numerical integration scheme, for example, the Gauss integration. In this context, the integrals are replaced by a sum of integrand functions evaluated at discrete sampling points, the so-called Gaussian-points, which are multiplied by certain weights. The coordinates of the Gaussian-points as well as the weighting factors can be found in the cited literature at the beginning of this chapter.

Solution of Non-Linear Equation Systems

The solution of non-linear equations, arising from kinematics or non-linear material behaviour, makes the use of an iterative procedure necessary. An often used iterative technique in, structural analysis, is the Newton-Raphson method, which is briefly described below. For detailed informations the reader is referred to the books by Wriggers [2008] or de Borst et al. [2012].

First of all, the concept of (pseudo-) time t should be employed to apply the external load in a number of loading increments. Applying this conception to equation (3.30) gives

$$^{t}\mathbf{K}\Delta\mathbf{U} = {}^{t+\Delta t}\mathbf{F}^{\mathrm{ext}} - {}^{t}\mathbf{F}^{\mathrm{int}} \, , \tag{3.31}$$

where $^{t}\mathbf{K}$ denotes the global tangent matrix at the time step t. The aim is now to determine the displacement increment $\Delta\mathbf{U}$ in the time step $t + \Delta t$, so that the forces $\mathbf{F}^{\mathrm{ext}}$ and $\mathbf{F}^{\mathrm{int}}$ are in equilibrium. This means, that in each iteration step n the global incremental displacement vector is updated as follows:

$$^{t+\Delta t}\mathbf{K}_{n-1}\Delta\mathbf{U}_n = {}^{t+\Delta t}\mathbf{F}^{\mathrm{ext}} - {}^{t+\Delta t}\mathbf{F}^{\mathrm{int}}_{n-1} \, , \tag{3.32}$$
$$^{t+\Delta t}\mathbf{U}_n = {}^{t+\Delta t}\mathbf{U}_{n-1} + \Delta\mathbf{U}_n \, . \tag{3.33}$$

This iteration process will be repeated until the norm of the residuum $\mathcal{R}$ is less than

a defined convergence tolerance η, i.e.

$$\mathcal{R}_n = \|^{t+\Delta t}\mathbf{F}^{\text{ext}} -^{t+\Delta t}\mathbf{F}^{\text{int}}_{n-1}\| < \eta\,. \tag{3.34}$$

3.4. Numerical Implementation of Plasticity

This section is addressed to the numerical implementation of the stress update algorithm and the tangent moduli, which are needed for the computation of the elastic-plastic constitutive equations, introduced in section 2.6. For additional informations to the presented theory here, the reader is referred to the textbooks by Simo and Hughes [1998]; Kojic and Bathe [2005]; Neto et al. [2008]; Wriggers [2008] or Shabana [2008].

First of all, an additive decomposition of the strain tensor (2.89) is done as follows:

$$\tilde{\boldsymbol{\epsilon}} = \tilde{\boldsymbol{\epsilon}}^{\text{el}} + \tilde{\boldsymbol{\epsilon}}^{\text{pl}}\,, \tag{3.35}$$

where only the deviatoric parts, labelled with $\tilde{\bullet}$, are of interest. Introducing Hooke's law, the stresses are also split into a deviatoric part $\mathbf{s}$ as well as into a hydrostatic part p, i.e.

$$\mathbf{s} = 2\mu\,\tilde{\boldsymbol{\epsilon}}^{\text{el}} = 2\mu\left(\tilde{\boldsymbol{\epsilon}} - \tilde{\boldsymbol{\epsilon}}^{\text{pl}}\right)\,, \quad p = K\,\text{tr}\left(\boldsymbol{\epsilon}^{\text{el}}\right)\,. \tag{3.36}$$

Here, μ denotes the shear modulus[1] and K is the bulk modulus[2]. With respect to the von Mises model with hardening properties, the yield condition reads

$$f(\boldsymbol{\eta}, \alpha) = \|\boldsymbol{\eta}\| - \sqrt{\frac{2}{3}}(\sigma_y + \text{H}_{\text{iso}}\alpha) \leq 0\,, \tag{3.37}$$

where $\boldsymbol{\eta} = \mathbf{s}(\boldsymbol{\sigma}) - \boldsymbol{\beta}$ is the relative stress tensor (back-stress tensor), already introduced in equation (2.138). The evolution equations for the plastic strain and the internal variables are defined by, e.g, cf. Wriggers [2008],

$$\dot{\tilde{\boldsymbol{\epsilon}}}^{\text{pl}} = \lambda\frac{\partial f}{\partial\mathbf{s}}\,, \qquad \dot{\alpha} = \sqrt{\frac{2}{3}}\lambda\,, \qquad \dot{\boldsymbol{\beta}} = -\frac{2}{3}\text{H}_{\text{kin}}\lambda\frac{\partial f}{\partial\mathbf{s}}\,. \tag{3.38}$$

After applying the implicit Euler rule to discretize the evolution equations, they can be reformulated as follows:

$$\begin{aligned}
\tilde{\boldsymbol{\epsilon}}^{\text{pl}}_{n+1} &= \tilde{\boldsymbol{\epsilon}}^{\text{pl}}_n + \Delta\lambda\mathbf{n}_{n+1}\,, \\
\alpha_{n+1} &= \alpha_n + \sqrt{\frac{2}{3}}\Delta\lambda\,, \\
\boldsymbol{\beta}_{n+1} &= \boldsymbol{\beta}_n + \frac{2}{3}\text{H}_{\text{kin}}\Delta\lambda\mathbf{n}_{n+1}\,,
\end{aligned} \tag{3.39}$$

where $\Delta\lambda = \lambda_{n+1} - \lambda_n$ and $\mathbf{n} \equiv \mathbf{N}(\boldsymbol{\sigma}, \mathbf{A})$. With respect to equation $(3.36)_1$, the

---

[1] $\mu = \frac{E}{2(1+\nu)}$
[2] $K = \left(\frac{3\lambda+2\mu}{3}\right)$ with $\lambda = \frac{\nu E}{(1+\nu)(1-2\nu)}$

deviatoric stresses at time-step t_{n+1} are calculated by

$$\mathbf{s}_{n+1} = 2\mu \left(\tilde{\boldsymbol{\epsilon}}_{n+1} - \tilde{\boldsymbol{\epsilon}}_{n+1}^{\mathrm{pl}} \right) , \tag{3.40}$$

and by substituting equation $(3.39)_1$ into equation (3.40) gives

$$\mathbf{s}_{n+1} = 2\mu \left(\tilde{\boldsymbol{\epsilon}}_{n+1} - \tilde{\boldsymbol{\epsilon}}_n^{\mathrm{pl}} \right) - 2\mu \, \Delta\lambda \mathbf{n}_{n+1} . \tag{3.41}$$

The next step is the formulation of the predictor-corrector method for the constitutive equations. In the first step (also denoted as the *elastic-predictor*) the variables are assumed as fixed. This assumption results in the *trial* state and the corresponding equations are

$$\begin{aligned}
\mathbf{s}_{n+1}^{\mathrm{trial}} &= 2\mu \left(\tilde{\boldsymbol{\epsilon}}_{n+1}^{\mathrm{trial}} - \tilde{\boldsymbol{\epsilon}}_n^{\mathrm{pl}} \right) , \\
\boldsymbol{\eta}_{n+1}^{\mathrm{trial}} &= \mathbf{s}_{n+1}^{\mathrm{trial}} - \boldsymbol{\beta}_n , \\
\alpha_{n+1}^{\mathrm{trial}} &= \alpha_n .
\end{aligned} \tag{3.42}$$

The set of plastic variables $\{\tilde{\boldsymbol{\epsilon}}_n^{\mathrm{pl}}, \alpha_n, \boldsymbol{\beta}_n\}$ are known from the last time step at t_n, the elastic strain $\boldsymbol{\epsilon}_{n+1}$ is computed from the global solution of the weak form and the *trial* parts in equation (3.42) can be calculated directly. The next step is to check the yield condition

$$f_{n+1}^{\mathrm{trial}}(\boldsymbol{\eta}_{n+1}^{\mathrm{trial}}, \alpha_{n+1}^{\mathrm{trial}}) = \|\boldsymbol{\eta}_{n+1}^{\mathrm{trial}}\| - \sqrt{\frac{2}{3}} \left(\sigma_y + \mathrm{H}_{\mathrm{iso}}\alpha_n \right) \leq 0 , \tag{3.43}$$

formulated here in terms of the *trial* variables. If the deviatoric stress $\mathbf{s}_{n+1}^{\mathrm{trial}}$ fulfils the yield condition within the (pseudo-) time interval $[t_n, t_{n+1}] \in [0, T]$, i.e. $f_{n+1}^{\mathrm{trial}}(\boldsymbol{\eta}_{n+1}^{\mathrm{trial}}, \alpha_{n+1}^{\mathrm{trial}}) \leq 0$, the material behaviour is purely elastic and the constitutive variables are updated as follows:

$$\begin{aligned}
\mathbf{s}_{n+1} &= \mathbf{s}_{n+1}^{\mathrm{trial}} , \\
\tilde{\boldsymbol{\epsilon}}_{n+1}^{\mathrm{pl}} &= \tilde{\boldsymbol{\epsilon}}_n^{\mathrm{pl}} , \\
\boldsymbol{\beta}_{n+1} &= \boldsymbol{\beta}_n , \\
\alpha_{n+1} &= \alpha_n .
\end{aligned} \tag{3.44}$$

Otherwise, the material shows an elastic-plastic behaviour within this time-step and the *trial* quantities have to be updated by the *radial-return* mapping procedure as outlined in the following. In this case, the solution for the plastic multiplier $\Delta\lambda$ and its direction $\mathbf{n}_{n+1}$ have to be determined for the deviatoric stress $\mathbf{s}_{n+1}$, defined in equation (3.41).

Using the equations $(3.42)_{1,2}$ and $(3.39)_3$ the relations

$$\begin{aligned}
\mathbf{s}_{n+1} - \boldsymbol{\beta}_{n+1} &= \boldsymbol{\eta}_{n+1}^{\mathrm{trial}} - \left(\frac{2}{3}\mathrm{H}_{\mathrm{kin}} + 2\mu \right) \Delta\lambda \, \mathbf{n}_{n+1} \\
\boldsymbol{\eta}_{n+1}^{\mathrm{trial}} &= \boldsymbol{\eta}_{n+1} \left[1 + \left(\frac{2}{3}\mathrm{H}_{\mathrm{kin}} + 2\mu \right) \frac{\Delta\lambda}{\|\boldsymbol{\eta}_{n+1}\|} \right] ,
\end{aligned} \tag{3.45}$$

can be determined form equation (3.41). From these relations, it is obvious that

the *trial* and the updated deviatoric parts of the relative stresses are co-linear. This implies that

$$\mathbf{n}_{n+1}^{\text{trial}} = \frac{\boldsymbol{\eta}_{n+1}^{\text{trial}}}{\|\boldsymbol{\eta}_{n+1}^{\text{trial}}\|} = \mathbf{n}_{n+1}$$

and the flow vectors at the *trial* and updated states are the same. Multiplying equation $(3.45)_2$ by $\mathbf{n}_{n+1}$ and noting that $\boldsymbol{\eta} \cdot \mathbf{n} = \|\boldsymbol{\eta}\|$ leads to

$$\|\boldsymbol{\eta}_{n+1}\| = \|\boldsymbol{\eta}_{n+1}^{\text{trial}}\| - \left(2\mu + \frac{2}{3}\mathrm{H}_{\text{kin}} \right) \Delta\lambda . \tag{3.46}$$

Inserting this relation into the yield condition (3.37) gives

$$f_{n+1} = \|\boldsymbol{\eta}_{n+1}^{\text{trial}}\| - \left(2\mu + \frac{2}{3}\mathrm{H}_{\text{kin}} \right) \Delta\lambda - \sqrt{\frac{2}{3}} \left[\sigma_y + \mathrm{H}_{iso} \left(\alpha_n + \sqrt{\frac{2}{3}}\Delta\lambda \right) \right] = 0 , \tag{3.47}$$

which has to be fulfilled at the current time step t_{n+1}. In the case of linear hardening, the plastic multiplier $\Delta\lambda$ can be calculated in a closed form by rearranging the previous equation as

$$\Delta\lambda = \frac{f_{n+1}^{\text{trial}}}{2\mu \left(1 + \frac{\mathrm{H}_{iso} + \mathrm{H}_{kin}}{3\mu} \right)} , \tag{3.48}$$

with $f_{n+1}^{\text{trial}} = \|\boldsymbol{\eta}_{n+1}^{\text{trial}}\| - \sqrt{\frac{2}{3}}(\sigma_y + \mathrm{H}_{iso}\alpha_n)$. With the computed increment of the plastic multiplier, the stresses, plastic strains and internal variables, given in equation (3.39), can be calculated. The actual stresses at t_{n+1} are given by

$$\boldsymbol{\sigma}_{n+1} = K \operatorname{tr}(\boldsymbol{\epsilon}) + 2\mu \left(\tilde{\boldsymbol{\epsilon}}_{n+1} - \tilde{\boldsymbol{\epsilon}}_n^{\text{pl}} \right) - 2\mu \, \Delta\lambda \, \mathbf{n}_{n+1}^{\text{trial}} . \tag{3.49}$$

By using the stresses $\boldsymbol{\sigma}_{n+1}$, the consistent elastic-plastic tangent modulus is determined by

$$\mathbb{C}_{n+1}^{\text{ep}} = \frac{\partial\boldsymbol{\sigma}_{n+1}}{\partial\boldsymbol{\epsilon}_{n+1}} , \tag{3.50}$$

$$= \mathbb{C}_{n+1}^{\text{el}} - 2\mu \, \mathbf{n}_{n+1}^{\text{trial}} \otimes \frac{\partial\Delta\lambda}{\partial\boldsymbol{\epsilon}_{n+1}} - 2\mu \, \Delta\lambda \frac{\partial\mathbf{n}_{n+1}^{\text{trial}}}{\partial\boldsymbol{\epsilon}_{n+1}} , \tag{3.51}$$

where the detailed derivations $\frac{\partial\Delta\lambda}{\partial\boldsymbol{\epsilon}_{n+1}}$ and $\frac{\partial\mathbf{n}_{n+1}^{\text{trial}}}{\partial\boldsymbol{\epsilon}_{n+1}}$ are given in Appendix C. The tensor $\mathbb{C}_{n+1}^{\text{el}}$ is the elasticity tensor

$$\mathbb{C}_{n+1}^{\text{el}} = K\,\mathbf{1} \otimes \mathbf{1} + 2\mu \left(\mathbb{I} - \frac{1}{3}\mathbf{1} \otimes \mathbf{1} \right) ,$$

with the fourth-order identity tensor $\mathbb{I}$.

4. Probability Theoretical Framework

Probability theory is the study of uncertainty and in the university engineering education non well established. Therefore, this chapter gives a brief introduction in the basics of the probability theory, which are applied in this thesis. For a thorough outline of the mathematical theory of probability, the reader is referred to the standard textbooks, for example, the ones by Loève [1977], Stark and Woods [1986], Papoulis [1991], Montgomery and Runger [1994], van Kampen [2007], Gardiner [2009].

4.1. Basic Definitions

In the following some frequently used definitions are listed and briefly explained, which are mainly inspired by the report of Sudret and der Kiureghian [2000].

Random Experiment

A *random experiment* is an experiment which can result in different outcomes, even though it is repeated in the same manner every time.

Sample Space

The set of all possible outcomes of a random experiment, denoted as the *sample space* of the experiment, is defined by Θ.

Event

An *event* is a subset of Θ containing outcomes $\theta \in \Theta$ of a random experiment, denoted by E, whereas the symbol θ always specifies an elementary event.

Probability of an Event

The *probability* $\mathcal{P}$ of an event E is equal to the sum of the probabilities of the outcomes in E.

σ-Algebra

The collection of all possible events having well-defined probabilities is referred to as the *σ-algebra* associated with Θ and defined by $\mathcal{F}$.

Probability Space

The *probability space* consists by means of the notations given above and is defined by $(\Theta, \mathcal{F}, \mathcal{P})$.

Random Variable

Let X be a real[1] *random variable* (RV), which is defined the mapping which assigns a real number to each outcome in the sample space of a random experiment by

$$X : (\Theta, \mathcal{F}, \mathcal{P}) \longrightarrow \mathbb{R}.$$

The value that a RV may take is defined by using lower case letters, such as x.

4.2. Properties of Single Random Variables

The objective of this section is the presentation of the mathematical tools which are available to analyse the complete probabilistic description of a continuous single RV X on the probability space $(\Theta, \mathcal{F}, \mathcal{P})$.

4.2.1. Probability Density Function

Let X be a continuous RV where any value in the range $-\infty < X < \infty$ is possible. The *probability density function* (PDF) $f_X(x)$ of a RV is a function which represents the probability that X takes a value in $[x_1, x_2]$ with the following definition:

$$f_X(x)\,\mathrm{d}x = \mathcal{P}(x_1 \leq X \leq x_2). \tag{4.1}$$

By integrating $f_X(x)$ over the interesting interval $[x_1, x_2]$, thus

$$\mathcal{P}(x_1 \leq X \leq x_2) = \int_{x_1}^{x_2} f_X(t)\,\mathrm{d}t, \tag{4.2}$$

leads to the probability that the RV takes a value within this interval. Any function that satisfies the following three conditions can be chosen as the PDF for a given RV X, cf. Montgomery and Runger [1994]:

1. $f_X(x) \geq 0$.

2. $\int_{-\infty}^{\infty} f_X(x)\,\mathrm{d}x = 1$.

3. $\mathcal{P}(x_1 \leq X \leq x_2) = \int_{x_1}^{x_2} f_X(t)\,\mathrm{d}t$.

---

[1] Only real valued random variables are considered in this work.
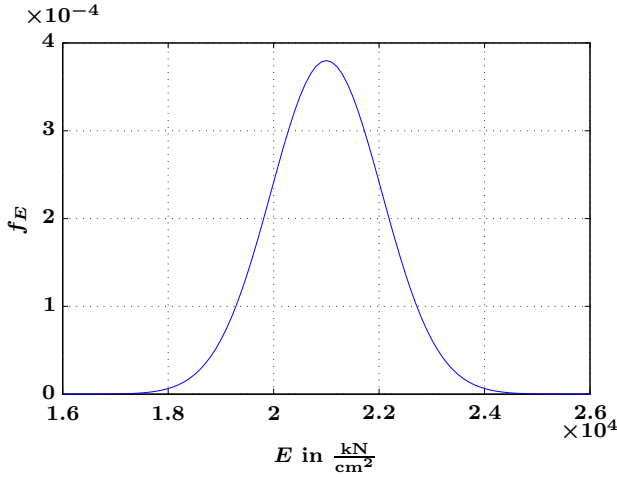
Figure 4.1.: Gaussian probability distribution function of E with mean $= 21000\frac{kN}{cm^2}$ and standard deviation of $\sigma_E = 5\%$.

The simplest probability density function is the Gaussian, or normal density function, which is for a single RV given by

$$f_E(x) = \frac{1}{\sqrt{2\pi\sigma_E^2}}e^{-\frac{(x-\mu_E)^2}{2\sigma_E^2}}\,. \tag{4.3}$$

Here, μ_E and σ_E are the mean and the standard deviation of the RV E. Fig. 4.1 shows the PDF of E, assuming a Gaussian distribution[2] with a mean of $\mu_E = 21000\frac{kN}{cm^2}$ and a standard deviation of $\sigma_E = 5\%$, which are typical values for steel of minor quality.

4.2.2. Cumulative Distribution Function

The *cumulative distribution function* (CDF) is a function $F_X(x) : \mathbb{R} \to [0,1]$, which specifies a probability measure as

$$F_X(x) = \mathcal{P}(X \leq x)\,. \tag{4.4}$$

---

[2]The use of Gaussian distributions is quiet common in the context of probabilistic mechanics. These distribution is not well suited to modelling material properties, for example, E or yield stress, which are by their nature positive valued. However, with respect to *small* standard deviations, the Gaussian distribution is a sufficient assumption.
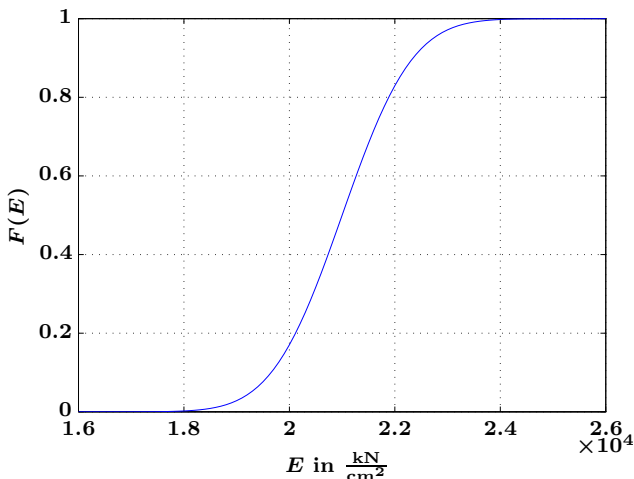
Figure 4.2.: Gaussian cumulative density function of Young's modulus E with a mean of $\mu_E = 21000 \frac{\text{kN}}{\text{cm}^2}$ and a standard deviation of $\sigma_E = 5\%$.

For a continuous RV the CDF is defined as

$$F_X(x) = \mathcal{P}(X \leq x) = \int_{-\infty}^{a} f_X(t)\, \mathrm{d}t\,, \qquad \text{for } -\infty < x < \infty\,, \tag{4.5}$$

and characterize the probability that X will take a value equal or less than a. The CDF is a monotonically increasing function with the following properties, cf. Montgomery and Runger [1994]:

1. $F_X(-\infty) = 0$.

2. $0 \leq F_X(x) \leq 1$.

3. $F_X(\infty) = 1$.

For some continuous RVs, the cumulative density function is differentiable everywhere and the PDF $f_X(x)$ can be determined from the CDF by differentiating

$$f_X(x) = \frac{\mathrm{d}F_X(x)}{\mathrm{d}x}\,. \tag{4.6}$$

As example consider the Gaussian distributed Young's modulus, where the integration of equation (4.3) leads to the CDF for this example, which is illustrated in Fig. 4.2. From this CDF, the probability that E is less than equal to $21000 \frac{\text{kN}}{\text{cm}^2}$ can be

read easily from Fig. 4.2, there is a likelihood of

$$\mathcal{P}(\mathbb{E}[E] \leq 21000 \, \frac{\text{kN}}{\text{cm}^2}) = 0.5 \, .$$

Here, $\mathbb{E}[\cdot]$ denotes the first moment of the RV, which is introduced in the following subsection. Both, the CDF and the PDF can be used to calculate the probabilities of events. Finally, it should be noted that the value of the PDF, at any given point x is not the probability of that event, i.e.

$$f_X(x) \neq \mathcal{P}(X = x) \, . \tag{4.7}$$

4.2.3. Moments of Probability Distributions

For a global characterization of a probability distribution, it is convenient to represent the distributions by their moments. In general, the nth moment of a probability distribution is defined as

$$\mathbb{E}[X^n] = \int_{-\infty}^{\infty} x^n f_X(x) \, \mathrm{d}x \, , \qquad \text{for } -\infty < x < \infty \, , \tag{4.8}$$

where $f_X(x)$ is the PDF of X. The most important quantities are related to the first and second moment of the probability distribution and will be introduced below.

Expected Value

Let $g(X) : \mathbb{R} \rightarrow \mathbb{R}$ be a function of X. In this case $g(X)$ is also a RV and the mathematical *expected value* (also denoted as expectation, mean value or simply as mean) of the function $g(X)$ is defined as

$$\mathbb{E}[X] = \mathbb{E}[g(X)] = \int_{-\infty}^{\infty} g(x) f_X(x) \, \mathrm{d}x \qquad \text{for } -\infty < x < \infty \, . \tag{4.9}$$

If $g(x) = x$, the expectation $\mathbb{E}[g(X)]$ becomes the expected value of X and reads

$$\mathbb{E}[X] = \mu_X = \int_{-\infty}^{\infty} x f_X(x) \, \mathrm{d}x \qquad \text{for } -\infty < x < \infty \, , \tag{4.10}$$

which is equivalent to $n = 1$ in equation (4.8).

Variance

The nth moment about the expected value is referred to as the nth central moment and is defined by the integral

$$\mathbb{E}[(X - \mu_X)^n] = \sigma^n = \int_{-\infty}^{\infty} (x - \mu_X)^n f_X(x) \, \mathrm{d}x \qquad \text{for } -\infty < x < \infty \, . \tag{4.11}$$

It is referred as the $(n^{th}\text{-})$ central moment, because the respective moment is related to the expected value of the RV and not to the origin of the coordinate system. The central moment, which represents the measure of the deviation of the RV X, from its expected value μ_X, is denoted as the *variance* of X. The variance is the second central moment and is defined as

$$
\begin{aligned}
\mathrm{Var}(X) &= \mathbb{E}[(X - \mu_X)^2] \\
&= \int_{-\infty}^{\infty} (x - \mu_X)^2 f_X(x)\, \mathrm{d}x \\
&= \int_{-\infty}^{\infty} x^2 f_X(x)\, \mathrm{d}x - \mu_X^2 \qquad \text{for } -\infty < x < \infty,
\end{aligned}
\tag{4.12}
$$

with the condition that μ_X exist. Considering equation (4.8) again and let $g(X) = X^2$. Then, the variance can be expressed as

$$
\mathbb{E}[X^2] = \int_{-\infty}^{\infty} x^2 f_X(x)\, \mathrm{d}x = \sigma_X^2,
\tag{4.13}
$$

where the positive square root of σ_X^2

$$
\sigma_X = \sqrt{\mathrm{Var}(X)},
\tag{4.14}
$$

is denoted as the standard deviation of X.

In addition to the unit-based moments, there are a number of dimensionless coefficients, which describe the shape of the probability distribution. Three of them are listed below:

1. The *coefficient of variation* α_X of a RV is given by

$$
\alpha_X = \frac{\sigma_X}{\mu_X},
\tag{4.15}
$$

if $\mu_X \neq 0$.

2. The *skewness* s_X is a measure for the symmetry of the distribution and is defined as

$$
s_X = \frac{\mathbb{E}[(X - \mu_X)^3]}{\sigma_X^3}.
\tag{4.16}
$$

3. The *kurtosis* κ_X is the fourth central moment which gives a statement for the slope or the peak of the distribution, and is given by

$$
\kappa_X = \frac{\mathbb{E}[(X - \mu_X)^4]}{\sigma_X^4}.
\tag{4.17a}
$$

For the normal distribution is $s_X = 0$ and $\kappa_X = 3$. Additionally, in some literature the *excess* is also specified. To distinguish between the excess and the

kurtosis the excess is denoted by κ_{X_e} and is indicated by

$$\kappa_{X_e} = \frac{\mathbb{E}[(X - \mu_X)^4]}{\sigma_X^4} - 3 \,. \tag{4.17b}$$

For the normal distribution the excess is $\kappa_{X_e} = 0$.

4.3. Properties of Two or More Random Variables

This section is focused on the complete probabilistic characterization of more than one continuous RV. For convenience the explanations are limited on two, the continuous RVs $X, Y \in (\Theta, \mathcal{F}, \mathcal{P})$. Basically, this theoretical framework is applicable and can be extended for the analysis to a various number of n RVs.

4.3.1. Joint and Marginal Probability Distribution

The probability distribution of X and Y which characterizes their common behaviour, in the same region, is referred as the *joint probability distribution* $f_{XY}(x, y)$. This distribution is specified by providing a method for calculating the probability that X and Y assume a value in any region of a two-dimensional space and satisfies the following three conditions, cf. Montgomery and Runger [1994]:

1. $f_{XY}(x, y) \geq 0 \quad \forall \, x, y$.

2. $\int\limits_{-\infty}^{\infty} \int\limits_{-\infty}^{\infty} f_{XY}(x, y) \, \mathrm{d}x \, \mathrm{d}y = 1$.

3. For any region B of a two-dimensional space $\mathcal{P}((X, Y) \in B) = \iint\limits_{B} f_{XY} \, \mathrm{d}x \, \mathrm{d}y$.

Consider the bivariate GAUSSIAN probability function for the RVs E and the Poisson ratio ν with μ_E and μ_ν as well as σ_E and σ_ν, where the associated bivariate PDF is defined by

$$\begin{aligned} f_{E\nu}(E, \nu) = &\frac{1}{2\pi\sigma_E\sigma_\nu\sqrt{1 - \rho_{E\nu}^2}} \exp\left(-\frac{1}{2(1 - \rho_{E\nu}^2)}\left[\frac{(E - \mu_E)^2}{\sigma_E^2} + \frac{(\nu - \mu_\nu)^2}{\sigma_\nu^2}\right.\right. \\ &\left.\left. - \frac{2\rho_{E\nu}(E - \mu_E)(\nu - \mu_\nu)}{\sigma_E\sigma_\nu}\right]\right) , \end{aligned} \tag{4.18}$$

where $\rho_{E\nu}$ denotes the correlation between the RVs E and ν. To represent the probability density function the following parameters are chosen: $\mu_E = 21000\,\frac{\mathrm{kN}}{\mathrm{cm}^2}$, $\sigma_E = 5\%$, $\mu_\nu = 0.3$, $\sigma_\nu = 10\%$. Furthermore, it is assumed that X and Y are independent, which results in a correlation $\rho_{E\nu}$ of zero. The corresponding probability density function is illustrated in Fig. 4.3.

For the probability of any outcome of the joint PDF, the double integral

$$\mathcal{P}((X, Y) \in B) = \iint\limits_{B} f_{XY} \, \mathrm{d}x \, \mathrm{d}y \,,$$
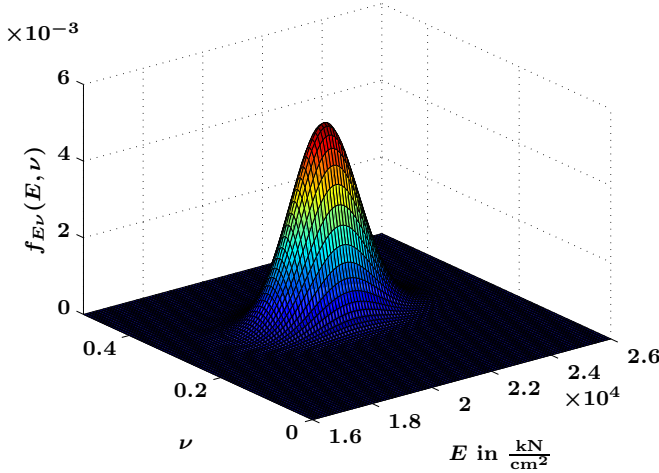
Figure 4.3.: GAUSSIAN joint probability density function of E with $\mu_E = 21000 \frac{\text{kN}}{\text{cm}^2}$, $\sigma_E = 5\%$ and Poisson ratio ν with $\mu_\nu = 0.3$, $\sigma_\nu = 10\%$.

can be evaluated at any specific region. For example, the probability $\mathcal{P}$ that $E = 21000 \frac{\text{kN}}{\text{cm}^2}$ and $\nu = 0.25$ reads

$$\mathcal{P}(E = 21000 \frac{\text{kN}}{\text{cm}^2}, \nu = 0.25) = \mathcal{P}(20900 \frac{\text{kN}}{\text{cm}^2} < E < 21100 \frac{\text{kN}}{\text{cm}^2}, 0.245 < \nu < 0.255)$$

$$= \int_{0.245}^{0.255} \int_{20900}^{21100} 0.00505 \, e^{-\frac{(E - 21000 \frac{\text{kN}}{\text{cm}^2})^2}{2 \cdot 1050^2 \frac{\text{kN}}{\text{cm}^2}^2} - \frac{(\nu - 0.3)^2}{0.0018}} \, \text{d}E \, \text{d}\nu$$

$$= 0.0025365 \,.$$

From the joint probability function of any continuous RV the *marginal probability density function* can be computed, which is defined for the RVs X and Y as follows:

$$f_X(x) = \int_{B_X} f_{XY}(x, y) \, \text{d}y \,,$$

$$f_Y(y) = \int_{B_Y} f_{XY}(x, y) \, \text{d}x \,, \tag{4.19}$$

where B_X and B_Y are the sets of all points, valid for the range $X = x$ and $Y = y$, respectively. For example, the requested probability of E can be calculated from the marginal probability distribution of E by integrating the joint PDF over the set of all

points for which $\mathbb{E}[E] = \mu_E$, i.e.

$$f_E(E) = \int\limits_{-\infty}^{\infty} f_{E\nu}(E,\nu)\,\mathrm{d}\nu \tag{4.20}$$

$$= \int\limits_{-\infty}^{\infty} 0.00505\,\mathrm{e}^{-\frac{(E-21000\,\frac{\mathrm{kN}}{\mathrm{cm}^2})^2}{2\cdot1050^2\,\frac{\mathrm{kN}}{\mathrm{cm}^2}^2} - \frac{(\nu-0.3)^2}{0.0018}}\,\mathrm{d}\nu$$

$$= \int\limits_{E} f_E(E)\,\mathrm{d}E \tag{4.21}$$

$$= 0.0003799\,\mathrm{e}^{-\frac{(E-21000\,\frac{\mathrm{kN}}{\mathrm{cm}^2})^2}{2\cdot1050^2\,\frac{\mathrm{kN}}{\mathrm{cm}^2}^2}}\,.$$

The resulting marginal PDF of E from the joint PDF of ν and E is plotted in Fig. 4.4.
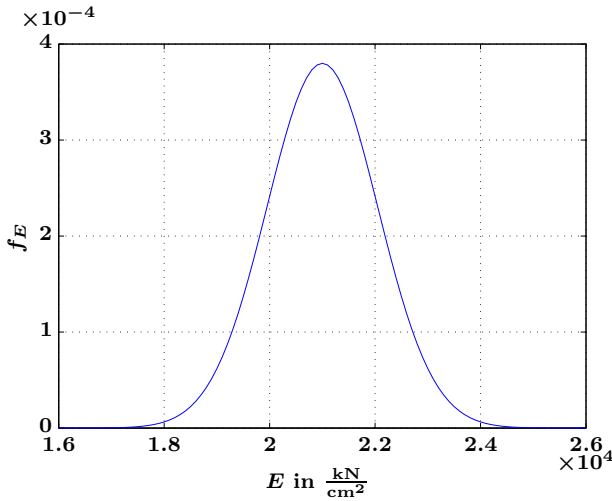
Figure 4.4.: Marginal PDF of E from joint PDF of ν and E.

Furthermore, the expected value and the variance of any of the two RVs X and Y can be obtained from the joint PDF as listed below:

$$\mathbb{E}[X] = \int\limits_{R_x}\int\limits_{R_y} f_{XY}(x,y)\,\mathrm{d}x\,\mathrm{d}y\,, \tag{4.22}$$

$$\mathrm{Var}(X) = \int\limits_{R_x}\int\limits_{R_y} (x-\mu_X)^2 f_{XY}(x,y)\,\mathrm{d}x\,\mathrm{d}y\,, \tag{4.23}$$

where R_x and R_y are the ranges over which X and Y are defined. Let $g(X, Y)$ be a function of X and Y. Then the expected value $\mathbb{E}[g(X, Y)]$ can be calculated from their joint PDF

$$\mathbb{E}[g(X, Y)] = \int\limits_{R_x} \int\limits_{R_y} g(x, y) f_{XY}(x, y) \, \mathrm{d}x \, \mathrm{d}y. \tag{4.24}$$

4.3.2. Joint Cumulative Probability Distribution

As already discussed for a single RV in subsection 4.2.2, the *cumulative probability distribution* is another way to characterize the simultaneous probabilistic behaviour of more than one RV. When more than one RV is considered, the corresponding distribution is denoted as the *joint cumulative probability distribution F_{XY}* and is given by

$$\begin{aligned} F_{XY}(x, y) &= \mathcal{P}(X \leq x, Y \leq y) \\ &= \int\limits_{-\infty}^{x} \int\limits_{-\infty}^{y} f_{XY}(s, t) \, \mathrm{d}s \, \mathrm{d}t. \end{aligned} \tag{4.25}$$

In Fig. 4.5, an example of the joint CDF for E and ν is illustrated, where the value of the probability $\mathcal{P}(E \leq 21000 \, \frac{\mathrm{kN}}{\mathrm{cm}^2}, \nu \leq 0.3)$ is calculated as 0.25.
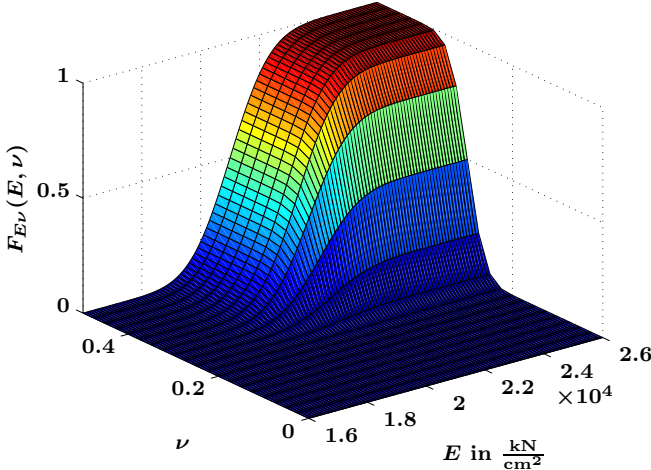
Figure 4.5.: Gaussian joint cumulative density function of E with $\mu_E = 21000 \frac{\mathrm{kN}}{\mathrm{cm}^2}$, $\sigma_E = 5\%$ and Poisson ration ν with $\mu_\nu = 0.3$ and $\sigma_\nu = 10\%$.

4.3.3. Conditional Probability Distribution

The *conditional probability distribution* describes the fact when not the hole sample space Θ of the probability space is of interest, but only a subset, for instance, $B \subset \Theta$, which is exemplary illustrated in Fig. 4.6. The triple $(B, \mathcal{F}_B, \mathcal{P}_B)$ with $\mathcal{F}_B = \{A \cap B; A \in \mathcal{F}\}$ is again a probability space. Such a conditional probability
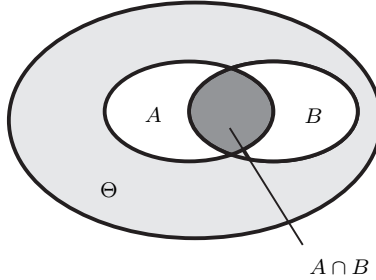
Figure 4.6.: Sample space $B, \mathcal{F}_B, \mathcal{P}_B$ of the probability space Θ.

function, denoted as $f_{Y|x}(y) \ \forall \ y$ in R_x satisfies the following three conditions, cf. Montgomery and Runger [1994]:

1. $f_{Y|x}(y) \geq 0$.

2. $\int_{R_x} f_{Y|x}(y) \, dy = 1$.

3. $\mathcal{P}(Y \in B | X = x) = \int_B f_{Y|x}(y) \, dy$, for any set B in the range of Y .

The conditional probability of Y given $X = x$ is by definition

$$f_{Y|x}(y) = \frac{f_{XY}(x,y)}{f_X(x)} \qquad \text{for } f_X(x) > 0 . \tag{4.26}$$

For example, looking at the previously defined joint distribution between E and ν. The conditional probability of $\underline{E}$, given $\underline{\nu} = \nu$ are:

$$
\begin{aligned}
f_{\underline{E}|\nu}(\nu) &= \frac{f_{\underline{E}\nu}(E,\nu)}{f_{\underline{\nu}}(\nu)} \\
&= \frac{0.00505\,\mathrm{e}^{-\frac{(E-21000\,\frac{\mathrm{kN}}{\mathrm{cm}^2})^2}{2\cdot 1050^2\,\frac{\mathrm{kN}}{\mathrm{cm}^2}^2} - \frac{(\nu-0.3)^2}{0.0018}}}{13.2981\,\mathrm{e}^{-\frac{(\nu-0.3)^2}{0.018}}} \\
&= 0.000379\,\mathrm{e}^{-\frac{(E-21000\,\frac{\mathrm{kN}}{\mathrm{cm}^2})^2}{2\cdot 1050^2\,\frac{\mathrm{kN}}{\mathrm{cm}^2}^2}} ,
\end{aligned}
$$

where $\bullet$ denotes the RVs of E and ν. The result of the conditional probability distribution of $\underline{E}$, given $\underline{\nu} = \nu$ coincides with the result in subsection 4.3.1. This is also obvious, because the RVs $\underline{E}$ and $\underline{\nu}$ are assumed to be uncorrelated, i.e. knowledge

which are obtained with the values of one RV can not change the probabilities which are received by the values of the other.

4.3.4. Covariance and Correlation between Random Variables

The *covariance* is a measure for the linear[3] dependency between two RVs. For the dependent RVs X and Y applies

$$f_{XY}(x, y) \neq f_X(x) f_Y(y). \tag{4.27}$$

To charaterize the covariance between X and Y it is assumed that the means $\mathbb{E}[X]$, $\mathbb{E}[Y]$ as well as

$$\mathbb{E}\left[(X - \mathbb{E}[X])(Y - \mathbb{E}[Y])\right], \tag{4.28}$$

exists. Then, equation (4.28) is defined by the *covariance*[4]

$$\begin{aligned} \mathrm{Cov}(X, Y) &= \mathbb{E}\left[(X - \mathbb{E}[X])(Y - \mathbb{E}[Y])\right] \\ &= \mathbb{E}[XY] - \mathbb{E}[X]\mathbb{E}[Y]. \end{aligned} \tag{4.29}$$

Note that the formula for the covariance is valid for continuous and discrete RVs. If the covariance is zero, thus

$$\mathrm{Cov}(X, Y) = 0, \tag{4.30}$$

the RVs X and Y are independent of each other. The *variance*, also derived in Appendix A, is given by

$$\mathrm{Var}(X + Y) = \mathrm{Var}(X) + \mathrm{Var}(Y) + 2\,\mathrm{Cov}(X, Y) = \mathrm{Var}(X) + \mathrm{Var}(Y). \tag{4.31}$$

A dimensionless measure of the relation between two RVs is the *correlation*, which is defined as

$$\begin{aligned} \rho_{XY} &= \frac{\mathrm{Cov}(X, Y)}{\sqrt{\mathrm{Var}(X)\mathrm{Var}(Y)}} \\ &= \frac{\sigma_{XY}}{\sigma_X \sigma_Y}. \end{aligned} \tag{4.32}$$

The correlation between any two RVs could have a value between $-1 \leq \rho_{XY} \leq 1$. If the value of (say) X increases and the value of Y also increases, the correlation is positive. On the other hand, means a negative correlation that, if the value of one RV is negative, the value of the other one is positive. The correlation is also zero if the two RVs are independent. Hence, independent RVs are uncorrelated, but a correlation equals to zero does not necessarily imply that the RVs are independent.

Random Vectors

In many applications exist a large number n of RVs and it is convenient to gather these variables into a vector. Such a vector, referred as random vector $\boldsymbol{X} : \Theta \to \mathbb{R}$, is

---

[3] The covariance of the RVs might not be sensitive if the relationship between them is non-linear.
[4] See Appendix A for a derivation.

given by

$$\boldsymbol{X} = \begin{pmatrix} X_1 \\ X_2 \\ \vdots \\ X_n \end{pmatrix} , \tag{4.33}$$

with the expected value

$$\bar{\boldsymbol{X}} = \mathbb{E}[\boldsymbol{X}] = \left[\bar{X}_1, \bar{X}_2, ..., \bar{X}_n \right]^T . \tag{4.34}$$

For a given random vector $\boldsymbol{X}$ the *covariance matrix* Σ is a $n \times n$ square matrix whose entries are given by $\Sigma_{ij} = \text{Cov}(X_i, X_j)$, which reads

$$\Sigma = \begin{bmatrix} \text{Cov}(X_1, X_1) & \text{Cov}(X_1, X_2) & \dots & \text{Cov}(X_1, X_n) \\ \text{Cov}(X_2, X_1) & \text{Cov}(X_2, X_2) & \dots & \text{Cov}(X_2, X_n) \\ \vdots & \vdots & \ddots & \vdots \\ \text{Cov}(X_n, X_1) & \text{Cov}(X_n, X_2) & \dots & \text{Cov}(X_n, X_n) \end{bmatrix} . \tag{4.35}$$

Note that $\text{Cov}(X_i, X_i) = \text{Var}(X_i)$. The covariance matrix is symmetric, because $\Sigma_{ij} = \Sigma_{ji}$ and in general positive definite. Further properties of Σ are:

- A positive value of the covariance matrix indicates that both dimensions increase or decrease together.

- A negative value indicates that one value increases while the other decreases.

- Two values X, Y are independent of each other if Σ is zero.[5]

4.3.5. Some useful Properties for Discrete Random Variables

In the following some useful properties of two discrete RVs $X, Y \in (\Theta, \mathcal{F}, P)$ are outlined.

- Let X and Y be two discrete RVs with existing μ_X and μ_Y then

$$\mathbb{E}[X \pm Y] = \mathbb{E}[X] \pm \mathbb{E}[Y] . \tag{4.36}$$

- For a set of discrete RVs $\{X_1, ... X_n\}$, with corresponding expectation values $\mathbb{E}[X_i]$, $1 \leq i \leq n$, applies

$$\mathbb{E}\left[\sum_{i=1}^{n} X_i \right] = \sum_{i=1}^{n} \mathbb{E}[X_i] . \tag{4.37}$$

- With respect to $\mathbb{E}[X]$, $\mathbb{E}[Y]$, $\text{Var}[X]$, $\text{Var}[Y]$, $\mathbb{E}[(X - \mathbb{E}[X])(Y - \mathbb{E}[Y])]$, the variance of X and Y becomes

$$\text{Var}[X + Y] = \text{Var}(X) + \text{Var}(Y) + 2\mathbb{E}[(X - \mathbb{E}[X])(Y - \mathbb{E}[Y])] , \tag{4.38}$$

---

[5]If two RVs are independent, the knowledge of the value of one of the two RVs does not change the chance for the value of the other according to $\mathbb{E}[XY] = \mathbb{E}[X]\mathbb{E}[Y]$, cf. equation (4.39).

where a derivation is given in Appendix A.

- The expectation of the two correlated RVs X and Y are defined by

$$\mathbb{E}[XY] = \mathbb{E}[X]\mathbb{E}[Y] + \mathrm{Cov}(X, Y) \ . \tag{4.39}$$

- Let X and Y are two independent RVs. In this case, the variance of their product[6] is given by

$$\mathrm{Var}(XY) = \mathbb{E}[X]^2\mathrm{Var}(Y) + \mathbb{E}[Y]^2\mathrm{Var}(X) + \mathrm{Var}(X)\mathrm{Var}(Y) \ . \tag{4.40}$$

4.4. Sampling Techniques

Almost all problems in stochastic structural analysis can be treated with the aid of random number generators, denoted in this work as *sampling techniques*. The advantage of such methods is their direct applicability to various systems to obtain the statistical informations of the system response. Not seldom these techniques are the only numerical useful method in solving the problem under uncertainty, especially for high dimensional problems. The purpose of the entire sampling process is to obtain probabilistic informations through the application of statistical methods to the generated samples. In order to fulfil the requirements, the samples need to follow the prescribed distribution function closely. Furthermore, the generated sample must be *statistically independent* of each other, which is a basic condition for the applicability of the available statistical methods. Finally, statistical methods are applied to estimate expected values and/or probabilities of the quantities of interest, e.g., the structural response. The flow chart displayed in Fig. 4.7 shows the typical sequence of an analysis process when applying a sampling technique.

There exist various methods for the selection of the values of the input variable(s), whereas in this section only these methods are proposed, which are applied in this thesis. First of all the simplest and maybe the most widespread technique, the *Monte Carlo Sampling* is presented in section 4.4.1, the two other presented techniques are the *Latin Hypercube Sampling*, introduced in section 4.4.2 and the *Quasi-Random* Sequences, discussed in section 4.4.3. For further sampling techniques and more theoretical background, the reader is referred to the textbooks by Sobol' [1994]; Fishman [1996] or Rubinstein and Kroese [2008].

4.4.1. Monte Carlo Sampling

The *Monte Carlo Sampling* (MCS) is one of the most frequently used simulation technique for quantifying the statistical response of a structural system with random input parameters. The MCS is based on (independent) realizations of random inputs with respect to their prescribed probability distribution. The sampling scheme for each realization becomes deterministic, because the data is fixed in each realization. Upon solving the deterministic realizations of the sampling scheme, the outcomes are collected into a vector. From this vector, statistical informations can be extracted, e.g., the expected value μ and the variance σ^2 of the structural response, the strains,

---

[6]For products of dependent RVs see, e.g., Goodman [1960].
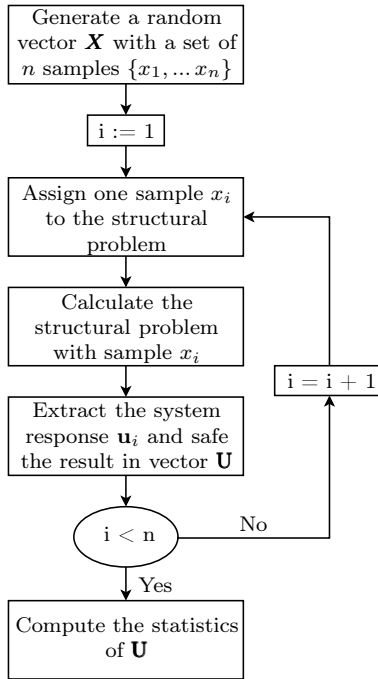
Figure 4.7.: Flow chart of computation for sample-based stochastic structural analysis.

the stresses etc. The corresponding point estimates (only unbiased[7] estimators considered here) are the sample mean $\hat{\mu} = \bar{y}$ and the sample variance $\hat{\sigma}^2 = s^2$, which are defined as

$$\hat{\mu} = \bar{y} = \frac{1}{n} \sum_{i=1}^{n} y_i \,, \tag{4.41}$$

where $y_i = f(x_i)$ and

$$\hat{\sigma}^2 = s^2 = \frac{1}{n-1} \sum_{i=1}^{n} (y_i - \hat{\mu})^2 \,, \tag{4.42}$$

---

[7] An estimator is unbiased if its mean value is equal to the true value of the parameter of interest.

for $i = 1, \dots n$. The accuracy of the estimator can be measured with the help of the *standard error*

$$\sigma_{\bar{y}} = \frac{\sigma}{\sqrt{n}} \, , \tag{4.43}$$

$$\hat{\sigma}_{\bar{y}} = \frac{s}{\sqrt{n}} \, , \tag{4.44}$$

where equation (4.44) is denoted as *estimated standard error*, which can be used when the standard deviation σ in equation (4.43) is unknown. Although the MCS is straightforward to apply, because it only requires repetitive runs of the deterministic system, the convergence rate of $\mathcal{O}(1/\sqrt{n})$ very slow. This fact has the effect, that a large number of sample runs is required to get a satisfactory solution. For example: A reduction of the error by a factor of (say) 10 leads to a drastically increasing sample size of factor 100. In summary:

Obtaining high accuracy is impossible. A good accuracy is only reachable by a large number of samples and for structural systems where the deterministic solution is already computationally expensive this method will be not the optimal choice.

On the other hand, the convergence rate is independent of the dimension of the random space, which is a notable benefit, because no other sample method possess this property.

4.4.2. Latin Hypercube Sampling

The *Latin Hypercube Sampling*, proposed by Mckay et al. [1979], is a sampling technique with the aim to generate a random set of a random input vector $\boldsymbol{X}$, which is more representative of the joint distribution of $\boldsymbol{X}$ than those generated by a MCS. In Fig. 4.8 a simple example is illustrated, where on the left side, the MCS is used and on the right side, the LHS is applied for the sampling. The RV, the Young's modulus E, is assumed to be log-normal distributed with a mean value of $\mu_E = 21000\frac{\text{kN}}{\text{cm}^2}$ and a standard deviation of $\sigma_E = 5\%$. This example already shows that the LHS generates a more accurate sample than those obtained by a MCS.

This subsection gives a brief overview and explains the schematic generation of a LHS, for a detailed explanation of the theory and the explicit generation of a LHS, the reader is referred to the publications by Mckay et al. [1979]; Iman and Conover [1980, 1982]; Stein [1987]; Florian [1992]; Helton and Davis [2003].

Let $\boldsymbol{x} = [x_1, x_2, \dots x_K]^T$ be a realization of the random input vector $\boldsymbol{X}$ with the dimension K, whereas each random input variable x_k, $k = 1, 2, \dots K$, is characterized by its own CDF F_{X_k}. The general procedure for the generation of a Latin Hypercube sample is as follows, cf. Helton and Davis [2003]:

1. The range of the known CDF $F_{X_k}(x)$ of each RV x_k is divided into N disjoint intervals S_{kn} with the property that each interval has the same probability $p_{kn} = \frac{1}{N}$.

2. Then, one value of each interval S_{kn} is chosen randomly.

3. The N values obtained for x_i are randomly paired with the N values obtained for x_j for $i, j = 1, \dots K$ and $i \neq j$, which implies that each value is used only once. This procedure is repeated until a set of N K-tuples is generated randomly,
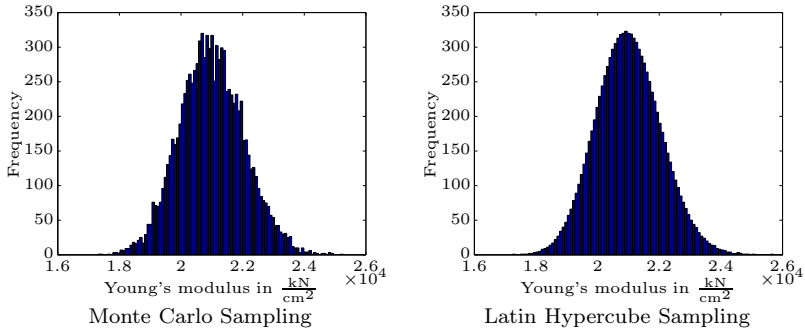
Figure 4.8.: Comparison of the approximation of sampling techniques for E as RV with $n = 10000$ samples.

where the K-tuples are of the form

$$\boldsymbol{x}_l = (x_{l1}, x_{l2}, \dots x_{lK}), \quad l = 1, 2, \dots N. \tag{4.45}$$

An example of a LHS, with $K = 2$ independent uniform RVs and $N = 6$ samples over the domain $[0, 1]^2$, is illustrated in Fig. 4.9. The superscript $\bullet^2$ characterises the dimension of a LHS and will be hereinafter omitted, because the dimension is already defined by K.

Mckay et al. [1979] shows that the LHS and MCS produces unbiased estimates for Υ, i.e. that repeated calculations of $\hat{\mu}_{LHS}$ results in the expected value of the population Υ

$$\hat{\mu}_{LHS} = \Upsilon, \tag{4.46}$$

where the subscript $\hat{\bullet}_{LHS}$ denotes the estimator of a LHS. The accuracy of this estimator is compared with the variance of the estimator of a MCS (4.42), which is repeated below:

$$\hat{\sigma}^2_{\text{MCS}} = s^2_{\text{MCS}} = \frac{1}{N-1} \sum_{i=1}^{N} (y_i - \hat{\mu})^2, \tag{4.47}$$

$$\text{for } i = 1, \dots N,$$

where the subscript $\hat{\bullet}_{\text{MCS}}$ represents the estimator of a MCS and for convenience n is replaced by N. The variance of the unbiased estimator of a LHS, as given in Mckay et al. [1979] or Helton and Davis [2003], reads

$$\hat{\sigma}^2_{LHS} = s^2_{LHS} = \hat{\sigma}^2_{\text{MCS}} + \frac{N-1}{N^{K+1}(N-1)^K} \sum_{\Omega_r} (\mu_r - \mu)(\mu_s - \mu), \tag{4.48}$$
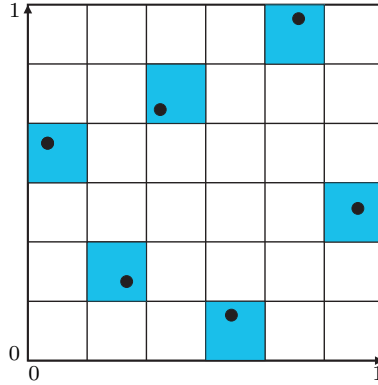
Figure 4.9.: Concept of a LHS for $K = 2$ and $N = 6$ over $[0, 1]$.

with

$$\mu = \mathbb{E}[y] \,, \tag{4.49}$$

$$\mu_r = \mathbb{E}\left[y \,|\, \boldsymbol{x} \in \text{cell } r\right] \,. \tag{4.50}$$

The sum over Ω_r includes the restricted space of all pairs (μ_r, μ_s) for which the associated cells have no coordinates in common, cf. Helton and Davis [2003]. The benefit of a LHS in comparison to a MCS is not directly visible when comparing the equations (4.47) and (4.48). However, the following theorem, cf. Helton and Davis [2003],

Theorem 4.1. *If* $y = f(x_1, x_2, \ldots x_K)$ *is monotonic in each sample element* x_j *and* $g(y)$ *is a monotonic function of* y, *then*

$$\text{Var}(T_{LHS}) \leq \text{Var}(T_{MCS}) \,, \tag{4.51}$$

implies that

$$\hat{\sigma}^2_{LHS} \leq \hat{\sigma}^2_{\text{MCS}} \,. \tag{4.52}$$

Here, T denotes the estimator defined by

$$T = \frac{1}{n} \sum_{i=1}^{n} y_i \,, \tag{4.53}$$

with $y_i = f(\boldsymbol{x}_i)$, which describes the random sample set $\boldsymbol{x} = \{x_1, \ldots x_i\}$. This relationship indicates, that the sampling variability of a sample, realized by a LHS, is smaller than the variance of a sample generated with a MCS. Mckay et al. [1979] shows by means of an example that the variance $\hat{\sigma}^2_{LHS}$ of a sample is considerably less than that for $\hat{\sigma}^2_{\text{MCS}}$. This is also illustrated in Fig. 4.10 where different sample sets[8] were

---

[8]The sets are represented by 100, 500, 1000, 2000, 3000, 4000, 5000, 7500, 10000 and 20000

created for E and the standard deviation of each sample is calculated. The samples based on a Gaussian distribution with $\mu_E = 21000\frac{\text{kN}}{\text{cm}^2}$ and $\sigma_E = 1050\frac{\text{kN}}{\text{cm}^2}$. From this plot the variance reduction is clearly visible. The generated LHS sets match the target value quite well, while significant fluctuations are visible by applied the MCS. Furthermore, the estimating error in the statistical moments is proportional to
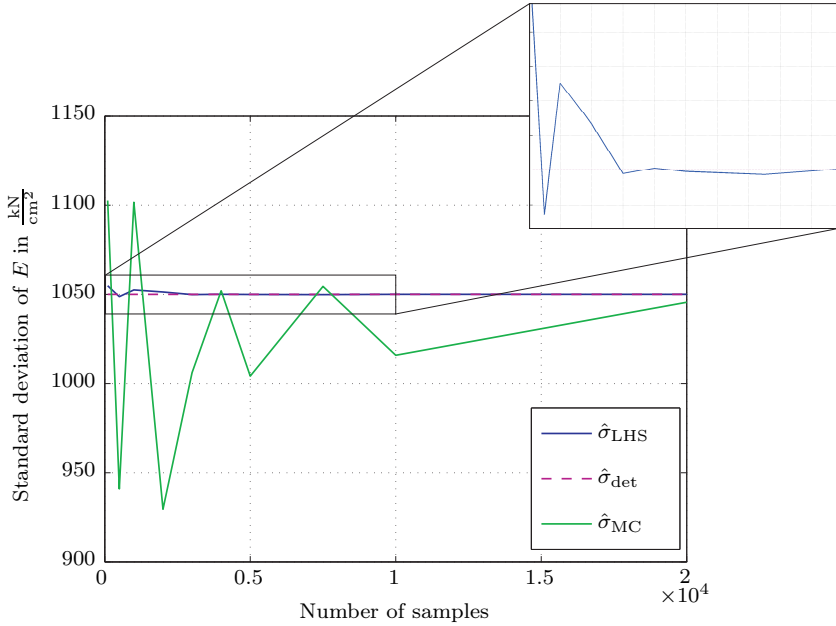
Figure 4.10.: Deterministic standard deviation σ_{det} (the target value) of E compared with the results received by a MCS $\hat{\sigma}_{\text{MCS}}$ and by a LHS $\hat{\sigma}_{\text{LHS}}$.

$\mathcal{O}(n^{-1})$, see Poles and Lovison [2009]. This means that for a reduction of the error (say) 10 the sample size also increases by a factor of 10.

4.4.3. Quasi-Random Sequences

The *Quasi-Random* or low discrepancy sequences are a deterministic counterpart to the (pseudo)-random integration used by the MCS. In conjunction with the Monte-Carlo procedure the term *Quasi-Monte* Carlo (QMC)-method is used in the following. One attribute of the QMC-method is that they are more uniformly distributed as the MCS. There are several ways of generating such quasi-random sequences, e.g., Halton [1960]; Sobol' [1967]; Niederreiter [1988, 1992]. Whereas in this work the so-called Sobol' sequences (Sobol' [1967]) are used, which are basically efficient to estimate high-dimensional integrals, cf. Morokoff and Caflisch [1995].

---

samples.

An introductory overview of the QMC-method is given by L'Ecuyer and Lemieux [2005] and for a detailed treatment of the QMC-method the reader is referenced to the textbooks by Fox [1999] and Lemieux [2009]. A detailed documentation of an algorithm for the generation of Sobol' sequences is presented in Bratley and Fox [1988].

The general idea of QMC-methods is to use a more regularly distributed point set $\boldsymbol{x} = \{x_1, x_2, \ldots x_n\}$ to build the approximation of equation (4.41) than the point set associated with a MCS. The basic one dimensional sequence is the VAN DER CORPUT sequence, where the first six sample values of the binary VAN DER CORPUT sequence are given below

$$0.1_2, 0.01_2, 0.11_2, 0.001_2, 0.101_2, 0.011_2, \ldots \tag{4.54}$$

or, equivalently

$$\frac{1}{2}, \frac{1}{4}, \frac{3}{4}, \frac{1}{8}, \frac{5}{8}, \frac{3}{8}, \cdots . \tag{4.55}$$

The VAN DER CORPUT prime $p = 2$ is the first dimension of the HALTON sequence, cf. Halton [1960]. The sequence of interest in this work, the SOBOL' sequence is a special case of the HALTON sequence where only the prime $p = 2$ is used. In the following a brief introduction on the generation of a SOBOL' sequence will be given, where for the sake of simplicity only a one-dimensional example is discussed. Consequently, a SOBOL' sequence is generated by expanding the set of integers $\{0, 1, 2, 3, \ldots n\}$ into base 2 notation, whereas the i-th term of the sequence is calculated as

$$x_i = \frac{b_0}{2} + \frac{b_1}{2^2} + \frac{b_2}{2^3} + \cdots + \frac{b_m}{2^{m+1}} , \tag{4.56}$$

where the b_m's are integers taken from the base 2 expansion of the number $i - 1$

$$[i-1]_2 = b_m b_{m-1} \cdots b_2 b_1 b_0 \qquad (m \in \mathbb{N}) , \tag{4.57}$$

with $b_m \in [0, 1]$. An evaluation of the representation in equation (4.56) together with equation (4.57) leads to the van der Corput sequence given in equation (4.55). In Fig. 4.11, the space-filling process of a one-dimensional unit "cube" using the technique described above is illustrated. The construction of a s-dimensional SOBOL' sequence is generated by s permutations of the one-dimensional sequence, where the result of a two-dimensional SOBOL' sequence is plotted in Fig. 4.12. To make out the difference between the three procedures presented in this section, consider Fig. 4.13 where the differences between a MCS, a LHS and the QMC-method are obvious. In the first two plots the clustering of points is still clearly visible. This phenomenon can be explained by the uncorrelated arrangement of the points. In the article by Caflisch [1998] such areas are investigated with the result that in the case of applying the MCS about $\sqrt{n}$ points of n points are lying in clumps. Beyond this publication, Morokoff and Caflisch [1993, 1994] give examples which show a significant improvement using quasi-random sequences over standard MC-Methods using (pseudo)-random sequences. The expectation error for the integration with a MCS is given by $\mathcal{O}_{\text{MCS}}(n^{-1/2})$. To get an error bound for the QMC-method, the probability theory can not be used due to the deterministic nature of quasi-random sequences. Such sequences have a convergence error of $\mathcal{O}(n^{-1})$ in optimal cases, where the theoretical upper (worst case) convergence bound is specified with $\mathcal{O}((\log n)^s n^{-1})$, cf. Morokoff and Caflisch [1994,
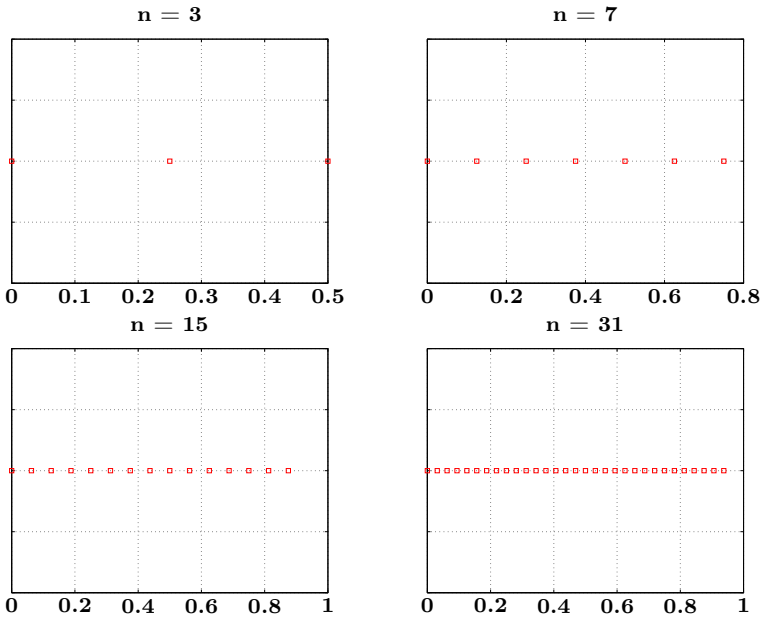
Figure 4.11.: Space-filling process of $[0,1]$ using a one-dimensional Sobol' sequence.
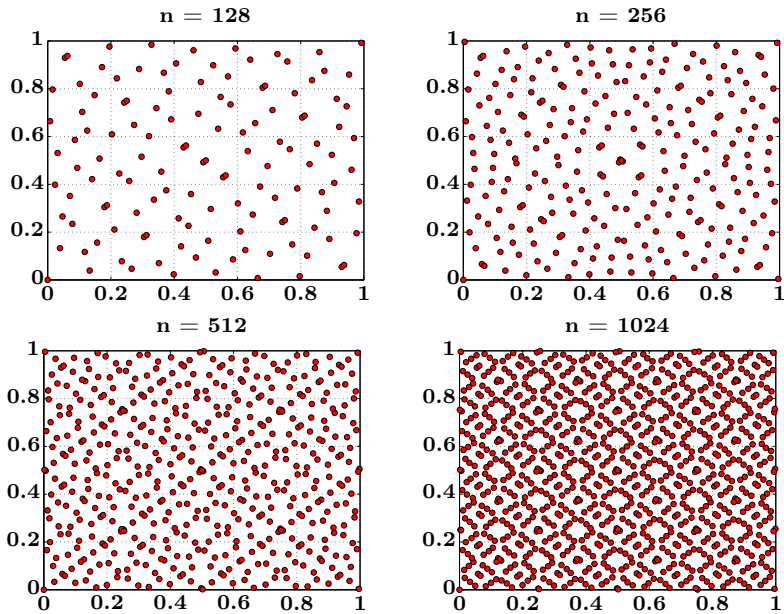
Figure 4.12.: Space-filling process of $[0,1]^2$ using a two-dimensional Sobol' sequence.
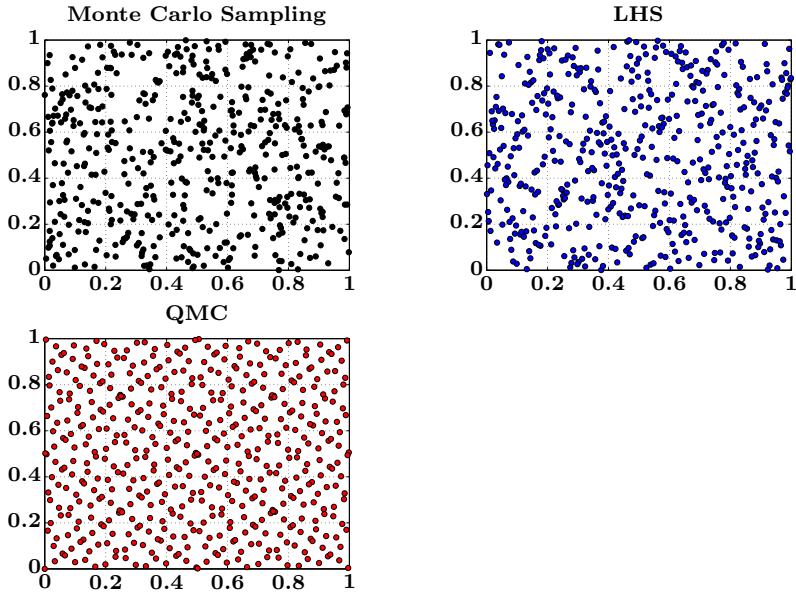
Figure 4.13.: Comparison of a space-filling process $[0, 1]^2$, each generated with $n = 512$ points.
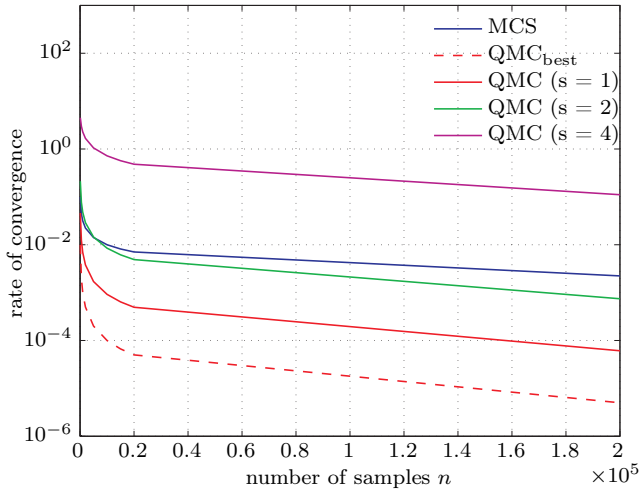
Figure 4.14.: Convergence rates of a MCS and a Sobol' sequences in different dimensions.

1995]. In Fig. 4.14 these two error measures[9] are plotted. Here, the QMC-method is plotted with the dimensions $s = 1, 2, 4$ and the best convergence rate for the QMC-method, denoted with QMC_{best}. The sample set, which are used for the curves, is $n = \{100, 500, 1000, 2000, 5000, 10000, 15000, 20000, 200000\}$. From the result shown in Fig. 4.14 it is obvious, that for small s the convergence rate of the QMC-method is faster than the MCS but for large s (in this example $s \geq 2$) the efficiency of the QMC-method might be considerably reduced. It significantly depends on the number of points used. However, Caflisch [1998] and Morokoff [1998] show that the QMC-method, even for integrating high-dimensional problems, can be extremely effective. Also, in Burhenne et al. [2011] it is pointed out, that Sobol' sequences perform as good as the LHS and with increasing number of input parameters Sobol' results even in a better sampling than the LHS.

---

[9]Note that the convergence error for the LHS is equal to the best Sobol' convergence error and therefore not separately plotted.

4.4.4. Summary

From the investigations in this section, it has been shown that the standard deviation of the estimates in the case of a LHS is much smaller than in the case of a MCS. Furthermore, it is by no means certain that the standard deviation of the MCS estimates with increasing sample number matches the target value. Whereas the LHS with appropriate sample number (here approximately by $n = 5000$ samples) closely approaches the target value. A direct comparison of the sampling with the QMC-method has not been performed at this point. The reason for this is based on the deterministic nature of the underlying sequence and the resulting correlations between the points of the quasi-random sequence.

In general, the sampling techniques discussed in this section can be applied to represent random input parameters. In view of correlated input parameters and if more complete information about a multivariate input distribution is available it should be applied in the sampling framework.

5. Quantification of Uncertainties and their Stochastic Modelling

As in any kind of scientific or technical prediction, uncertainties exist in structural engineering analysis. In practice, the estimation of the input parameters of a structural system may be difficult or inaccurate, i.e. *uncertain*. The fact, that the input parameters are uncertain also leads to an uncertainty of the system response, thus in the prediction of the structural response. If the informations of the input parameters are vague or not known and the statistics of these parameters cannot be evaluated, the theory of *fuzzy sets* can be applied, for further informations on this topic, the reader is referred to de Lima and Ebecken [2000] or Moens and Vandepitte [2005]. In the case of known statistical informations, e.g., the probability distributions of the input parameters are known, the system response can be determined with the aid of the probability theory using random processes or fields, see Matthies and Bucher [1999]; Ghanem and Spanos [2003]; Chen and Soares [2008]. Also in this work, the focus lies on the categorization of uncertainties in various categories and the subsequent consideration of these uncertainties by means of the probability theory. The branch for the quantification of uncertainties in structural analysis is too large to be conveyed more detailed here. Therefore, the reader is referred to the publications by Matheron [1989]; Oberkampf et al. [2002a,b]; Christian [2004]; Field Jr. and Grigoriu [2007]; Helton et al. [2008]; Kiureghian and Ditlevsen [2009].

The chapter is structured as follows: First of all, a brief survey of different types of uncertainties is given and how to deal with them. After this, section 5.2 is addressed to give a brief overview of stochastic processes. The subsections 5.3.1 to 5.3.3 are devoted to methods for the representation of random processes and fields, with special emphasis on these methods which are applied in this thesis. A detailed discussion of these methods are afterwards presented in the chapters 6 to 9. Subsection 5.3.4 gives a short overview of non-GAUSSIAN models, which are interesting for the representation of data which is characterized by statistics that are inconsistent with the GAUSSIAN distribution. At the end of this chapter, section 5.4 provides an insight into the modelling of uncertain material parameters applying random fields. In addition, a clear distinction between random processes and random fields is given in this section.

5.1. Introductory Comments on Uncertainties in Structural Analysis

All types of engineering problems based in a multitude of cases on a deterministic approach. Observed variations, e.g., in loading conditions, material properties or geometry are taken into account by either selecting extremely high or low average values for representing the parameters. But, as already mentioned in the introduction of this chapter, uncertainties exist in all engineering branches. There are several strategies how to deal with these uncertainties, where Christian [2004] distinguishes in his article between the following four strategies:

1. Ignoring the uncertainty.

2. Being conservative.

3. Using the observational method.

4. Quantifying the uncertainty.

For the quantification and the mathematical description of uncertainties, statistical and probabilistic procedures provide a sound framework for a reasonable treatment of the analysis of these uncertainties. Moreover, there are various sources of uncertainties to be dealt with, where hereinafter some common ones are listed. These could be, e.g., *inherent* uncertainties, *statistical* uncertainties, *model* uncertainties or *measurement* uncertainties. A graphical illustration of the confines of the uncertainties is given in Fig. 5.1 and is named after Kiureghian and Ditlevsen [2009] as the *model universe*.
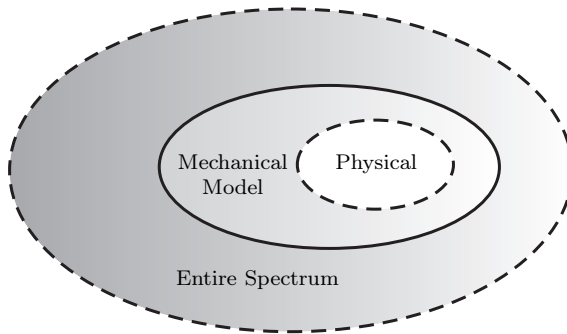
Figure 5.1.: Graphical depiction of the universe of uncertainties (according to Schenk and Schuëller [2005]).

While the uncertainties in mechanical modelling can be reduced, for instance, when additional knowledge becomes available, the physical or intrinsic uncertainties cannot. In the literature, these uncertainties are often categorized into *epistemic* and *aleatoric*, which are described below:

Epistemic uncertainty describes potential deficiency in any phase of modelling that is due to imperfect knowledge, ignorance or limitations of information in building the mathematical model of a physical system and/or in its numerical computation. Examples could include the vagueness in structural parameters or in boundary conditions, deficiency in modelling of the physical system and/or a subjective implementation. From the foregoing description it is clear that such uncertainties can be **reduced** by collecting more informations.

Aleatoric uncertainty is an inherent randomness or variability in the physical properties, such as variability/scatter in material properties, geometrical parameters etc., of a system over time and/or space. IAdditional information **cannot reduce** this type of uncertainty.

Conceptually, analyses which involve epistemic and aleatoric uncertainties involve the following three distinct mathematical entities, cf. Helton et al. [2008].

1. A characterization of the aleatoric uncertainty.

2. A function that predicts results of interest.

   3. A characterization of the epistemic uncertainty.

There are various methods for dealing with these two types of uncertainties available. For the representation of aleatoric uncertainties mathematical models of the probability theory are available, cf. chapter 4. For the representation of the epistemic uncertainty, Helton et al. [2008] identifies the following four different mathematical structures: the *Interval analysis*, *possibility theory*, *evidence theory* and the *probability theory*. Whereas this thesis focuses on the probability methods, which are widely used and rely upon a sound mathematical framework. Coming back to Fig. 5.1, where the entire spectrum is still not categorized. This last area is also of the aleatory type and therefore also not reducible, because no physical system is truly isolated, which is illustrated by the dashed line.

Until now, the FEM is not taken into account in the classification of uncertainties. This will be now done with respect to structural systems, including general outlines. Hereby, the focus lies on the explanation of the discrepancy between the prediction and the measurement of the system parameters, by neglecting the discretization error[1]. One reason for such kind of discrepancy is the finite element model, which is only a mathematical idealization of the physical system and does not represents the physical behaviour of the system exactly but with a certain accuracy. This sort of uncertainty can be categorized as model uncertainty, where typical examples could be strongly non-linear interactions in a linear model or ignoring theses non-linear interactions as well as inaccurate modelling of the boundary conditions etc. A further point is the level of detail of the mathematical model which represents the system behaviour. Also when assuming that the mathematical model represents the system behaviour quite well, the system parameters exhibit deviations from their true values. Such deviations (resp. uncertainties) could be loading uncertainties, such as *wind, snow, life loads*[2], *water waves* or *earthquakes* as well as uncertainties in structural properties like *geometry imperfections*, *Young's modulus*, *material strength*, *damping characteristics* or *tensile strength*.

In general, the deterministic values are the so called *nominal* values, where no scattering is taken into account. Such a parameter, for instance, the Young's modulus E can be quantified in terms of their CDF as

$$\mathcal{P}_E(a \leq E \leq b) = \int\limits_a^b f_E(x)\, \mathrm{d}x\,.$$

In general, experimental data are extremely scarce in most areas of engineering applications. In reference to practical applications, most of the system parameters are assumed as nominal values, because no statistical informations are available. In this work only stochastic material parameters are considered and this kind of uncertainties are normally epistemic in nature. Here, the motivation lies on the fact that, with more available information, the uncertainty of the estimation decreases and may be theoretically vanish when the sample of observations is large, i.e. infinit. Furthermore, it has been taken into account that a stochastic input data sample also results in an uncertain output, i.e. the system response. Since the input is random and specified by probability distributions, the output also follows such probability distributions,

---

[1]For further information to discretization errors the reader is referred to Zienkiewicz and Taylor [2000].

[2]Life loads may be categorized either as quasi-static load processes such as floor loads, or as actual dynamic loads such as those generated by traffic on bridges, cf. Vanmarcke et al. [1986].

i.e. has a well defined unique distribution, where an illustration can be found in the PhD thesis of Geistefeldt [2003].

5.2. Stochastic Processes

The classical probability theory is concerned with those random variables whose values do not depend upon time, or any other set of parameters. However, in the analysis of many phenomena it is necessary to study a family of random variables, which depend upon groups of parameters, most often including time. This section gives a brief survey in the characterization of random processes, which is mainly inspired by the textbook by Kleiber and Hien [1992]. For further informations, the reader is referred to this book, as well as to the textbooks by Papoulis [1991] or Gardiner [2009].

A *stochastic process* is a family of RVs $X(t), t \in T$. In many engineering problems the parameter t will be the time and the underlying intuitive notion will be that of a random variable developing in time. A standard example for a simple stochastic process is illustrated in Fig. 5.2, where an ensemble of all possible realizations $H(t, \theta)$ of the random process $X(t)$ is illustrated.
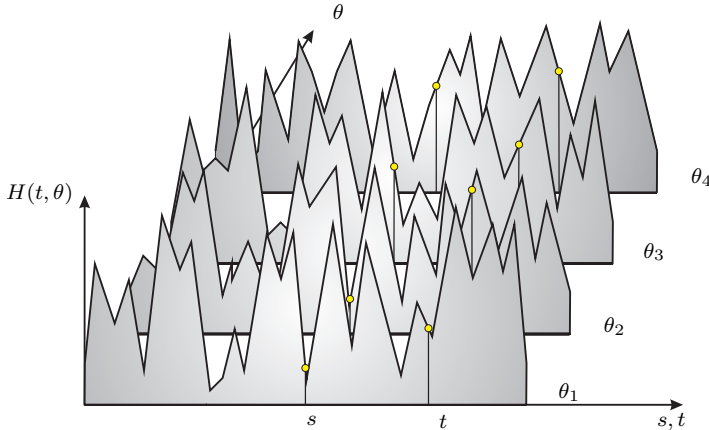
Figure 5.2.: Ensemble of realizations of a one-dimensional random process.

On the basis of the previous chapter, some mathematical definitions for stochastic processes are summarized below.

Let $X(t)$ be a stochastic process, which is characterized by a two dimensional CDF as

$$F_2(x_1, t_1; x_2, t_2) = \mathcal{P}(X(t_1) \le x_1; X(t_2) \le x_2), \tag{5.1}$$

where the corresponding PDF is given by

$$f_2(x_1, t_1; x_2, t_2) = \frac{\partial^2 F_2(x_1, t_1; x_2, t_2)}{\partial x_1 \partial x_2}. \tag{5.2}$$

If f_n is known all functions with a number less than n, i.e. $(n-1)$, can be determined, such as f_1 by f_2,

$$f_1(x_1, t_1) = \int_{-\infty}^{\infty} f_2(x_1, t_1; x_2, t_2) \, \mathrm{d}x_2 \,.$$

In general, a n-dimensional CDF is defined by

$$F_n(x_1, t_1; ...; x_n, t_n) = \mathcal{P}(X(t_1) \le x_1; ...; X(t_n) \le x_n) \,, \tag{5.3}$$

and a n-dimensional PDF by

$$f_n(x_1, t_1; ...; x_n, t_n) = \frac{\partial^n F_n(x_1, t_1; ...; x_n, t_n)}{\partial x_1 \ldots \partial x_n} \,. \tag{5.4}$$

The m-th moment of $X(t)$ is given in terms of its first density function, i.e. $f_1(x_1, t)$ as

$$\mu_x^m(t) = \mathbb{E}[X^m] = \int_{-\infty}^{\infty} x^m f_1(x, t) \, \mathrm{d}x \,. \tag{5.5}$$

The expected value $\mathbb{E}$ of the stochastic process $X(t)$ is defined by the first moment $\mu_x^1(t) = \mu_x(t)$ and the second moment $\mu_x^2(t)$ denotes the mean square value of $X(t)$.

The m-th central moment of a stochastic process $X(t)$ is defined by,

$$\overline{\mu}_x^m(t) = \mathbb{E}[(X^m - x^0)^m)] = \int_{-\infty}^{\infty} (x - \mu_x^1)^m f_1(x, t) \, \mathrm{d}x \,, \tag{5.6}$$

and the variance of $X(t)$ is given by $\overline{\mu}_x^2(t) = \sigma_x^2(t)$. The mn-th joint moment, at the given times t_1 and t_2 reads

$$\mu_x^{mn}(t_1, t_2) = \mathbb{E}[X^n(t_1)X^m(t_2)]$$
$$= \int_{-\infty}^{\infty} \int_{-\infty}^{\infty} x_1^m x_2^n f_2(x_1, t_1; x_2, t_2)) \, \mathrm{d}x_1 \mathrm{d}x_2 \,. \tag{5.7}$$

A measure for the independence between $X(t_1)$ and $X(t_2)$ is the *correlation function*, defined by $\mu_x^{11}(t_1, t_2)$. The *autocovariance function* is a further measure, which is given by

$$C_{xx}(t_1, t_2) = \mathbb{E}\left[(X(t_1) - \mu_x(t_1))(X(t_2) - \mu_x(t_2))\right] \,,$$
$$= \int_{-\infty}^{\infty} \int_{-\infty}^{\infty} (x_1 - \mu_x(t_1))(x_2 - \mu_x(t_2)) f_2(x_1, t_1; x_2, t_2) \, \mathrm{d}x_1 \mathrm{d}x_2 \,, \tag{5.8}$$
$$= \mu_{xx}(t_1, t_2) - \mu_x(t_1)\mu_x(t_2) \,.$$

This equation describes the covariance of the variable against a time-shifted version of itself. If $t_1 = t_2 = t$, the autocovariance function becomes the variance of the

stochastic process $X(t)$, i.e.

$$C_{xx}(t,t) = \text{Var}_x(t) = \sigma_x^2(t) = \mu_x^2(t) - (\mu_x^1(t))^2 \,. \tag{5.9}$$

If the stochastic process $X(t)$ has the following properties:

$$\begin{aligned}
\mathbb{E}[X(t)] &= \mu_x^1 & \forall\, t \in T \\
\text{Var}(X(t)) &= \sigma_x^2 & \forall\, t \in T \\
C_{xx}(t_1, t_2) &= C_{xx}(t_2 - t_1) = C_{xx}(\tau) & \forall\, t \in T \,,
\end{aligned} \tag{5.10}$$

it is denoted as *weakly* stationary process. All given remarks in the listing above do not depend on time t. To be more specific, these moments are invariant by a translation of the time origin. A stronger condition for a stochastic process $X(t)$ is the requirement, that all possible moments are not affected by a shift in time, which is denoted as *strongly* stationary process.

A further property are the Wiener-Khintchine-realization of the autocovariance function C_{xx}. When assuming that the time separation τ tends to infinity, the autocovariance function tends to zero. Therefore, the Fourier-transform pair of C_{xx} exists and by definition the spectral density $S(\omega)$ of the weakly stationary process $X(t)$ is given by

$$S_{xx}(\omega) = \frac{1}{2\pi} \int\limits_{-\infty}^{\infty} C_{xx}(\tau) e^{i\omega\tau} \,\mathrm{d}\tau \,. \tag{5.11}$$

By performing the inversion of $S_{xx}(\omega)$ recovering the autocovariance function, i.e.

$$C_{xx}(\tau) = \int\limits_{-\infty}^{\infty} S_{xx}(\omega) e^{-i\omega\tau} \,\mathrm{d}\omega \,. \tag{5.12}$$

This realization states that the autocovariance function, of a weakly stationary process is the Fourier-transformation of the corresponding spectral density and vice versa, see also Appendix D.

A central stochastic process, which achieves the stationary condition, is the stationary Gaussian process, which plays a central role in the theory as well as in the application of probabilistic methods. In general, a stochastic process $X(t)$ is called a Gaussian stochastic process, if for every finite set $\{t_1, t_2, ..., t_n\} \in T$, the set of random parameters $\{x(t_1), x(t_2), ..., x(t_n)\}$ have the joint probability density function

$$f_n(x_1, t_1; ...; t_n, x_n) = \frac{1}{\sqrt{(2\pi)^n \det(\Sigma_{\boldsymbol{xx}})}} e^{-\frac{1}{2}(\boldsymbol{x} - \boldsymbol{\mu_x}(t))^T \Sigma_{\boldsymbol{xx}}(t)^{-1}(\boldsymbol{x} - \boldsymbol{\mu_x}(t))} \,, \tag{5.13}$$

where $\boldsymbol{\mu_x}(t) = \mathbb{E}[\boldsymbol{x}(t)]$ denotes the expectation vector, $\Sigma_{\boldsymbol{xx}}(t)$ is referred to as the covariance matrix and $\boldsymbol{x} = [x_1, x_2, ... x_n]^{\mathrm{T}}$. It can be shown that the multivariate Gaussian probability density function is fully specified by its average $\mathbb{E}[X(t)]$ and its second moment $\mathbb{E}[X(t_1)X(t_2)]$, cf. Xiu [2010]. In practice, many variables are empirically well approximated by Gaussians. The reason for this is based on the *central limit theorem*, which states that a random variable composed of the result of many additive parts, each independent but arbitrarily distributed, is Gaussian, cf. van Kampen [2007]; Gardiner [2009].

5.3. Representation of Stochastic Processes and Fields

The uncertainties of physical quantities can be characterized by stochastic processes or stochastic fields very well. In engineering applications there are typical examples of interest, such as earthquake ground motion, sea waves, wind and snow loads, road roughness, imperfections of structures or fluctuating properties in random media. For many of these parameters, stochastic properties were determined over the years, through a variety of measurements and investigations.

In view of structural engineering, the structural response is often non-linear, see for example, Augusti et al. [1984]; Sundararajan [1995]; Ditlevsen and Madsen [2007], and as already discussed in subsection 4.4.1 it might be too complex to determine such non-linear response statistics by other means than sampling techniques. Such a sampling is realized by a sample function, where this function should be chosen in such a way that the underlying stochastic process/field is characterized accurately. This sample function might be stationary or non-stationary, univariate or multivariate, Gaussian or non-Gaussian. What properties a sample function finally has, strongly depends on the requirements of the accuracy of the realistic representation of the physical behaviour as well as on the available statistical data. Besides these standard sampling techniques, quite different representation methods have been developed, such as the *Spectral Representation Method*, Karhunen-Loève Expansion and the *Polynomial Chaos Expansion* (PCE). These three discretization methods are applied in this thesis and in the following three subsections a briefly overview of some developments is given. Detailed theoretical informations with respect to this methods will be given in the following chapters.

5.3.1. Spectral Representation Method

The *Spectral Representation* Method has been introduced by Shinozuka and Jan [1972] and appears to be one of the most used spectral representation methods, e.g., Shinozuka and Deodatis [1991]; Grigoriu [1993]; Deodatis [1997]; Grigoriu [2000a]. According to this method, sample functions of the stochastic processes/fields are generated with specified power spectral density informations. In the case of stationary or homogeneous cases, the fast Fourier transform technique (FFT) is used for a significantly improvement of the computationally efficiency, e.g., Shinozuka and Deodatis [1991]. The SPRM generates ergodic sample functions of which each generated sample function is identical to the corresponding target power spectrum. The method was continually developed through the years in various ways, for example, for the simulation of stochastic waves, cf. Deodatis and Shinozuka [1989], or non-Gaussian stochastic fields, see Yamazaki and Shinozuka [1988]; Bocchini and Deodatis [2008], spatially incoherent multidimensional and multivariate random processes and fields, see Ramadan and Novak [1993], as well as to simulate multivariate ergodic stochastic processes, presented by Deodatis [1996b], multivariate nonstationary stochastic processes, cf. Deodatis [1996a], and non-Gaussian multidimensional multivariate fields, proposed by Popescu et al. [1998].

5.3.2. Karhunen-Loève Expansion

A quiet general spectral representation, utilized for Gaussian stochastic processes / fields, is the Karhunen-Loève Expansion (KLE) of the covariance function.

This representation technique is the most efficient method for the discretisation of a random process/field, because it requires the smallest number of random variables to represent a random process or field within a given level of accuracy, cf. Ghanem and Spanos [2003]; Li and Der Kiureghian [1993]; Zhang and Ellingwood [1994]; Le Maître and Knio [2010]. In Phoon et al. [2002b], the author directly applies the KLE for the representation of non-Gaussian fields. A further study by Phoon et al. [2002a] presents a wavelet Galerkin approach to solve the Fredholm integral equation for a large number of KL terms accurately and cheaply. In stochastic finite element analysis, the KLE is often applied in conjunction with the Polynomial Chaos approximation, for instance, Anders and Hori [2001]; Ghanem and Spanos [2003]; Xiu and Karniadakis [2003]; Keese [2004]; Chung et al. [2005]; Sachdeva et al. [2006]; Sett et al. [2011]. In these articles and textbooks, the input parameters are characterized by the KLE while the statistics of the system response are evaluated using the PCE. This combination of the KLE and the PCE in the context of FEM is well known as *Spectral Stochastic Finite Element Method* (SSFEM). To the end of this brief review of the KLE, the articles of Huang et al. [2001] and Stefanou and Papadrakakis [2007] should be mentioned, where a detailed overview including a direct assessment of the SPRM and the KLE is presented.

5.3.3. Polynomial Chaos Expansion

The *Polynomial Chaos* Expansion provides a generalization of the Karhunen-Loève expansion and was first presented by Wiener [1938]. Based on Wiener's ideas, Cameron and Martin [1947] constructed an orthogonal basis for non-linear functionals in terms of Fourier-Hermite functionals. A detailed review of the development steps is given in Ghanem and Spanos [2003]. When the PCE is applied in the context of a stochastic finite element analysis it is used to represent the structural system response by a set of coefficients in a suitable so-called *polynomial chaos* basis. The following collection focuses on some publications which use the PCE for the evaluation of the covariance function of the underlying solution process. These are: Ghanem and Kruger [1996]; Sakamoto and Ghanem [2002]; Debusschere et al. [2005]; Field Jr. and Grigoriu [2004]. The PCE has two major advantages compared to the KLE, cf. Anders [2000]:

1. The PCE can be used to expand random variables of any distribution, i.e. not only Gaussian.

2. The PCE doesn't require any a priori knowledge on the probability distribution of the expanded random process or field.

5.3.4. Non-Gaussian Models

In almost all previously cited studies a Gaussian distribution is applied for the representation of the random variables or random vectors. One reason for assuming a Gaussian distribution is the simplicity and the lack of relevant experimental data. As already mentioned earlier, the most physical phenomena and therefore practical engineering problems, such as material and geometric properties exhibit non-Gaussian probabilistic characteristics. Furthermore, the non-Gaussian assumption permits to efficiently treat the case of large input variability without violating the physical constraints of the material and geometric properties, as remarked in Stefanou [2011]. The generation of a sample functions of a non-Gaussian processes / fields can be realized
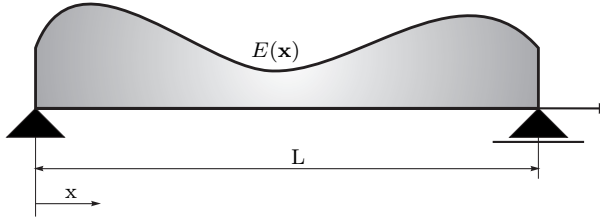
Figure 5.3.: Sample function of a random variable described by an one-dimensional random field.

in various ways. One widely applied technique is the memoryless non-linear transformation of Gaussian processes, e.g., Yamazaki and Shinozuka [1988], which utilizes the spectral representation method. Bocchini and Deodatis [2008] compare in their article the three simulation algorithms, proposed by Yamazaki and Shinozuka [1988]; Deodatis and Micaletti [2001] and Shi and Deodatis [2004]. Furthermore, Grigoriu [2000b] considers two different non-Gaussian models, whereas Stefanou [2011] used non-Gaussian transformation in connection with the stochastic finite element method to estimate the response variability of cylindrical shells. For the application of non-Gaussian polynomials Xiu and Karniadakis [2002, 2003]; Xiu [2009] presented the *Askey* scheme, see also the following chapter.

A further method for the characterization of non-Gaussian processes/fields is the application of non-linear filters. Such filters are utilized to generate a stationary non-Gaussian stochastic process in agreement with a given first-order probability density function and the spectral density, see e.g., Cai and Lin [1996].

5.4. Modelling of Uncertain Material Properties

So far, the definitions *random process* and *random field* were always called synonymous. Now, a distinction between these definitions is made and afterwards some important definitions of random fields are listed.

Typical examples for the description, in terms of random processes have already been given in this section. Such processes could be, for instance, wind loads on structures which exhibit random spatial and temporal fluctuations, whereas spatially correlated fluctuations, such as material properties are generally characterized by random fields. An example could be the simple beam in Fig. 5.3, where a random field is applied to represent the randomness of the Young's modulus $E(\mathbf{x})$, where the vector $\mathbf{x} = (x_1, x_2, ..., x_n)$ defines the spatial location of E. When performing such a measurement for different beams and different realizations of the beam the value of $E(x)$, $x \in \mathbf{x}$ will be randomly vary from measurement to measurement. Mathematically, this connection is defined through a random variable $E(x, \theta)$, $\theta \in \Theta$. The same measurement at a different location $y \in \mathbf{y}$ results in a different value, $E(y, \theta)$. This means that the measurement will again vary from one measurement to another and this difference in turn is random. A further observation is that values from adjacent locations do not differ as much as values that are measured at locations further apart. Such a behaviour is an example of a covariance structure, many different

types of which may be modelled by random fields.

Mathematically spoken, a random field $H(\mathbf{x})$ is a real valued random variable whose statistics, such as the expected value, standard deviation etc., may be different for each $\mathbf{x} \in \mathbf{x}$, i.e.

$$H \in \mathbb{R}; \quad \mathbf{x} = [x_1, x_2, ..., x_n]^T \in \mathcal{D} \subset \mathbb{R}^n. \tag{5.14}$$

The expected value function of $H(\mathbf{x})$ is defined by

$$\bar{H}(\mathbf{x}) = \mu_H = \mathbb{E}[H(\mathbf{x})], \tag{5.15}$$

where the expectation operator $\mathbb{E}$ is to be taken at a fixed location $\mathbf{x}$ over all possible realizations $H(\mathbf{x}, \theta)$, see Fig. 5.4 where four realizations $(\theta_1, \theta_2, \theta_3, \theta_4)$ at the locations x and y are illustrated. As by stochastic processes, a specific dependency structure of
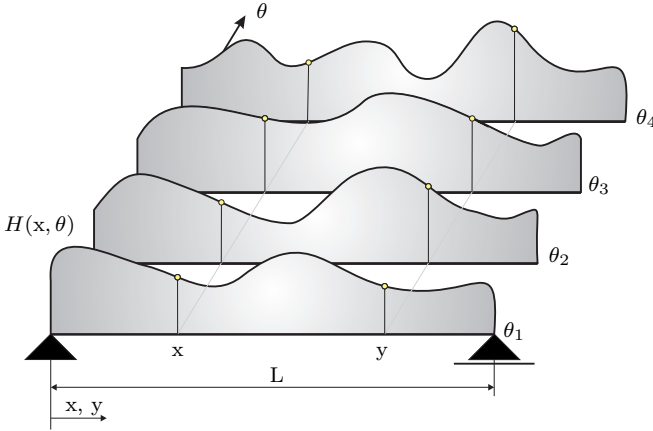
Figure 5.4.: Ensemble realizations of a one-dimensional random field.

random field values $H(\mathbf{x})$ and $H(\mathbf{y})$ is characterized by the autocovariance function

$$C_{HH}(\mathbf{x}, \mathbf{y}) = \mathbb{E}\left[(H(\mathbf{x}) - \bar{H}(\mathbf{x}))(H(\mathbf{y}) - \bar{H}(\mathbf{y}))\right]. \tag{5.16}$$

A random field $H(\mathbf{x})$ is called *weakly homogeneous* if

$$\bar{H}(\mathbf{x}) = \text{const.} \quad \forall\, \mathbf{x} \in \mathcal{D} \tag{5.17}$$
$$C_{HH}(\mathbf{x}, \mathbf{x} + \xi) = C_{HH}(\xi) \quad \forall\, \mathbf{x} \in \mathcal{D}, \tag{5.18}$$

where ξ defines the separation distance along the axes. This properties are equivalent to a stationary random process, cf. the listing in (5.10). If the autocovariance function $C_{HH}(\cdot)$ depends on the distance but not on the direction, i.e.

$$C_{HH}(\mathbf{x}, \mathbf{x} + \xi) = C_{HH}(\|\xi\|) \quad \forall\, \mathbf{x} \in \mathcal{D}, \tag{5.19}$$

$H(\mathbf{x})$ is referred as a *isotropic* random field.

6. Random Field Modelling

An experiment may be defined as an operation designed to discover some unknown truth. For example, consider a steel beam where an investigator observes the material properties in an experimental study. The observed measures, denoted as outcomes, are described in the elementary probability theory usually in terms of *random variables*. Projecting this onto a numerical method, for example, a sampling method, it works well. Performs the investigator a variety of trials with a large number of steel beams, the outcomes of all experimental studies are equivalent to observing the realization of a *random field*. Each outcome, in the terminology of random fields, identified by its coordinates $\mathbf{x} = [\mathrm{x}, \mathrm{y}, \mathrm{z}]$ and with respect to a n-dimensional space. The points of the outcomes are grouped in a random vector $\boldsymbol{X} = [\mathbf{x}_1, \dots \mathbf{x}_n]^{\mathrm{T}}$ whose elements are the structural coordinates of the mechanical system.

This chapter contains the background of the theory of *random fields*, which is later used in conjunction with the FEM for the representation of material uncertainties. In section 6.1 some general remarks about random fields are presented. Section 6.2 gives an overview about discretization methods for random fields. Further discretization methods are the series expansion methods, such as the Karhune-Loève Expansion and the Spectral Representation Method, which are discussed in detail in sections 6.3 and 6.4.

The bandwidth over the theory of random fields is large and can not be treated here comprehensively. For a broad treatment of random fields the reader is referred to the literature. For an illustrative textbook with some applications the reader is referred to Christakos [1992] or Vanmarcke [2010], whereas a detailed mathematical background of random fields can be found in the textbook of Adler and Taylor [2007].

6.1. Preliminary Remarks on Random Fields

The term *random field* has already been introduced in section 5.4 and some properties of such fields are already given there. In this section the theory of random fields is presented in detail.

Let $(\Theta, \mathcal{F}, \mathcal{P})$ be the probability space and considering a $\mathcal{L}^p(\Theta, \mathcal{F}, \mathcal{P})$ space, which is a linear normed space of a set of random variables $\{X_1, \dots X_n\}$ on $(\Theta, \mathcal{F}, \mathcal{P})$. The $\mathcal{L}^p$ space satisfies the condition

$$\mathbb{E}[X]^p = \int_{\Theta} |X(\mathrm{x})|^p \, \mathrm{d}\mathcal{P}(\mathrm{x}), \tag{6.1}$$

with the norm

$$\|X\| = (\mathbb{E}[X]^p)^{\frac{1}{p}}, \tag{6.2}$$

whereby $\mathcal{L}^p$ is defined completely. In this work, only second-order random variables are considered, i.e. $p = 2$. Per definition a $\mathcal{L}^2$ space is being defined with the inner

product

$$\langle X_1, X_2 \rangle = \mathbb{E}[X_1 X_2] = \int_{\Theta} X_1(\mathrm{x}) X_2(\mathrm{x}) \, \mathrm{d}\mathcal{P}(\mathrm{x}) \,, \tag{6.3}$$

where X_1 and X_2 are random variables and $\mathcal{L}^2$ is denoted as Hilbert space.

A random field should be assumed as a set of random variables indexed by the continuous value $\mathbf{x}$, with $\mathbf{x} \in \Theta$. For a given parameter $\mathbf{x}_0$, $H(\mathbf{x}_0, \theta)$ is per definition a random variable and for an outcome θ_0, $H(\mathbf{x}, \theta_0)$ is a realization of the random field, cf. Sudret and der Kiureghian [2000].

In the following, some properties are listed into which random fields can be classified, where similar discussions can be found in Sudret and der Kiureghian [2000]. Furthermore, some of these properties are already mentioned in section 5.4 and will be reviewed here for convenience.

- A random field is referred to as *univariate* when the value $H(\mathbf{x})$ coupled with the point $\mathbf{x}$ is a random variable. On the other hand a random field is called *multivariate*, when the value $H(\mathbf{x})$ attached to the point $\mathbf{x}$ is a random vector.

- A random field is denoted as *one-dimensional* if the dimension d of $\mathbf{x}$ is one. The *multidimensional* case occurs when the dimension d of $\mathbf{x}$ is larger than one.

- Random fields can be distinguished by means of the chosen probability density law. In general, random fields are subdivided into Gaussian and non-Gaussian fields. As mentioned earlier in this work, the Gaussian distribution is often applied in engineering applications and has several important properties. Probably the most important property is the complete characterization by its mean and its covariance[1] .

- A random field can be classified by the spatial variability of $\mathbf{x}$. To be more specific, it can be distinguished between homogeneous fields, i.e. when the mean and the covariance are being constant. Otherwise the field is referred to as non-homogeneous.

With respect to this work, only univariate multidimensional homogeneous Gaussian fields are applied. This is sufficient for the representation of physical parameters, like Young's modulus, Poisson's ratio, yield stress, hardening parameters etc. as independent random fields.

6.2. Categories of Discretization Methods for Random Fields

Until now, the set of points $\{\mathbf{x_1}, \mathbf{x_2}, ...\}$ is infinite and not sufficient to express all the properties of the random field $H(\mathbf{x}_i, \theta)$, $i = 1, ...$. Therefore, a discretization technique is needed to approximate the random field by a finite number of random variables into a measurable set in $\mathbb{R}^n$. Besides the discretization methods mentioned in the previous chapter, several methods have been developed for the discretization of random fields. This section gives a summary of the discussions given in the report of Sudret and der Kiureghian [2000]. For further details reference is made to this report as well as to the references given in the following subsections.

---

[1] In the multidimension case it is the covariance matrix.

Starting from the previous considerations and using the notation style of Sudret and der Kiureghian [2000], the following definition has been be made:

The discretization of $H(\cdot)$ is done by an approximation, denoted by $\hat{H}(\cdot)$, with a finite set of random variables $\{X_i, i = 1, \dots n\}$, $X_i \in (\Theta, \mathcal{F}, \mathcal{P})$ at points x_i, which can be formally expressed as

$$H(\mathbf{x}) \stackrel{\text{discretization}}{\longrightarrow} \hat{H}(\mathbf{x}) = \mathcal{F}(\mathbf{x}, \boldsymbol{X}(\theta)) \,. \tag{6.4}$$

After Sudret and der Kiureghian [2000], the discretization methods can be separated into the three following categories:

1. **Point discretization**: Here, each random variable X_i is a selected value of the random field $H(\cdot)$ at some given point $\mathbf{x}_i$.

2. **Average discretization**: By applying this method, the set of random variables $\{X_i\}$ are weighted integrals of $H(\cdot)$ over a domain Ω_e

$$X_i = \int\limits_{\Omega_e} H(\mathbf{x})w(\mathbf{x}) \, \mathrm{d}\Omega_e \,, \tag{6.5}$$

   with the weighting function $\omega(\mathbf{x})$.

3. **Series expansion methods**: Here, $H(\cdot)$ is in principal represented by a infinite series involving random variables and deterministic spatial functions, where the approximation $\hat{H}(\cdot)$ is received by truncating the infinite series after a certain number of terms.

6.2.1. Point Discretization Methods

In general, the uncertainty of a random field $H(\cdot)$ is represented by specific points, for example, the nodes of a finite element mesh or the integration points, where the number of considered points characterizes the number of random variables.

The Midpoint (MP-) Method

This technique, proposed by Kiureghian and Ke [1988], is the simplest method for the discretization of a random field. Hereby, the approximation $\hat{H}(\cdot)$ is realized within each element domain Ω_e by a single random variable, which is characterized by the value of the field at the centroid $\mathbf{x}_c$ of the element, i.e.

$$\hat{H}(\mathbf{x}) = H(\mathbf{x}_c) \,, \quad \mathbf{x} \in \Omega_e \,. \tag{6.6}$$

The approximated field is characterized by the random vector $\boldsymbol{X}$, including all element centroids $\mathbf{x}_c^1, \dots \mathbf{x}_c^{ne}$, i.e. $\boldsymbol{X} = \left[H(\mathbf{x}_c^1), \dots H(\mathbf{x}_c^{ne})\right]^{\mathrm{T}}$. The mean is directly available by the mean of $H(\cdot)$ as well as the variance, where both values are evaluated at the centroids of the elements.

The Shape Function (SF-) Method

This method, introduced by Liu et al. [1986a,b], approximated the random field $H(\cdot)$ within an element in terms of the nodal values $\mathbf{x}_i$ and the corresponding shape functions N_i as follows, cf. Sudret and der Kiureghian [2000]:

$$\hat{H}(\mathbf{x}) = \sum_{i=1}^{n_n} N_i(\mathbf{x}) H(\mathbf{x}_i), \quad \mathbf{x} \in \Omega_e \tag{6.7}$$

where n_n is the number of nodes of element e and $\mathbf{x}_i$ defines the coordinates of the i-th node. In this case $\hat{H}(\cdot)$ is represented by the random vector $\boldsymbol{X} = [H(\mathbf{x}_1), ..., H(\mathbf{x}_{n_n})]$. The statistics of the mean and the covariance matrix of $\hat{H}(\cdot)$ can be found in the references at the beginning of this subsection. In view of the MP-method, where discontinuities occur at the element boundaries has this method the advantage that $\hat{H}(\cdot)$ is continuous over the entire domain Ω.

The Integration Point (IP-) Method

Here, $H(\cdot)$ is implicitly discretized by the total number of integration points. The discretization scheme where each integration point associated with one random variable, gives accurate results for a short correlation length. Furthermore, this method uses the same integration rules as the standard FE-method. On the one hand, the number of random variables is limited to the total number of integration points. To be more specific, when the set of random variables is larger than the total number of existing integration points the correlation matrix will be singular. On the other hand grows the number of RVs drastically with a finer FE-mesh, respectively by increasing mechanical systems.

The Optimal Linear Estimation (OLE-) Method

This method, also denoted as *Kriging technique* (Matthies et al. [1997]) was proposed by Li and Der Kiureghian [1993]. Here, the random field is approximated by a linear function of nodal values as follows, cf. Li and Der Kiureghian [1993]:

$$\hat{H}(\mathbf{x}) = a(\mathbf{x}) + \sum_{i=1}^{n_a} b_i(\mathbf{x}) X_i = a(\mathbf{x}) + \mathbf{b}^{\mathrm{T}}(\mathbf{x}) \cdot \boldsymbol{X}, \quad \mathbf{x} \in \Omega \tag{6.8}$$

where $\boldsymbol{X} = [H(\mathbf{x}_1), ..., H(\mathbf{x}_{n_a})]$ and n_a denotes the number of nodal points, used in the approximation. The functions $a(\mathbf{x})$ and $\mathbf{b}(\mathbf{x})$ have to be evaluated, therefore see the references at the beginning of this subsection. The error of this method can be determined by, cf. Li and Der Kiureghian [1993],

$$\mathrm{Var}\left[H(\mathbf{x}) - \hat{H}(\mathbf{x})\right] = \sigma^2(\mathbf{x}) - \underbrace{\sum\nolimits_{H(\mathbf{x})\boldsymbol{X}}^{\mathrm{T}} \sum\nolimits_{\boldsymbol{XX}}^{-1} \sum\nolimits_{H(\mathbf{x})\boldsymbol{X}}}_{\mathrm{Var}\,[\hat{H}(\mathbf{x})]}, \tag{6.9}$$

where $\sum_{\boldsymbol{XX}}$ denotes the covariance matrix of $\boldsymbol{X}$, $\sum_{H(\mathbf{x})\boldsymbol{X}}$ is a vector containing the covariances of $H(\mathbf{x})$ with the elements of $\boldsymbol{X}$ and $\sigma^2(\mathbf{x})$ represents the variance of $H(\cdot)$. Since the error (resp. the variance) is always positive indicates that

$\hat{H}(\mathbf{x})$ always under-represents the variance of the original random field $H(\mathbf{x})$, cf. Sudret and der Kiureghian [2000].

6.2.2. Averaging Discretization Methods

Spatial Average (SA-) Method

This method was proposed by Vanmarcke and Grigoriu [1983]. Here, $\hat{H}(\cdot)$ within each element e is realized as the spatial average of $H(\cdot)$ as follows, cf. Sudret and der Kiureghian [2000]:

$$\hat{H}(\mathbf{x}) = \frac{\int_{\Omega_e} H(\mathbf{x})\,\mathrm{d}\Omega_e}{|\Omega_e|} = \bar{H}_e\,, \quad \mathbf{x} \in \Omega_e\,. \tag{6.10}$$

The random vector $\boldsymbol{X}$ is assembled by the average values $\bar{H}(\mathbf{x})$, thus $\boldsymbol{X} = [\bar{H}_e]$, $e = 1,\dots n_e$. The mean and the covariance of $\boldsymbol{X}$ are evaluated in terms of the mean and covariance function of $H(\mathbf{x})$ over the domain Ω_e. Usually, the spatial average over an element e with respect to the variance is smaller than the local variance of the random field, i.e. it under-represents the local variance of the random field, cf. Sudret and der Kiureghian [2000].

Weighted Integral (WI-) Method

The WI-method was introduced in the early 1990s by Deodatis [1990, 1991]; Deodatis and Shinozuka [1991]. At the same time, Takada [1990a,b] applied this method in conjunction with the finite element method. The method seems to be more attractive than the previous ones, because no extra discretization of the random field is necessary.

Let $\mathbf{k}^e$ be the deterministic element stiffness matrix

$$\mathbf{k}^e = \int\limits_{\Omega_e} \mathbf{B}^{\mathrm{T}}\,\mathbb{C}\,\mathbf{B}\,\mathrm{d}\Omega_e\,, \tag{6.11}$$

with the linear elasticity tensor $\mathbb{C}$. The (until now) deterministic matrix $\mathbf{k}^e$ is now extended by a univariate random field $H(\mathbf{x},\theta)$, which represents the fluctuating material properties within element e by

$$\mathbb{C}(\mathbf{x},\theta) = \mathbb{C}_0\left[1 + H(\mathbf{x},\theta)\right]\,. \tag{6.12}$$

Here, $\mathbb{C}_0$ denotes the constant part of the elasticity tensor and $H(\mathbf{x},\theta)$ is a zero-mean homogeneous random field. By substituting the expression (6.12) into equation (6.11), the element stiffness matrix can be rewritten as

$$\mathbf{k}^e(\theta) = \mathbf{k}_0^e + \Delta\mathbf{k}^e(\theta) \quad \text{with} \quad \Delta\mathbf{k}^e(\theta) = \int\limits_{\Omega_e} H(\mathbf{x},\theta)\mathbf{B}^{\mathrm{T}}\mathbb{C}_0\mathbf{B}\,\mathrm{d}\Omega_e\,, \tag{6.13}$$

where $\theta \in \Theta$. After some algebra (see the references at the beginning of this subsec-

tion) the *stochastic* element stiffness matrix is obtained as follows:

$$\mathbf{k}^e(\theta) = \mathbf{k}_0^e + \sum_{i=1}^{n_{WI}} \Delta \mathbf{k}_i^e X_i^e \,, \tag{6.14}$$

where $\mathbf{k}_0^e$ denotes the mean element stiffness matrix, $\Delta\mathbf{k}_i^e$ are deterministic matrices, X_i^e are variables of the random field, referred to as the *weighted integrals* and n_{WI} denotes the number of the weighted integrals of element e. The number of the weighted integrals depends on the type of the used element.

The method depends strictly on the FE-mesh and for a small correlation length the accuracy of the result is questionable compared to the integration domain Ω_e. Some further drawbacks, discussed in Sudret and der Kiureghian [2000], are summarized in the following:

- The method is limited to elastic structures.

- The input parameters are restricted to small Cov's when applying the first-order perturbation method.

- The method is time intensive when the system contains a large number of elements.

In the habilitation treatise of Sudret [2007], the author concludes that this method has been given less attention in the recent years. Moreover, through the literature review which has been done in this thesis, this statement should be generalized to the fact that the proposed methods in this section have little to no longer be applied in SFEM applications in the last years.

6.2.3. Series Expansion Methods

In view of the previous presented discretization methods the series expansion methods differs by the fact, that the random field is exactly represented by a (formally) infinit series involving random variables and deterministic spatial functions. The realization of a random field is then obtained by a truncation of this series. Such methods are the two already mentioned ones, namely the KLE, see Ghanem and Spanos [2003] and the SPRM, cf. Shinozuka and Jan [1972]. Further related methods are the Expansion Optimal Linear Estimation (EOLE-) method, cf. Li and Der Kiureghian [1993] and the Orthogonal Series Expansion (OSE), see Zhang and Ellingwood [1994].

One of the pioneering works in the field of series expansion methods is the approach proposed by Lawrence [1987], where the series expansion of $H(\mathbf{x})$ is defined by

$$H(\mathbf{x}) = \sum_{j=1}^{\infty} H_{0j}\varphi_j(\mathbf{x}) + \sum_{i=1}^{\infty}\sum_{j=1}^{\infty} H_{ij}\xi_i(\theta)\varphi_j(\mathbf{x}) \,. \tag{6.15}$$

Here, $\varphi_j(\mathbf{x})$, $j = 1,\dots$ is a set of linear independent deterministic functions and $\xi_i(\theta)$, $i = 1,\dots$ are statistically independent random variables. The basis random variables have the following properties:

$$\mathbb{E}\left[\xi_i\right] = 0 \quad \text{for } i = 1, 2, \dots, \tag{6.16}$$

$$\mathbb{E}\left[\xi_i\xi_j\right] = \delta_{ij} \,, \tag{6.17}$$

where δ_{ij} denotes the Kronecker delta. Truncating the series in equation (6.15) after M basis random variables and N deterministic functions leads to

$$H(\mathbf{x}) \approx \sum_{j=1}^{N} H_{0j}\varphi_j(\mathbf{x}) + \sum_{i=1}^{M}\sum_{j=1}^{N} H_{ij}\xi_i(\theta)\varphi_j(\mathbf{x}) = \hat{H}(\mathbf{x}) \,. \tag{6.18}$$

For the solution, including some descriptions for the calculation of the coefficients H_{ij}, the reader is referred to Lawrence [1989].

6.3. Karhunen-Loève Expansion

Let $H(\mathbf{x}, \theta)$ be a random field where $\theta \in \Theta$ belonging to the space of random events $(\Theta, \mathcal{F}, \mathcal{P})$. Furthermore, the mean $\mu(\mathbf{x})$ and the variance $\sigma^2(\mathbf{x})$ are defined on this probability space and indexed on a bounded domain $\mathcal{D}$.

The general idea is to decompose a general second-order random field $H(\mathbf{x}, \theta)$ into an orthonormal set of series expansion functions $f(\mathbf{x})$ whose coefficients are uncorrelated random variables $\xi(\theta)$. The deterministic functions $f(\cdot)$ have been orthonormalized to serve as a basis set for the decomposition, where the expanded Fourier-type series reads, cf. Ghanem and Spanos [2003]:

$$H(\mathbf{x}, \theta) = \sum_{i=0}^{\infty} \sqrt{\lambda_i} f_i(\mathbf{x})\xi_i(\theta) \,, \tag{6.19}$$

with a set of constants $\{\lambda_i\}_{i=1}^{\infty}$ as well as a set of orthonormal deterministic eigenfunctions $\{f_i(\mathbf{x})\}_{i=1}^{\infty}$ and $\{\xi_i(\theta)\}_{i=1}^{\infty}$ denotes a set of uncorrelated random variables with a mean equal to zero. The definition in equation (6.19) is denoted as the Karhunen-Loève expansion of the random field $H(\mathbf{x}, \theta)$. Any realization of the random field $H(\mathbf{x}, \theta)$ is expanded by a set of $\{f_i(\mathbf{x})\}_{i=1}^{\infty}$, which can be expressed as an eigenvalue problem as follows, cf. Ghanem and Spanos [2003]:

$$\forall\, i = 1, \ldots \quad \int_{\mathcal{D}} C(\mathbf{x}_1, \mathbf{x}_2) f_i(\mathbf{x}_2) \,\mathrm{d}\mathcal{D}_{\mathbf{x}_2} = \lambda_i f_i(\mathbf{x}_1) \,, \tag{6.20}$$

where $C(\mathbf{x}_1, \mathbf{x}_2)$ is the covariance function of $H(\mathbf{x}, \theta)$, λ_i denotes the i-th eigenvalue and $f_i(\mathbf{x})$ are the corresponding eigenfunction of the covariance function. Equation (6.20) is referred as Fredholm integral equation. The eigenfunctions $f_i(\mathbf{x})$ can be normalized by

$$\int_{\mathcal{D}} f_i(\mathbf{x}) f_j(\mathbf{x}) \,\mathrm{d}\mathcal{D} = \delta_{ij} \,. \tag{6.21}$$

The covariance function is *bounded*, *symmetric* and *positive definite*, cf. Sudret and der Kiureghian [2000]; Ghanem and Spanos [2003]; Le Maître and Knio [2010], where a set of $\{f_i(\mathbf{x})\}_{i=0}^{\infty}$ forms a complete orthonormal basis of $\mathcal{L}^2(\mathcal{D})$.[2] The set of eigenvalues $\{\lambda_i\}_{i=0}^{\infty}$ is real, numerable and the only possible accumulation point of the eigenvalues is zero. Due to the aforementioned properties, any realization of

---

[2] A proof can be found, e.g., in the textbook by Stark and Woods [1986].

$H(\mathbf{x}, \theta)$ can be expanded over $\mathcal{L}^2(\mathcal{D})$ as, cf. Sudret and der Kiureghian [2000],

$$H(\mathbf{x}, \theta) = \mu(\mathbf{x}) + \sum_{i=1}^{\infty} \sqrt{\lambda_i} f_i(\mathbf{x}) \xi_i(\theta) \, . \tag{6.22}$$

Further, the following relation applies:

$$\mathbb{E}[\xi_i \xi_j] = \delta_{ij} \, , \tag{6.23}$$

which can be checked when calculating $\text{Cov}[H(\mathbf{x}_1, \theta), H(\mathbf{x}_2, \theta)]$ by means of equation (6.19) and requiring that the result is equal to $C(\mathbf{x}_1, \mathbf{x}_2)$, see also Appendix D.

With respect to the definition in expression (6.4) a discretized random field $\hat{H}(\cdot)$ is obtained by truncating the series expansion in equation (6.22) after the M-th term, i.e.

$$\hat{H}(\mathbf{x}, \theta) = \mu(\mathbf{x}) + \sum_{i=1}^{M} \sqrt{\lambda_i} f_i(\mathbf{x}) \xi_i(\theta) \, . \tag{6.24}$$

The variance and the covariance functions of this series are given by

$$\text{Var}\left[\hat{H}(\mathbf{x}, \theta)\right] = \sum_{i=1}^{M} \lambda_i f_i^2(\mathbf{x}) \, , \tag{6.25}$$

$$\text{Cov}\left[\hat{H}(\mathbf{x}_1, \theta), \hat{H}(\mathbf{x}_2, \theta)\right] = \sum_{i=1}^{M} \lambda_i f_i(\mathbf{x}_1) f_i(\mathbf{x}_2) \, . \tag{6.26}$$

Properties of the Karhunen-Loève Expansion

In the following, a few properties of the KLE are listed, which are summarized from the report by Sudret and der Kiureghian [2000]. Further properties can be found in this report as well as in the textbook by Ghanem and Spanos [2003] and the references therein.

- The set of basis functions $\{f_i(\mathbf{x})\}$, of the covariance function $C(\cdot)$, is optimal in the mean square error. This means, that the mean square error of the truncated expansion $\hat{H}(\cdot)$ is minimized and no other series expansion method leads to a smaller mean square error after the truncation of M terms, see also Le Maître and Knio [2010].

- The variance of $\hat{H}(\cdot)$ always *underestimates* the variance of $H(\cdot)$, because the variance of $\hat{H}(\cdot)$ is always smaller than the variance of $H(\cdot)$, which becomes clear by considering the following equation:

$$\text{Var}\left[H(\mathbf{x}) - \hat{H}(\mathbf{x})\right] = \sigma_H^2(\mathbf{x}) - \sum_{i=1}^{M} \lambda_i f_i^2(\mathbf{x}) = \text{Var}[H(\mathbf{x})] - \text{Var}[\hat{H}(\mathbf{x})] \, . \tag{6.27}$$

- A set of random variables $\{\xi_i(\theta)\}$ is orthonormal if and only if the set of basis functions $\{f_i(\mathbf{x})\}$ as well as the constants $\{\lambda_i\}$ are solutions of the eigenvalue problem (6.20), cf. Sudret and der Kiureghian [2000].

- If the investigated random field is Gaussian each random variable $\xi_i(\theta)$ is also Gaussian. It follows, that any set of random variables $\{\xi_i(\theta)\}$ forms a set of *independent* standard normal variables, cf. Sudret and der Kiureghian [2000]; Nouy [2009].

6.3.1. Analytical Solution of the Integral Equation

In this subsection the *analytical* solution of the Fredholm integral is presented. Closed form solutions of this equation do seldom exist and only for some simple geometries an analytical solution is available. Analytical solutions, for instance, of rectangular or quadratic domains, can be found in Ghanem and Spanos [2003]. For complex geometries no analytical solution exists and numerical methods must be applied to solve the covariance function. This fact is discussed in subsection 6.3.2, where a Galerkin type procedure is applied to compute the covariance function numerically.

A covariance function commonly applied is the *exponential* function, where the expressions for one-, two- and three-dimensional domains are given below:

$$C_{1D}(\mathbf{x}_1, \mathbf{x}_2) = e^{-\frac{|x_1 - x_2|}{c_x}}, \tag{6.28}$$

$$C_{2D}(\mathbf{x}_1, \mathbf{y}_1; \mathbf{x}_2, \mathbf{y}_2) = e^{-\frac{|x_1 - x_2|}{c_x} - \frac{|y_1 - y_2|}{c_y}}, \tag{6.29}$$

$$C_{3D}(\mathbf{x}_1, \mathbf{y}_1, \mathbf{z}_1; \mathbf{x}_2, \mathbf{y}_2, \mathbf{z}_2) = e^{-\frac{|x_1 - x_2|}{c_x} - \frac{|y_1 - y_2|}{c_y} - \frac{|z_1 - z_2|}{c_z}}, \tag{6.30}$$

where the first index of C_{iD}, $i = 1, 2, 3$ refers to the dimensionality of the function and $c_{x,y,z}$ denotes the correlation length in the corresponding direction.

In Fig. 6.1 the one-dimensional covariance function is exemplary plotted. The function is defined over the domain $\mathcal{D} = [0, 1]$, where different correlation lengths $c_x = 0.01, 0.1, 1.0, 10.0$ are applied to demonstrate the influence of c on the covariance function. The limit of the correlation function is zero, i.e. when the covariance function takes the form of a delta function $C(\mathbf{x}_1, \mathbf{x}_2) = \delta(\mathbf{x}_1 - \mathbf{x}_2)$, see Fig. 6.1 (a). Here, the eigenvalues will not decrease, i.e. they are constant. A further discussion can be found in subsection 6.3.3, where the resulting eigenvalues for different correlation lengths are evaluated.

In the following, the analytical solutions for the eigenfunctions f_i and the eigenvalues λ_i are calculated for the one-, two- and three-dimensional exponential covariance function, defined in equations (6.28) to (6.30). The approximation of the random field is expressed by

$$\hat{H}(\mathbf{x}, \theta) = \mu(\mathbf{x}) + \sigma_{\hat{H}} \sum_{i=1}^{M} \sqrt{\lambda_i} f_i(\mathbf{x}) \xi_i(\theta), \quad \mathbf{x} \in \mathcal{D}, \tag{6.31}$$

where $\sigma_{\hat{H}}$ denotes the standard deviation of the approximated field $\hat{H}(\cdot)$.

(a) Correlation length $c_{\mathbf{x}} = 0.01$

(b) Correlation length $c_{\mathbf{x}} = 0.1$

(c) Correlation length $c_{\mathbf{x}} = 1.0$

(d) Correlation length $c_{\mathbf{x}} = 10.0$
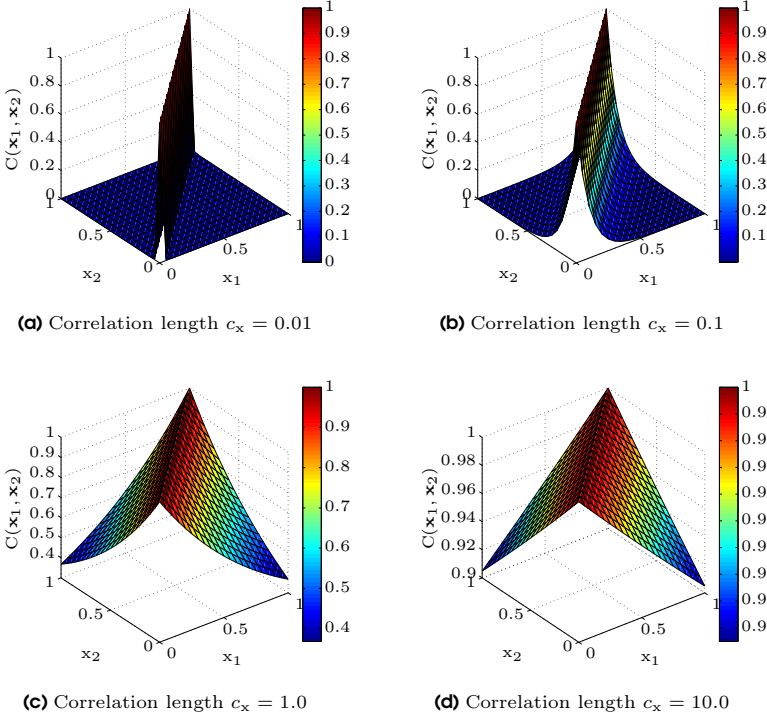
Figure 6.1.: Surface plots of the covariance function (6.28) over the domain $\mathcal{D} = [0, 1]$ with different correlation lengths.

One-Dimensional Case

The solution of the one-dimensional random field is computed by the approximate random field $\hat{H}$, given in (6.31) and repeated here again

$$\hat{H}(\mathbf{x}, \theta) = \mu(\mathbf{x}) + \sigma_{\hat{H}} \sum_{i=1}^{M} \sqrt{\lambda_i} f_i(\mathbf{x}) \xi_i(\theta), \quad \mathbf{x} \in \mathcal{D}. \tag{6.32}$$

The variables λ_i and $f_i(\mathbf{x})$ are the solutions of the eigenvalue problem

$$\int_{\mathcal{D}} C(\mathbf{x}_1, \mathbf{x}_2) f_i(\mathbf{x}_2) \, d\mathcal{D}_{\mathbf{x}_2} = \lambda_i f_i(\mathbf{x}_1). \tag{6.33}$$

By use of the one-dimensional exponential covariance function (6.28), the FREDHOLM integral equation can be solved in closed form. Therefore, when substituting the

function (6.28) into the eigenvalue problem (6.33) yields

$$\int\limits_{-a}^{a} e^{-\frac{|\mathbf{x}_1 - \mathbf{x}_2|}{c_{\mathbf{x}}}} f_i(\mathbf{x}_2) \, d\mathcal{D}_{\mathbf{x}_2} = \lambda_i f_i(\mathbf{x}_1),$$ (6.34)

where the domain is defined within the interval $[-a, a]$. Based on Ghanem and Spanos [2003] the exact solutions of (6.34) are listed below:

- The eigenpairs $(\lambda_i, f_i(\mathbf{x}))$ for $i = 1, 3, 5, \dots$ are calculated by

$$\lambda_i = \frac{2\,c}{\omega_i^2 c^2 + 1},$$ (6.35)

$$f_i(\mathbf{x}) = \alpha_i \cos(\omega_i \mathbf{x}),$$ (6.36)

  where c is the correlation length and α_i is defined by

$$\alpha_i = \frac{1}{\sqrt{a + \frac{\sin(2\omega_i a)}{2\omega_i}}}.$$ (6.37)

  The variable ω_i is the solution of the transcendental equation

$$\frac{1}{c} - \omega_i \tan(\omega_i a) = 0 \quad \text{in the range} \quad \left[(i-1)\frac{\pi}{a}, \, (i - \frac{1}{2})\frac{\pi}{a}\right].$$ (6.38)

- Similar for $i = 2, 4, 6, \dots$:

$$\lambda_i = \frac{2\,c}{\omega_i^2 c^2 + 1},$$ (6.39)

$$f_i(\mathbf{x}) = \alpha_i \sin(\omega_i \mathbf{x}),$$ (6.40)

  in the case of even permutations, α_i is given by

$$\alpha_i = \frac{1}{\sqrt{a - \frac{\sin(2\omega_i a)}{2\omega_i}}}.$$ (6.41)

  With the associated term ω_i, where the solution of the transcendental equation reads

$$\frac{1}{c} \tan(\omega_i a) + \omega_i = 0 \quad \text{in the range} \quad \left[(i - \frac{1}{2})\frac{\pi}{a}, \, i\frac{\pi}{a}\right].$$ (6.42)

With these derivatives all coefficients for the analytical solution of the eigenvalue problem can be calculated.

One-Dimensional Example

Let $\mathcal{D} = [0, a]$ be a domain in $\mathbb{R}^1$ with $a = 1$. The associated covariance function, given in equation (6.28), with the coordinates $\mathbf{x} \in \mathcal{D}$ has a correlation length of $c_{\mathbf{x}} = 1$. The analysed field $H_\alpha(\mathbf{x}, \theta)$ is the zero mean part of equation (6.32) with

the corresponding covariance function $C_{1D}(\mathbf{x}_1, \mathbf{x}_2)$. For the analysis, this function is truncated after the first six terms, i.e.

$$\hat{H}_\alpha(\mathbf{x}, \theta) \approx \sigma_\alpha \sum_{i=1}^{6} \sqrt{\lambda_i} f_i(\mathbf{x}) \xi_i(\theta) \,. \tag{6.43}$$

The first six eigenfunctions $f_i(\mathbf{x})$ are calculated as

$$f_1(\mathbf{x}) = 1.0725 \cos(1.3065\,\mathbf{x})$$
$$f_2(\mathbf{x}) = 1.3257 \sin(3.6732\,\mathbf{x})$$
$$f_3(\mathbf{x}) = 1.3834 \cos(6.5846\,\mathbf{x})$$
$$f_4(\mathbf{x}) = 1.3994 \sin(9.6317\,\mathbf{x})$$
$$f_5(\mathbf{x}) = 1.4056 \cos(12.7232\,\mathbf{x})$$
$$f_6(\mathbf{x}) = 1.4086 \sin(15.8341\,\mathbf{x})$$

with the corresponding eigenvalues λ_i

$$\lambda_1 = 0.7388, \qquad \lambda_2 = 0.1380, \qquad \lambda_3 = 0.0451,$$
$$\lambda_4 = 0.0213, \qquad \lambda_5 = 0.0123, \qquad \lambda_6 = 0.0079 \,.$$

The resulting curves for the variance and the covariance profiles are plotted in Fig. 6.2, where the target curve, the two-, four- and the six-term KLE is illustrated. The corresponding equations for the curves are given by, cf. Anders [2000],

$$\text{Cov}\,(\mathbf{x}, \mathbf{x}) = \hat{H}_\alpha\left(-\frac{a}{2} + \mathbf{x}a, -\frac{a}{2} + \mathbf{x}a\right), \quad \mathbf{x} \in [0, 1]\,, \tag{6.44}$$

$$\text{Cov}\,(\mathbf{x}, 1 - \mathbf{x}) = \hat{H}_\alpha\left(-\frac{a}{2} + \mathbf{x}a, -\frac{a}{2} + (1 - \mathbf{x})\,a\right), \quad \mathbf{x} \in [0, 1]\,, \tag{6.45}$$

where the standard deviation σ_α is assumed to $\sigma_\alpha = 1$.

Two-Dimensional Case

The previously presented procedures can be applied analogically to the two-dimensional case, where the rectangular domain

$$\mathcal{D} = [-a,\, a] \times [-b,\, b]$$

is considered. With respect to the two-dimensional function $C_{2D}(\mathbf{x}, \mathbf{y})$, given in equation (6.29), the corresponding eigenvalue problem reads

$$\int_{-a}^{a} \int_{-b}^{b} \mathrm{e}^{\left(-\frac{|\mathbf{x}_1 - \mathbf{x}_2|}{c_{\mathbf{x}}} - \frac{|\mathbf{y}_1 - \mathbf{y}_2|}{c_{\mathbf{y}}}\right)} f_i(\mathbf{x}_2, \mathbf{y}_2)\, \mathrm{d}\mathcal{D}_{\mathbf{x}_2} \mathrm{d}\mathcal{D}_{\mathbf{y}_2} = \lambda_i f_i(\mathbf{x}_1, \mathbf{y}_1)\,. \tag{6.46}$$

The solutions of equation (6.46) are obtained by products of the one-dimensional solutions, see Ghanem and Spanos [2003] or Sudret and der Kiureghian [2000]. The eigenvalues λ_i are determined by

$$\lambda_i = \lambda_{i_{\mathbf{x}}}^{1D} \lambda_{i_{\mathbf{y}}}^{1D}\,, \tag{6.47}$$

(a) Covariance function $C_{\mathbf{xx}}(\mathbf{x}, \mathbf{x})$ **(b)** $C_{\mathbf{xx}}$ with shift distance $(1 - \mathbf{x})$
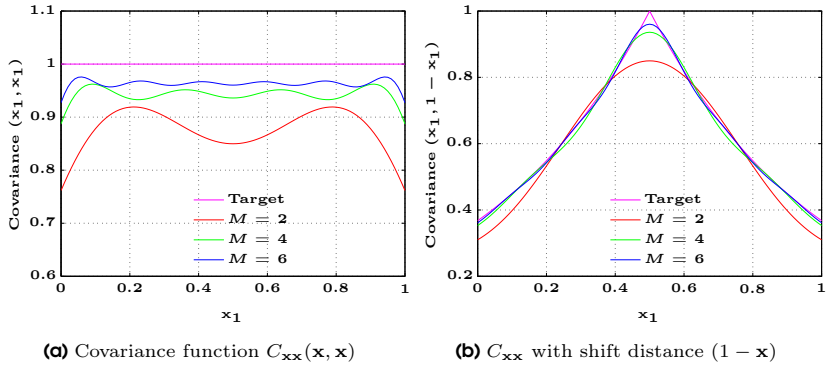
Figure 6.2.: (a) Comparison of the covariance for different dimensions M. (b) Covariance with a shift distance representation in the one-dimensional case for different dimensions M.

and the eigenfunctions $f_i(\mathbf{x}, \mathbf{y})$ are computed by

$$f_i(\mathbf{x}, \mathbf{y}) = f_{i_{\mathbf{x}}}(\mathbf{x}) f_{i_{\mathbf{y}}}(\mathbf{y}). \tag{6.48}$$

Here, the superscript $\bullet^{1D}$ indicates the one-dimensional solution of the eigenvalues and eigenfunctions.

Two-Dimensional Example

Let $\mathcal{D} = [0, a] \times [0, b]$ be a domain in $\mathbb{R}^2$ with edge lengths $a = 1$ and $b = 1$. The covariance function defined in equation (6.29) has the coordinates $(\mathbf{x}_1, \mathbf{y}_1)$, $(\mathbf{y}_1, \mathbf{y}_2) \in \mathcal{D}$ and the correlation lengths are $c_{\mathbf{x}} = c_{\mathbf{y}} = 1$. The two-dimensional KLE, truncated after the first six terms and reads

$$\hat{H}_\alpha(\mathbf{x}, \mathbf{y}, \theta) \approx \sigma_\alpha \sum_{i=1}^{6} \sqrt{\lambda_i} f_i(\mathbf{x}, \mathbf{y}) \xi_i(\theta). \tag{6.49}$$

The first six eigenfunctions $f_i(\mathbf{x}, \mathbf{y})$ are computed by

$$f_1(\mathbf{x}, \mathbf{y}) = 1.1502 \cos(1.3065\mathbf{x}) \cos(1.3065\mathbf{y})$$
$$f_2(\mathbf{x}, \mathbf{y}) = 1.4218 \sin(3.6732\mathbf{x}) \cos(1.3065\mathbf{y})$$
$$f_3(\mathbf{x}, \mathbf{y}) = 1.4218 \cos(1.3065\mathbf{x}) \sin(3.6732\mathbf{y})$$
$$f_4(\mathbf{x}, \mathbf{y}) = 1.4837 \sin(6.5846\mathbf{x}) \cos(1.3065\mathbf{y})$$
$$f_5(\mathbf{x}, \mathbf{y}) = 1.4837 \cos(1.3065\mathbf{x}) \sin(6.5846\mathbf{y})$$
$$f_6(\mathbf{x}, \mathbf{y}) = 1.7575 \sin(3.6732\mathbf{x}) \sin(3.6732\mathbf{y})$$

(a) Covariance function $C_{\mathbf{xx}}(\mathbf{x}, \mathbf{x})$ **(b)** $C_{\mathbf{xx}}$ with shift distance $(1 - \mathbf{x})$
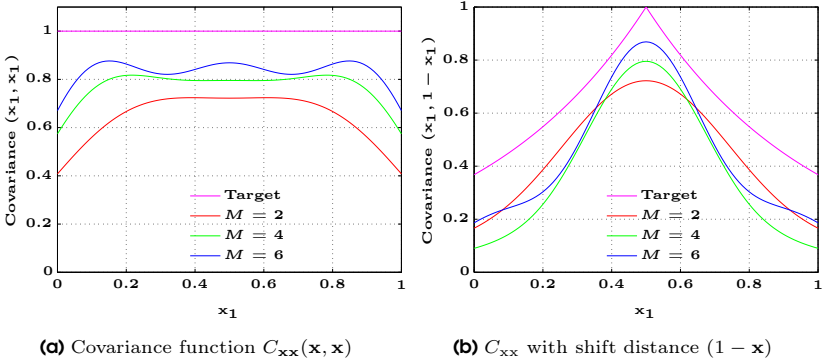
Figure 6.3.: (a) Comparison of the covariance for different dimensions M. (b) Covariance with a shift distance representation in the two-dimensional case for different dimensions M.

with the associated eigenvalues λ_i

$$\lambda_1 = 0.5458, \qquad \lambda_2 = 0.1020, \qquad \lambda_3 = 0.1020,$$
$$\lambda_4 = 0.0333, \qquad \lambda_5 = 0.0333, \qquad \lambda_6 = 0.0190 \,.$$

The resulting curves for the variance and the covariance profiles are depicted in Fig. 6.3. Plotted are the target curve, the two-, four- and the six-term KLE. The corresponding equations for the curves are given by, cf. Anders [2000],

$$\text{Cov}(\mathbf{x}, \mathbf{x}) = \hat{H}_\alpha \left(-\frac{1}{2}(a, b) + \mathbf{x}(a, b), -\frac{1}{2}(a, b) + \mathbf{x}(a, b) \right) , \tag{6.50}$$

$$\text{Cov}(\mathbf{x}, 1 - \mathbf{x}) = \hat{H}_\alpha \left(-\frac{1}{2}(a, b) + \mathbf{x}(a, b), -\frac{1}{2}(a, b) + (1 - \mathbf{x})(a, b) \right) , \tag{6.51}$$

where $\mathbf{x} \in [0, 1]$ and the standard deviation σ_α in each direction is assumed to $\sigma_\alpha = 1$.

Three-Dimensional Case

The extension of the KLE to three-dimensional random fields has been established in a manner analogous to the two-dimensional case. To be more specific, the eigenvalues and eigenfunctions of the one-dimensional solutions are multiplied with each other.

Let $\mathcal{D}$ be a domain in $\mathbb{R}^3$ which is defined by a hexahedron with the edge lengths

$$\mathcal{D} = [-a, a] \times [-b, b] \times [-c, c]$$

and the corresponding eigenvalue problem is given by

$$
\int\limits_{-a}^{a} \int\limits_{-b}^{b} \int\limits_{-c}^{c} C(\mathbf{x}_1, \mathbf{y}_1, \mathbf{z}_1; \mathbf{x}_2, \mathbf{y}_2, \mathbf{z}_2) f_i(\mathbf{x}_2, \mathbf{y}_2, \mathbf{z}_2) \, \mathrm{d}\mathcal{D}_{\mathbf{x}_2} \mathrm{d}\mathcal{D}_{\mathbf{y}_2} \mathrm{d}\mathcal{D}_{\mathbf{z}_2}
$$
$$
= \lambda_i f_i(\mathbf{x}_1, \mathbf{y}_1, \mathbf{z}_1) \, .
$$

(6.52)

Substituting the three-dimensional covariance kernel (6.30) into equation (6.52) leads to the solution of the corresponding eigenvalue problem, which is, for simplicity reasons, split into the three one-dimensional solutions as follows:

$$
\int\limits_{-a}^{a} e^{-\frac{|\mathbf{x}_1 - \mathbf{x}_2|}{c_{\mathbf{x}}}} f_{i_{\mathbf{x}}}(\mathbf{y}) \, \mathrm{d}\mathcal{D}_{\mathbf{x}_2} = \lambda_{i_{\mathbf{x}}} f_{i_{\mathbf{x}}}(\mathbf{x}_1) \, ,
$$

(6.53a)

$$
\int\limits_{-b}^{b} e^{-\frac{|\mathbf{y}_1 - \mathbf{y}_2|}{c_{\mathbf{y}}}} f_{i_{\mathbf{y}}}(\mathbf{y}_2) \, \mathrm{d}\mathcal{D}_{\mathbf{y}_2} = \lambda_{i_{\mathbf{y}}} f_{i_{\mathbf{y}}}(\mathbf{y}_1) \, ,
$$

(6.53b)

$$
\int\limits_{-c}^{c} e^{-\frac{|\mathbf{z}_1 - \mathbf{z}_2|}{c_{\mathbf{z}}}} f_{i_{\mathbf{z}}}(\mathbf{z}_2) \, \mathrm{d}\mathcal{D}_{\mathbf{z}_2} = \lambda_{i_{\mathbf{z}}} f_{i_{\mathbf{z}}}(\mathbf{z}_1) \, .
$$

(6.53c)

Similarly to the two-dimensional case, the resulting eigenvalues λ_i are products of the one-dimensional solutions, i.e.

$$
\lambda_i = \lambda_{i_{\mathbf{x}}}^{1D} \lambda_{i_{\mathbf{y}}}^{1D} \lambda_{i_{\mathbf{z}}}^{1D} \, ,
$$

(6.54)

and for the eigenfunctions $f(\mathbf{x}, \mathbf{y}, \mathbf{z})$ the procedure is analogously, i.e.

$$
f_i(\mathbf{x}, \mathbf{y}, \mathbf{z}) = f_{i_{\mathbf{x}}}(\mathbf{x}) f_{i_{\mathbf{y}}}(\mathbf{y}) f_{i_{\mathbf{z}}}(\mathbf{z}) \, .
$$

(6.55)

Three-Dimensional Example

Let $\mathcal{D}$ be a domain in $\mathbb{R}^3$ with the dimensions $[0, a] \times [0, b] \times [0, c]$, with $a = b = c = 1$. The covariance function has the properties $(\mathbf{x}_1, \mathbf{y}_1, \mathbf{z}_1)$, $(\mathbf{x}_2, \mathbf{y}_2, \mathbf{z}_2) \in \mathcal{D}$ and the correlation length is $c_{\mathbf{x}} = c_{\mathbf{y}} = c_{\mathbf{z}} = 1$. The corresponding approximation of the random field, truncated after the first six terms reads

$$
\hat{H}_\alpha(\mathbf{x}, \mathbf{y}, \mathbf{z}, \theta) \approx \sigma_\alpha \sum_{i=1}^{6} \sqrt{\lambda_i} f_i(\mathbf{x}, \mathbf{y}, \mathbf{z}) \xi_i(\theta) \, ,
$$

(6.56)

with the corresponding eigenfunctions $f_i(\mathbf{x}, \mathbf{y}, \mathbf{z})$, given on the next page.

$$f_1(\mathbf{x}, \mathbf{y}, \mathbf{z}) = 1.2336 \cos(1.3065\mathbf{x}) \cos(1.3065\mathbf{y}) \cos(1.3065\mathbf{z})$$
$$f_2(\mathbf{x}, \mathbf{y}, \mathbf{z}) = 1.5249 \sin(3.6732\mathbf{x}) \cos(1.3065\mathbf{y}) \cos(1.3065\mathbf{z})$$
$$f_3(\mathbf{x}, \mathbf{y}, \mathbf{z}) = 1.5249 \cos(1.3065\mathbf{x}) \sin(3.6732\mathbf{y}) \cos(1.3065\mathbf{z})$$
$$f_4(\mathbf{x}, \mathbf{y}, \mathbf{z}) = 1.5249 \cos(1.3065\mathbf{x}) \cos(1.3065\mathbf{y}) \sin(3.6732\mathbf{z})$$
$$f_5(\mathbf{x}, \mathbf{y}, \mathbf{z}) = 1.5913 \cos(6.5846\mathbf{x}) \cos(1.3065\mathbf{y}) \cos(1.3065\mathbf{z})$$
$$f_6(\mathbf{x}, \mathbf{y}, \mathbf{z}) = 1.5913 \cos(1.3065\mathbf{x}) \cos(6.5846\mathbf{y}) \cos(1.3065\mathbf{z})$$

and the associated eigenvalues λ_i are determined as

$$\lambda_1 = 0.4032, \qquad \lambda_2 = 0.0753, \qquad \lambda_3 = 0.0753,$$
$$\lambda_4 = 0.0753, \qquad \lambda_5 = 0.0246, \qquad \lambda_6 = 0.0246.$$

The resulting curves for the variance and the covariance profiles are depicted in Fig. 6.4, where the target curve, the two-, four- and the six-term KLE are illustrated. The corresponding equations for the curves are defined by, cf. Anders [2000],

$$\text{Cov}(\mathbf{x}, \mathbf{x}) = \hat{H}_\alpha \left(-\frac{1}{2}(a, b, c) + \mathbf{x}(a, b, c), -\frac{1}{2}(a, b, c) + \mathbf{x}(a, b, d) \right), \qquad (6.57)$$

$$\text{Cov}(\mathbf{x}, 1 - \mathbf{x}) = \hat{H}_\alpha \left(-\frac{1}{2}(a, b, c) + \mathbf{x}(a, b, c), -\frac{1}{2}(a, b, c) + (1 - \mathbf{x})(a, b, c) \right) \qquad (6.58)$$

where $\mathbf{x} \in [0, 1]$ and the standard deviation σ_α in each direction is assumed to $\sigma_\alpha = 1$.

(a) Covariance function $C_{\mathbf{xx}}(\mathbf{x}, \mathbf{x})$ **(b)** $C_{\mathbf{xx}}$ with shift distance $(1 - \mathbf{x})$
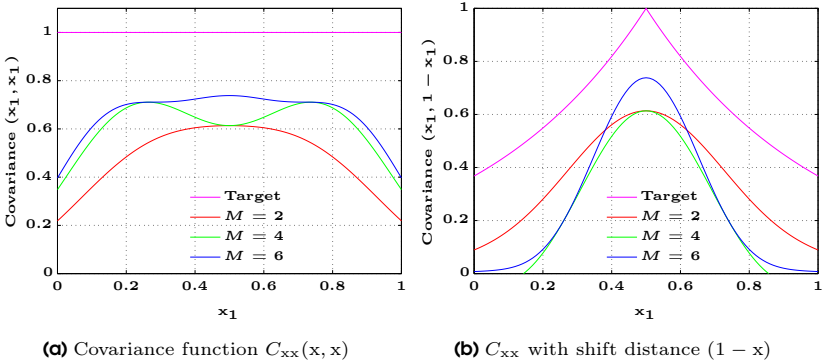
Figure 6.4.: (a) Comparison of the covariance for different dimensions M. (b) Covariance with a shift distance representation in the three-dimensional case for different dimensions M.

Concluding Remarks

From the results displayed on the left hand side in Figs. 6.2−6.4, it is obvious that the variance is fluctuating with regard to the spatial coordinate x and the error at the boundaries of the domain $\mathcal{D}$ is larger compared to that of the middle region. Furthermore, it can be noticed that the convergence to the target value ($\sigma^2 = 1$) is faster for the one-dimensional case than for the two- and three-dimensional cases, because the solution for the multi-dimensional case are products of the solutions of the one-dimensional case, as can be seen when considering equations (6.48) and (6.55). The graphs on the right hand side in Figs. 6.2−6.4 show the cross-section of the covariance function. From these plots it is obvious that the KLE comes closer to the target curve by an increasing M. Furthermore, it should be remarked that the number of dimensions of M, which are applied in this work, corresponds to the number of terms that are used in most applications in the literature, for instance, Sudret and der Kiureghian [2000] or Ghanem and Spanos [2003]. This is also a reasonable choice in this work, because the material properties of steel, which are exclusively used in this work, varies smoothly at the interesting scales and these variations can be sufficiently capture by a moderat number of M. For a detailed discussion of the convergence properties, the truncation order should have at least $M = 20$ and more terms, see e.g., Stefanou and Papadrakakis [2007] where a detailed assessment of the KLE is presented. It is emphasized that this applies only for the KLE alone. When the KLE is used for the characterization of random input parameters in the framework of SSFEM[3], the dimension M should be small, because the resulting polynomial basis P increases drastically with increasing M. A detailed discussion on the polynomial chaos will be given in the next chapter.

6.3.2. Numerical Solution of the Integral Equation

As already remarked in the previous subsection, analytical solutions for the Fredholm integral equation (6.20) are only available for a few autocovariance functions and simple geometries. Closed form solutions for exponential and triangular covariance functions for one-dimensional homogeneous fields are given in Spanos and Ghanem [1989] and Ghanem and Spanos [2003]. Except for these particular examples the Fredholm integral equation has to be solved numerically. A widely used strategy is the approximation of the eigenfunctions $\{f_k(\mathbf{x})\}_{k=1}^{\infty}$ by a combination of basis functions $h_i(\mathbf{x})$. For the choice of the basis different approaches are available, which are listed below:

- Piecewise polynomials used by Ghanem and Spanos [2003],

- orthogonal Legendre polynomials used by Zhang and Ellingwood [1994] and

- wavelets used by Phoon et al. [2004].

In this work, the approach, presented by Ghanem and Spanos [2003] is pursued. They developed a Galerkin-type procedure for numerical solutions and illustrated this approach through its application to a two-dimensional curved geometry. This formulation will be presented below (for the sake of clarity) for the one-dimensional case. Similar derivations of the numerical solution can be also found in Sudret and der Kiureghian [2000]; Ghanem and Spanos [2003]; Le Maître and Knio [2010].

---

[3]SSFEM: **S**pectral **S**tochastic **F**inite **E**lement **M**ethod. For a detailed discussion see chapter 8.

Let $h_i(\mathbf{x})$ be a complete set of functions in the Hilbert space $\mathcal{L}^2(\mathcal{D})$. It is possible to write the eigenfunctions of the covariance function $C(\mathbf{x}_1, \mathbf{x}_2)$ as a linear combination of the interpolation functions $\{h_i(\mathbf{x})\}_{i=1}^{\infty}$ as follows, cf. Ghanem and Spanos [2003]:

$$f_k(\mathbf{x}) = \sum_{i=1}^{\infty} d_i^k h_i(\mathbf{x}), \tag{6.59}$$

where the coefficients $\{d_i^k\}_{i=1}^{\infty}$ are the unknown nodal values of the eigenfunctions of the k-th element. Truncating equation (6.59) after the N-th term, and substituting it afterwards into equation (6.20) gives the residual, cf. Ghanem and Spanos [2003],

$$\epsilon_N(\mathbf{x}) = \sum_{i=1}^{N} d_i^k \left[\int_{\mathcal{D}} C(\mathbf{x}_1, \mathbf{x}_2) h_i(\mathbf{x}_2) \, d\mathcal{D}_{\mathbf{x}_2} - \lambda_k h_i(\mathbf{x}_1) \right]. \tag{6.60}$$

Requiring that the truncated series being the projection of $f_k(\cdot)$ onto the space $\mathcal{H}_N$, spanned by the set $\{h_i(\cdot), i = 1, 2, \ldots N\}$ implies that ϵ_M is orthogonal to $\mathcal{H}_N$ in $\mathcal{L}^2(\mathcal{D})$. With this at hand and with respect to the inner product (6.3), the following expression is obtained, cf. Sudret and der Kiureghian [2000]:

$$\langle \epsilon_N, h_j(\mathbf{x}) \rangle = \int_{\mathcal{D}} \epsilon_N(\mathbf{x}) h_j(\mathbf{x}) \, d\mathcal{D}_{\mathbf{x}_1} = 0, \quad j = 1, 2, \ldots N. \tag{6.61}$$

Substituting (6.60) into equation (6.61) and after some rearrangement leads to

$$\sum_{i=1}^{N} d_i^k \left[\int_{\mathcal{D}} \left[\int_{\mathcal{D}} C(\mathbf{x}_1, \mathbf{x}_2) h_i(\mathbf{x}_2) d\mathcal{D}_{\mathbf{x}_2} \right] h_j(\mathbf{x}_1) \, d\mathcal{D}_{\mathbf{x}_1} - \lambda_k \int_{\mathcal{D}} h_i(\mathbf{x}) h_j(\mathbf{x}) \, d\mathcal{D}_{\mathbf{x}_1} \right] = 0, \tag{6.62}$$

which finally results in the generalized algebraic eigenvalue problem

$$\mathbf{W} \, \mathbf{D} = \mathbf{\Lambda} \, \mathbf{A} \, \mathbf{D}. \tag{6.63}$$

This linear system may be solved for the matrix $\mathbf{D}$ and the eigenvalues $\{\lambda_i\}_{i=1}^{N}$, where the individual matrices are given by

$$\mathbf{A}_{ij} = \int_{\mathcal{D}} h_i(\mathbf{x}) h_j(\mathbf{x}) \, d\mathcal{D}_{\mathbf{x}_1}, \tag{6.64}$$

$$\mathbf{W}_{ij} = \int_{\mathcal{D}} \int_{\mathcal{D}} C(\mathbf{x}_1, \mathbf{x}_2) h_i(\mathbf{x}_1) h_j(\mathbf{x}_2) \, d\mathcal{D}_{\mathbf{x}_1} d\mathcal{D}_{\mathbf{x}_2}, \tag{6.65}$$

$$\mathbf{D}_{ij} = d_i^k, \tag{6.66}$$

$$\Lambda_{ij} = \delta_{ij} \lambda_j. \tag{6.67}$$

This solution scheme can be implemented using the FE-mesh shape functions as the basis set $\{h_i(\cdot)\}$ and $\{h_j(\cdot)\}$. The eigenvalues $\{\lambda_i\}_{i=1}^{N}$ are the diagonal elements of the matrix Λ and the set of eigenfunctions $\{f_k(\mathbf{x})\}_{k=1}^{N}$ of the covariance function are

obtained by substituting the solutions of the matrix $\mathbf{D}$ back into equation (6.59). Based on the correlation structure over the hole domain the matrix $\mathbf{W}$ is a dense matrix whereas the matrix $\mathbf{A}$ is usually sparse and both matrices are positive definite.

In general, by a KLE other than by a classical eigenvalue calculation the highest eigenvalues are sought, because the highest eigenfunctions represents the longest wavelengths. For smaller eigenvalues the associated eigenfunctions are short waves. The precision of the approximation for the eigenvalues decreases with smaller eigenvalues, because the fluctuation of the associated eigenvalues are on higher frequency over the domain and with linear shape functions are no longer satisfactory mappable. Hence only a few solutions of equation (6.63) should be used for the representation of the random field since there is a risk of tampering by the solution with small eigenvalues. In view of the representation of material properties, a higher number of random variables ξ_i captures higher frequency random fluctuations, whereas a few random variables should only be used for the approximation of slow varying material properties. In addition, for a good representation of the correlation structure, especially for small correlation lengths, the FE-discretization must be fine.

6.3.3. Example for the Numerical Solution of the Integral Equation

In this subsection, the analytical and the numerical KLE are compared by using a Gaussian homogeneous random field with zero mean and unit variance where the investigated domains are shown in Fig. 6.5. The two-dimensional FE models are discretized using shell elements with piecewise linear shape functions and the three-dimensional FE models are discretized with brick elements using piecewise linear shape functions. In the table below, the investigated FE models, with their number of elements and degrees of freedom (d.o.f.), are summarized.

Table 6.1.: Number of elements and degrees of freedom of the investigated FE models.

Dimension of the domain $\mathcal{D}$	Number of Elements	Degrees of Freedom
Plate with a coarse mesh	16	50
Plate with a fine mesh	1600	≈ 3360
Cube with a coarse mesh	64	375
Cube with a fine mesh	2197	≈ 8230

The applied covariance functions are given by equations (6.29) and (6.30), where for each case different correlation lengths $c = 0.01, 0.1, 1.0, 10$ are applied to show the influence of the scale of correlation, on the quality of the solution of the eigenvalues. Note, that the correlation lengths in each direction are identical, i.e. $c_x = c_y = c_z = 1.0$ or $c_x = c_y = c_z = 10$ etc. The exact eigenvalues are calculated by solving the Fredholm integral equation (6.20) with respect to the dimension, i.e. two- or three-dimensional and the numerical values are computed by evaluating equation (6.63). As already mentioned in subsection 6.3.2 one limit of the correlation length is zero, i.e. the covariance function takes the form of a delta function, as depicted in Fig. 6.1 (a). In this case, the eigenvalues remain constant, as can be seen in Figs. 6.6 and 6.7, where this case is illustrated by the straight lines. The other limit is the completely correlated field, i.e. the correlation length is infinite. Here, only the first eigenvalue is non-zero and the remaining eigenvalues are very small in comparison to the first eigenvalue. The strong decrease of the eigenvalues in this
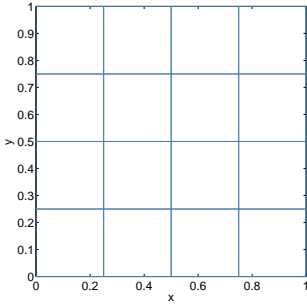
(a) Plate with 16 elements
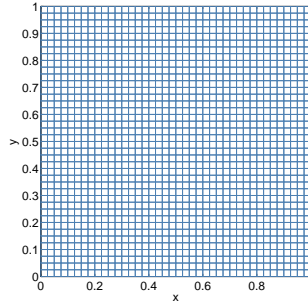
(b) Plate with 1600 elements
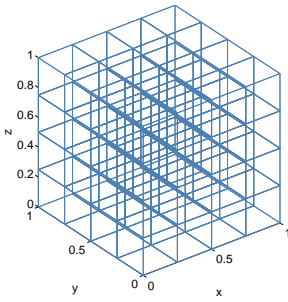
(c) Cube with 64 elements
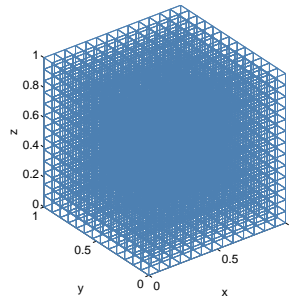
(d) Cube with 2197 elements

Figure 6.5.: Investigated FE models.
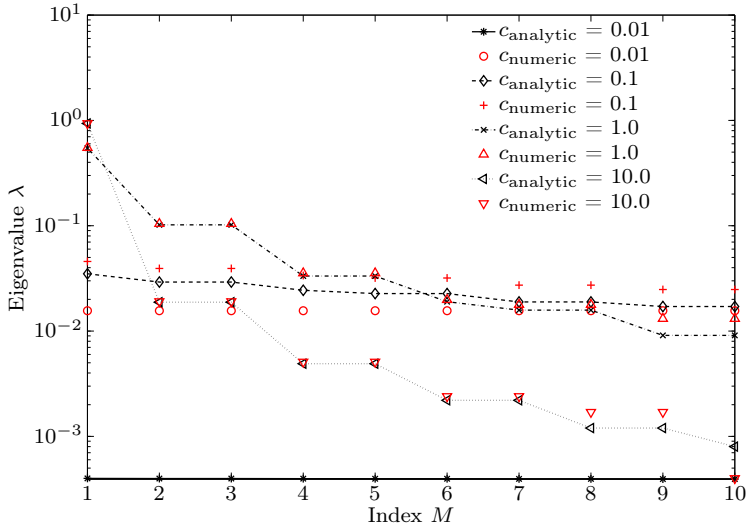
(a) Eigenvalue λ_M of the two-dimensional covariance function using the coarse mesh
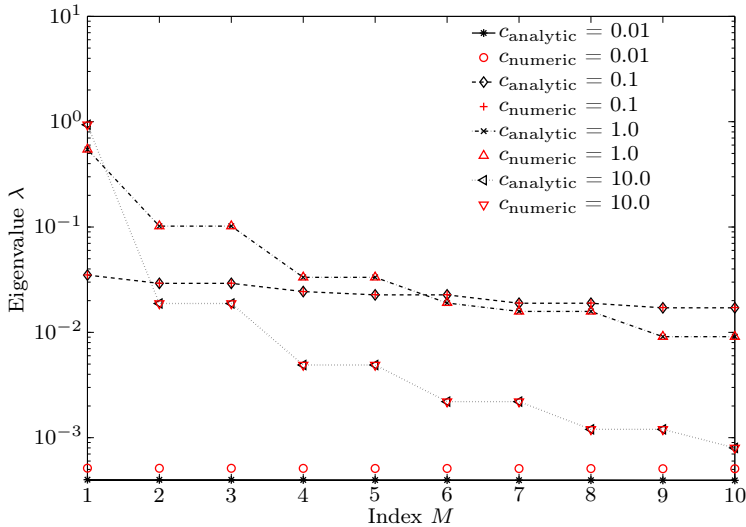
(b) Eigenvalue λ_M of the two-dimensional covariance function using the fine mesh

Figure 6.6.: Exact and approximate Eigenvalues λ_M of the covariance function given by equation (6.29), $M = 1, \ldots 10$ and using different correlation lengths c.
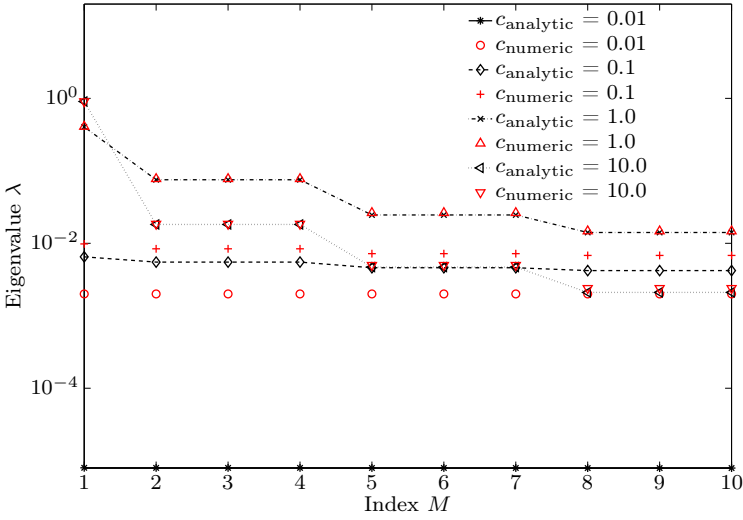
(a) Eigenvalue λ_M of the three-dimensional covariance function using the coarse mesh
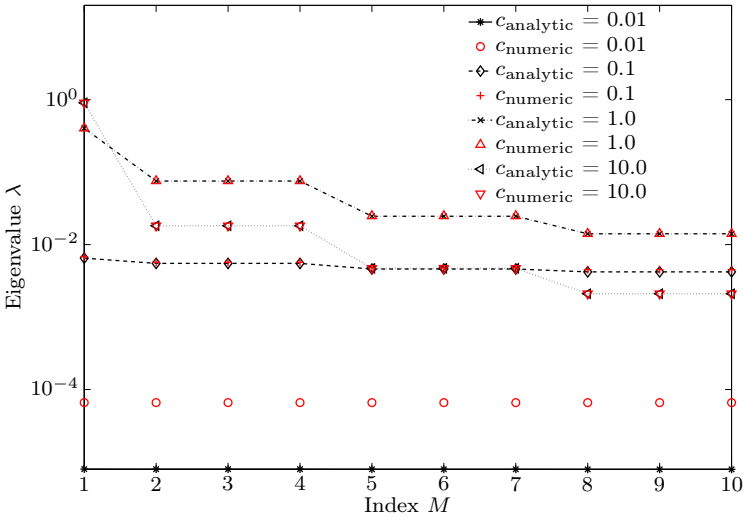
(b) Eigenvalue λ_M of the three-dimensional covariance function using the fine mesh

Figure 6.7.: Exact and approximate Eigenvalues λ_M of the covariance function given by equation (6.30), $M = 1, \ldots 10$ and using different correlation lengths c.

Table 6.2.: Computational time for the numerical solution of the eigenvalues.

Dimension of the domain $\mathcal{D}$	Computational time in sec.
Plate with a coarse mesh	< 1 sec.
Plate with a fine mesh	≈ 8000 sec.
Cube with a coarse mesh	≈ 30 sec.
Cube with a fine mesh	≈ 74500 sec.

case can is illustrated by the dotted lines in Figs. 6.6 and 6.7. Moreover, the results in these figures show the generally good match between the analytical (lines) and numerical evaluation (only markers) of the eigenvalues, whereas the large discrepancy by applying a small correlation length of $c = 0.01$ is also obvious in these figures. The similarities/deviations of the results can be seen very good in Figs. 6.8 and 6.9, where the relative errors

$$\epsilon_\lambda = \frac{c_{\text{numeric}} - c_{\text{analytic}}}{c_{\text{analytic}}} \cdot 100\% \,, \tag{6.68}$$

of the analytical and the corresponding numerical evaluation of the eigenvalues are shown. Theoretically, the numerical and analytical eigenvalues are identical if an infinite small interval for the FE discretization is used. However, in practical applications the computational costs for the realization of such a fine discretization for the mechanical structure as well as for the random field realization are disproportional, which becomes clear when comparing the computation times[4] for the determination of the eigenvalues in Tab. 6.2.

Concluding Remarks

With the numerical investigations in this subsection, an important property of the KLE has been demonstrated, namely the influce of the correlation length on the accuracy of the solution of the eigenvalues. For a given covariance function the decay rate of the eigenvalues depends inversely on the correlation length. For instance, a long correlation length implies that the field is strongly correlated and the eigenvalues drops faster. The limit of this, the infinite correlation length, is the fully correlated field where the eigenvalues decay to zero immediately. On the other hand, a weakly correlated field has a short correlation length, where the decay of the eigenvalues is slow. Here is the limit the uncorrelated field, i.e. where the correlation length is zero. In this case, the eigenvalues have no eigenvalue decay, i.e. are being constant. Finally, regarding to the solution time of the two- and three-dimensional calculation of the eigenvalues, which are reported in Tab. 6.2. From this listing, it is obvious that the fine discretizations requires drastically more computation time than the coarse meshes by no significantly improving results.

---

[4]All computations are performed on a Intel Xeon server with 32 Intel Xeon E5-2680 processors, each of them with 2,7 GHz and a total memory of 256 GB.
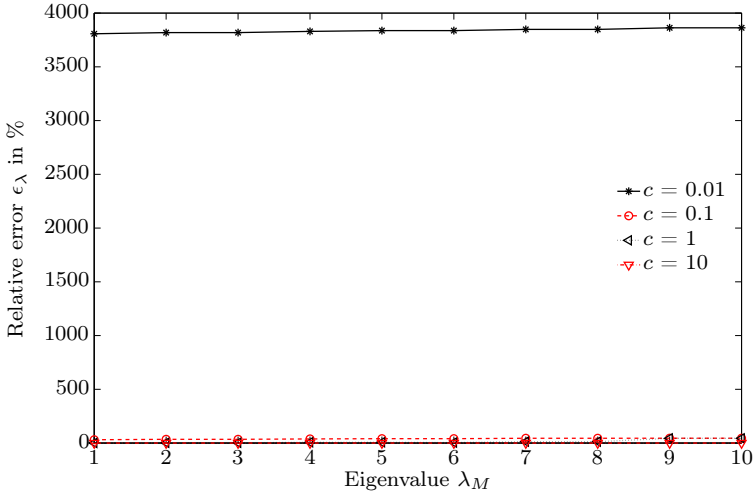
(a) Relative error ϵ_λ of the eigenvalues using the two-dimensional coarse mesh
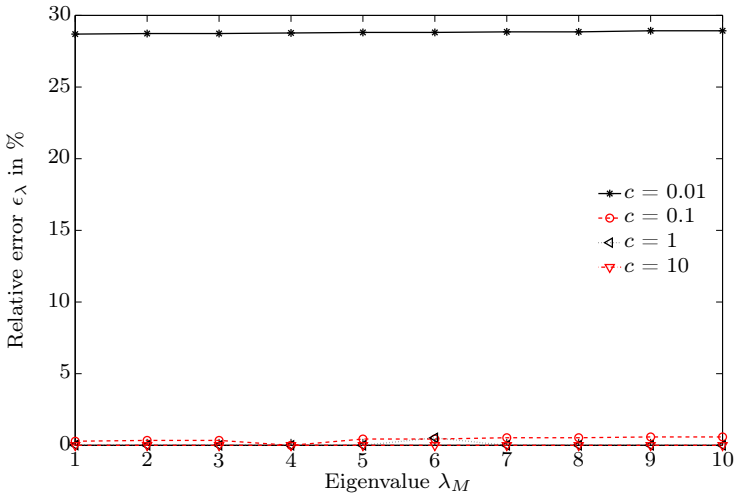
(b) Relative error ϵ_λ of the eigenvalues by using the two-dimensional fine mesh

Figure 6.8.: Relative error ϵ_λ of the eigenvalues using different correlation lengths c for the two-dimensional plate.
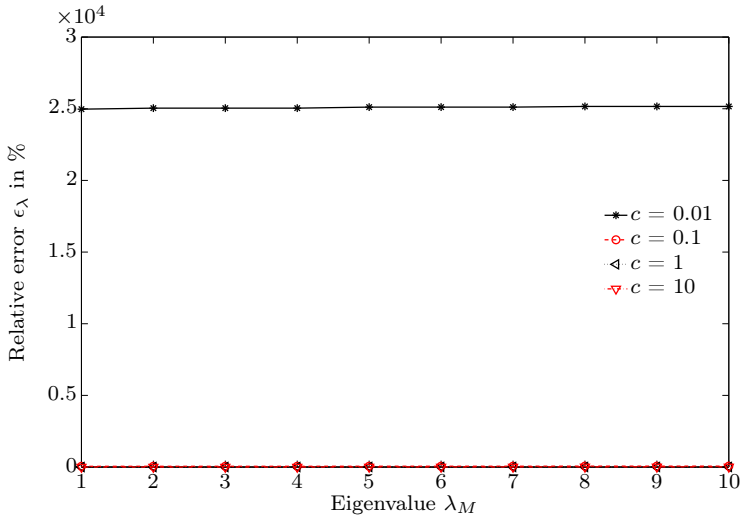
(a) Relative error ϵ_λ of the eigenvalues using the three-dimensional coarse mesh
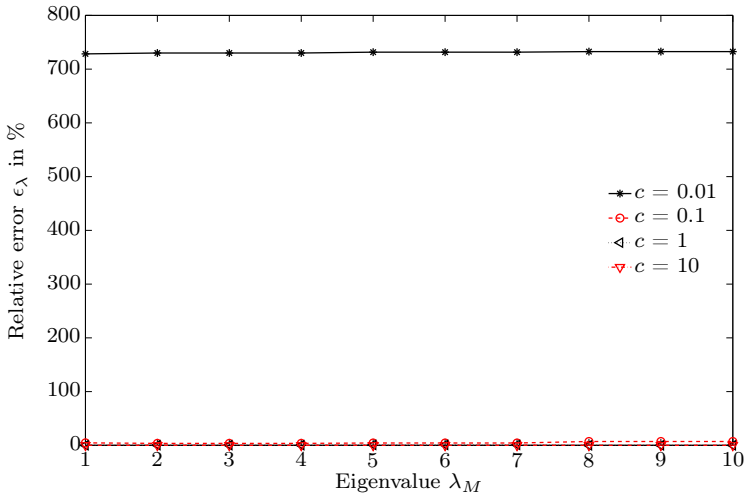
(b) Relative error ϵ_λ of the eigenvalues by using the three-dimensional fine mesh

Figure 6.9.: Relative error ϵ_λ of the eigenvalues using different correlation lengths c for the three-dimensional cube.

6.4. Spectral Representation Method

The *Spectral Representation Method* is a further method that is commonly applied for the representation of Gaussian stochastic fields. The generation of sample functions for stochastic fields, which describe the random parameters of the underlying system, can also be done by using the spectral representation theorem. Shinozuka and Deodatis [1991] show that sample functions produced by the spectral representation theorem are not ergodic. They provide an alternative formulation which generates sample functions by a cosine series formula of the SPRM and shows that this formulation results in ergodic sample functions. Besides the KLE this formulation seems simultaneously the most applied one in engineering applications for the representation of random properties. This method is also applied in this thesis for the analysis of elastic-plastic problems with respect to random material parameters.

Numerous papers dealing with simulations of random processes / fields have been published in the last four decades. Apart from the cited publications in the subsection 5.3.1 here are some publications listed which deal with uncertain material and geometry properties. These are: Shinozuka and Lenoe [1976]; Shinozuka and Deodatis [1996]; Stefanou and Papadrakakis [2004]. One of the first publications which deals with the representation of uncertain material parameters is the article, presented by Shinozuka and Lenoe [1976]. An extended formulation of stochastic fields realized by the SPRM can be found in Shinozuka and Deodatis [1996] where the simulation of multi-dimensional *univariate* Gaussian fields are presented and a specific application can be found in Stefanou and Papadrakakis [2004]. Here, the SPRM is applied to represent material and geometrical uncertainties of shells by uncorrelated two-dimensional stochastic fields. The SPRM is well suited in the context of the Monte Carlo simulation technique whereas the application of parallel computing is straight forward.

In the following subsections the methodology of the SPRM is presented for two-dimensional and three-dimensional random fields. The theoretical contexts are essentially a summary of the article proposed by Shinozuka and Deodatis [1996]. It should be remarked that the Fast Fourier Transform (FFT) version, cf. Shinozuka and Deodatis [1991, 1996], is not applied in this thesis, because the values of the stochastic field are needed at non-uniformly spaced points. Finally, the generation of random fields with multivariate variables, cf. Deodatis [1996b, 1997], is also not being considered here, because all random parameters are assumed to be independent from each other.

6.4.1. Simulation of 2-D Univariate Homogeneous Stochastic Fields

Let $H_S(\mathbf{x}, \mathbf{y}, \theta)$ be a two-dimensional univariate (2D-1V) homogeneous real valued stochastic field with mean value equal to zero and bi-quadrant power spectral density function $S_{H_S H_S}(\omega_{\mathrm{x}}, \omega_{\mathrm{y}})$. The corresponding spectral representation of the random field reads, cf. Shinozuka and Deodatis [1996]:

$$
\begin{aligned}
H_S(\mathbf{x}, \mathbf{y}, \theta) = \int_{-\infty}^{\infty} \int_{0}^{\infty} & [\cos(\kappa_{\mathrm{x}} \mathbf{x} + \kappa_{\mathrm{y}} \mathbf{y}) \, \mathrm{d}u(\kappa_{\mathrm{x}}, \kappa_{\mathrm{y}}) \\
& + \sin(\kappa_{\mathrm{x}} \mathbf{x} + \kappa_{\mathrm{y}} \mathbf{y}) \, \mathrm{d}\nu(\kappa_{\mathrm{x}}, \kappa_{\mathrm{y}})] \; .
\end{aligned}
\tag{6.69}
$$

The parameters $du(\kappa_x, \kappa_y)$ and $d\nu(\kappa_x, \kappa_y)$ are the orthogonal increments of the independent real valued random fields $u(\kappa_x, \kappa_y)$ and $\nu(\kappa_x, \kappa_y)$ where both have a mean value equal to zero and the requirements

$$\mathbb{E}\left[u(\kappa_x, \kappa_y)\right] = \mathbb{E}\left[\nu(\kappa_x, \kappa_y)\right] = 0, \tag{6.70}$$

$$\mathbb{E}\left[du(\kappa_x, \kappa_y)\right] = \mathbb{E}\left[d\nu(\kappa_x, \kappa_y)\right] = 0, \tag{6.71}$$

must be satisfied by each random field of this kind. The power spectral density function $S_{H_S H_S}(\kappa_x, \kappa_y)$ and the autocovariance function $C_{H_S H_S}(\tau_x, \tau_y)$ constitute the two-dimensional Wiener-Khintchine[5] transform pair

$$S_{H_S H_S}(\kappa_x, \kappa_y) = \frac{1}{(2\pi)^2} \int\limits_{-\infty}^{\infty} \int\limits_{-\infty}^{\infty} C_{H_S H_S}(\tau_x, \tau_y) e^{-i(\kappa_x \tau_x + \kappa_y \tau_y)}\, d\tau_x d\tau_y, \tag{6.72}$$

$$C_{H_S H_S}(\tau_x, \tau_y) = \int\limits_{-\infty}^{\infty} \int\limits_{-\infty}^{\infty} S_{H_S H_S}(\kappa_x, \kappa_y) e^{i(\kappa_x \tau_x + \kappa_y \tau_y)}\, d\kappa_x d\kappa_y, \tag{6.73}$$

where τ_x and τ_y are the separation distances along the x and y axes, respectively, and κ_x, κ_y are the corresponding wave numbers. After some algebraic manipulations, see Shinozuka and Deodatis [1996], equation (6.69) can be rewritten as

$$H_S(\mathbf{x}, \mathbf{y}, \theta) = \sqrt{2} \sum_{n_x=0}^{\infty} \sum_{n_y=0}^{\infty}$$

$$\left\{ \sqrt{2 S_{H_S H_S}(\kappa_{x_{n_x}}, \kappa_{y_{n_y}}) \Delta\kappa_x \Delta\kappa_y} \cos\left(\kappa_{x_{n_x}} \mathbf{x} + \kappa_{y_{n_y}} \mathbf{y} + \Phi^{(1)}_{n_x n_y}(\theta)\right)\right\} + \tag{6.74}$$

$$\left\{ \sqrt{2 S_{H_S H_S}(\kappa_{x_{n_x}}, -\kappa_{y_{n_y}}) \Delta\kappa_x \Delta\kappa_y} \cos\left(\kappa_{x_{n_x}} \mathbf{x} - \kappa_{y_{n_y}} \mathbf{y} + \Phi^{(2)}_{n_x n_y}(\theta)\right)\right\}.$$

Here, $\Phi^{(1)}_{n_x n_y}(\theta)$ and $\Phi^{(2)}_{n_x n_y}(\theta)$ are two different sets of random phase angles, which are uniformly distributed in the range $[0, 2\pi]$. By making use of the symmetry properties

$$\begin{aligned} C_{H_S H_S}(\tau_x, \tau_y) &= C_{H_S H_S}(-\tau_x, -\tau_y), \\ S_{H_S H_S}(\kappa_x, \kappa_y) &= S_{H_S H_S}(-\kappa_x, -\kappa_y), \end{aligned} \tag{6.75}$$

and truncating the infinite series in equation (6.74) after a finite number the following formulation is obtained, Shinozuka and Deodatis [1996]:

$$\hat{H}_S(\mathbf{x}, \mathbf{y}, \theta) =$$

$$\sqrt{2} \sum_{n_x=0}^{N_x-1} \sum_{n_y=0}^{N_y-1} \left[A_{n_x n_y} \cos\left(\kappa_{x_{n_x}} \mathbf{x} + \kappa_{y_{n_y}} \mathbf{y} + \Phi^{(1)}_{n_x n_y}(\theta)\right) \right. \tag{6.76}$$

$$\left. + \tilde{A}_{n_x n_y} \cos\left(\kappa_{x_{n_x}} \mathbf{x} - \kappa_{y_{n_y}} \mathbf{y} + \Phi^{(2)}_{n_x n_y}(\theta)\right) \right],$$

---

[5] See also Appendix D

where the $\hat{\bullet}$ denotes the discretized formulation of the random field. The parameters in equation (6.76) are given by

$$A_{n_x n_y} = \sqrt{2 S_{\hat{H}_S \hat{H}_S}(\kappa_{x_{n_x}}, \kappa_{y_{n_y}}) \Delta \kappa_x \Delta \kappa_y} \tag{6.77}$$

$$\tilde{A}_{n_x n_y} = \sqrt{2 S_{\hat{H}_S \hat{H}_S}(\kappa_{x_{n_x}}, -\kappa_{y_{n_y}}) \Delta \kappa_x \Delta \kappa_y} \tag{6.78}$$

$$\kappa_{x_{n_x}} = n_x \Delta \kappa_x \quad ; \quad \kappa_{y_{n_y}} = n_y \Delta \kappa_y \tag{6.79}$$

$$\Delta \kappa_x = \frac{\kappa_{x_u}}{N_x} \quad ; \quad \Delta \kappa_x = \frac{\kappa_{y_u}}{N_y}, \tag{6.80}$$

with the subsequent relations

$$\begin{aligned}
A_{0 n_y} = A_{n_x 0} = 0 \text{ for } n_x = 0, 1, 2, ... N_x - 1 \text{ and } n_y = 0, 1, 2, ... N_y - 1, \\
\tilde{A}_{0 n_y} = \tilde{A}_{n_x 0} = 0 \text{ for } n_x = 0, 1, 2, ... N_x - 1 \text{ and } n_y = 0, 1, 2, ... N_y - 1.
\end{aligned} \tag{6.81}$$

Here, κ_{x_u} and κ_{y_u} in equation (6.79) are the cut-off wave numbers defining the space domain along the corresponding axes x and y of the power spectral density function $S_{\hat{H}_S \hat{H}_S}(\mathbf{x}, \mathbf{y})$. To be more specific, this means, that $S_{\hat{H}_S \hat{H}_S}(\cdot)$ is set to zero for any mathematical or physical reason when it lies outside the regions

$$-\kappa_{x_u} \leq \kappa_x \leq \kappa_{x_u} \quad \text{and} \quad -\kappa_{y_u} \leq \kappa_y \leq \kappa_{y_u}. \tag{6.82}$$

Due to the fact that κ_{x_u} and κ_{y_u} have fixed values, the wave number steps $\Delta \kappa_x$ and $\Delta \kappa_y$ tends to zero when N_x and N_y tends to infinity. For a given number of terms for N_x and N_y, $\Delta \kappa_x$ and $\Delta \kappa_y$ are constant and it yields

$$\begin{aligned}
N_x \Delta \kappa_x = \kappa_{x_u}, \\
N_y \Delta \kappa_y = \kappa_{y_u}.
\end{aligned} \tag{6.83}$$

In the following listing the properties of $\hat{H}_S(\mathbf{x}, \mathbf{y}, \theta)$ are summarized, see also Shinozuka and Deodatis [1996]:

- The simulated stochastic field $\hat{H}_S(\mathbf{x}, \mathbf{y}, \theta)$ is periodic with

$$L_{x0} = \frac{2\pi}{\Delta \kappa_x} \quad \text{along the x axis} \tag{6.84}$$

$$L_{y0} = \frac{2\pi}{\Delta \kappa_y} \quad \text{along the y axis}. \tag{6.85}$$

  This means, that with a smaller $\Delta \kappa_i$, $i = $ x, y or equivalently with a larger n under a specific cut-off wave number κ_{i_u}, $i = $ x, y the longer the period of the simulated field $\hat{H}_S(\mathbf{x}, \mathbf{y}, \theta)$ gets.

- The stochastic field $\hat{H}_S(\mathbf{x}, \mathbf{y}, \theta)$ is asymptotically Gaussian as $N_x, N_y \to \infty$ due to the central limit theorem, cf. Shinozuka and Deodatis [1991].

- The expected value and the autocorrelation function of the simulated field are

both identical to the corresponding targets, i.e.

$$\mathbb{E}\left[\hat{H}_S(\mathbf{x}, \mathbf{y}, \theta)\right] = \mathbb{E}\left[H_S(\mathbf{x}, \mathbf{y}, \theta)\right] \tag{6.86}$$

$$C_{\hat{H}_S \hat{H}_S}(\tau_x, \tau_y) = C_{H_S H_S}(\tau_x, \tau_y) . \tag{6.87}$$

To generate a sample function $\hat{H}_S^{(i)}(\mathbf{x}, \mathbf{y}, \theta)$ the random phase angles $\Phi^{(1)}_{n_x n_y}(\theta)$ and $\Phi^{(2)}_{n_x n_y}(\theta)$; $n_x = 0, 1, 2, ...N_x - 1$; $n_y = 0, 1, 2, ...N_y - 1$ must be substituted by their corresponding i-th realizations $\phi^{(1)(i)}_{n_x n_y}(\theta)$ and $\phi^{(2)(i)}_{n_x n_y}(\theta)$; $n_x = 0, 1, 2, ...N_x - 1$; $n_y = 0, 1, 2, ...N_y - 1$. With respect to the realizations of the phase angles, equation (6.76) can be rewritten as

$$\hat{H}_S^{(i)}(\mathbf{x}, \mathbf{y}, \theta) =$$
$$\sqrt{2} \sum_{n_x=0}^{N_x-1} \sum_{n_y=0}^{N_y-1} \left[A_{n_x n_y} \cos\left(\kappa_{x_{n_x}} \mathbf{x} + \kappa_{y_{n_y}} \mathbf{y} + \phi^{(1)(i)}_{n_x n_y}(\theta) \right) \right. \tag{6.88}$$
$$\left. + \tilde{A}_{n_x n_y} \cos\left(\kappa_{x_{n_x}} \mathbf{x} - \kappa_{y_{n_x}} \mathbf{y} + \phi^{(2)(i)}_{n_x n_y}(\theta) \right) \right] ,$$

where the realizations of $\phi^{(1)(i)}_{n_x n_y}(\theta)$ and $\phi^{(2)(i)}_{n_x n_y}(\theta)$ can be sampled by the methods discussed in section 4.4. The space increments $\Delta\mathbf{x}$ and $\Delta\mathbf{y}$ separate the generated values $H_S^{(i)}(\mathbf{x}, \mathbf{y}, \theta)$ by

$$\begin{aligned} \Delta x &\leq \frac{2\pi}{2\kappa_{x_u}} , \\ \Delta y &\leq \frac{2\pi}{2\kappa_{y_u}} , \end{aligned} \tag{6.89}$$

where this restriction must be set to prevent aliasing according to the sampling theorem, cf. Eveleigh [1996]. Every sample function generated by equation (6.88) is ergodic in the mean value and in the autocorrelation when the rectangular area $L_x \times L_y$ over which $\hat{H}_S^{(i)}(\mathbf{x}, \mathbf{y}, \theta)$ is simulated is equal to one period, i.e.

$$L_x = L_{x0} \quad \text{and} \quad L_y = L_{y0} , \tag{6.90}$$

or when it approaches infinity

$$L_x = \infty \quad \text{and} \quad L_y = \infty . \tag{6.91}$$

The only randomness in equation (6.88) occours through the uniformly distributed phase angle θ. It is also possible to generate weakly ergodic sample functions with a random phase angle as well as random amplitudes, but this is not considered further at this point. Therefore, the reader is referred to the textbook by Grigoriu [1993].

The Special Case of Two-Dimensional Quadratic Fields

The simulation formula for a quadratic homogeneous stochastic field, denoted by $\hat{H}_{S_\square}(\mathbf{x}, \mathbf{y}, \theta)$, differs only in one term of the general case for homogeneous two-dimensional stochastic fields as defined in equation (6.76).

The quadratic stochastic field $\hat{H}_{S_\square}(\mathbf{x}, \mathbf{y}, \theta)$ can be computed by, cf. Shinozuka and Deodatis [1996],

$$\hat{H}_{S_\square}(\mathbf{x}, \mathbf{y}, \theta) =$$

$$\sqrt{2} \sum_{n_x=0}^{N_x-1} \sum_{n_y=0}^{N_y-1} A_{n_x n_y} \left[\cos\left(\kappa_{x_{n_x}}\mathbf{x} + \kappa_{y_{n_y}}\mathbf{y} + \Phi^{(1)}_{n_x n_y}(\theta) \right) \right. \tag{6.92}$$

$$\left. + \cos\left(\kappa_{x_{n_x}}\mathbf{x} - \kappa_{y_{n_y}}\mathbf{y} + \Phi^{(2)}_{n_x n_y}(\theta) \right) \right] .$$

The only difference is $\tilde{A}_{n_x n_y}$, which is replaced through $A_{n_x n_y}$, because the terms are equal in the quadratic case, with the symmetry conditions

$$C_{\hat{H}_S \hat{H}_S}(\tau_x, \tau_y) = C_{\hat{H}_S \hat{H}_S}(\tau_x, -\tau_y) = C_{\hat{H}_S \hat{H}_S}(-\tau_x, \tau_y) = C_{\hat{H}_S \hat{H}_S}(-\tau_x, -\tau_y) , \tag{6.93}$$

and

$$S_{\hat{H}_S \hat{H}_S}(\kappa_x, \kappa_y) = S_{\hat{H}_S \hat{H}_S}(\kappa_x, -\kappa_y) = S_{\hat{H}_S \hat{H}_S}(-\kappa_x, \kappa_y)$$
$$= S_{\hat{H}_S \hat{H}_S}(-\kappa_x, -\kappa_y) , \tag{6.94}$$

as listed in Shinozuka and Deodatis [1996]. All parameters in equation (6.92) have already been defined with reference to equation (6.76) and therefore are not repeated here again.

6.4.2. Two-Dimensional Numerical Example

A first example will be given with respect to the generation of the randomly and uniformly distributed phase angle Φ, introduced in equation (6.74). The only input parameter for Φ is the range where the uniform distribution is defined, i.e. $[0, 2\pi]$. The used sample sizes are listed in Tab. 6.3. By use of equations (B.12) and (B.13), given in Appendix B, the mean value of Φ computed as $\mu_\Phi = \pi$ and the standard deviation is calculated as $\sigma_\Phi \approx 1,8138$. The results for the sampling are also reported in Tab. 6.3 and plotted in Fig. 6.10. The MCS shows relatively large deviations from the target values, where the target values even with 20000 samples are not being achieved. On the other hand, the LHS and the Sobol' sequence[6] reached the target mean relatively fast while the standard deviation is only achieved at 20000 samples. The errors of the LHS and the Sobol' sequence occur during the study of small size, i.e. for $\hat{\mu}_\Phi$ and $\hat{\sigma}_\Phi$ less than 1%, while the maximal errors for the MCS are nearly 5% for $\hat{\mu}_\Phi$ and around 4% for $\hat{\sigma}_\Phi$. It should be remarked, that the used quasi-random sequences, cf. subsection 4.4.3, are deterministic point sets. This means, that these sequences are not directly applicable to simulations due to the correlations between the sample points (Morokoff and Caflisch [1993, 1994, 1995]; Morokoff [1998]) and a direct efficient simulation of material parameters is only possible if the samples are reordered. To overcome this drawback some scrambling, cf. Owen [1994]; Matoušek [1998], is used to put enough randomness in the sequences.

---

[6]This term will be used instead of QMC-Method, because a Sobol' sequence is exclusively used to generate a deterministic point set.

Table 6.3.: Results of the sampled values for $\hat{\mu}_\Phi$ and $\hat{\sigma}_\Phi$ of the uniformly distributed phase angle Φ.

Sample size	Sampling technique	Sampled value $\hat{\mu}_\Phi$	Sampled value $\hat{\sigma}_\Phi$
	MCS	2.9922	1.7439
100	LHS	3.1400	1.8250
	Sobol' sequence	3.1411	1.8290
	MCS	3.2399	1.7603
500	LHS	3.1418	1.8156
	Sobol' sequence	3.1417	1.8186
	MCS	3.1353	1.8003
1000	LHS	3.1417	1.8147
	Sobol' sequence	3.1416	1.8134
	MCS	3.1308	1.7878
2500	LHS	3.1416	1.8142
	Sobol' sequence	3.1416	1.8144
	MCS	3.1500	1.8131
5000	LHS	3.1416	1.8140
	Sobol' sequence	3.1416	1.8137
	MCS	3.1195	1.8263
10000	LHS	3.1416	1.8139
	Sobol' sequence	3.1416	1.8139
	MCS	3.1423	1.8170
20000	LHS	3.1416	1.8138
	Sobol' sequence	3.1416	1.8138

Two-Dimensional Representation of a Stochastic Field

The generation of a zero-mean Gaussian stochastic field is based on the generation of a set of sample functions $\hat{H}_S(\cdot)$, given by equation (6.76). The power spectral density function $S_{\hat{H}_S \hat{H}_S}$ appearing in equations (6.77) and (6.78) is given below:

$$S_{\hat{H}_S \hat{H}_S}(\kappa_{\mathrm{x}}, \kappa_{\mathrm{y}}) = \sigma^2 \frac{c_{\mathrm{x}} c_{\mathrm{y}}}{4\pi} \exp\left[-\left(\frac{c_{\mathrm{x}} \kappa_{\mathrm{x}}}{2}\right)^2 - \left(\frac{c_{\mathrm{y}} \kappa_{\mathrm{y}}}{2}\right)^2 \right], \tag{6.95}$$

which has also been applied by Shinozuka and Deodatis [1996] and Stefanou and Papadrakakis [2004]. The parameters that are used to generate a discretized stochastic field $\hat{H}_S(\mathbf{x}, \mathbf{y}, \theta)$ are listed below.

- The correlation length parameters c_{x} and c_{y} and the standard deviation σ of the random field are

$$c_{\mathrm{x}} = 1.0\,\mathrm{m}, \quad c_{\mathrm{y}} = 1.0\,\mathrm{m}, \quad \sigma = 1. \tag{6.96}$$

- The upper cut-off wave numbers, defined in equation (6.80), are specified by

$$\kappa_{\mathrm{x}_u} = 5.00\,\frac{\mathrm{rad}}{\mathrm{m}} \quad \text{and} \quad \kappa_{\mathrm{y}_u} = 5.00\,\frac{\mathrm{rad}}{\mathrm{m}}. \tag{6.97}$$
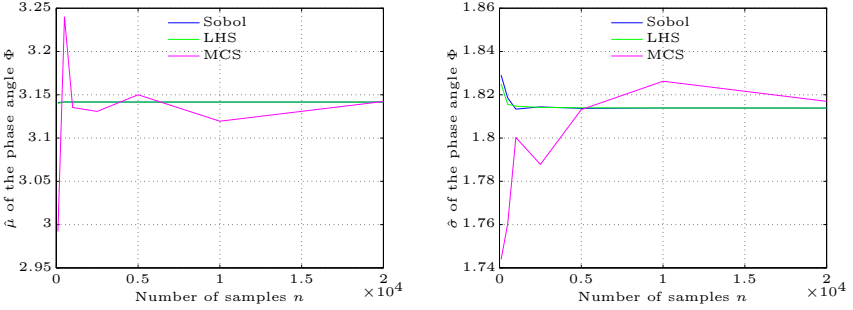
Figure 6.10.: Plot of the results from Tab. 6.3.

- The parameters N_x and N_y, also appearing in equation (6.80), are chosen to

$$N_x = N_y = 48 \,, \tag{6.98}$$

  with which the parameters $\Delta\kappa_x$ and $\Delta\kappa_y$ in equation (6.80) are determined to

$$\Delta\kappa_x = \Delta\kappa_y = 0.1042 \, \frac{\text{rad}}{\text{m}} \,. \tag{6.99}$$

- The periods L_{x_0} and L_{y_0}, given in equations (6.84) and (6.85), are calculated as

$$L_{x_0} = L_{y_0} = 60.32 \, \text{m} \,. \tag{6.100}$$

With this parameters and with the aid of a LHS and Sobol' sequences, Gaussian stochastic fields are generated. For comparison a simulation with a MCS with 1000 samples has also been performed. All sample functions are realized over a range with the dimensions $L_x = 20.11\,\text{m}$ and $L_y = 20.11\,\text{m}$. In Fig. 6.11 the results for the sample functions with $n = 1000$ samples are plotted.

To see how well a stationary Gaussian field, applying the SPRM, is simulated the sampled skewness $\hat{s}_{\hat{H}_S}$ and the sampled excess[7] $\hat{\kappa}_{\hat{H}_{S_e}}$ of the generated fields are compared. The results of this investigation are reported in Tab. 6.4. The comparison of the obtained values with the target values clearly shows that the target skewness is quite good approximated with already $n = 100$ samples. The target value for the skewness is achieved by $n = 250$ samples using a LHS, while the Sobol' sequence shows an asymptotic line against $\hat{\kappa}_{\hat{H}_{S_e}} = 0.6$. This result is further discussed with respect to Fig. 6.12, where the histograms for the stochastic fields in Fig. 6.11 are plotted. Besides the histogram the fitted Gaussian curves are also plotted, where it can be clearly seen that the sampled values by the Sobol' sequence are accumulated closer to the expected value what correlates with the value for the excess. Also the obtained result with a MCS shows a good or even more accurate solution than this

---

[7]For a Gaussian distribution the target values for $\hat{s}_{\hat{H}_S}$ and for $\hat{\kappa}_{\hat{H}_{S_e}}$ are both equal to zero.

(a) Generated with a LHS.

(b) Generated with a Sobol' sequence.

(c) Generated with a MCS.
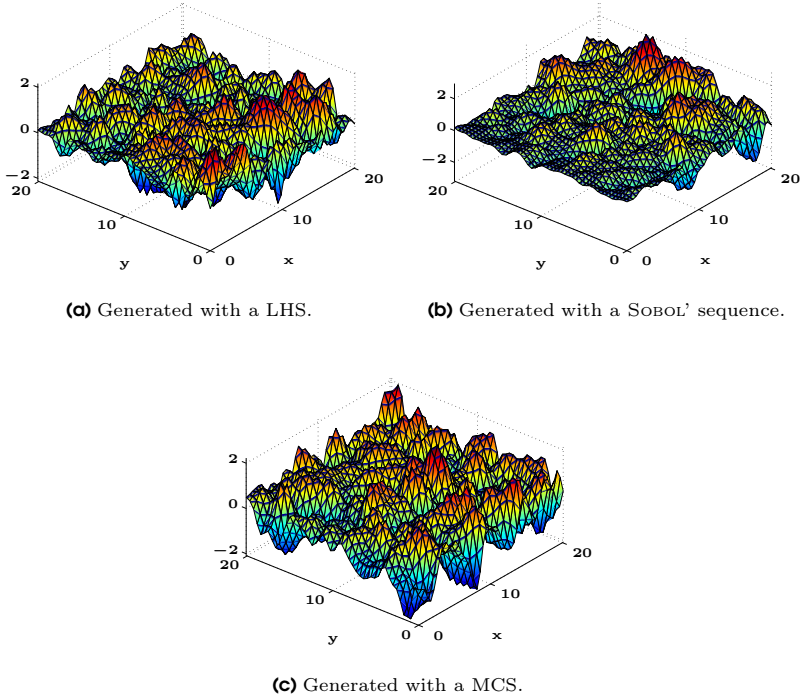
Figure 6.11.: Sample functions of a stochastic field $\hat{H}_S(\mathbf{x}, \mathbf{y}, \theta)$.

one reached with a Sobol' sequence. In summary, the sampled skewness and excess are relatively near to the target values, where a LHS performs better than a Sobol' sequence. Furthermore, the sampled values shows a decreasing trend as the number of samples increases, but no further improvement is visible from a certain sample size when comparing the results in Tab. 6.4. The obtained result with respect to a MCS shows a quite well approximation, which has not been expected. In addition, the evolution of the skewness and excess over the samples are plotted in Appendix D.

Table 6.4.: Reached values for the sampled skewness and sampled excess for $\hat{H}_{S_e}(\mathbf{x}, \mathbf{y})$.

Samples	Sampling technique for Φ	$\hat{s}_{\hat{H}_S}$	$\hat{\kappa}_{\hat{H}_{S_e}}$
100	LHS	0.01172	0.04589
	SOBOL'	-0.01078	0.60408
250	LHS	0.00632	0.00691
	SOBOL'	-0.00678	0.60278
500	LHS	-0.00958	0.01563
	SOBOL'	-0.01229	0.60940
1000	MCS	-0.00262	-0.03962
	LHS	0.00425	0.00942
	SOBOL'	0.00219	0.58486
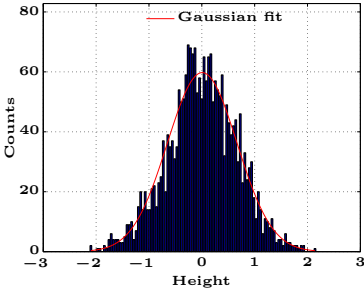
(a) Generated with a LHS.
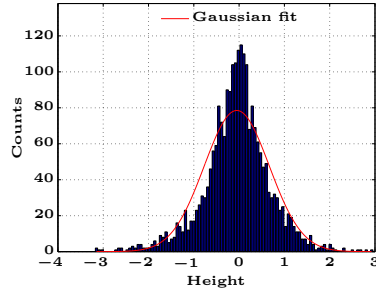
(b) Generated with a SOBOL' sequence.
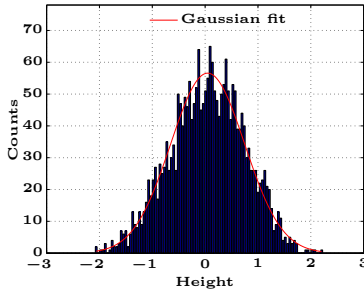
(c) Generated with a MCS.

Figure 6.12.: Histograms and GAUSSIAN fit of the sample functions of $\hat{H}_S(\mathbf{x}, \mathbf{y}, \theta)$ displayed in Fig. 6.11.

6.4.3. Simulation of 3-D Univariate Homogeneous Stochastic Fields

The three-dimensional simulation of a homogeneous stochastic field is a straight forward extension of the two-dimensional case. First, the extended formulas and relations are specified. Afterwards, the simulation formula for the three-dimensional case will be given.

Let $H_S(\mathbf{x}, \mathbf{y}, \mathbf{z}, \theta)$ be a three-dimensional univariate (3D-1V) homogeneous real valued stochastic field with mean value equal to zero, a power spectral density function $S_{H_S H_S}(\kappa_\mathrm{x}, \kappa_\mathrm{y}, \kappa_\mathrm{z})$ and an autocovariance function $C_{H_S H_S}(\tau_\mathrm{x}, \tau_\mathrm{y}, \tau_\mathrm{z})$. The power spectral density function and the autocovariance function constitute the three-dimensional Wiener-Khintchine transform pair, cf. Shinozuka and Deodatis [1996],

$$
S_{H_S H_S}(\kappa_\mathrm{x}, \kappa_\mathrm{y}, \kappa_\mathrm{z}) = \frac{1}{(2\pi)^3} \int\limits_{-\infty}^{\infty} \int\limits_{-\infty}^{\infty} \int\limits_{-\infty}^{\infty}
$$
$$
C_{H_S H_S}(\tau_\mathrm{x}, \tau_\mathrm{y}, \tau_\mathrm{z}) e^{-i(\kappa_\mathrm{x}\tau_\mathrm{x} + \kappa_\mathrm{y}\tau_\mathrm{y} + \kappa_\mathrm{z}\tau_\mathrm{z})} \,\mathrm{d}\tau_\mathrm{x}\mathrm{d}\tau_\mathrm{y}\mathrm{d}\tau_\mathrm{z} \,,
$$
$$(6.101)$$

$$
C_{H_S H_S}(\tau_\mathrm{x}, \tau_\mathrm{y}, \tau_\mathrm{z}) = \int\limits_{-\infty}^{\infty} \int\limits_{-\infty}^{\infty} \int\limits_{-\infty}^{\infty}
$$
$$
S_{H_S H_S}(\kappa_\mathrm{x}, \kappa_\mathrm{y}, \kappa_\mathrm{z}) e^{i(\kappa_\mathrm{x}\tau_\mathrm{x} + \kappa_\mathrm{y}\tau_\mathrm{y} + \kappa_\mathrm{z}\tau_\mathrm{z})} \,\mathrm{d}\kappa_\mathrm{x}\mathrm{d}\kappa_\mathrm{y}\mathrm{d}\kappa_\mathrm{z} \,.
$$
$$(6.102)$$

Here, τ_x, τ_y and τ_z are the separation distances along the x, y and z coordinate axes and κ_x, κ_y and κ_z are the corresponding wave numbers. The simulation formula for the three-dimensional series is extended to the third direction z, similar to the two-dimensional case defined in equation (6.76). The simulation formula $\hat{H}_S(\mathbf{x}, \mathbf{y}, \mathbf{z}, \theta)$ of a three-dimensional stochastic field $H_S(\mathbf{x}, \mathbf{y}, \mathbf{z}, \theta)$, with $S_{\hat{H}_S \hat{H}_S}(\kappa_\mathrm{x}, \kappa_\mathrm{y}, \kappa_\mathrm{z})$, $C_{\hat{H}_S \hat{H}_S}(\tau_\mathrm{x}, \tau_\mathrm{y}, \tau_\mathrm{z})$ and the symmetries

$$
\begin{aligned}
C_{\hat{H}_S \hat{H}_S}(\tau_\mathrm{x}, \tau_\mathrm{y}, \tau_\mathrm{z}) &= C_{\hat{H}_S \hat{H}_S}(-\tau_\mathrm{x}, -\tau_\mathrm{y}, -\tau_\mathrm{z}) \,, \\
S_{\hat{H}_S \hat{H}_S}(\kappa_\mathrm{x}, \kappa_\mathrm{y}, \kappa_\mathrm{z}) &= S_{\hat{H}_S \hat{H}_S}(-\kappa_\mathrm{x}, -\kappa_\mathrm{y}, -\kappa_\mathrm{z}) \,,
\end{aligned}
$$
$$(6.103)$$

is given ba, cf. Shinozuka and Deodatis [1996],

$$
\hat{H}_S(\mathbf{x}, \mathbf{y}, \mathbf{z}, \theta) = \sqrt{2} \sum_{n_\mathrm{x}=0}^{N_\mathrm{x}-1} \sum_{n_\mathrm{y}=0}^{N_\mathrm{y}-1} \sum_{n_\mathrm{z}=0}^{N_\mathrm{z}-1}
$$
$$
\begin{aligned}
\Big[\; & A^{(1)}_{n_\mathrm{x} n_\mathrm{y} n_\mathrm{z}} \cos\left(\kappa_{\mathrm{x}_{n_\mathrm{x}}}\mathbf{x} + \kappa_{\mathrm{y}_{n_\mathrm{y}}}\mathbf{y} + \kappa_{\mathrm{z}_{n_\mathrm{z}}}\mathbf{z} + \Phi^{(1)}_{n_\mathrm{x} n_\mathrm{y} n_\mathrm{z}}(\theta)\right) \\
+ \; & A^{(2)}_{n_\mathrm{x} n_\mathrm{y} n_\mathrm{z}} \cos\left(\kappa_{\mathrm{x}_{n_\mathrm{x}}}\mathbf{x} - \kappa_{\mathrm{y}_{n_\mathrm{y}}}\mathbf{y} + \kappa_{\mathrm{z}_{n_\mathrm{z}}}\mathbf{z} + \Phi^{(2)}_{n_\mathrm{x} n_\mathrm{y} n_\mathrm{z}}(\theta)\right) \\
+ \; & A^{(3)}_{n_\mathrm{x} n_\mathrm{y} n_\mathrm{z}} \cos\left(\kappa_{\mathrm{x}_{n_\mathrm{x}}}\mathbf{x} + \kappa_{\mathrm{y}_{n_\mathrm{y}}}\mathbf{y} - \kappa_{\mathrm{z}_{n_\mathrm{z}}}\mathbf{z} + \Phi^{(3)}_{n_\mathrm{x} n_\mathrm{y} n_\mathrm{z}}(\theta)\right) \\
+ \; & A^{(4)}_{n_\mathrm{x} n_\mathrm{y} n_\mathrm{z}} \cos\left(\kappa_{\mathrm{x}_{n_\mathrm{x}}}\mathbf{x} - \kappa_{\mathrm{y}_{n_\mathrm{y}}}\mathbf{y} - \kappa_{\mathrm{z}_{n_\mathrm{z}}}\mathbf{z} + \Phi^{(4)}_{n_\mathrm{x} n_\mathrm{y} n_\mathrm{z}}(\theta)\right) \Big] \,,
\end{aligned}
$$
$$(6.104)$$

with the following parameters:

$$A^{(1)}_{n_x n_y n_z} = \sqrt{2S_{\hat{H}_S \hat{H}_S}(\kappa_{x_{n_x}}, \kappa_{y_{n_y}}, \kappa_{z_{n_z}})\Delta\kappa_x \Delta\kappa_y \Delta\kappa_z}\,, \tag{6.105}$$

$$A^{(2)}_{n_x n_y n_z} = \sqrt{2S_{\hat{H}_S \hat{H}_S}(\kappa_{x_{n_x}}, -\kappa_{y_{n_y}}, \kappa_{z_{n_z}})\Delta\kappa_x \Delta\kappa_y \Delta\kappa_z}\,, \tag{6.106}$$

$$A^{(3)}_{n_x n_y n_z} = \sqrt{2S_{\hat{H}_S \hat{H}_S}(\kappa_{x_{n_x}}, \kappa_{y_{n_y}}, -\kappa_{z_{n_z}})\Delta\kappa_x \Delta\kappa_y \Delta\kappa_z}\,, \tag{6.107}$$

$$A^{(4)}_{n_x n_y n_z} = \sqrt{2S_{\hat{H}_S \hat{H}_S}(\kappa_{x_{n_x}}, -\kappa_{y_{n_y}}, -\kappa_{z_{n_z}})\Delta\kappa_x \Delta\kappa_y \Delta\kappa_z}\,, \tag{6.108}$$

$$\kappa_{x_{n_x}} = n_x \Delta\kappa_x \quad ; \quad \kappa_{y_{n_y}} = n_y \Delta\kappa_y \quad ; \quad \kappa_{z_{n_z}} = n_z \Delta\kappa_z\,, \tag{6.109}$$

$$\Delta\kappa_x = \frac{\kappa_{x_u}}{N_x} \quad ; \quad \Delta\kappa_y = \frac{\kappa_{y_u}}{N_y} \quad ; \quad \Delta\kappa_z = \frac{\kappa_{z_u}}{N_z}\,, \tag{6.110}$$

and the relations

$$A^{(j)}_{0 n_y n_z} = A^{(j)}_{n_x 0 n_z} = A^{(j)}_{n_x n_y 0} = 0 \quad \text{for} \quad j = 1, 2, 3, 4 \quad \text{and}$$
$$n_x = 0, 1, 2, ... N_x - 1; \; n_y = 0, 1, 2, ... N_y - 1; \; n_z = 0, 1, 2, ... N_z - 1\,. \tag{6.111}$$

Here, κ_{x_u}, κ_{y_u} and κ_{z_u} are the cut-off wave numbers defining the space domain along the x, y and z axes of the power spectral density function $S_{\hat{H}_S \hat{H}_S}(\mathbf{x}, \mathbf{y}, \mathbf{z})$, which is set to zero for any mathematical or physical reason if it lies outside the region defined by

$$-\kappa_{x_u} \le \kappa_x \le \kappa_{x_u}\,, \quad -\kappa_{y_u} \le \kappa_y \le \kappa_{y_u} \quad \text{and} \quad -\kappa_{z_u} \le \kappa_z \le \kappa_{z_u}\,. \tag{6.112}$$

Due to the fact that κ_{x_u}, κ_{y_u} and κ_{z_u} have fixed values, the wave number steps $\Delta\kappa_x$, $\Delta\kappa_y$ and $\Delta\kappa_z$ tends to zero while N_x, N_y and N_z tends to infinity. For a given number of terms N_x, N_y and N_z, $\Delta\kappa_x$, $\Delta\kappa_y$ and $\Delta\kappa_z$ are constant and it follows

$$N_x \Delta\kappa_x = \kappa_{x_u}\,, \tag{6.113}$$

$$N_y \Delta\kappa_y = \kappa_{y_u}\,, \tag{6.114}$$

$$N_z \Delta\kappa_z = \kappa_{z_u}\,. \tag{6.115}$$

The independent random phase angles $\Phi^{(j)}_{n_x n_y n_z}(\theta)$, $n_k = 0, 1, 2, ... N_k - 1$, $j = 1, 2, 3, 4$, $k = $ x, y, z in equation (6.104) are uniformly distributed in the range $[0, 2\pi]$. The properties of $\hat{H}_S(\mathbf{x}, \mathbf{y}, \mathbf{z}, \theta)$ are identical to those listed for the two-dimensional case $\hat{H}_S(\mathbf{x}, \mathbf{y}, \theta)$, so they will only be summarized shortly below.

- The simulated stochastic field $\hat{H}_S(\mathbf{x}, \mathbf{y}, \mathbf{z}, \theta)$ is periodic with period

$$L_{x0} = \frac{2\pi}{\Delta\kappa_x} \quad \text{along the x axis}\,, \tag{6.116}$$

$$L_{y0} = \frac{2\pi}{\Delta\kappa_y} \quad \text{along the y axis}\,, \tag{6.117}$$

$$L_{z0} = \frac{2\pi}{\Delta\kappa_z} \quad \text{along the z axis}\,. \tag{6.118}$$

- The simulated stochastic field $\hat{H}_S(\mathbf{x}, \mathbf{y}, \mathbf{z}, \theta)$ is asymptotically Gaussian as $N_x, N_y, N_z \to \infty$.

- The expected value and the autocorrelation function of the simulated field are both identical to the corresponding targets

$$
\begin{aligned}
\mathbb{E}\left[\hat{H}_S(\mathbf{x}, \mathbf{y}, \mathbf{z}, \theta)\right] &= \mathbb{E}\left[H_S(\mathbf{x}, \mathbf{y}, \mathbf{z}, \theta)\right], \\
C_{\hat{H}_S \hat{H}_S}(\tau_x, \tau_y, \tau_z) &= C_{H_S H_S}(\tau_x, \tau_y, \tau_z).
\end{aligned}
\tag{6.119}
$$

To generate a sample function $\hat{H}_S^{(i)}(\mathbf{x}, \mathbf{y}, \mathbf{z}, \theta)$ the random phase angles $\Phi^{(1)}_{n_x n_y n_z}(\theta)$, $\Phi^{(2)}_{n_x n_y n_z}(\theta)$, $\Phi^{(3)}_{n_x n_y n_z}(\theta)$ and $\Phi^{(4)}_{n_x n_y n_z}(\theta)$, $n_k = 0, 1, 2, ..., N_k - 1$, $k = $ x, y, z are substituted by their corresponding i-th realizations $\phi^{(1)(i)}_{n_x n_y n_z}(\theta)$, $\phi^{(2)(i)}_{n_x n_y n_z}(\theta)$, $\phi^{(3)(i)}_{n_x n_y n_z}(\theta)$ and $\phi^{(4)(i)}_{n_x n_y n_z}(\theta)$, $n_k = 0, 1, 2, ..., N_k - 1$, $k = $ x, y, z. With respect to the realizations of the phase angles $\phi^{(j)(i)}_{n_x n_y n_z}(\theta)$, $j = 1, 2, 3, 4$, the series representation in equation (6.104) can be rewritten, cf. Shinozuka and Deodatis [1996],

$$
\begin{aligned}
\hat{H}_S^{(i)}(\mathbf{x}, \mathbf{y}, \mathbf{z}, \theta) = \sqrt{2} \sum_{n_x=0}^{N_x-1} \sum_{n_y=0}^{N_y-1} \sum_{n_z=0}^{N_z-1} \\
\Big[\; A^{(1)}_{n_x n_y n_z} \cos\left(\kappa_{x_{n_x}} \mathbf{x} + \kappa_{y_{n_y}} \mathbf{y} + \kappa_{z_{n_z}} \mathbf{z} + \phi^{(1)(i)}_{n_x n_y n_z}(\theta)\right) \\
+ A^{(2)}_{n_x n_y n_z} \cos\left(\kappa_{x_{n_x}} \mathbf{x} - \kappa_{y_{n_y}} \mathbf{y} + \kappa_{z_{n_z}} \mathbf{z} + \phi^{(2)(i)}_{n_x n_y n_z}(\theta)\right) \\
+ A^{(3)}_{n_x n_y n_z} \cos\left(\kappa_{x_{n_x}} \mathbf{x} + \kappa_{y_{n_y}} \mathbf{y} - \kappa_{z_{n_z}} \mathbf{z} + \phi^{(3)(i)}_{n_x n_y n_z}(\theta)\right) \\
+ A^{(4)}_{n_x n_y n_z} \cos\left(\kappa_{x_{n_x}} \mathbf{x} - \kappa_{y_{n_y}} \mathbf{y} - \kappa_{z_{n_z}} \mathbf{z} + \phi^{(4)(i)}_{n_x n_y n_z}(\theta)\right)\Big],
\end{aligned}
\tag{6.120}
$$

where the realizations $\phi^{(j)(i)}_{n_x n_y n_z}(\theta)$, $j = 1, ... 4$ are generated by a LHS. To avoid aliasing the space increments Δx, Δy and Δz, which separate the generated values $\hat{H}_S^{(i)}(\mathbf{x}, \mathbf{y}, \mathbf{z}, \theta)$, have to obey

$$
\Delta x \leq \frac{2\pi}{2\kappa_{x_u}}, \quad \Delta y \leq \frac{2\pi}{2\kappa_{y_u}} \quad \text{and} \quad \Delta z \leq \frac{2\pi}{2\kappa_{z_u}}.
\tag{6.121}
$$

Every sample function, generated by equation (6.120) is ergodic in the mean value and autocorrelation when the domain $L_x \times L_y \times L_z$ over which $\hat{H}_S^{(i)}(\mathbf{x}, \mathbf{y}, \mathbf{z}, \theta)$ is simulated, is equal to one period

$$
L_x = L_{x0}, \qquad L_y = L_{y0} \quad \text{and} \quad L_z = L_{z0},
\tag{6.122}
$$

or when it approaches infinity, i.e.

$$
L_x = \infty, \qquad L_y = \infty \qquad \text{and} \quad L_z = \infty.
\tag{6.123}
$$

Special Case of Three-Dimensional Cubic Fields

A homogeneous cubic stochastic field is represented by the following series, cf. Shinozuka and Deodatis [1996]:

$$
\hat{H}_{S_\square}(\mathbf{x}, \mathbf{y}, \mathbf{z}, \theta) = \sqrt{2} \sum_{n_x=0}^{N_x-1} \sum_{n_y=0}^{N_y-1} \sum_{n_z=0}^{N_z-1} A^{(1)}_{n_x n_y n_z}
$$

$$
\begin{aligned}
\Big[\ & \cos\left(\kappa_{x_{n_x}} \mathbf{x} + \kappa_{y_{n_y}} \mathbf{y} + \kappa_{z_{n_z}} \mathbf{z} + \Phi^{(1)}_{n_x n_y n_z}(\theta) \right) \\
+ & \cos\left(\kappa_{x_{n_x}} \mathbf{x} - \kappa_{y_{n_y}} \mathbf{y} + \kappa_{z_{n_z}} \mathbf{z} + \Phi^{(2)}_{n_x n_y n_z}(\theta) \right) \\
+ & \cos\left(\kappa_{x_{n_x}} \mathbf{x} + \kappa_{y_{n_y}} \mathbf{y} - \kappa_{z_{n_z}} \mathbf{z} + \Phi^{(3)}_{n_x n_y n_z}(\theta) \right) \\
+ & \cos\left(\kappa_{x_{n_x}} \mathbf{x} - \kappa_{y_{n_y}} \mathbf{y} - \kappa_{z_{n_z}} \mathbf{z} + \Phi^{(4)}_{n_x n_y n_z}(\theta) \right) \Big] \ .
\end{aligned}
\tag{6.124}
$$

Because of the symmetry property $A^{(1)}_{n_x n_y n_z} = A^{(2)}_{n_x n_y n_z} = A^{(3)}_{n_x n_y n_z} = A^{(4)}_{n_x n_y n_z}$ the series formula for three-dimensional cubic fields is slightly simpler than the corresponding formula for the general case in equation (6.104). As in the two-dimensional case there are also symmetry conditions of $C_{\hat{H}_S \hat{H}_S}(\tau_x, \tau_y, \tau_z)$ and $S_{\hat{H}_S \hat{H}_S}(\kappa_x, \kappa_y, \kappa_z)$ in the three dimensional case, which are

$$
\begin{aligned}
C_{\hat{H}_S \hat{H}_S}(\tau_x, \tau_y, \tau_z) &= C_{\hat{H}_S \hat{H}_S}(-\tau_x, \tau_y, \tau_z) &= C_{\hat{H}_S \hat{H}_S}(\tau_x, -\tau_y, \tau_z) \\
C_{\hat{H}_S \hat{H}_S}(\tau_x, \tau_y, -\tau_z) &= C_{\hat{H}_S \hat{H}_S}(\tau_x, -\tau_y, -\tau_z) &= C_{\hat{H}_S \hat{H}_S}(-\tau_x, \tau_y, -\tau_z) \\
C_{\hat{H}_S \hat{H}_S}(-\tau_x, -\tau_y, \tau_z) &= C_{\hat{H}_S \hat{H}_S}(-\tau_x, -\tau_y, -\tau_z) \ ,
\end{aligned}
\tag{6.125}
$$

and

$$
\begin{aligned}
S_{\hat{H}_S \hat{H}_S}(\kappa_x, \kappa_y, \kappa_z) &= S_{\hat{H}_S \hat{H}_S}(-\kappa_x, \kappa_x, \kappa_z) &= S_{\hat{H}_S \hat{H}_S}(\kappa_x, -\kappa_y, \kappa_z) \\
S_{\hat{H}_S \hat{H}_S}(\kappa_x, \kappa_y, -\kappa_z) &= S_{\hat{H}_S \hat{H}_S}(\kappa_x, -\kappa_y, -\kappa_z) &= S_{\hat{H}_S \hat{H}_S}(-\kappa_x, \kappa_y, -\kappa_z) \\
S_{\hat{H}_S \hat{H}_S}(-\kappa_x, -\kappa_y, \kappa_z) &= S_{\hat{H}_S \hat{H}_S}(-\kappa_x, -\kappa_y, -\kappa_z) \ .
\end{aligned}
\tag{6.126}
$$

All parameters in equation (6.124) have already been defined with reference to equation (6.104) and are therefore not repeated here.

6.4.4. Three-Dimensional Numerical Realization

The generation of a multidimensional Gaussian zero-mean stochastic field is based on the generation of a set of sample functions $\hat{H}_S(\cdot)$, defined in equation (6.104). The applied power spectral density function $S_{\hat{H}_S \hat{H}_S}(\cdot)$, appearing in the equations (6.105) to (6.108), is a direct extension of the equation (6.95) and reads

$$
S_{\hat{H}_S \hat{H}_S}(\kappa_x, \kappa_y, \kappa_z) = \sigma^2 \frac{c_x c_y c_z}{4\pi} \exp\left[-\left(\frac{c_x \kappa_x}{2}\right)^2 - \left(\frac{c_y \kappa_y}{2}\right)^2 - \left(\frac{c_z \kappa_z}{2}\right)^2 \right] \ , \tag{6.127}
$$

which has been also applied in the publication by Papadrakakis and Kotsopulos [1999]. The calculation in the three-dimensional case is exemplary performed with 100 sam-

ples, where the parameters are listed in a short manner below.

- The correlation length parameters c_x, c_y and c_z and the standard deviation σ of the random field are

$$c_x = 1.0\,\text{m}, \quad c_y = 1.0\,\text{m}, \quad c_z = 1.0\,\text{m}, \quad \sigma = 1\,. \tag{6.128}$$

- The upper cut-off wave numbers defined in equation (6.110) are specified by

$$\kappa_{xu} = 5.00\,\frac{\text{rad}}{\text{m}}, \quad \kappa_{yu} = 5.00\,\frac{\text{rad}}{\text{m}} \quad \text{and} \quad \kappa_{zu} = 5.00\,\frac{\text{rad}}{\text{m}}\,. \tag{6.129}$$

- For computational purposes the parameters N_x, N_y and N_z also appearing in equation (6.110) are chosen as

$$N_x = N_y = N_z = 20\,, \tag{6.130}$$

with which the parameters $\Delta\kappa_x$, $\Delta\kappa_y$ and $\Delta\kappa_z$ in equation (6.110) computed as

$$\Delta\kappa_x = \Delta\kappa_y = \Delta\kappa_z = 0.25\,\frac{\text{rad}}{\text{m}}\,. \tag{6.131}$$

- The periods L_{x0}, L_{y0} and L_{z0} defined in the equations (6.116) to (6.118), are calculated as

$$L_{x0} = L_{y0} = L_{z0} = 25.13\,\text{m}\,. \tag{6.132}$$

For simplicity reasons, a detailed discussion, such as in the two dimensional random fields, given in subsection 6.4.2, will be waived here[8]. Some properties of the SPRM are discussed at a concrete example in section 8.6. At this point only a remark regarding to the computational time will be given. With respect to the defined parameters above, the calculation time for 100 sample functions is about 470 seconds, which was done on a server[9] using a parallel code and 12 CPUs.

6.4.5. Concluding Remarks

The computational simulations and analysis discussed in this section show that Sobol' sequences can give a valid Monte-Carlo based simulation result for the considered problem. When comparing the results for the sampled phase angles, it can be seen that a LHS and the Sobol' sequence show better results with a much lower number of samples than the MCS. The result for the skewness and the kurtosis obtained from the LHS seems to be more precise than those obtained with a MCS as well as the Sobol' sequence. The computational effort for the realization of a sample set of random fields grows in the three dimensional case drastically. For example takes the calculation of a two-dimensional field with 100 sample functions, applying the parameters of section 6.4.2 about 7 seconds, while the realization of 100 sample functions in the three dimensional case takes about 470 seconds.

---

[8] For multivariate statistical analysis, see, e.g., Anderson [1958]; Tabachnick and Fidell [2013].

[9] The server consists of 32 Intel Xeon E5-2680 processors, each of them with 2,7 GHz and a total memory of 256 GB.

6.5. Summary

In this chapter various discretization methods for the characterization of random material properties are presented. After some general remarks on random fields, gives section 6.2 a brief summary of some existing techniques for the discretization of random fields. In sections 6.3 and 6.4 the theory of the methods applied in this work is discussed in detail. First, the theoretical background of the KLE and SPRM is presented. Afterwards, some numerical studies have been carried out for both methods and the results are discussed. The results of the realized random fields are quite good, but as might be expected the computational time for the realization of a representation of a three-dimensional random field increases drastically by increasing degrees of freedom of the FE mesh. In future research, special attention should be paid on the reduction of the computational time, especially in view of three-dimensional random fields, where the calculation time increases drastically. Especially in view of the KLE, several methods are developed in the last decade to reduce the computational time. One example, is the fast multipole methods, e.g., Schwab and Todor [2006], whereas for the interested reader is referred to the cited article and the references therein as well as to the textbook by Le Maître and Knio [2010] for a general overview.

In this work, the KLE is exclusively used to represent the fluctuations of the input parameters in a series expansion. The fact that the KLE requires knowing the covariance function of the field being expanded makes it impossible to use it for the representation of the system response. To circumvent this lack of knowledge, the system response is approximated by the Polynomial Chaos Expansion, which is outlined in the next chapter. Furthermore, the SPRM is coupled with a MCS and used as reference solution of the system response, which are compared with the results obtained from the SSFEM (the KLE coupled with the Polynomial Chaos Expansion) in the linear elastic formulation in section 8.6 and with the proposed elastic-plastic formulation in chapter 9.

7. Polynomial Chaos Expansion

As already pointed out in the previous chapter, the KLE is a powerful method to characterize the fluctuations of the input parameters of a (e.g., mechanical) system. However, by applying this technique, the covariance kernel $C(\cdot)$ is explicitly required to represent the random field in terms of their eigenfunctions. In view of the representation of the system response it is not optimal, because the covariance function of the system response is not known a priori. A possibility to represent the system response by random variables is the Polynomial Chaos Expansion, which is presented in this chapter. With respect to various engineering applications, this methodology is well documented, see for instance, Ghanem and Spanos [2003]; Matthies et al. [1997]; Schuëller [1997]; Sudret and der Kiureghian [2000]; Le Maître and Knio [2010]; Xiu [2010]. In addition to this works, the mathematical textbooks by Funaro [1992] and Gautschi [2004] should be also mentioned here, where the theory of orthogonal polynomials is discussed in detail.

This chapter is structured as follows: In section 7.1 important definitions are introduced, which are used in the subsequent sections and chapters. The main focus of this chapter is the construction of the Polynomial Chaos, which is presented in section 7.2. Besides the basic construction contains this section the definition of the Polynomial Basis, presented in subsection 7.2.1. For computational reasons, it is necessary to conduct system analysis with a finite number of random variables, which is discussed in subsection 7.2.2. In section 7.2.3, the approximation of a random variable is explained, because there are various ways possible to represent a random variable in terms of polynomials and for an accurate approximation of the system response, an optimal choice of these polynomials is important. The section ends with a brief overview of the generalized PCE, which is applied when non-GAUSSIAN random variables are used. In the last paragraph of this chapter the general implementation of the polynomial chaos is presented in detail.

7.1. Basic Definitions and Functional Spaces

First of all, the basic definitions and notations, which are used in the subsequent sections and chapters are introduced. More detailed informations can be found in Ghanem and Spanos [2003] or Le Maître and Knio [2010].

Let X be a $\mathbb{R}$-valued random variable defined on the probability space $\mathcal{L}^2(\Theta, \mathcal{F}, P)$, i.e.

$$X : \Theta \to \mathbb{R} \,. \tag{7.1}$$

Furthermore, a set of GAUSSIAN variables $\{\xi_i(\theta)\}_{i=1}^{\infty}$ is introduced, which is centred, normalized and mutually orthogonal. With $\hat{\Gamma}_p$ the space of polynomials in $\{\xi_i(\theta)\}_{i=1}^{\infty}$ is defined, which have a degree that not exceeds p. The set of polynomials that belongs to the space $\hat{\Gamma}_p$ is defined by Γ_p and is orthogonal to $\hat{\Gamma}_{p-1}$. Finally, the space $\tilde{\Gamma}_p$ should be introduced, which is spanned by Γ_p. With these definitions at

hand the so-called Wiener Chaos decomposition should be defined as follows, cf. Le Maître and Knio [2010]:

$$\hat{\Gamma}_p = \hat{\Gamma}_{p-1} \oplus \tilde{\Gamma}_p \,, \qquad \mathcal{L}^2(\Theta, \mathcal{F}, P) = \bigoplus_{i=0}^{\infty} \tilde{\Gamma}_i \,, \tag{7.2}$$

where $\oplus$ denotes the operator of orthogonal summation. The subspace $\tilde{\Gamma}_p$ of $\mathcal{L}^2(\Theta, \mathcal{F}, P)$ is referred to as the p-th homogeneous chaos, whereas Γ_p denotes the polynomial chaos of order p. Thus, the polynomial chaos of order p consists of all polynomials of order p, involving all possible combinations of the random variables $\{\xi_i(\theta)\}_{i=1}^{\infty}$. The random variables are functions and the polynomial chaos accordingly are functions of functions and therefore denoted as *functionals*, cf. Ghanem and Spanos [2003]; Le Maître and Knio [2010].

7.2. Construction of the Polynomial Chaos

The polynomial chaos based on the concept of the homogeneous chaos, proposed by Wiener [1938], has been refined and extended in the subsequent decades by various researchers. This representation technique was applied in the late 1980s, respectively early 1990s by Ghanem and Spanos [2003] in order to solve boundary value problems with random coefficients. This publication can be seen as the "pioneer work" of the PCE in the area of engineering applications. The polynomial chaos expansion has been successfully applied for stochastic analysis in various applications, where some of the recent publications are listed in the below: Xiu and Karniadakis [2002]; Field Jr. and Grigoriu [2004]; Sudret [2007]; Blatman and Sudret [2008]; Blatman [2009] as well as the two reviews by Najm [2009] and Xiu [2009].

Let X be a Gaussian random variable, which should be expressed via a series expansion. Based on the probability space $(\Theta, \mathcal{F}, P)$, $\{\xi_i(\theta)\}_{i=1}^{\infty}$ denotes a set of independent standard Gaussian random variables on Θ. Each second order random variable X, as introduced in equation (7.1), can be represent by a polynomial chaos expansion as follows, cf. Ghanem and Spanos [2003]; Le Maître and Knio [2010]:

$$X = a_0 \Gamma_0 \tag{7.3}$$

$$+ \sum_{i_1=1}^{\infty} a_{i_1} \Gamma_1(\xi_{i_1}(\theta))$$

$$+ \sum_{i_1=1}^{\infty} \sum_{i_2=1}^{i_1} a_{i_1 i_2} \Gamma_2(\xi_{i_1}(\theta), \xi_{i_2}(\theta))$$

$$+ \sum_{i_1=1}^{\infty} \sum_{i_2=1}^{i_1} \sum_{i_3=1}^{i_2} a_{i_1 i_2 i_3} \Gamma_3(\xi_{i_1}(\theta), \xi_{i_2}(\theta), \xi_{i_3}(\theta)) + \dots \,,$$

where Γ_p are successive polynomial chaoses of order p and $a_\bullet \in \mathbb{R}$ are deterministic coefficients. This series expansion is convergent in the mean-square sense, cf.

Le Maître and Knio [2010]:

$$\lim_{p \to \infty} \mathbb{E}\left[\left(a_0 \Gamma_0 + \cdots + \sum_{i_1=1}^{\infty} \cdots \sum_{i_p=1}^{i_{p-1}} a_{i_1 \cdots i_p} \Gamma_p(\xi_{i_1}, \ldots \xi_{i_p}) - x\right)^2\right] = 0. \quad (7.4)$$

An important property of Γ_p is the orthogonality where the polynomials with order $p > 0$ have an expectation equal to zero

$$\mathbb{E}[\Gamma_i] = 0, \quad i > 0. \quad (7.5)$$

The mean value of the product of two polynomials, with respect to the inner product, is also zero

$$\mathbb{E}[\Gamma_i \Gamma_j] = 0, \quad i \neq j. \quad (7.6)$$

Equation (7.3) should be recast in a more compact manner by the univocal relation

$$\psi(\cdot) \Longleftrightarrow \Gamma(\cdot). \quad (7.7)$$

With this relation, the PC-expansion of X can be subsequently rewritten as

$$X = \sum_{j=0}^{\infty} a_j \psi_j(\boldsymbol{\xi}(\theta)), \quad \boldsymbol{\xi} = \{\xi_1, \ldots\}. \quad (7.8)$$

The construction of the PCE outlined above is realized with an infinite number of normalized uncorrelated Gaussian random variables ξ_i, $i = 1, \ldots$. For computational purposes, this series expansion needs to be truncated after a finite number M of random variables, which leads to a PCE with a finite dimension P. To be more specific, the PC-expansion of dimension M and order p is the subspace of $\tilde{\Gamma}_p$ generated by the elements of Γ_p involving only the set of random variables up to order M, i.e. $\{\xi_1, \ldots \xi_M\}$, see also subsection 7.2.2. This fact is exemplary expressed for equation (7.3) with a dimension of $M = 2$ in the following:

$$X = a_0 \Gamma_0 \quad (7.9)$$

$$+ \sum_{i_1=1}^{2} a_{i_1} \Gamma_1(\xi_{i_1}(\theta))$$

$$+ \sum_{i_1=1}^{2} \sum_{i_2=1}^{i_1} a_{i_1 i_2} \Gamma_2(\xi_{i_1}(\theta), \xi_{i_2}(\theta))$$

$$+ \sum_{i_1=1}^{2} \sum_{i_2=1}^{i_1} \sum_{i_3=1}^{i_2} a_{i_1 i_2 i_3} \Gamma_3(\xi_{i_1}(\theta), \xi_{i_2}(\theta), \xi_{i_3}(\theta)) + \ldots,$$

or when the summations are evaluated explicitly, it reads

$$X = a_0 \Gamma_0 \tag{7.10}$$
$$+ a_1 \Gamma_1(\xi_1(\theta)) + a_2 \Gamma_1(\xi_1(\theta))$$
$$+ a_{11} \Gamma_2(\xi_1(\theta), \xi_1(\theta)) + a_{21} \Gamma_2(\xi_2(\theta), \xi_1(\theta)) + a_{22} \Gamma_2(\xi_2(\theta), \xi_2(\theta))$$
$$+ a_{111} \Gamma_3(\xi_1(\theta), \xi_1(\theta), \xi_1(\theta)) + a_{211} \Gamma_3(\xi_2(\theta), \xi_1(\theta), \xi_1(\theta))$$
$$+ a_{221} \Gamma_3(\xi_2(\theta), \xi_2(\theta), \xi_1(\theta)) + a_{222} \Gamma_3(\xi_2(\theta), \xi_2(\theta), \xi_2(\theta)) + \dots .$$

By applying the compact form of equation (7.8) the expansion above can be recast in terms of $\psi_j(\cdot)$ (where only the first six terms are specified here) as

$$X = a_0 \ \psi_0 + a_1 \ \psi_1 + a_2 \ \psi_2 + a_3 \ \psi_3 + a_4 \ \psi_4 + a_5 \ \psi_5 + a_6 \ \psi_6 + \dots, \tag{7.11}$$

where, for instance, the term $a_{22}\Gamma_2(\xi_2(\theta), \xi_2(\theta))$ becomes $a_6 \ \psi_6$. Closed form expressions for $\Gamma_\bullet$ up to order $p = 4$ are given in Ghanem and Spanos [2003] and also listed here:

$$\Gamma_0 = 1,$$
$$\Gamma_1(\xi_{i_1}) = \xi_{i_1},$$
$$\Gamma_2(\xi_{i_1}, \xi_{i_2}) = \xi_{i_1}\xi_{i_2} - \delta_{i_1 i_2},$$
$$\Gamma_3(\xi_{i_1}, \xi_{i_2}, \xi_{i_3}) = \xi_{i_1}\xi_{i_2}\xi_{i_3} - \xi_{i_1}\delta_{i_2 i_3} - \xi_{i_2}\delta_{i_1 i_3} - \xi_{i_3}\delta_{i_1 i_2} \quad \text{and} \tag{7.12}$$
$$\Gamma_4(\xi_{i_1}, \xi_{i_2}, \xi_{i_3}, \xi_{i_4}) = \xi_{i_1}\xi_{i_2}\xi_{i_3}\xi_{i_4} - \xi_{i_1}\xi_{i_2}\delta_{i_3 i_4} - \xi_{i_1}\xi_{i_3}\delta_{i_2 i_4} - \xi_{i_1}\xi_{i_4}\delta_{i_2 i_3}$$
$$- \xi_{i_2}\xi_{i_3}\delta_{i_1 i_4} - \xi_{i_2}\xi_{i_4}\delta_{i_1 i_3} - \xi_{i_3}\xi_{i_4}\delta_{i_1 i_2} + \delta_{i_1 i_2}\delta_{i_3 i_4}$$
$$+ \delta_{i_1 i_3}\delta_{i_2 i_4} + \delta_{i_1 i_4}\delta_{i_2 i_3} .$$

In principle, a multi-dimensional PC can be computed as, cf. Sudret and der Kiureghian [2000],

$$\Gamma_M(\boldsymbol{\xi}) = (-1)^M \ e^{\frac{1}{2}\boldsymbol{\xi}^T \boldsymbol{\xi}} \ \frac{\partial^M}{\partial \xi_{i_1} \dots \partial \xi_{i_M}} \ e^{-\frac{1}{2}\boldsymbol{\xi}^T \boldsymbol{\xi}}, \tag{7.13}$$

where $\boldsymbol{\xi} = \{\xi_{i_1}, \xi_{i_2}, \dots \xi_{i_M}\}$ denotes a set of M Gaussian random variables.

7.2.1. Polynomial Basis

Up to now, no specification about the basis of the polynomial chaoses Γ or the corresponding ψ's was made. If the random variable ξ is assumed to be Gaussian, a one-dimensional Hermite polynomial chaos basis is optimal, because an expansion with $p = 1$ results in an exact representation, cf. Le Maître and Knio [2010]. This will be discussed in detail along this subsection.

One-dimensional PC-Basis

In the one-dimensional case (polynomials of only one random variable ξ), Γ and ψ can be generated directly from the definition of the Hermite polynomials as follows,

cf. Sudret and der Kiureghian [2000]:

$$\mathfrak{h}_M(\xi) = (-1)^M \, \frac{\partial^M \left(e^{-\frac{1}{2}\xi^2}\right)}{\partial \xi^M} \, e^{\frac{1}{2}\xi^2} \,, \tag{7.14}$$

which is simply the single variable version of equation (7.13). Some of these polynomials are tabulated in Ghanem and Spanos [2003], where the first five one-dimensional Hermite polynomials ($\mathfrak{h}_0, \ldots \mathfrak{h}_4$) are listed below:

$$\mathfrak{h}_0 = 1 \,, \quad \mathfrak{h}_1 = \xi \,, \quad \mathfrak{h}_2 = \xi^2 - 1 \,, \quad \mathfrak{h}_3 = \xi^3 - 3\xi \,, \quad \mathfrak{h}_4 = \xi^4 - 6\xi^2 + 3 \,, \tag{7.15}$$

as well as illustrated in Fig. 7.1 for $\xi \in [-2, 2]$. Substituting these polynomials into equation (7.8) the random response X becomes

$$X = a_0 + a_1 \xi + a_2(\xi^2 - 1) + a_3(\xi^3 - 3\xi) + a_4(\xi^4 - 6\xi^2 + 3) \,. \tag{7.16}$$
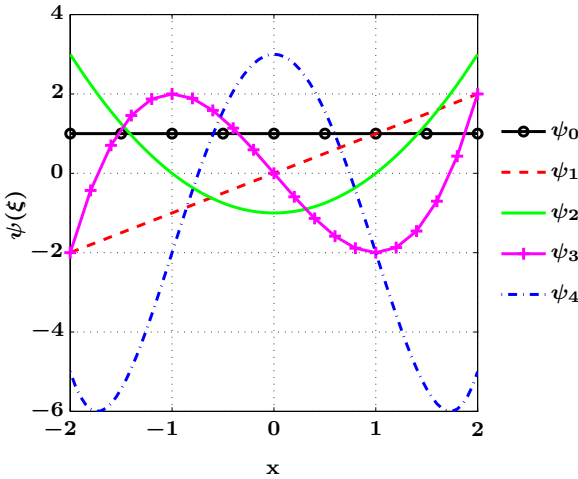
Figure 7.1.: One-dimensional ($M = 1$) Hermite polynomials of order up to $p = 4$.

The orthogonality of the one-dimensional Hermite polynomials, with respect to the inner product of $\mathcal{L}^2(\Theta, \mathcal{F}, P)$, leads to

$$
\begin{aligned}
\langle \mathfrak{h}_m, \mathfrak{h}_n \rangle &= \int_\Theta \mathfrak{h}_m(\xi(\theta)) \mathfrak{h}_n(\xi(\theta)) \, d\mathcal{P}(\theta) \,, \\
&= \int_\mathbb{R} \mathfrak{h}_m(\xi) \mathfrak{h}_n(\xi) \rho_\xi \, d\xi \,, \\
&= \delta_{mn} \langle \mathfrak{h}_n^2 \rangle \,,
\end{aligned}
\tag{7.17}
$$

where ρ_ξ defines the probability density of ξ.

Multi-Dimensional PC Basis

If more than one random variable occurs in the investigated system, a multi-dimensional PC basis is needed. in the presented work, such a basis is constructed by products of the one-dimensional HERMITE polynomials. Therefore, let $\boldsymbol{\alpha} = \{\alpha_1, \ldots \alpha_p\} \in \mathbb{N}^p$ be a multi-indices. Then, the p-variate M-th degree PC basis functions are the products of the one-dimensional PC polynomials of total degree less than or equal to M. To be more specific, the p-th order HERMITE polynomial can be constructed by, see, e.g., Sudret and der Kiureghian [2000],

$$\psi_{\boldsymbol{\alpha}}(\theta) = \prod_{k=1}^{M} \mathfrak{h}_{\alpha_k} \left(\xi_k(\theta) \right) . \qquad (7.18)$$

Each multi-dimensional polynomial is defined by a sequence of M non-negative integers $\boldsymbol{\alpha} = \{\alpha_1, \ldots \alpha_M\}$ whose sum is smaller than or equal to p. Ghanem and Spanos [2003] tabulated the polynomial chaos for different dimensions M and orders p, which are listed in the table below for a two-dimensional polynomial chaos up to order $p = 4$. An example of a two-dimensional ($M = 2$) polynomial chaos up to order $p = 3$ are illustrated in Figs. 7.2 and 7.3.

Table 7.1.: Two-dimensional polynomial chaos up to order $p = 4$ and their corresponding variances.

j	p, order of the homogeneous chaos	j-th polynomial chaos ψ_j	$\langle \psi_j^2 \rangle$
0	$p = 0$	1	1
1	$p = 1$	ξ_1	1
2		ξ_2	1
3	$p = 2$	$\xi_1^2 - 1$	2
4		$\xi_1 \xi_2$	1
5		$\xi_2^2 - 1$	2
6	$p = 3$	$\xi_1^3 - 3\xi_1$	6
7		$\xi_1^2 \xi_2 - \xi_2$	2
8		$\xi_1 \xi_2^2 - \xi_1$	2
9		$\xi_2^3 - 3\xi_2$	6
10	$p = 4$	$\xi_1^4 - 6\xi_1^2 + 3$	24
11		$\xi_1^3 \xi_2 - 3\xi_1 \xi_2$	6
12		$\xi_1^2 \xi_2^2 - \xi_1^2 - \xi_2^2 + 1$	4
13		$\xi_1 \xi_2^3 - 3\xi_1 \xi_2$	6
14		$\xi_2^4 - 6\xi_2^2 + 3$	24

7.2.2. Truncation of the Polynomial Chaos Expansion

As already mentioned earlier in this chapter, for computations it is important to truncate the number of random variables ξ_i, $i = 1, \ldots M$ and the series expansion after a finite number p of PC coefficients. When truncating equation (7.8) after the
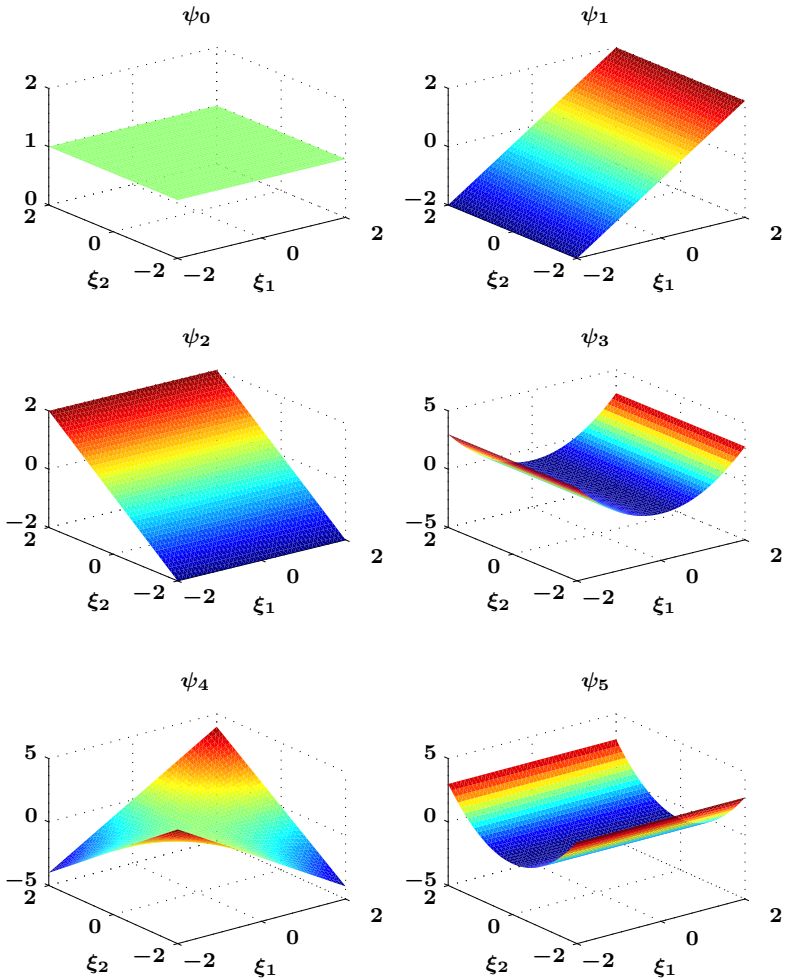
Figure 7.2.: Two-dimensional $(M = 2)$ Hermite polynomials of order $p = 0, 1, 2$.
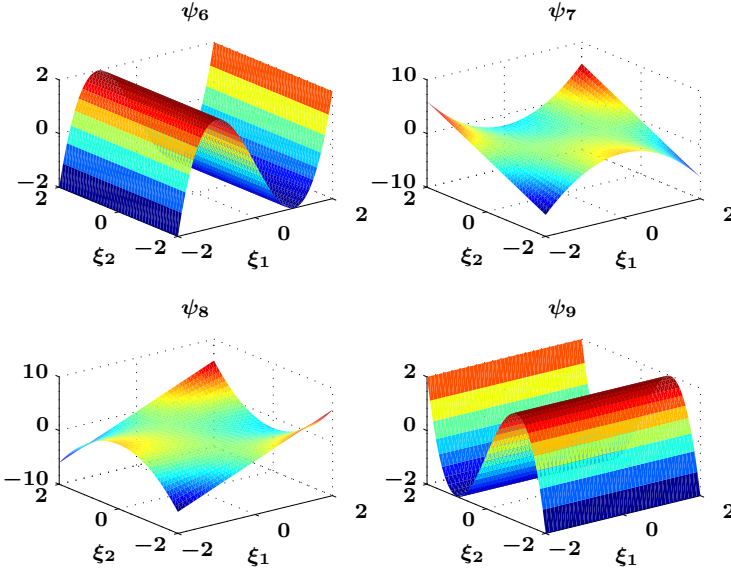
Figure 7.3.: Two-dimensional ($M = 2$) Hermite polynomials of order $p = 3$.

M-th dimensions and p-th order, the dimension dim of the polynomial basis P can be determined by

$$\dim P = \frac{(M + p)!}{M!\,p!}.$$ (7.19)

Evaluating this formula for different dimensions M and orders p leads to a number of basis polynomials P where the results up to $M = p = 6$ are reported in Tab. 7.2.

Table 7.2.: Number of basis polynomials P in a M-dimensional PCE truncated after order p.

M	$p = 1$	$p = 2$	$p = 3$	$p = 4$	$p = 5$	$p = 6$
2	3	6	10	15	21	28
4	5	15	35	70	126	210
6	7	28	84	210	462	924

The interpretation of this values is as follows: Each scalar value, for instance, the system response $u_x(\theta)$ at a certain node, is represented by a series expansion of P coefficients. This means, that the whole stochastic of $u_x(\theta)$ is approximated by a number of coefficients equal to dim P. As already mentioned in the previous chapter,

Table 7.3.: Correspondence of the probability law and their corresponding orthogonal polynomials.

	PDF	Orthogonal polynomials	Support range
Continuous	Gaussian	Hermite	$(-\infty, \infty)$
	Gamma	Laguerre	$[0, \infty)$
	Uniform	Jacobi	$[a, b]$
	Beta	Legendre	$[a, b]$
Discrete	Possion	Charlier	$\{0, 1, 2, ...\}$
	Binomial	Krawtchouk	$\{0, 1, 2, ... N\}$
	negative Binomial	Meixner	$\{0, 1, 2, ...\}$
	Hypergeometric	Hahn	$\{0, 1, 2, ... N\}$

a higher dimension M reflects higher random fluctuations better, whereas, with a higher order of p, non-linearities of the system response can be represented more accurate.

7.2.3. Stochastic Approximation

The optimal choice of the stochastic basis is essential to get an accurate representation of the random variable. For example, consider the series expansion of X in equation (7.16). Theoretically, X can also be expanded by

$$X = a_0 F_0(\xi(\theta)) + a_1 F_1(\xi(\theta)) + a_2 F_2(\xi(\theta)) + a_3 F_3(\xi(\theta)), \tag{7.20}$$

where F_i are polynomials, which can be constructed by any basis. For this example, the polynomials

$$F_0 = 1, \quad F_1 = \xi(\theta), \quad F_2 = \xi^2(\theta), \quad F_3 = \xi^3(\theta), \tag{7.21}$$

are assumed to approximate the system response. However, these polynomials are not the ideal choice. For example, large positive values of $\xi(\theta)$ lead to large positive values of the system response. Furthermore, when $\xi(\theta)$ is negative the odd power terms result in negative values and the even terms give positive values. Since they are not orthogonal, small changes in $F(\xi(\theta))$ result in relatively large changes in the coefficients a_i. This collinearity will make the associated least-squares problem ill-conditioned, cf. Choi et al. [2007]. The crucial point of this example is that a more reasonable polynomial basis, that satisfies the orthogonality, should be used. In the literature several orthogonal polynomials are described whose orthogonality weighting functions match the standard probability density functions. A few of the most common PDFs, with their corresponding orthogonal polynomials, are listed in Tab. 7.3, see also Schoutens [2000]; Xiu and Karniadakis [2002]; Xiu [2010]:

Generalized Polynomial Chaos Expansion

For a Gaussian distribution of X the Hermite polynomial basis is the optimal choice, see also Tab. 7.3. In order to represent various probability distributions with the polynomial chaos expansion, Xiu and Karniadakis [2002, 2003] presented the Askey scheme. Here, not only Hermite polynomials could be used to represent a Gaussian

or non-Gaussian system response, but also any orthogonal polynomials to characterize the system response. For detailed informations of this scheme, the reader is referred to Xiu and Karniadakis [2002, 2003].

In general: For the class of problems of interest the probability distribution of the system response to be determined is generally not known a priori and the construction of the optimal orthogonal basis is therefore (a priori) not possible. However, by knowledge of the probability laws of the input data, it may be useful to utilize these measures to generate a suitable PC basis for the system response. This means, that the basis will at least be optimal with respect to the uncertain input data representation. If, e.g., the system response cannot be captured with an orthogonal polynomial basis, because no orthogonal basis can be constructed, a numerical construction is possible, see Stoer and Bulirsch [2002], where this methodology is discussed in detail.

7.3. Implementation of the Polynomial Chaos Expansion

The construction of the polynomial chaos basis is an add-on of the institutes internal FE-code, realized in the programming environment of Matlab. For the implementation of the polynomial chaos basis the formulation presented in Sudret and der Kiureghian [2000]; Sudret et al. [2006] will be summarized in this section. This approach was realized in collaboration with Schmidt [2013] in the context of his bachelor thesis.

The goal is to compute all possible non negative integer sequences of M whose sum is equal to $q = \{1, ...p\}$ where $q = \sum_{i=1}^{M} \alpha_i$. This problem is equivalent to that of filling $(M + q - 1)$ boxes with $(M - 1)$ balls, see Tab. 7.4, where an example for the generation of such an integer sequences $\boldsymbol{\alpha}$ is given.

Table 7.4.: Relation between the reverse integer sequences $\boldsymbol{\alpha}$, the ball samples and the resulting chaos polynomials.

Arrangement of the balls	Reverse Integer Sequence	Chaos Polynomial
⊡ ⊡ ⊡ ☐ ☐	2 0 0 0	$\mathfrak{h}_2(\xi_1) = \xi_1^2 - 1$
⊡ ☐ ☐ ☐ ⊡	0 1 1 0	$\mathfrak{h}_1(\xi_2)\mathfrak{h}_1(\xi_3) = \xi_2\,\xi_3$

The relation between the integers α_i of the sequences $\boldsymbol{\alpha}$ and the box samples is listed below:

- For each integer α_i of the sequence $\boldsymbol{\alpha}$ skip α_i empty boxes and put a ball in the next box.

- Conversely, for each ball sample, each integer α_i of the sequence is equal to the number of empty boxes between two consecutive balls.

The recursive algorithm for the generation of all possible ball samples is summarized in the following. For example, let $M = 4$ and $q = 2$, which is equivalent to put three balls in a certain sequence into five boxes ☐ ☐ ☐ ☐ ☐, whereas the idea is sub-divided into the following two steps.

1. In the first step the initial sample is obtained by putting the balls in the $M - 1$ first boxes. The corresponding integer sequence reads $\boldsymbol{\alpha} = \{0, 0, 0, q\}$ and the associated box sample results to ⊡ ⊡ ⊡ ☐ ☐.

2. From the second up to the last step, the rightmost ball is shifted one box to the right. If this is not possible, i.e. the rightmost ball is already rightmost and the rightmost ball, which can be shifted by one box to the right, is picked and the balls lying to the right of this ball shifted one box back to the left.

This procedure is illustrated in Tab. 7.5 for all sequences of $M = 4$ and $q = 2$, where it should be remarked that the polynomial basis ψ_i is based on the reversed integer sequence that corresponds to this one used in Ghanem and Spanos [2003].

Concluding Remark

As already mentioned in the last subsection based the polynomial chaos mainly on the explanations of Ghanem and Spanos [2003]; Sudret and der Kiureghian [2000]; Sudret et al. [2006]. It has been realized, that effective techniques for the reduction of CPU time has been developed. Such methods are, e.g., an adaptive choice of the PC basis or an refinement during the computation as well as an p-refinement of the polynomial chaos. These techniques will not be covered here in detail and the reader is referred to the textbook by Le Maître and Knio [2010] and the references therein, where such newer developments are discussed.

Table 7.5.: Integer-sequences of four-dimensional ($M = 4$) chaos-polynomials of order $p = 2$, respectively $q = 2$.

Arrangement of the Balls	Integer Sequence	Reverse Integer Sequence	Polynomial Basis
⊡ ⊡ ⊡ □ □	0 0 0 2	2 0 0 0	$\xi_1^2 - 1$
⊡ ⊡ □ ⊡ □	0 0 1 1	1 1 0 0	$\xi_1 \xi_2$
⊡ ⊡ □ □ ⊡	0 0 2 0	1 0 1 0	$\xi_1 \xi_3$
⊡ □ ⊡ ⊡ □	0 1 0 1	1 0 0 1	$\xi_1 \xi_4$
⊡ □ ⊡ □ ⊡	0 1 1 0	0 0 2 0	$\xi_2^2 - 1$
⊡ □ □ ⊡ ⊡	0 2 0 0	0 1 1 0	$\xi_2 \xi_3$
□ ⊡ ⊡ ⊡ □	1 0 0 1	0 1 0 1	$\xi_2 \xi_4$
□ ⊡ ⊡ □ ⊡	1 0 1 0	0 0 2 0	$\xi_3^2 - 1$
□ ⊡ □ ⊡ ⊡	1 1 0 0	0 0 1 1	$\xi_3 \xi_4$
□ □ ⊡ ⊡ ⊡	2 0 0 0	0 0 0 2	$\xi_4^2 - 1$

8. Stochastic Finite Element Method

The *Stochastic Finite Element Method* (SFEM) is meanwhile a well established technique to investigate (e.g., structural) systems with stochastic properties in various engineering branches. It is an extension of the standard FEM, which combines the probability theory with the deterministic approach. The focus lies on the solution of mechanical systems whose parameters, such as material, geometry or loads are uncertain. The motivation of any SFEM approach is to get an alternative and more effective method to the time-consuming Monte Carlo Sampling techniques. Stefanou [2011] identifies two factors for the constantly growing attention of the SFEM received over the last three decades, which are:

- The understanding of the significant influence of the inherent system uncertainties on the system response and

- the enormous increase of the computational performance in the last years.

Some publications, which reflect some of the early developments of the SFEM are the works from Contreras [1980]; Vanmarcke et al. [1986]; Liu et al. [1986a,b, 1987]; Shinozuka and Deodatis [1988]; Takada [1990a,b]; Zhu et al. [1992]; Kleiber and Hien [1992].

The general formulation in the SFEM is a simple extension of the deterministic linear formulation $\mathbf{KU} = \mathbf{F}$, i.e.

$$\mathbf{K}(\theta)\,\mathbf{U}(\theta) = \mathbf{F}(\theta)\,, \quad \text{with } \theta \in (\Theta, \mathcal{F}, \mathcal{P})\,, \tag{8.1}$$

where $(\Theta, \mathcal{F}, \mathcal{P})$ denotes a HILBERT space. To shorten the notation, the random character θ is not explicitly written in the following sections. It will only be used when a clear distinction between the deterministic and the stochastic variable is needed, for instance, to distinguish the deterministic stiffness matrix $\mathbf{K}$ from its stochastic counter part $\mathbf{K}(\theta)$.

After the discretization of the random field with the KLE, the fluctuations of the input parameters are characterized by a finite number of random variables. The system response may be also represent by a suitable space, which is spanned by a polynomial chaos basis P. The statistics of the system response (beyond the mean) reached if the PC coefficients are evaluated. This methodology is well known as the *Spectral Stochastic Finite Element Method* (SSFEM) where the pioneered work, which was applied to mechanical problems, was presented by Ghanem and Spanos [2003]. The vast amount of research is reflected in a large number of publications. In addition to the reference textbook by Ghanem and Spanos [2003], the recently published textbooks by Le Maître and Knio [2010] and Xiu [2010] are mentioned in this context, which cover a wide range of the stochastic finite element analysis.

This chapter is structured as follows: A brief overview of techniques for the analysis of stochastic mechanical systems is presented in section 8.1. This section ends with a short explanation of the distinction between the non-intrusive and the intrusive approach. The detailed formulation of the SSFEM, for linear elastic material behaviour, is presented in section 8.2. Then, some remarks on the computational implementation

of the SSFEM are discussed and illustrated by means of pseudo-algorithms. Afterwards, the post-processing step is presented. Here, it is explained how the polynomial chaos coefficients must be evaluated to make practical predictions for the quantities of interest, for example, the system response, which is outlined in section 8.4. Then, some extensions of the SSFEM are presented in section 8.5, with a particular emphasis on multiple input random fields. A numerical example is presented and discussed in section 8.6 and the major findings of this chapter are summarised in section 8.7.

8.1. Overview of Numerical Techniques

The discretization of the random input parameters has already been addressed in chapter 6 and will not be described here any more. This section is addressed to give a brief summary of some alternative stochastic finite element methods besides the SSFEM. Namely, these are the *perturbation method*, the *weighted integral method* and the Neumann expansion. The following subsections are essentially a summary of the works of Matthies et al. [1997]; Schuëller [1997]; Anders [2000]; Sudret and der Kiureghian [2000]; Choi et al. [2007]. Due to the "overview-character", detailed expressions of the formulations of the presented methods will be omitted in this section. Therefore, the reader is referred to the cited works above as well as to the citations in the subsequent subsections.

8.1.1. Perturbation Method

The perturbation method is a commonly used non-sampling method, where the input parameters are expanded around their corresponding mean values and truncated after a certain order. This method is mainly limited to second-order expansions, because the evaluation of the statistical moments needs higher order statistical moments, which makes it complicated as well as computationally extensive.

Let $\boldsymbol{X} = [X_1, ... X_N]$ be a zero-mean random vector including the variations of the input parameters around their means with the total number of the input parameters defined by N. The expansion of the terms, appearing in equation 8.1, in a Taylor-Series reads, cf. Sudret and der Kiureghian [2000]:

$$\mathbf{K}(\theta) = \mathbf{K}_0 + \sum_{i=1}^{N} \mathbf{K}_i^I X_i + \frac{1}{2} \sum_{i=1}^{N} \sum_{j=1}^{N} \mathbf{K}_{ij}^{II} X_i X_j + ... , \tag{8.2}$$

$$\mathbf{U} = \mathbf{U}_0 + \sum_{i=1}^{N} \mathbf{U}_i^I X_i + \frac{1}{2} \sum_{i=1}^{N} \sum_{j=1}^{N} \mathbf{U}_{ij}^{II} X_i X_j + ... , \tag{8.3}$$

$$\mathbf{F} = \mathbf{F}_0 + \sum_{i=1}^{N} \mathbf{F}_i^I X_i + \frac{1}{2} \sum_{i=1}^{N} \sum_{j=1}^{N} \mathbf{F}_{ij}^{II} X_i X_j + ... , \tag{8.4}$$

where $\bullet_i^I$ and $\bullet_{ij}^{II}$ are the first and the second derivatives with respect to $\boldsymbol{X} = 0$. For example, the partial derivatives $\mathbf{K}_i^I$ and $\mathbf{K}_{ij}^{II}$ are given by

$$\mathbf{K}_i^I = \frac{\partial \mathbf{K}(\theta)}{\partial X_i} \bigg|_{\boldsymbol{X}=0} \quad \text{and} \quad \mathbf{K}_{ij}^{II} = \frac{\partial^2 \mathbf{K}(\theta)}{\partial X_i X_j} \bigg|_{\boldsymbol{X}=0} . \tag{8.5}$$

The coefficient vectors $\mathbf{U}_0$, $\mathbf{U}_i^I$ and $\mathbf{U}_{ij}^{II}$ are evaluated by substituting the equations $(8.2)-(8.4)$ into equation (8.1) and identifying terms with the same order. This leads to the following recursive equations, cf. Sudret and der Kiureghian [2000]:

$$\mathbf{U}_0 = \mathbf{K_0}^{-1}\mathbf{F}_0\,, \tag{8.6}$$

$$\mathbf{U}_i^I = \mathbf{K}_0^{-1}\left(\mathbf{F}_i^I - \mathbf{K}_i^I\mathbf{U}_0\right)\,, \tag{8.7}$$

$$\mathbf{U}_{ij}^{II} = \mathbf{K}_0^{-1}\left(\mathbf{F}_{ij}^{II} - \mathbf{K}_i^I\mathbf{U}_j^I - \mathbf{K}_j^I\mathbf{U}_i^I - \mathbf{K}_{ij}^{II}\mathbf{U}_0\right)\,. \tag{8.8}$$

The expected value of the system response $\mathbf{U}$ can be evaluated by using equation (8.3), thus

$$\mathbb{E}[\mathbf{U}] \approx \mathbf{U}_0 + \frac{1}{2}\sum_{i=1}^{N}\sum_{j=1}^{N}\mathbf{U}_{ij}^{II}\,\mathrm{Cov}(X_i,\,X_j)\,, \tag{8.9}$$

with $\mathbf{U}_0 = \mathbb{E}[\mathbf{U}_0]$. The second-order approximation of the covariance matrix $\mathrm{Cov}(\cdot,\cdot)$ can be found in Yamazaki et al. [1988].

The perturbation-based SFEM has been applicated to a wide range of problems, such as elastic problems, dynamic problems, eigenvalue problems, non-linear problems etc. However, this method is practically restricted to input parameters, which have only small fluctuations. The coefficient of variation α_X, where X denotes an arbitrary stochastic variable, depends on the non-linearity of the system and is specified in many publications to $\alpha_X \leq 20\%$. In the recently published textbooks by Le Maître and Knio [2010] and Xiu [2010], α_X is even specified to $\alpha_X \leq 10\%$.

This method can be coupled with random field discretization techniques. Examples are the spatial average method, discussed in the subsection 6.2.1 or the shape function method, which was introduced in the subsection 6.2.2. For more informations about the coupling between the perturbation method and these discretization methods, see Sudret and der Kiureghian [2000] and the references therein.

8.1.2. Weighted Integral Method

The weighted integral method is a perturbation-based approach with the discretization scheme presented in section 6.2.2. This method was first introduced amongst others by Deodatis [1991] and Deodatis and Shinozuka [1991].

For convenience, the *stochastic* element stiffness matrix $\mathbf{k}^e(\theta)$, introduced in equation (6.14), is written here again

$$\mathbf{k}^e(\theta) = \mathbf{k}_0^e + \sum_{i=1}^{n_{WI}}\Delta\mathbf{k}_i^e X_i^e\,, \tag{8.10}$$

where $\Delta\mathbf{k}_i^e$ are deterministic matrices, X_i^e are the *weighted integrals* and n_{WI} denotes the number of weighted integrals of element e. The assembling procedure of the parts in equation (8.10) leads to a global stiffness matrix of $N \times n_{WI}$ random variables in the linear equation system

$$\mathbf{K}(\theta)\,\mathbf{U} = \mathbf{F}\,, \tag{8.11}$$

which has to be solved for $\mathbf{U}$. For more details on the assembling see Deodatis [1991]. The response statistics are evaluated from equation (8.11), where the first-order Taylor series expansion is applied to $\mathbf{U}$ about the mean values of the weighted integrals X_i^e. Evaluating this expansion leads to, cf. Sudret and der Kiureghian [2000],

$$\mathbf{U} = \mathbf{U}_0 + \sum_{e=1}^{N} \sum_{i=1}^{n_{WI}} X_i^e \frac{\partial \mathbf{U}}{\partial X_i^e}\bigg|_{X_i^e=0}. \tag{8.12}$$

In the case of a deterministic load vector $\mathbf{F}$, the partial derivative $\frac{\partial \mathbf{U}}{\partial X_i^e}$ is calculated by partially differentiating equation (8.11) with respect to X_i^e, i.e.

$$\frac{\partial \mathbf{U}}{\partial X_i^e} = -\mathbf{K_0}^{-1} \frac{\partial \mathbf{K}}{\partial X_i^e}\bigg|_{X_i^e=0} \mathbf{U}_0\,, \tag{8.13}$$

with $\mathbf{U}_0 = \mathbf{K}_0^{-1}\mathbf{F}$. Substituting this derivative back into equation (8.12) it becomes

$$\mathbf{U} = \mathbf{U}_0 - \sum_{e=1}^{N} \sum_{i=1}^{n_{WI}} X_i^e \mathbf{K_0}^{-1} \frac{\partial \mathbf{K}}{\partial X_i^e}\bigg|_{X_i^e=0} \mathbf{U}_0\,. \tag{8.14}$$

The mean value of $\mathbf{U}$ can be evaluated directly from equation (8.14) as

$$\mathbb{E}[\mathbf{U}] = \mathbf{U}_0 = \mathbf{K}_0^{-1}\mathbf{F}\,. \tag{8.15}$$

For the evaluation of the Var and Cov of $\mathbf{U}$, the reader is referred to, e.g., the article by Deodatis [1990].

8.1.3. Neumann Expansion Method

The Neumann expansion is an effective technique when coupled with the Monte-Carlo Method, cf. Yamazaki et al. [1988]. The key advantage lies in the factorization of the global stochastic stiffness matrix $\mathbf{K}(\theta)$, which avoids repeating inversion of the stochastic stiffness matrix $\Delta\mathbf{K}$ during the calculation process, cf. Yamazaki et al. [1988]; Chakraborty and Bhattacharyya [2002].

The *stochastic* global stiffness matrix $\mathbf{K}(\theta)$ is defined by

$$\mathbf{K}(\theta) = \mathbf{K}_0 + \Delta\mathbf{K}\,, \tag{8.16}$$

where $\mathbf{K}_0$ denotes the mean stiffness matrix and $\Delta\mathbf{K}$ is a matrix which includes the fluctuating components of the considered parameter. Inserting equation (8.16) into equation (8.1), by neglecting randomness in $\mathbf{F}$, leads to

$$[\mathbf{K}_0 + \Delta\mathbf{K}]\,\mathbf{U} = \mathbf{F}\,. \tag{8.17}$$

The evaluation of this equation, with respect to $\mathbf{U}_0$, gives

$$\mathbf{U}_0 = \mathbf{K}_0^{-1}\mathbf{F}\,. \tag{8.18}$$

Applying a Neumann expansion to the inverted stochastic global stiffness matrix

$\mathbf{K}^{-1}(\theta)$ gives, cf. Yamazaki and Shinozuka [1988],

$$\mathbf{K}^{-1}(\theta) = (\mathbf{K}_0 + \Delta\mathbf{K})^{-1} = (\mathbf{I} - \mathbf{P} + \mathbf{P}^2 - \mathbf{P}^3 + \cdots)\,\mathbf{K}_0^{-1}\,, \tag{8.19}$$

with the relation $\mathbf{P} = \mathbf{K}_0^{-1}\Delta\mathbf{K}(\theta)$ and $\mathbf{I}$ is an identity matrix. After substituting equation (8.19) into $\mathbf{U} = \mathbf{K}^{-1}(\theta)\,\mathbf{F}$, the following result is obtained:

$$\mathbf{U} = (\mathbf{I} - \mathbf{P} + \mathbf{P}^2 - \mathbf{P}^3 + \cdots)\,\mathbf{K}_0^{-1} \tag{8.20}$$

$$= \mathbf{U}_0 + \sum_{n=0}^{\infty}(-1)^n\mathbf{P}^n\mathbf{U}_0\,, \tag{8.21}$$

where $\mathbf{U}_0\mathbf{F}^{-1} = \mathbf{K}_0^{-1}$. Statistics of the system response $\mathbf{U}$ are calculated by Shinozuka and Deodatis [1988], whereas only the first two terms of equation (8.21) are used, with the remark of the authors that the approximated results of $\mathbf{U}$ are good if the coefficient of variation is small, i.e. $\alpha_X \leq 20\%$. The mean value of the displacement vector is given by

$$\mathbb{E}[\mathbf{U}] = \mathbf{U}_0\,, \tag{8.22}$$

where $\mathbf{U}_0$ is already defined in equation (8.18). For this expansion method, the covariance matrix of $\mathbf{U}$ can be written in a compact form as follows, cf. Matthies et al. [1997]:

$$\mathrm{Cov}(\mathbf{U},\,\mathbf{U}) = \mathbf{E}\left[\mathbf{P}\mathbf{U}_0\mathbf{U}_0^{\mathrm{T}}\mathbf{U}^{\mathrm{T}}\right]\,. \tag{8.23}$$

8.1.4. Improved Neumann Method

A similar approach to the Neumann Expansion method is presented by Spanos and Ghanem [1989], where the KLE is applied to represent the fluctuations of the input parameters. The Neumann expansion is also utilised to obtain the evaluation of the system response $\mathbf{U}$.

Let $H(\mathbf{x}, \theta)$ be a random field, defined by

$$H(\mathbf{x}, \theta) = H_0 + \Delta H\,, \tag{8.24}$$

where the fluctuating part ΔH is represented by a KLE as

$$\Delta H(\mathbf{x}, \theta) = \sum_{i=1}^{\infty}\sqrt{\lambda_i}f_i(\mathbf{x})\xi_i(\theta)\,. \tag{8.25}$$

Here, ξ_i are Gaussian random variables with respect to the corresponding set of eigenfunctions $\{f_i\}$ and λ_i is the i-th eigenvalue. Substituting this representation into equation (8.24) leads to

$$H(\mathbf{x}, \theta) = H_0 + \sum_{i=1}^{\infty}\sqrt{\lambda_i}f_i(\mathbf{x})\xi_i(\theta)\,. \tag{8.26}$$

Now the formulation with respect to the FEM is presented below. The stochastic

element stiffness matrix can be written in a compact form by

$$\mathbf{k}^e(\theta) = \mathbf{k}_0^e + \sum_{i=1}^{\infty} \mathbf{k}_i^e \xi_i(\theta) \,, \tag{8.27}$$

where $\mathbf{k}_i^e$ is the i-th deterministic matrix of element e, defined by

$$\mathbf{k}_i^e = \sqrt{\lambda_i} \int_{\Omega_e} \mathbf{B}^{\mathrm{T}} \mathbb{C}_0 f_i(\mathbf{x}) \mathbf{B} \, \mathrm{d}\Omega_e \,, \tag{8.28}$$

with $\mathbb{C}_0$[1] being a constant matrix and the matrix $\mathbf{B}$ relates the components of the strains to the element nodal displacements. Assembling all element contributions leads to the global stochastic stiffness matrix $\mathbf{K}(\theta)$ and the stochastic counterpart of the deterministic FEM formulation

$$\left[\mathbf{K}_0 + \sum_{i=1}^{\infty} \mathbf{K}_i \xi_i(\theta) \right] \mathbf{U}(\theta) = \mathbf{F} \,. \tag{8.29}$$

Note, that the load vector $\mathbf{F}$ is assumed to be deterministic. The system random response $\mathbf{U}(\theta)$ is obtained by inverting equation (8.29). However, no closed solution of such an inverse exists, cf. Sudret and der Kiureghian [2000]. To circumvent this problem, Spanos and Ghanem [1989] proposed a Neumann series expansion to obtain an approximation for this inverse operator, which is presented below.

First of all, multiplying both sides of equation (8.29) by $\mathbf{K}_0^{-1}$, which leads to

$$\left[\mathbf{I} + \sum_{i=1}^{\infty} \mathbf{K}_0^{-1} \mathbf{K}_i \xi_i(\theta) \right] \mathbf{U} = \mathbf{U}_0 \,, \tag{8.30}$$

with $\mathbf{U}_0 = \mathbf{K}_0^{-1} \mathbf{F}$. The inversion of equation (8.30) reads

$$\mathbf{U} = \left[\mathbf{I} + \sum_{i=1}^{\infty} \mathbf{K}_0^{-1} \mathbf{K}_i \xi_i(\theta) \right]^{-1} \mathbf{U}_0 \,. \tag{8.31}$$

By applying a Neumann series expansion to equation (8.31), the following result is obtained, cf. Spanos and Ghanem [1989]:

$$\mathbf{U} = \sum_{h=0}^{\infty} (-1)^h \left[\mathbf{I} + \sum_{i=1}^{\infty} \mathbf{K}_0^{-1} \mathbf{K}_i \xi_i(\theta) \right]^h \mathbf{U}_0 \,, \tag{8.32}$$

where an explicit expression of the first terms is given by

$$\mathbf{U} = \left[\mathbf{I} - \sum_{i=1}^{\infty} \mathbf{Q}_i \xi_i(\theta) + \sum_{i=1}^{\infty} \sum_{j=1}^{\infty} \mathbf{Q}_i \mathbf{Q}_j \xi_i(\theta) \xi_j(\theta) + \cdots \right] \mathbf{U}_0 \,,$$

with $\mathbf{Q}_i = \mathbf{K}_0^{-1} \mathbf{K}_i$ and $\mathbf{Q}_j = \mathbf{K}_0^{-1} \mathbf{K}_j$. Truncating the KLE (index i) and the Neumann expansion series (index h) in equation (8.32) gives an approximation for

---

[1] The explicit definition of $\mathbb{C}_0$ for an isotropic material will be given in the next section.

the displacement vector $\mathbf{U}$. The first moment of the system response $\mathbf{U}$ can be evaluated from equation (8.32) by applying the expectation operator, i.e.

$$\mathbb{E}[\mathbf{U}] = \sum_{h=0}^{\infty} (-1)^h \, \mathbb{E}\left[\mathbf{I} - \sum_{i=1}^{\infty} \mathbf{Q}_i \xi_i(\theta) + \sum_{i=1}^{\infty} \sum_{j=1}^{\infty} \mathbf{Q}_i \mathbf{Q}_j \xi_i(\theta) \xi_j(\theta) + \cdots \right] \mathbf{U}_0 \,. \quad (8.33)$$

For the determination of the covariance matrix the reader is referred to Spanos and Ghanem [1989] or Matthies et al. [1997].

Each random displacement u^i from $\mathbf{U}$ in equation (8.32) can be represented by a series of polynomials $\mathbb{P}$ by a set of variables $\{\xi_h\}_{h=1}^{\infty}$. By use of the single index j, the response of a specific nodal displacement u^i can be formally written as follows:

$$\mathrm{u}^i = \sum_{j=0}^{\infty} u_j^i \mathbb{P}_j \left(\{\xi_h(\theta)\}_{h=1}^{\infty}\right) \,, \quad (8.34)$$

where $\mathbb{P}_0 \equiv 1$ and $\mathbb{P}_j \left(\{\xi_h(\theta)\}_{h=1}^{\infty}\right)$ are polynomials in standard normal variables. The choice of the polynomials is important and must be made carefully to achieve an accurate approximation of the random variables. Orthogonal polynomials are an optimal choice, where a detailed discussion of this fact has been given in the previous chapter.

In this section, an overview of a few numerical methods for the representation of stochastic systems are presented. These methods are mainly applied at the beginning of the SFEM developments. The recent applications and developments are primary restricted the spectral stochastic methods, see, e.g., the article of Nouy [2009]. In view of the following section the input parameters are characterized by a KLE and the system response is represented by a PCE. This approach as well as the methods presented in this section are called *intrusive*, hence it requires an expansion (new formulation) of the computer code to handle the reformulated equations. An alternative approach is the *non-intrusive* one. In this context, the PC coefficients of the system response are evaluated by a deterministic or random sampling of the original deterministic model/computer code. Also the sampling techniques, which has been presented in section 4.4, are non-intrusive methods. The former method calculates the system response in terms of a PCE directly in one computer run, which is a great advantage to the non-intrusive approach where a large number of computer runs are necessary. On the other hand, the non-intrusive methods requires no modifications on the existing computer code, which makes it attractive for industrial applications in connection with a commercial code.

8.2. Spectral Stochastic Finite Element Method

The basis of the SSFEM was proposed by Ghanem and Spanos [1989]; Spanos and Ghanem [1989]; Ghanem and Spanos [2003] in the early 1990s. In its first version, the fluctuations of the input quantities are represented by GAUSSIAN random fields, which are discretized by the KARHUNEN-LOÈVE Expansion. As mentioned earlier, the KLE can not be used to represent the system response. Due to this, Ghanem and Spanos [2003] used the PCE to overcome this drawback.

The basic approach, presented by Ghanem and Spanos [2003], has received a wide acceptance and has been applied in various engineering application areas, what is

documented by a large number of publications. A few of these applications are (cf. also Sudret [2007]): Transport media problems, as presented in Ghanem and Dham [1998], non-linear vibrations, see Li and Ghanem [1998] and heat conduction problems, discussed in Ghanem [1999].

Beside this listing, there are also some applications in the field of fluid dynamics that give some benefit in view of the first proposed PCE. With respect to this area of research it is referenced to the paper by Najm [2009] as well as to the recently published textbook by Le Maître and Knio [2010].

Some mathematically based publications completed PCE approach in the early 2000s. In this context, the works by Deb et al. [2001]; Babuška and Chatzipantelidis [2002]; Babuška et al. [2004] and Frauenfelder et al. [2005] are mentioned, see also Sudret [2007]. The main focus of this works lies on the solution of elliptic differential equations with stochastic coefficients.

Apart from the detailed discussions in the referred books and papers above, a more general overview of the SSFEM can be found in the reports by Matthies et al. [1997]; Schuëller [1997]; Sudret and der Kiureghian [2000] or Gutiérrez and Krenk [2004].

After this brief historical review the following subsections are devoted to the SSFEM with respect to linear elastic problems where the entire field of a stochastic calculation will be considered. Starting with the equilibrium equation in a stochastic context over the representation of the system response by a PCE up to the post-processing of the results. Afterwards, some remarks on the computational implementation and on the extension of the SSFEM are given.

8.2.1. Formulation of the Stochastic Elliptic Boundary Value Problem

The following subsections are addressed to the formulation of the stochastic counterpart of the deterministic balance of linear momentum with the boundary conditions summarized in equation 3.4, which are repeated here for convenience reasons:

$$\begin{cases} \operatorname{div}\boldsymbol{\sigma} + \mathbf{b} &= \mathbf{0}\,, \\ \mathbf{u} &= \bar{\mathbf{u}} \qquad \text{on} \quad \partial\Omega_{\mathrm{u}}\,, \\ \boldsymbol{\sigma}\cdot\mathbf{n} &= \bar{\mathbf{t}} \qquad \text{on} \quad \partial\Omega_{\sigma}\,. \end{cases} \tag{8.35}$$

In the stochastic formulation of this thesis, neither the domain Ω nor the parts $\partial\Omega_{\mathrm{u}}$ and $\partial\Omega_{\sigma}$ of its boundaries are random. Furthermore, the loading terms are also assumed to be deterministic. In contrast, the Young's modulus E is represented by a random field, denoted by $H_E(\mathbf{x}, \theta)$. As a consequence the system response $\mathbf{u}$ (respectively $\mathbf{U}$ for the global system response) is also a random field, denoted by $\mathbf{u}(\mathbf{x}, \theta)$, respectively $\mathbf{U}(\mathbf{x}, \theta)$, and almost surely[2] satisfies the following linear stochastic boundary value problem (without body forces $\mathbf{b}$):

$$\begin{cases} \operatorname{div}\boldsymbol{\sigma}(\mathbf{x}, \theta) &= \mathbf{0}\,, \\ \mathbf{u} &= \bar{\mathbf{u}} \qquad \text{on} \quad \partial\Omega_{\mathrm{u}}\,, \\ \boldsymbol{\sigma}\cdot\mathbf{n} &= \bar{\mathbf{t}} \qquad \text{on} \quad \partial\Omega_{\sigma}\,. \end{cases} \tag{8.36}$$

---

[2] Let $(\Theta, \mathcal{F}, \mathcal{P})$ be a probability space. In this space an event $\mathrm{E} \in \mathcal{F}$ happens almost surely if the probability $\mathcal{P}(\mathrm{E})$ is 1, formally written as $\mathcal{P}(\mathrm{E}) = 1$.

8.2.2. Stochastic Variational Form

The deterministic space for the random solution is denoted by $\mathcal{V}$ and the complete functional space for the displacement field $\mathbf{u}(\mathbf{x}, \theta)$ is given by the tensor product space $\mathcal{V} \otimes \mathcal{S}$, where $\mathcal{S} = \mathcal{L}^2(\Theta, \mathcal{F}, \mathcal{P})$ is a reasonable choice in practice. The variational form of the linearized weak form of the stochastic problem (8.36) then reads:

Find $\mathbf{u}(\mathbf{x}, \theta) \in \mathcal{V} \otimes \mathcal{S}$ such that

$$\mathscr{A}(\mathbf{u}, \boldsymbol{\delta}_\mathrm{u}(\theta)) = \mathscr{B}(\boldsymbol{\delta}_\mathrm{u}(\theta)) \qquad \forall \boldsymbol{\delta}_\mathrm{u}(\theta) \in \mathcal{V} \otimes \mathcal{S}, \tag{8.37}$$

where

$$\begin{aligned} \mathscr{A}(\mathbf{u}, \boldsymbol{\delta}_\mathrm{u}(\theta)) &= \int_\Theta \left[\int_\Omega \boldsymbol{\sigma}(\mathbf{x}, \theta) : \nabla^{\mathrm{sym}\cdot} \boldsymbol{\delta}_\mathrm{u}(\theta)\, \mathrm{d}v \right] \mathrm{d}\mathcal{P}(\theta) \\ &\equiv \mathbb{E}[\mathscr{A}(\mathbf{u}, \boldsymbol{\delta}_\mathrm{u}(\theta))], \end{aligned} \tag{8.38}$$

and

$$\mathscr{B}(\boldsymbol{\delta}_\mathrm{u}(\theta)) = \int_\Theta \left[\int_{\partial\Omega} \bar{\mathbf{t}} \cdot \boldsymbol{\delta}_\mathrm{u}(\theta)\, \mathrm{d}a \right] \mathrm{d}\mathcal{P}(\theta) \equiv \mathbb{E}[\mathscr{B}(\boldsymbol{\delta}_\mathrm{u}(\theta))], \tag{8.39}$$

with the mathematical expectation

$$\mathbb{E}[f] = \int_\Theta f(\theta)\, \mathrm{d}\mathcal{P}(\theta).$$

Discretization of the Stochastic Problem by the Galerkin Method

In order to solve the problem, given in equation (8.37), by the GALERKIN method, it is suitable to split the discretization procedure into the following two parts.

1. The first part of the discretization is similar to the discretization of the deterministic finite element formulation, where suitable subspaces of $\mathcal{V} \otimes \mathcal{S}$ are selected. Such a subspace $\mathcal{V}^h \subset \mathcal{V}$, denoted as finite element approximation space, is

$$\mathcal{V}^h = \mathrm{span}\,\{N_i\}_{i \in \mathcal{N}}, \tag{8.40}$$

   where $\mathcal{N}$ denotes the set of nodes of the FE mesh and N_i is the shape function associated with the i-th node.

2. The second part is related to the stochastic discretization, which requires an introduction of a finite-dimensional subspace $\mathcal{S}^P \subset \mathcal{S}$. This subspace $\mathcal{S}^P$ is spanned by a polynomial chaos

$$\mathcal{S}^P = \mathrm{span}\{\psi_j(\theta),\ j = 0, \dots P - 1\}, \tag{8.41}$$

   where the ψ_j's form a set of orthogonal multidimensional HERMITE Polynomials. Here, when applying the polynomial chaos expansion it is assumed that the input random field is characterized by a KLE, using M random variables. Both parts,

the discretization by the KLE and the approximation of the stochastic dimension via the polynomial chaos will be illustrated in the following two subsections.

8.2.3. Spatial Discretization applying the KLE

The spatial discretization of the stochastic problem is straightforward. After applying the procedure described in subsection 3.3 and with respect to the operators $\mathscr{A}(\cdot)$ and $\mathscr{B}(\cdot)$, introduced in the previous section, the discretized stochastic weak form is obtained as follows:

$$\mathscr{A}\left(\hat{\mathbf{u}}, \boldsymbol{\delta}_{\hat{\mathbf{u}}}(\theta)\right) \approx \mathbb{E}\left[\boldsymbol{\delta}_{\hat{\mathbf{u}}}(\theta) \underbrace{\int_{\Omega} \mathbf{B}^{\mathrm{T}} \mathbb{C}(\mathbf{x}, \theta) \mathbf{B} \, \mathrm{d}v}_{\mathbf{k}^e(\theta)} \, \hat{\mathbf{u}}(\theta)\right], \tag{8.42}$$

and

$$\mathscr{B}\left(\hat{\mathbf{u}}, \boldsymbol{\delta}_{\hat{\mathbf{u}}}(\theta)\right) \approx \mathbb{E}\left[\boldsymbol{\delta}_{\hat{\mathbf{u}}}(\theta)\left(\underbrace{\int_{\partial\Omega} \mathbf{H}^{\mathrm{T}} \bar{\mathbf{t}} \, \mathrm{d}a}_{\mathbf{f}^{e\,\mathrm{ext}}}\right)\right], \tag{8.43}$$

where $\mathbf{f}^{e\,\mathrm{ext}}$ are the deterministic[3] external element forces and $\mathbf{k}^e(\theta)$ denotes the stochastic element stiffness matrix.

Since the Young's modulus is discretized by a KLE using a set of M Gaussian random variables $\{\xi_i(\theta), \, i = 1, \dots M\}$, the stochastic elasticity tensor $\mathbb{C}(\mathbf{x}, \theta)$ can be expressed as

$$\mathbb{C}(\mathbf{x}, \theta) \equiv \hat{H}_E(\mathbf{x}, \theta)\, \mathbb{C}_0\,. \tag{8.44}$$

Here, $\hat{H}_E(\cdot)$ is the discretized random Young's modulus field and $\mathbb{C}_0$ is the constant part of the isotropic[4] material tensor in equation (2.88), which is given by

$$\mathbb{C}_0 = \frac{1}{(1+\nu)(1-2\nu)} \begin{bmatrix} 1-\nu & \nu & \nu & & & \\ \nu & 1-\nu & \nu & & \mathbf{0} & \\ \nu & \nu & 1-\nu & & & \\ & & & \frac{1-2\nu}{2} & & \\ & \mathbf{0} & & & \frac{1-2\nu}{2} & \\ & & & & & \frac{1-2\nu}{2} \end{bmatrix}. \tag{8.45}$$

---

[3] Stochastic external forces are also possible but not applied in this thesis.

[4] For the sake of simplicity only isotropic materials are considered in this thesis. For further research also anisotropic materials should be applied, because it could not a priori be assumed, that the material properties which are characterized by random fields, has an isotropic microstructure.

With respect to equation (6.31) the elasticity tensor can be recast as

$$\mathbb{C}(\mathbf{x}, \theta) = \left[\mu_E + \sigma_E \sum_{i=1}^{M} \sqrt{\lambda_i} f_i(\mathbf{x}) \xi_i(\theta) \right] \mathbb{C}_0 \,, \tag{8.46}$$

where σ_E is the standard deviation of the Young's modulus. Inserting equation (8.46) into the deterministic stiffness matrix

$$\mathbf{k}^e = \int_{\Omega_e} \mathbf{B}^{\mathrm{T}} \mathbb{C} \mathbf{B} \, \mathrm{d}\Omega_e \,,$$

results in the stochastic counterpart $\mathbf{k}^e(\theta)$

$$\mathbf{k}^e(\theta) = \int_{\Omega_e} \mu_E \mathbf{B}^{\mathrm{T}} \mathbb{C}_0 \mathbf{B} \, \mathrm{d}\Omega_e + \int_{\Omega_e} \sigma_E \sum_{i=1}^{M} \sqrt{\lambda_i} f_i(\mathbf{x}) \xi_i(\theta) \mathbf{B}^{\mathrm{T}} \mathbb{C}_0 \mathbf{B} \, \mathrm{d}\Omega_e \tag{8.47}$$

$$= \mathbf{k}_0^e + \hat{H}_{E_i} \mathbf{k}_i^e \,, \tag{8.48}$$

where $\mathbf{k}_0^e$ denotes the mean element stiffness matrix and $\mathbf{k}_i^e$ is the i-th weighted element stiffness matrix. Applying the same assembling procedure as for the deterministic case, cf. section 3.3, the global mean stiffness matrix and the weighted global stiffness matrices are obtained by assembling the element matrices, i.e.

$$\mathbf{K}_0 = \bigcup_{e=1}^{n_e} \mathbf{k}_0^e = \bigcup_{e=1}^{n_e} \int_{\Omega_e} \mu_E \mathbf{B}^{\mathrm{T}} \mathbb{C}_0 \mathbf{B} \, \mathrm{d}\Omega_e \,, \tag{8.49}$$

$$\mathbf{K}_i = \bigcup_{e=1}^{n_e} \mathbf{k}_i^e = \bigcup_{e=1}^{n_e} \int_{\Omega_e} \hat{H}_{E_i}(\mathbf{x}) \mathbf{B}^{\mathrm{T}} \mathbb{C}_0 \mathbf{B} \, \mathrm{d}\Omega_e \,. \tag{8.50}$$

The components of the displacement and force vectors are arranged in a similar way to the deterministic case, which finally leads to the stochastic counterpart of the global variational problem:

$$\boldsymbol{\delta}_{\mathrm{U}}^{\mathrm{T}}(\theta) \left(\left[\mathbf{K}_0 + \sum_{i=1}^{M} \mathbf{K}_i \xi_i(\theta) \right] \mathbf{U}(\theta) \right) = \boldsymbol{\delta}_{\mathrm{U}}^{\mathrm{T}}(\theta) \mathbf{F}$$

$$\boldsymbol{\delta}_{\mathrm{U}}^{\mathrm{T}}(\theta) \left(\left[\sum_{i=0}^{M} \mathbf{K}_i \xi_i(\theta) \right] \mathbf{U}(\theta) \right) = \boldsymbol{\delta}_{\mathrm{U}}^{\mathrm{T}}(\theta) \mathbf{F} \,, \tag{8.51}$$

with the usual convention $\xi_0 \equiv 1$. Hence, the *semi-discretized* version of the variational problem, given in equation (8.37), reads:

Find $\mathbf{U}(\theta) \in \mathcal{V}$ such that $\forall \, \mathbf{U}(\theta)$

$$\mathbb{E}[\boldsymbol{\delta}_{\mathrm{U}}^{\mathrm{T}}(\theta) \mathbf{K}(\theta) \mathbf{U}(\theta)] = \mathbb{E}[\boldsymbol{\delta}_{\mathrm{U}}^{\mathrm{T}}(\theta) \mathbf{F}] \,. \tag{8.52}$$

8.2.4. Stochastic Discretization applying the PCE

To represent the solution in the stochastic dimension by the Galerkin method, a subspace $\mathcal{S}^P \in \mathcal{S}$ is required. Such a subspace can be defined by

$$\mathcal{S}^P = \mathrm{span}\{\psi_j(\theta)\}_{j=0}^{P-1}\,, \tag{8.53}$$

which is a span of second-order functionals in $\boldsymbol{\xi}$, by the truncated polynomial chaos basis. Here, $\{\psi_j(\theta)\}_{j=0}^{P-1}$ is a complete set of orthogonal random variables, defined as polynomials in $\{\xi_i(\theta)\}_{i=1}^{M}$.[5] The random variables ψ_j have to satisfy the following properties, cf. Sudret and der Kiureghian [2000]:

$$\psi_0 \equiv 1\,, \tag{8.54}$$
$$\mathbb{E}[\psi_j(\theta)] = 0\,, \quad j > 0\,, \tag{8.55}$$
$$\mathbb{E}[\psi_j(\theta)\psi_k(\theta)] = 0\,, \quad j \neq k\,. \tag{8.56}$$

Every random variable, for instance, a random nodal displacement $\mathrm{u}(\theta)$ may be sought in the subspace $\mathcal{S}^P$ and can be therefore represented by

$$\mathrm{u}(\theta) = \sum_{j=0}^{P-1} u_j \psi_j(\theta)\,. \tag{8.57}$$

In the same way, the expansion of the global stochastic nodal displacement vector $\mathbf{U}(\theta)$ can be expressed as:

$$\mathbf{U}(\theta) = \sum_{j=0}^{P-1} \mathbf{U}_j \psi_j(\theta)\,, \tag{8.58}$$

where the $\mathbf{U}_j$'s are deterministic vectors. Gathering the vectors $\mathbf{U}_j$, $j = 0, \dots P-1$ and $\boldsymbol{\delta}_{\mathrm{U}_k}^{\mathrm{T}}(\theta)$, $k = 0, \dots P-1$ into the block vectors $\boldsymbol{\mathcal{U}}$ and $\boldsymbol{\delta_{\mathcal{U}}^{\mathrm{T}}}(\theta)$ of size $(\mathcal{N} \cdot \bar{P}) \times 1$ leads to the following *fully discretized* variational problem:

Find $\boldsymbol{\mathcal{U}} \in \mathbb{R}^{(\mathcal{N} \cdot \bar{P}) \times 1}$ such that $\forall \boldsymbol{\delta_{\mathcal{U}}^{\mathrm{T}}}(\theta) \in \mathbb{R}^{(\mathcal{N} \cdot \bar{P}) \times 1}$

$$\sum_{j=0}^{P-1}\sum_{k=0}^{P-1} \boldsymbol{\delta}_{\mathrm{U}_k}^{\mathrm{T}}(\theta)\mathbb{E}[\mathbf{K}(\theta)\psi_j(\theta)\psi_k(\theta)]\mathbf{U}_j = \sum_{k=0}^{P-1} \boldsymbol{\delta}_{\mathrm{U}_k}^{\mathrm{T}}(\theta)\mathbb{E}[\mathbf{F}\psi_k]\,, \tag{8.59}$$

where $\bar{P} := P - 1$. Since the test functions $\boldsymbol{\delta}_{\mathrm{U}_k}^{\mathrm{T}}(\theta)$ are arbitrary the remaining parts must be zero, so equation (8.59) becomes

$$\sum_{j=0}^{P-1} \mathbb{E}[\mathbf{K}(\theta)\psi_j(\theta)\psi_k(\theta)]\mathbf{U}_j = \mathbb{E}[\mathbf{F}\psi_k]\,, \quad k = 0, \dots P-1\,. \tag{8.60}$$

This set of systems of (usually coupled) deterministic equations can be formally written in the compact block form

$$\boldsymbol{\mathcal{K}\mathcal{U}} = \boldsymbol{\mathcal{F}}\,. \tag{8.61}$$

---

[5]The detailed expression $\{\psi_j(\{\xi_i(\theta)\}_{i=1}^{M})\}_{j=0}^{P-1}$ is omitted to shorten the notation.

Alternative Derivation of the Spectral Problem

In order to obtain the expression (8.60) (resp. expression (8.61)), the subsequently outlined steps are necessary. First, substituting equation (8.58) into equation $(8.51)_2$ (since $\boldsymbol{\delta}^{\mathrm{T}}_{\mathrm{U}_k}(\theta)$ is arbitrary) leads to

$$\left(\sum_{i=0}^{M}\mathbf{K}_i\xi_i(\theta)\right)\left(\sum_{j=0}^{P-1}\mathbf{U}_j\psi_j(\theta)\right) - \mathbf{F} = 0. \tag{8.62}$$

The residual of this equation reads, cf. Sudret and der Kiureghian [2000],

$$\epsilon_{M,P} = \sum_{i=0}^{M}\sum_{j=0}^{P-1}\mathbf{K}_i\xi_i(\theta)\mathbf{U}_j\psi_j(\theta) - \mathbf{F} = 0. \tag{8.63}$$

The Galerkin method is applied to minimize the previously defined residual, which is equivalent to the requirement that this residual is orthogonal to the space $\mathcal{S}^P$, i.e.

$$\mathbb{E}[\epsilon_{M,P}\psi_k] = 0, \quad k = 0, ... P - 1. \tag{8.64}$$

With respect to equation (8.63) and by using the relations

$$c_{ijk} = \mathbb{E}[\xi_i\psi_j\psi_k], \tag{8.65}$$
$$\mathbf{F}_k = \mathbb{E}[\mathbf{F}\psi_k], \tag{8.66}$$

equation (8.64) can be rewritten as

$$\sum_{i=0}^{M}\sum_{j=0}^{P-1}c_{ijk}\mathbf{K}_i\mathbf{U}_j = \mathbf{F}_k, \quad k = 0, ... P - 1. \tag{8.67}$$

The occurring third order tensor c_{ijk} in equation (8.67) is essential in the assembling process and will from now on be referred as *multiplication* tensor. This tensor is symmetric with regard to the last two indices $c_{ijk} = c_{ikj}$, which highlights some symmetries in the structure of the global stochastic stiffness matrix. Through the properties of the stochastic basis, cf. equations (8.55) and (8.56), many of the entries of c_{ijk} are zero. A further important property of c_{ijk} is that it only depends on the stochastic basis P. This means, that the computation and the storage of the non-zero entries can be done in a pre-processing step.

With the introduction of a further relation $\mathbf{K}_{jk}$, which is defined by

$$\mathbf{K}_{jk} = \sum_{i=0}^{M}c_{ijk}\mathbf{K}_i, \tag{8.68}$$

equation (8.67) can be rewritten as

$$\sum_{j=0}^{P-1}\mathbf{K}_{jk}\mathbf{U}_j = \mathbf{F}_k, \quad k = 0, ... P - 1. \tag{8.69}$$

This set of linear equation systems can be also expressed by the block structure

$$\mathcal{K}\mathcal{U} = \mathcal{F} ,$$

which is identical to equation (8.61). Finally, this structure can also be also written in a matrix form, i.e.

$$\underbrace{\begin{pmatrix} \mathbf{K}_{0,0} & \cdots & \mathbf{K}_{0,P-1} \\ \mathbf{K}_{1,0} & \cdots & \mathbf{K}_{1,P-1} \\ \vdots & \ddots & \vdots \\ \mathbf{K}_{P-1,0} & \cdots & \mathbf{K}_{P-1,P-1} \end{pmatrix}}_{\mathcal{K}} \underbrace{\begin{pmatrix} \mathbf{U}_0 \\ \mathbf{U}_1 \\ \vdots \\ \mathbf{U}_{P-1} \end{pmatrix}}_{\mathcal{U}} = \underbrace{\begin{pmatrix} \mathbf{F}_0 \\ 0 \\ \vdots \\ 0 \end{pmatrix}}_{\mathcal{F}} . \tag{8.70}$$

Note that $\mathbf{F}_k$ is zero for $k > 0$ when assuming only deterministic loadings, as in this work. The matrix $\mathbf{K}_{0,0}$ contains the deterministic parameters and the matrices $\mathbf{K}_i$ in equation (8.68) for $i > 0$ along with c_{ijk} corresponds to the spatial varying parameters. Utilizing the KLE, the variations of these parameters are represented by a set of eigenfunctions $\{f_i(\mathbf{x})\}_{i=1}^M$. In view of the sparse structure of the multiplication tensor only a few $\mathbf{K}_{jk}$'s are non zero and the global block matrix $\mathcal{K}$ shows a distinctive sparse structure, which is illustrated in Fig. 8.1 for different dimensions M and expansion orders p, where the coloured squares highlights the non-zero entries.

General remark: As already mentioned and illustrated by the figure 8.1, grows the stochastic system of equations drastically with increasing dimension M and polynomial order p. In view of the sparse structure of $\mathcal{K}$, there are effective approximation techniques developed, such as low-rank approximation techniques of the tensor structure of c_{ijk} (resp. the stochastic system of equations). These methods makes the calculation of the stochastic system quiet efficient with respect to the computation time as well as to an effective usage of the memory. A recently published paper, which has been specifically addressed to these topics is this one presented by Espig et al. [2014]. Further model reduction techniques can be found in the article by Nouy [2009].

8.3. Remarks on the Computational Implementation of the SSFEM

The implementation of the SSFEM is not straightforward. Often moments of orthogonal one-dimensional polynomials as well as multi-dimensional polynomials are essential. This section outlines some ingredients of the computational implementation of these tasks and illustrates, by pseudo-algorithmic options, how to realize it in a computer code. If built-in functions of MATLAB are used in the presented algorithms, these functions are highlighted by italic characters.

8.3.1. Variance of the Chaos-Polynomials

The expectation of two one-dimensional HERMITE polynomials can be evaluated by, cf. Sudret and der Kiureghian [2000],

$$\mathbb{E}[\mathfrak{h}_p(\xi)\mathfrak{h}_q(\xi)] = \delta_{pq}p! . \tag{8.71}$$

By the fact that the polynomials $\{\psi_j, j = 1, \dots P - 1\}$ are also orthogonal to each other, the multi-dimensional case can be expressed as products of the one-dimensional
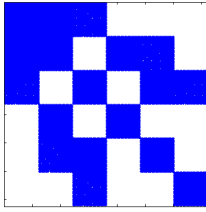
(a) Dimension $M = 2$, order $p = 2$ $\Rightarrow$ basis $P = 6$.
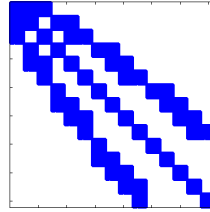
(b) Dimension $M = 2$, order $p = 4$ $\Rightarrow$ basis $P = 15$.
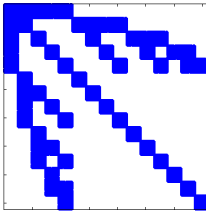
(c) Dimension $M = 4$, order $p = 2$ $\Rightarrow$ basis $P = 15$.
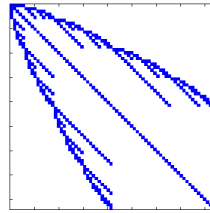
(d) Dimension $M = 4$, order $p = 4$ $\Rightarrow$ basis $P = 70$.
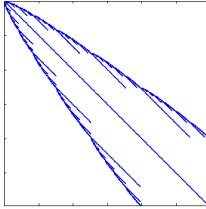
(e) Dimension $M = 4$, order $p = 8$ $\Rightarrow$ basis $P = 495$.
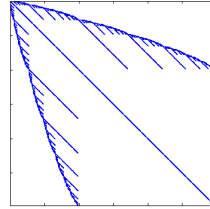
(f) Dimension $M = 8$, order $p = 4$ $\Rightarrow$ basis $P = 495$.
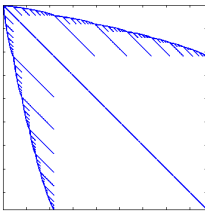
(g) Dimension $M = 12$, order $p = 4$ $\Rightarrow$ basis $P = 1820$.
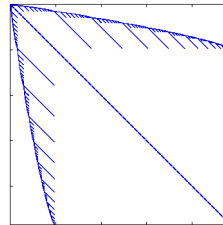
(h) Dimension $M = 16$, order $p = 4$ $\Rightarrow$ basis $P = 4845$.

Figure 8.1.: Illustration of the sparse structure of $\mathcal{K}$ for different dimensions M and expansion orders p.

polynomials as follows, cf. Sudret and der Kiureghian [2000]:

$$\mathbb{E}[\psi_{\boldsymbol{\alpha}}\psi_{\boldsymbol{\beta}}] = \delta_{\boldsymbol{\alpha}\boldsymbol{\beta}} \prod_{i=1}^{M} \alpha_i! \,, \tag{8.72}$$

where $\boldsymbol{\alpha}$ and $\boldsymbol{\beta}$ are multi-indices. The Kronecker delta is equal to 1 if the integer sequences of $\boldsymbol{\alpha}$ and $\boldsymbol{\beta}$ are identical, otherwise zero. In view of the post-processing, the variances are needed for the calculation of the covariance in equation (8.77). Note that ψ_0 is not explicitly stored in the workspace, because of the convention $\mathbb{E}[\psi_0^2] = 1$. The corresponding pseudo-code for the calculation of the variances (see equations (8.71) and (8.72)) is illustrated in Algorithm 1.

Algorithm 1 Calculating the variances $\mathbb{E}[\psi_j^2]$

Require: M, P and C
 1: initialise: sn = *ones*(1, P-1)
 2: **for** j = 1 : P - 1 **do**
 3:   **for** i = 1 : M **do**
 4:     sn(j) = sn(j)*factorial*(C{j}(i))
 5:   **end for**
 6: **end for**

Here, M denotes the dimension of the KLE, P is the number of basis polynomials calculated by equation (7.19) and C contains all $(P-1)$ integer sequences of the polynomial chaos.

8.3.2. Multiplication-Tensor c_{ijk}

The multiplication-tensor c_{ijk}, introduced in equation (8.65), is essential when applying Gaussian random fields in the context of the (normal distributed) SSFEM. This tensor is required for the computation of the stiffness matrices $\mathbf{K}_{jk}$ in equation (8.68). The multiplication-tensor and the variances of the polynomials are equivalent if one of the indices i, j, k is zero and the other two have the same value. Due to the properties of c_{ijk}, this tensor is calculated only once and stored in the workspace during the pre-processing.

Following the work of Sudret and der Kiureghian [2000], the coefficients of c_{ijk} are calculated by

$$c_{ijk} = \left(p!\delta_{P-1,q} + q!\delta_{p,q-1}\right) \prod_{l\neq i} \alpha_l! \,, \tag{8.73}$$

where a detailed derivation can be also found in this work. This derivation style was also used for the implementation, which is illustrated in the pseudo-code of Algorithm 2.

The variables M, P and C are already defined in the previous subsection. Using multi-indices to define the integer-sequences $\boldsymbol{\alpha}$ and $\boldsymbol{\beta}$, this algorithm computes and stores all coefficients of c_{ijk}, which are not equal to zero. This means, the terms whose Hermite polynomials are not orthogonal to each other, i.e $\mathfrak{h}_{\alpha_{j_0}}$ and $\mathfrak{h}_{\beta_{j_0}}$ with $\alpha_{j_0} = \beta_{j_0}$.

Algorithm 2 Storing the values of the multiplication-tensor c_{ijk}

Require: M, P und C
1: **for** i $= 1 :$ M **do**
2:    initialise: CC{i} = $sparse$(P-1, P-1)
3:    **for** j $= 1 :$ P-1 **do**
4:      **for** k $=$ j $:$ P-1 **do**
5:        $\boldsymbol{\alpha}_j$ =C{j}
6:        $\boldsymbol{\beta}_k$ =C{k}
7:        dif = C{j}-C{k}
8:        **if** dif $==$ i **then**
9:          the i-th integer are
10:          p = C{j}(i)
11:          q = C{k}(i)
12:          a = $factorial$(p)$isequal$(P-1, q) + $factorial$(q)$isequal$(p, q-1)
13:          al = C{j}
14:          al(i) = ( )
15:          b = $prod$($gamma$(al+1))
16:          CC{i}(j,k) = ab
17:        **end if**
18:      **end for**
19:    **end for**
20: **end for**

As a *first* example, let $M = 4$, $p = 2$ and consider the loop-indices $i = 1$, $j = 1$, $k = 5$. With respect to the algorithm above, this set of indices leads to the integer sequences of $\boldsymbol{\alpha}$ and $\boldsymbol{\beta}$, which are listed in the first two rows of Tab. 8.1. From this listing, it is

Table 8.1.: Examples for integer sequences of different loop-indices i, j, k of c_{ijk}.

	Reverse Integer Sequence	Polynomial basis
First example	1 0 0 0	ξ_1
$i = 1$, $j = 1$, $k = 5$	2 0 0 0	$\xi_2^2 - 1$
Second example	1 0 0 0	ξ_1
$i = 2$, $j = 1$, $k = 6$	1 1 0 0	$\xi_1 \xi_2$

obvious that the integer sequences $\boldsymbol{\alpha}_j$ and $\boldsymbol{\beta}_k$ are only different in their i-th integer. Thus the corresponding coefficient of c_{ijk} is computed by using equation (8.73), which results in $c_{115} = 2$. The following coefficients for $i = 1$ are constructed in the same way, i.e. with respect to the orthogonal property of the HERMITE polynomials, where only four coefficients of c_{1jk} are non-zero.

As a *second* example consider the loop-indices $i = 2$, $j = 1$, $k = 6$ where the corresponding sequences of $\boldsymbol{\alpha}_j$ and $\boldsymbol{\beta}_k$ are also listed in Tab. 8.1. Again, using equation (8.73) the coefficient of the multiplication-tensor $c_{216} = 2$ is obtained. For this example ($M = 4$, $p = 2$) a total number of sixteen terms (without taking into account the expectation values ψ_0) of c_{ijk} are non-zero. Note that the coefficients of c_{ijk} also provides the variances of the basis polynomials, which are discussed in the foregoing subsection.

When operating with three[6] polynomials, the tensor $d_{ijk} = \mathbb{E}[\psi_i \psi_j \psi_k]$ is required. The implementation has also been realized with regard to Sudret and der Kiureghian [2000], whereas a detailed pseudo-code is omitted here.

8.4. Post-Processing of the Results

The formulation of the linear SSFEM leads to a system response, for example, of a displacement $u(\theta)$ of a specific node in terms of its polynomial chaos expressed by

$$u(\theta) = \sum_{i=0}^{P-1} u_i \psi_i \,.$$

For practical predictions, the polynomial chaos coefficients (here u_i) must be evaluated in order to derive the quantities of interest. This section gives a brief overview to the computation of some stochastic moments using the PC coefficients. These are the mean value, variance, skewness and the kurtosis as well as the approximation of the PDF of the system response.

8.4.1. Probability Density Function of the System Response

The computation of the probability density function of a specific value of the system response can be realized by evaluating the series expansion of the PC coefficients by applying a sampling technique. In this work, this is realized by use of the LHS, which leads to a set of system responses $\{u^i(\theta), i = 1, \dots n\}$. Using this set, a histogram may be created as an estimator of the PDF. However, this result is not very smooth[7] and approximation methods are developed, which give a smooth estimation of the system response. Such *kernel smoothing* techniques have been discussed, for example, in Wand and Jones [1995], where a general equation for the kernel density estimation is defined by

$$\hat{f}_{u(\theta)}(u) = \frac{1}{n\,h_K} \sum_{i=1}^{n} K\left(\frac{u - u^i}{h_K}\right) \,. \tag{8.74}$$

Here, K denotes the kernel function and h_K is a smoothing parameter referred to as bandwidth parameter. This parameter has a strong influence on the estimated results and is selected with respect to the kernel. Commonly used kernels, such as the Gaussian or the Epanechnikov kernel, are also provided in Matlab.

8.4.2. Computation of the Statistical Moments

The statistical moments of a certain system response $u(\theta)$ can be analytically evaluated from the polynomial chaos coefficients. In particular, this leads for the mean

---

[6] In the case of algebraic operations with more than three polynomials, a splitting of the polynomials on tensors with lower-order is appropriate, therefore see subsection 9.2.2.

[7] One example has been given in subsection 4.4.2 where the MCS and LHS has been compared by their resulting histograms, cf. Fig. 4.8.

value and the variance to

$$\mu_{\mathrm{u,PC}} \equiv \mathbb{E}[\mathrm{u}(\theta)] = u_0 \,, \tag{8.75}$$

$$\sigma_{\mathrm{u,PC}}^2 \equiv \mathrm{Var}(\mathrm{u}(\theta)) = \sum_{i=1}^{P-1} u_i^2 \,, \tag{8.76}$$

$$\mathrm{Cov}_{\mathrm{uu,PC}} \equiv \mathrm{Cov}(\mathrm{u}(\theta), \mathrm{u}(\theta)) = \sum_{i=1}^{P-1} \mathbb{E}[\psi_i^2] u \cdot u^{\mathrm{T}} \,, \tag{8.77}$$

where $\bullet_{\mathrm{PC}}$ indicates that the moments are evaluated with respect to the polynomial chaos expansion. The higher order moments can also be computed in the same manner. The skewness is approximated by a PCE as, cf. Sudret [2007],

$$s_{\mathrm{u}(\theta),\mathrm{PC}} = \frac{1}{\sigma_{\mathrm{u}(\theta),\mathrm{PC}}^3} \sum_{i=1}^{P-1} \sum_{j=1}^{P-1} \sum_{k=1}^{P-1} d_{ijk} u_i u_j u_k \,. \tag{8.78}$$

The kurtosis and accordingly its PC-based approximation reads, cf. Sudret [2007],

$$\kappa_{\mathrm{u}(\theta),\mathrm{PC}} = \frac{1}{\sigma_{\mathrm{u}(\theta),\mathrm{PC}}^4} \sum_{i=1}^{P-1} \sum_{j=1}^{P-1} \sum_{k=1}^{P-1} \sum_{l=1}^{P-1} d_{ijkl} u_i u_j u_k u_l \,. \tag{8.79}$$

For the accurate computation of the mean values and variances, a PCE of order $p = 2$ seems to be sufficiently. However, for the calculation of higher statistical moments a PCE of at least of $p = 3$ should be used.

8.5. Extensions of the Spectral Stochastic Finite Element Method

Beside a quite common consideration of fluctuating material properties using Gaussian random variables, there are also a lot of studies that use non-Gaussian random fields to characterize the stochastic material properties. On the one hand, when using a Gaussian field, the implementation is easier, because no transformation of the Gaussian random variables is necessary. On the other hand, when using Gaussian variables, it is theoretically possible to get negative outcomes, which physically makes no sense. With this in mind, log-normal random fields can be the better choice. However, in this work only small standard deviations $\sigma \leq 10\%$ are considered, which is typically a reasonable choice for material parameters, for instance, of steel. Investigations on the yield stress of $\sigma_y = 23.5\,\mathrm{kN/cm}^2$ and $\sigma(\sigma_y) = 10\%$ show that no negative sampling value occurs when a LHS with $n = 10000$ is used. Negative values occured only when utilizing a LHS with $n = 1000000$ and with a standard deviation of $\sigma(\sigma_y) \geq 20\%$. Negative values (if occur) are intercepted, what indeed leads to an approximation, which is sufficiently accurate due to the sporadic occurring of negative values.

The following two subsections briefly outline the generation of non-Gaussian random variables and fields by means of the KLE. In subsection 8.5.3 the extension to multiple random variables will be discussed, which is afterwards applied in chapter 9.

8.5.1. Log-Normal Random Variables

Let $g(\theta) = \mu_g + \sigma_g \xi(\theta)$ be a single random variable with the standard Gaussian random variable $\xi(\theta)$. The transformation of $g(\theta)$ into a log-normal random variable can be written as follows, cf. Sudret and der Kiureghian [2000],

$$\mathfrak{l}(\theta) = e^{\mu_g + \sigma_g \xi(\theta)} \,, \tag{8.80}$$

where the PCE of $\mathfrak{l}(\theta)$ is defined by

$$\mathfrak{l}(\theta) = \sum_{i=0}^{\infty} \mathfrak{l}_i \, \psi_i(\xi) \,, \tag{8.81}$$

where $\psi_i(\xi)$ denotes the i-th Hermite polynomial. With respect to the orthogonality properties of the $\psi_i(\xi)$'s, the coefficients $\mathfrak{l}_i$ are obtained by, cf. Sudret and der Kiureghian [2000],

$$\mathfrak{l}_i = \frac{\mathbb{E}\left[\exp(\mu_g + \sigma_g \xi)\,\psi_i(\xi)\right]}{\mathbb{E}(\psi_i^2)} \,. \tag{8.82}$$

After Sudret and der Kiureghian [2000], the expansion of a log-normal random variable into the polynomial chaos can be done by

$$\mathfrak{l}(\theta) = \mu_{\mathfrak{l}} \sum_{i=0}^{\infty} \frac{\sigma_g^i}{i!} \, \psi_i(\xi) \,. \tag{8.83}$$

8.5.2. Log-Normal Random Fields

Let $g(\mathbf{x})$ be a truncated Gaussian random field. This field can be transformed into a log-normal field by $\mathfrak{l}(\mathbf{x}, \theta)$ as follows, cf. Sudret and der Kiureghian [2000]:

$$\mathfrak{l}(\mathbf{x}, \theta) = \exp\left(\mu_g(\mathbf{x}) + \sum_{i=1}^{M} g_i(\mathbf{x})\, \xi_i\right) = \exp\left(\mu_g(\mathbf{x}) + \boldsymbol{g}(\mathbf{x})^{\mathrm{T}} \cdot \boldsymbol{\xi}\right) \,, \tag{8.84}$$

with $\boldsymbol{g} = (g_1, \dots g_M)$ and $\boldsymbol{\xi} = (\xi_1, \dots \xi_M)$. The corresponding polynomial chaos reads

$$\mathfrak{l}(\mathbf{x}, \theta) = \sum_{j=0}^{P-1} \mathfrak{l}_j(\mathbf{x})\, \psi_j(\boldsymbol{\xi}) \,. \tag{8.85}$$

The use of a log-normal random field in the context of a SSFEM simulation is analogous to the steps described in section 8.2, where the random field realization, as defined in equation (8.44), is replaced by equation (8.84). The global equilibrium system then reads

$$\left(\sum_{i=0}^{M} \mathbf{K}_i \, \psi_i(\theta) \right) \left(\sum_{j=0}^{P-1} \mathbf{U}_j \, \psi_j(\theta) \right) = \mathbf{F} \,, \tag{8.86}$$

$$\Leftrightarrow \quad \sum_{i=0}^{M} \sum_{j=0}^{P-1} d_{ijk} \mathbf{K}_i \, \mathbf{U}_j = \mathbf{F}_k \,, \quad k = 0, \dots P - 1 \,, \tag{8.87}$$

with the coefficients of the multiplication tensor d_{ijk} and $\mathbf{F}_k = \mathbb{E}[\psi_k \, \mathbf{F}]$.

8.5.3. Multiple Input Random Fields

In almost all engineering applications, more than one material property is uncertain. Examples could be the Young's modulus and the Poisson's ratio in elastic analysis or in the case of elastic-plastic applications, the yield stress and the hardening parameters could be uncertain as well. Until now, only one input variable is assumed to be random, which should now be extended to multiple random input variables, see also Ghanem [1999] for a similar framework.

In view of chapter 9 the Young's modulus, yield stress, isotropic hardening modulus and the kinematic hardening modulus are characterized as random quantities. With respect to the presented framework in this chapter, the four random variables are characterized as follows:

$$E(\mathbf{x}, \theta) = \mu_E + \xi_1 E_1 + \xi_2 E_2 + \cdots + \xi_M E_M \tag{8.88}$$

$$\sigma_y(\mathbf{x}, \theta) = \mu_{\sigma_y} + \xi_1 \sigma_{y_1} + \xi_2 \sigma_{y_2} + \cdots + \xi_M \sigma_{y_M} \tag{8.89}$$

$$\mathbb{H}_{\text{iso}}(\mathbf{x}, \theta) = \mu_{\text{H}_{\text{iso}}} + \xi_1 H_{\text{iso}_1} + \xi_2 H_{\text{iso}_2} + \cdots + \xi_M H_{\text{iso}_M} \tag{8.90}$$

$$\mathbb{H}_{\text{kin}}(\mathbf{x}, \theta) = \mu_{\text{H}_{\text{kin}}} + \xi_1 H_{\text{kin}_1} + \xi_2 H_{\text{kin}_2} + \cdots + \xi_M H_{\text{kin}_M} \,, \tag{8.91}$$

where $\mu_\bullet$ denotes the expected value of the corresponding material parameter and M is the dimension of the KLE. As shown in the expressions above, it is assumed that each material parameter is represented by one random variable, which is equivalent to a relatively slow variation of each material parameter over space. To combine these four expansions into the same numerical environment, it is suitable to formulate them as follows (with $M = 4$):

$$E(\mathbf{x}, \theta) = \mu_E + \xi_1 E_1 + \xi_2 0 + \xi_3 0 + \xi_4 0 = \sum_{i=0}^{4} E_i \xi_i \,, \tag{8.92}$$

$$\sigma_y(\mathbf{x}, \theta) = \mu_{\sigma_y} + \xi_1 0 + \xi_2 \sigma_{y_2} + \xi_3 0 + \xi_4 0 = \sum_{i=0}^{4} \sigma_{y_i} \xi_i \,, \tag{8.93}$$

$$\mathbb{H}_{\text{iso}}(\mathbf{x}, \theta) = \mu_{\text{H}_{\text{iso}}} + \xi_1 0 + \xi_2 0 + \xi_3 H_{\text{iso}_3} + \xi_4 0 = \sum_{i=0}^{4} H_{\text{iso}_i} \xi_i \,, \tag{8.94}$$

$$\mathbb{H}_{\text{kin}}(\mathbf{x}, \theta) = \mu_{\text{H}_{\text{kin}}} + \xi_1 0 + \xi_2 0 + \xi_3 0 + \xi_4 H_{\text{kin}_4} = \sum_{i=0}^{4} H_{\text{kin}_i} \xi_i \,, \tag{8.95}$$

with the standard convention $\xi_0 \equiv 1$ and the zero order material term is defined as the

expected value, e.g., $E_0 = \mu_E$. The expansions above are not restricted to any specific order p of the polynomial chaos. For example, let the polynomial order $p = 2$. Then, the basis P of the polynomial chaos includes 15 terms. A higher order expansion can be realized without any restriction. However, the choice of the dimension M and the order of the polynomial chaos p must be carried out carefully, because the basis P of the polynomial chaos grows drastically with increasing M and p, cf. Tab. 7.2.

8.6. Numerical Example

The accuracy of the analytical and the numerical approximation of the KLE has been examined in subsection 6.3.2. As it was observed there both methods are quite similar. The accuracy of the SPRM using different sampling techniques for the random phase angle was discussed in subsection 6.4.2. From these investigations, it is obvious that the random phase angle sampled with a LHS leads to the best accuracy. In this section, a numerical example with different dimensions M, orders p and correlation lengths c is investigated, where the special emphasis is placed on the influence of these parameters on the system response u_y and the standard deviation $\sigma(u_y)$ of a node at the top of the plate. Due to the fact that the numerical example has a hole at the centre, the realization of the random field, when using the KLE, has been performed in a numerical manner. The results from the SSFEM are compared with those obtained from a coupled SPRM-MCS and a simple Latin Hypercube Sampling. The three-dimensional plate is illustrated in Fig. 8.2 (**a**). The domain $\mathcal{D}$ of the model is specified by $10 \times 10 \times 1$ [cm] and the circular hole at the center of the plate has a radius of $r = 1$ cm. The plate is loaded by a distributed load of $10\,\text{kN/cm}^2$. The constitutive behaviour of the model is represented by a linear-elastic material formulation. The elastic behaviour is represented by an isotropic linear-elastic material law with a deterministic Poisson ration of $\nu = 0.25$ and a spatial varying Young's modulus of $E(\mathbf{x}, \theta) = 21.000\,\text{kN/cm}^2$. The spatial fluctuations of $E(\mathbf{x}, \theta)$ are represented in two ways, i.e with the Karhunen-Loève Expansion and the *Spectral Representation Method*.

Spatial Discretization of the Domain

By applying the Karhunen-Loève Expansion, the Young's modulus is represented by a discretized three-dimensional random field $\hat{H}(\mathbf{x}, \mathbf{y}, \mathbf{z}, \theta)$, $\mathbf{x}, \mathbf{y}, \mathbf{z} \in \mathcal{D}$ with zero mean and values in $\mathbb{R}_+$. To be more specific, $E(\mathbf{x}, \theta)$ is characterized by the covariance function

$$C_E(\mathbf{x}_1, \mathbf{y}_1, \mathbf{z}_1; \mathbf{x}_2, \mathbf{y}_2, \mathbf{z}_2) = e^{-\frac{|\mathbf{x}_1 - \mathbf{x}_2|}{c_\mathbf{x}} - \frac{|\mathbf{y}_1 - \mathbf{y}_2|}{c_\mathbf{y}} - \frac{|\mathbf{z}_1 - \mathbf{z}_2|}{c_\mathbf{z}}}. \tag{8.96}$$

The standard deviation of $E(\mathbf{x}, \theta)$ is $\sigma_E = 10\%$, which spatially varies over $\mathcal{D}$. The correlation length c is varied by $c = 0.01, 0.1, 1.0, 10.0$ [cm]. It is worth remembering that an analytical solution of equation (6.20) is valid only for simple geometries and, because of the hole at the center of the plate, the random field has to be calculated numerically.

By using the Spectral Representation Method the Young's modulus is characterized by the discretized three-dimensional random field $\hat{H}_S(\mathbf{x}, \mathbf{y}, \mathbf{z}, \theta)$, $\mathbf{x}, \mathbf{y}, \mathbf{z} \in \mathcal{D}$ with zero
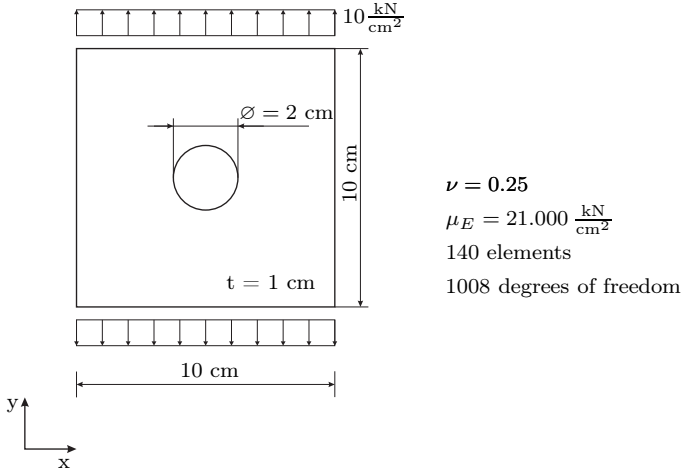
(a) Schematic illustration of the plate.
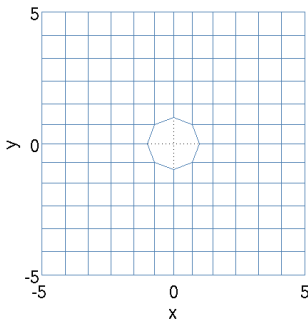
(b) Discretization of the plate.
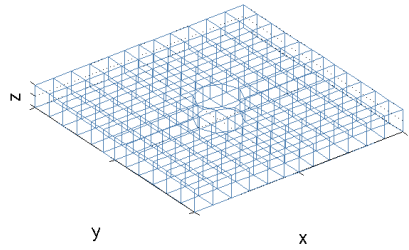
(c) 3D view of the discretized plate.

Figure 8.2.: Numerical linear elastic example.

mean and values in $\mathbb{R}_+$. The Young's modulus is represented by

$$
\begin{aligned}
\hat{H}_S(\mathbf{x}, \mathbf{y}, \mathbf{z}, \theta) = \sqrt{2} \sum_{n_{\mathrm{x}}=0}^{N_{\mathrm{x}}-1} \sum_{n_{\mathrm{y}}=0}^{N_{\mathrm{y}}-1} \sum_{n_{\mathrm{z}}=0}^{N_{\mathrm{z}}-1} & \\
\Big[\ A^{(1)}_{n_{\mathrm{x}} n_{\mathrm{y}} n_{\mathrm{z}}} \cos &\left(\kappa_{\mathrm{x}_{n_{\mathrm{x}}}} \mathbf{x} + \kappa_{\mathrm{y}_{n_{\mathrm{y}}}} \mathbf{y} + \kappa_{\mathrm{z}_{n_{\mathrm{z}}}} \mathbf{z} + \Phi^{(1)}_{n_{\mathrm{x}} n_{\mathrm{y}} n_{\mathrm{z}}}(\theta) \right) \\
+ A^{(2)}_{n_{\mathrm{x}} n_{\mathrm{y}} n_{\mathrm{z}}} \cos &\left(\kappa_{\mathrm{x}_{n_{\mathrm{x}}}} \mathbf{x} - \kappa_{\mathrm{y}_{n_{\mathrm{y}}}} \mathbf{y} + \kappa_{\mathrm{z}_{n_{\mathrm{z}}}} \mathbf{z} + \Phi^{(2)}_{n_{\mathrm{x}} n_{\mathrm{y}} n_{\mathrm{z}}}(\theta) \right) \\
+ A^{(3)}_{n_{\mathrm{x}} n_{\mathrm{y}} n_{\mathrm{z}}} \cos &\left(\kappa_{\mathrm{x}_{n_{\mathrm{x}}}} \mathbf{x} + \kappa_{\mathrm{y}_{n_{\mathrm{y}}}} \mathbf{y} - \kappa_{\mathrm{z}_{n_{\mathrm{z}}}} \mathbf{z} + \Phi^{(3)}_{n_{\mathrm{x}} n_{\mathrm{y}} n_{\mathrm{z}}}(\theta) \right) \\
+ A^{(4)}_{n_{\mathrm{x}} n_{\mathrm{y}} n_{\mathrm{z}}} \cos &\left(\kappa_{\mathrm{x}_{n_{\mathrm{x}}}} \mathbf{x} - \kappa_{\mathrm{y}_{n_{\mathrm{y}}}} \mathbf{y} - \kappa_{\mathrm{z}_{n_{\mathrm{z}}}} \mathbf{z} + \Phi^{(4)}_{n_{\mathrm{x}} n_{\mathrm{y}} n_{\mathrm{z}}}(\theta) \right) \Big] \ .
\end{aligned}
\tag{8.97}
$$

The power spectral density function $S_{\hat{H}_S \hat{H}_S}$ characterizing the approximated random field is assumed by

$$
S_{\hat{H}_S \hat{H}_S}(\kappa_{\mathrm{x}}, \kappa_{\mathrm{y}}, \kappa_{\mathrm{z}}) = \sigma_E^2 \frac{c_{\mathrm{x}} c_{\mathrm{y}} c_{\mathrm{z}}}{4\pi} \exp \left[-\left(\frac{c_{\mathrm{x}} \kappa_{\mathrm{x}}}{2} \right)^2 - \left(\frac{c_{\mathrm{y}} \kappa_{\mathrm{y}}}{2} \right)^2 - \left(\frac{c_{\mathrm{z}} \kappa_{\mathrm{z}}}{2} \right)^2 \right] \ . \tag{8.98}
$$

The standard deviation of $E(\mathbf{x}, \theta)$ is $\sigma_E = 10\%$, which spatially varies over $\mathcal{D}$ where the correlation lengths are the same as for the KLE. The response statistics are evaluated using a sample size of $n_{\mathrm{SPRM}} = 1000$, where the random phase angles are sampled by applying the LHS.

Sampling Method

The accuracy of the spatial discretization methods is compared with a simple LHS using a sample size of $n_{\mathrm{LHS}} = 2000$. As already discussed in section 4.4.2, the LHS has a convergence rate of $\mathcal{O}(n^{-1})$, while the convergence rate of the standard MCS is $\mathcal{O}(1/\sqrt{n})$. By comparing these two methods it is obvious, that the convergence rate of LHS is better than those of the MCS using the same number of samples. Therefore, the LHS is applied as reference solution for this example.

Parameter Variation

The standard deviation of the system response σ_{u} of a node at the top of the plate, with respect to the coefficient of variation α_E of the Young's modulus, has been investigated. For the subsequent calculations, the parameters $(M, p, c$ and $\alpha_E)$ are varied, which are summarized in the following:

- Different dimensions M of the KLE and polynomial orders p of the PCE.

- Various correlation lengths c_i, $i = $ x, y, z for both methods, i.e. for the KLE and SPRM.

- Different coefficients of variation α_E of E.

As already remarked in chapter 6, the values of the KLE as well as of the SPRM are values, which are used in most applications in the literature and sufficiently reasonable for system responses. However, for a detailed parameter study the values must be significantly larger than those applied here.

Finite Element Model

The discretized plate is illustrated in Figs. 8.2 (**b**) and 8.2 (**c**). The model consists of 140 FE elements with a total number of 1008 degrees of freedom, where linear shape functions are applied to approximate the structural response.

Results of the Numerical Example

The results obtained by using the SSFEM, coupled SPRM-MCS and the LHS, are depicted in Figs. 8.3 to 8.6. The accuracy of the linear SSFEM and the coupled SPRM-MCS is examined by comparing the approximated standard deviation of the system response σ_u with those of a LHS. The obtained curves using the SSFEM shows an increasing standard deviation by a increasing correlation length, see Figs. 8.3−8.5. This phenomena were also observed in subsection 6.3.2, where the influence of the correlation length of the eigenvalues of the KLE was investigated. It implies, that the field is strongly correlated by a long correlation length, which results in a fast decay of the eigenvalues. A fully correlated field, i.e. where the correlation length is infinite, leads to a rapidly decay of the corresponding eigenvalues, where only one eigenvalue is one and all others are zero. On the other hand, a weakly correlated field has a slow decay of the eigenvalues, where the fully uncorrelated field has no decay in the eigenvalues. The under-representation of the variance of the random field, cf. equation (6.27), is also visible in Figs. 8.3−8.5 when comparing the results of the SSFEM with those of a LHS. It should be noticed that the deviation to a LHS decreases with an increasing c. The influence of the dimension M and the order p is also observed in these figures with a quantitatively similar trend. The curve using $M = 2$ and $p = 2$ is still slightly different from the counterparts. However, when applying $M = 4$ and $p = 2$ the parameter pair $M = 4$ and $p = 4$, the curves match each other quite well. This result implies, that for this numerical example only a few terms for the dimension ($M = 4$) and order ($p = 2$) are needed to achieve an accurate approximation of the system response, measured in terms of the standard deviation σ_u. As already remarked at the end of subsection 6.3.1, the number of terms (i.e. M and p) should be small, otherwise the basis P of the PCE increases drastically. More discussions about the truncation orders of M and p can be found in Xiu [2010] and Le Maître and Knio [2010].

The results of the coupled SPRM-MCS are depicted in Fig. 8.6. The trend of the curves using the correlation lengths $c = 0.01$, $c = 0.1$ and $c = 1.0$ are comparable to those obtained from the SSFEM, plotted in Figs. 8.3−8.5. A noticeable difference is seen by using a SPRM-MCS with $c = 10$. On the one hand, the curve is still above the reference solution and on the other hand it seems so that there is no convergence in the standard deviation.

In Fig. 8.7, all graphs from Figs. 8.3 to 8.6 with a correlation length of $c = 1.0$ are plotted again. From this plot, the differences in the standard deviations of the system response become quite obvious. the SPRM-MCS is the closest to the reference (LHS) solution. Furthermore, the above mentioned matching between $M = 4$, $p = 2$ and $M = 4$, $p = 4$ becomes quite clear here. In general, a good approximation, in view of the solution of the LHS, is obtained with both methods.

Figure 8.3.: Standard deviation of the plate deflection versus the coefficient of variation α_E of the plate by using a dimension of $M = 2$ and a order of $p = 2$.

Figure 8.4.: Standard deviation of the plate deflection versus the coefficient of variation α_E of the plate by using a dimension of $M = 4$ and a order of $p = 2$.
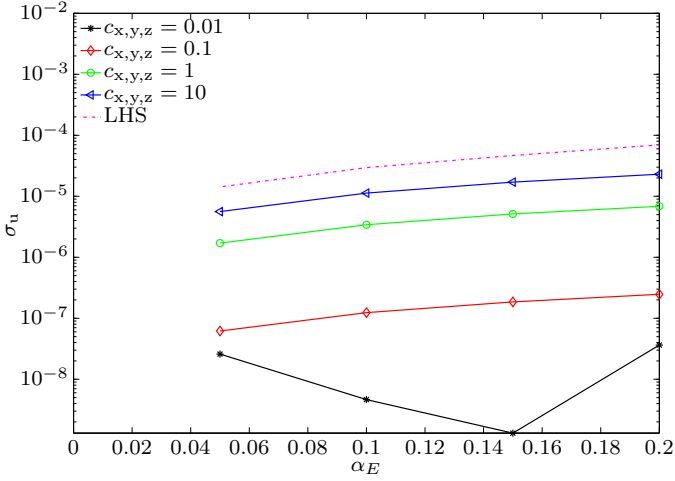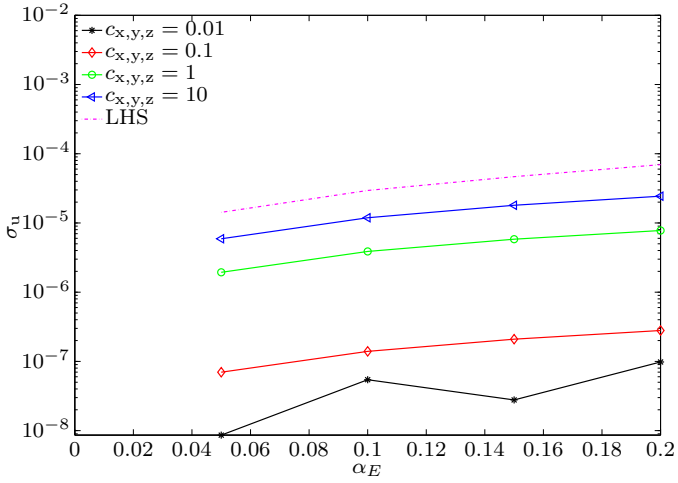
Figure 8.5.: Standard deviation of the plate deflection versus the coefficient of variation α_E of the plate by using a dimension of $M = 4$ and a order of $p = 4$.
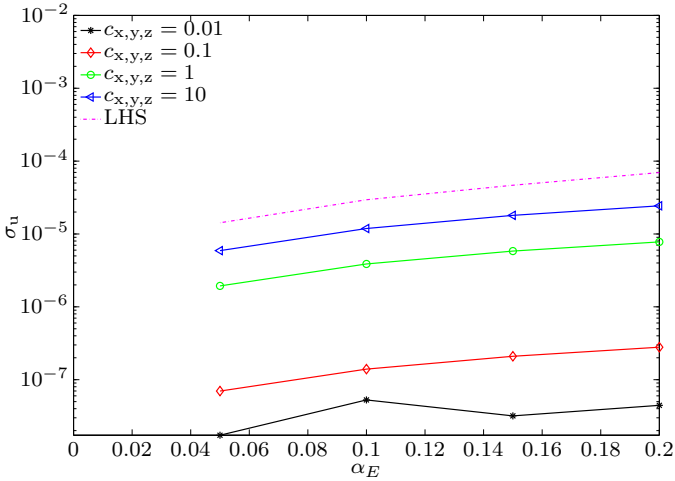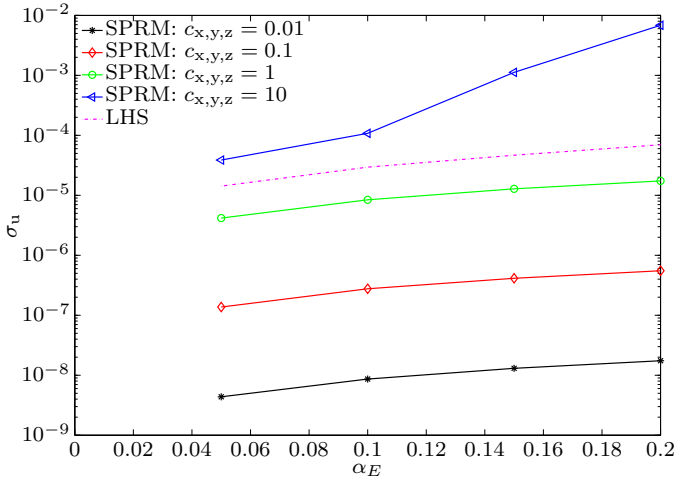

Figure 8.6.: Standard deviation of the plate deflection versus the coefficient of variation α_E of the plate by using the coupled SPRM-MCS.
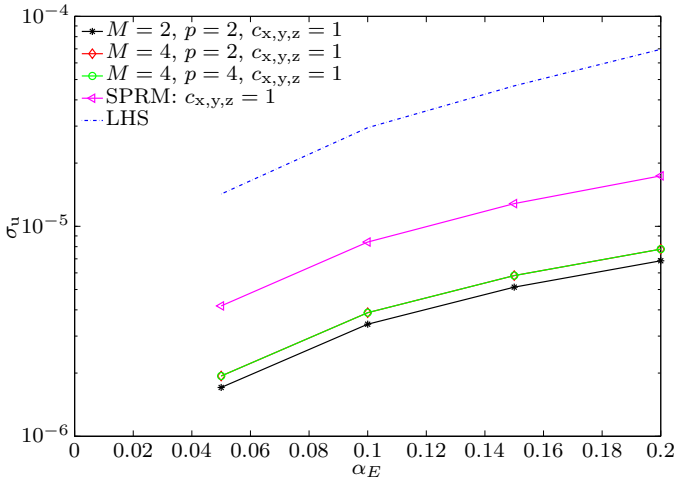
Figure 8.7.: Comparison of the standard deviation of the plate deflection versus the coefficient of variation α_E for $c = 1.0$ of the SSFEM, coupled SPRM-MCS and the LHS.

8.7. Summary

In this chapter, the linear spectral stochastic finite element method was discussed in detail. First, a brief overview of some solution methods, for the evaluation of the stochastic system response, has been presented in section 8.1. At the end of this subsection, a brief distinction between intrusive and non-intrusive methods has been given. The emphasis of this chapter was the formulation of the linear SSFEM, which was presented in detail in sections 8.2 to 8.5. First, the stochastic elliptic boundary value problem is defined. Then, the variational form of the linearized stochastic problem is introduced and afterwards discretized. The discretization is split into two parts, namely the deterministic part and the stochastic part, which was presented in detail in subsection 8.2.3 and 8.2.4. After that, some remarks on the computational implementation of important parts of the stochastic formulation are given in 8.3. To this point, only preprocessing steps are explained and the next step is the post-processing, which was outlined in section 8.4. Here, the theoretical background was provided to make practical predictions, such as the standard deviation, skewness, kurtosis etc. for the quantities of interest. Some important extensions of the linear SSFEM are presented in section 8.5, with particular emphasis on multiple input random fields. In section 8.6, the influence of the parameters M, p, c and α_E are discussed by a three-dimensional numerical example. By this, an assessment on the capability of the linear SSFEM and the coupled SPRM-MCS for the simulation of a three-dimensional plate with a circular hole at the center has been performed. The evaluation of the FREDHOLM integral equation was performed numerically by applying a GALERKIN projection. A three-dimensional homogeneous GAUSSIAN field with zero

mean, unit variance and an exponential autocovariance function has been applied. The solution of the random field with the SPRM has been done by using an exponential power spectral density function and applying a LHS for the sampling of the random phase angles. The accuracy of these methods are compared with a standard LHS. In general, it has been shown that the solution comes closer to the reference solution (the LHS) with an increasing correlation length. Furthermore, it has been observed, that an increasing correlation coefficient has an influence on the stability of the coupled SPRM-MCS approach. It has also been verified that, by applying the SSFEM, only a few KLE terms M and a low polynomial order p is necessary in order to achieve a sufficiently accurate approximation of the system response. In general, the linear SSFEM provides an adequate approximation by using only a few terms M and p. The coupled SPRM-MCS seems to provide slightly better solutions than the SSFEM, when comparing it with the solution of a LHS. However, two remarks should be given. The first one is the correlation length, which must be selected carefully otherwise some stability problems could occur. The second is the computational time, which is relatively high in comparison to the linear SSFEM.

9. Spectral Stochastic Finite Element Method in the Context of Plasticity

The deterministic theory of plasticity as well as the realization in a computer code was discussed in sections 2.6 and 3.4. This is equivalent with the assumption that the material parameters are assumed to be exactly known in every point of the body. However, this is not true in reality, because the material parameters are actually not the same at every point in the considered domain. To get a more general formulation, the standard deterministic J_2 flow theory has to be extended in such a way that random material parameters are taken into account. In this chapter, an approach is developed where such material fluctuations can be taken into account. To be more specific, the linear SSFEM approach, which has been presented in the previous chapter, is used as basis and extended in the subsequent sections to solve elastic-plastic problems with uncertain material parameters. The stochastic variational inequality is solved by a novel mixed method, consisting of an algebraic (PCE)−sampling (regression method) formulation. The problem is projected in a GALERKIN manner similar to the one in the classical finite element approach onto the polynomial basis of the discretized space. The *stochastic closest point projection*[1] (SCPP) is done in an algebraic-sampling manner to determine the relevant quantities in the stochastic radial return scheme. This is achieved by using the polynomial chaos algebra (PCA) as well as the regression method. The numerical realization of this formulation is straightforward, which means that it is efficient but the intrusive character of this approach requires the reformulation of the existing program code.

The structure of this chapter is as follows: In section 9.1, some existing approaches for the stochastic analysis of elastic-plastic material behaviour are briefly summarized. In view of the presented linear SSFEM the system response is represented in terms of the PCE, i.e. as a function of the known random variables of some simple type. Commonly used random variables for the PCE are normalised GAUSSIAN RVs and, with respect to some mathematical conditions, elementary mathematical operations can be done on the PCE of these random variables. The necessary mathematical operations for the novel non-linear approach will be presented in sections 9.2 and 9.3. The main part of this chapter, the formulation of the VON MISES (J_2) plasticity in the stochastic context is presented in section 9.4. The subsequent realization of this novel theoretical formulation in the in-house FE-computer program is presented in section 9.5. In section 9.6, different approaches for the probabilistic yielding are discussed and some remarks to these approaches are given. The verification of the presented approach is done on two numerical examples, which are discussed in section 9.7. A summary as well as a conclusion of this chapter is given in section 9.8.

---

[1] cf. Rosić [2013].

9.1. Overview of Existing Approaches

The major difficulty in extending the available formulations of the linear SSFEM to elastic-plastic problems is the highly non-linear coupling in the elastic-plastic constitutive rate equation. There exist only a few formulations, where random material properties are taken into account. In the following, a summary of the review, given in section 1.2, is presented.

The first approach to be mentioned here was published by Anders and Hori [1999] and Anders [2000]. In these publications, the authors dealt with elastic-plastic constitutive equations by assuming a stochastic Young's modulus. It is based on the perturbation expansion at the stochastic mean behaviour. As already mentioned several times in this thesis, the coefficient of variation α_X is limited to $\alpha_X \leq 20\%$ and in the recently published book by Xiu [2010] the COV is even specified by $\alpha_X \leq 10\%$. The approach was generalized to three-dimensional problems by Anders and Hori [2001], but the limitations by applying the perturbation method are still present there. Another drawback of this method is the always necessary need of information on higher order moments in order to calculate lower-order moments. In the literature, this problem is referred to as a *closure-problem*.

A further approach was presented in a series of papers by Sett et al. [2007b,a]; Jeremić et al. [2007]; Jeremić and Sett [2009]; Sett and Jeremić [2010]; Sett et al. [2011]. This approach based on the EULERIAN-LAGRANGIAN (EL) form of the FOKKER–PLANCK–KOLMOGOROV equation, which was formulated by Kavvas [2003]. The presented methodology is second-order accurate and does not suffer from the drawbacks of the MCS as well as the perturbation method. To be more specific, neither does the *closure problem*, as in the perturbation method, occur nor does it require the repetitive use of a computationally expensive deterministic elastic-plastic model as when a MCS is used. Nevertheless, the formulation of the constitutive equation is complicated and this approach is currently only applied to one-dimensional constitutive problems.

In the recently published paper by Arnst and R.Ghanem [2012], the authors presented a formulation for stochastic boundary value problems (SBVPs) whose formulation involves inequality constraints. They formulated a class of stochastic variational inequalities (SVIs) which is well adapted to characterize the solution of specified inequality constrained SBVPs. The discretization of the SVIs is performed via a projection onto PCEs and collocation of the inequality constraints. Besides the application on contact problems, the presented formulation is also applied to elastic-plastic problems where the general VON MISES elastic-plastic material formulation is used. However, in the numerical example, the isotropic hardening modulus is the only stochastic material parameter. The solution of the problem is done by applying the sparse grid approach, where the stochastic convex domain of admissible stresses is represented by a set of collocation points. This is a "drawback" of this method at the same time, because the number of collocation points increases exponentially when a large number of random variables are required, to represent the fluctuations of the system parameters.

The last reviewed approach was presented by Rosić and Matthies [2008]; Rosić et al. [2010]; Rosić and Matthies [2012]; Rosić [2013]. Here, the authors proposed a stochastic variational inequality formulation of stochastic elastic-plastic material behaviour. The solution algorithm in their work is an extension of the standard return-mapping algorithm, cf. Simo and Hughes [1998]. They employed a stochastic closest point

projection, whereas the predictor and corrector are formulated with the help of the stochastic GALERKIN method in its fully intrusive and non-intrusive variant. The proposed techniques tested on a series of two-dimensional examples where the bulk modulus, shear modulus, yield stress and the isotropic hardening modulus are assumed to be uncertain. Indeed, no mixed linear hardening, i.e., isotropic and kinematic hardening is taken into account and the numerical examples are limited to two-dimensional problems.

9.2. Calculating Non-Linearities via Polynomial Chaos Algebra

This section is devoted to the relevant algebraic operations of PC variables, such as the subtraction/addition, multiplication/division and inversion of a system consisting of PC variables. For further details to the discussed operations here as well as on the evaluation of non-polynomial functions, such as exponential functions or differential equations, the reader is referred to the publication by Debusschere et al. [2005] and to the textbooks by Springer [1979] and Le Maître and Knio [2010].

Let $a(\theta)$, $b(\theta)$ and $c(\theta)$ be three random variables, which are mapped from the probability space $\mathcal{L}^2(\Theta, \mathcal{F}, \mathcal{P})$ into $\mathbb{R}$. This (approximated) mapping is realized by its truncated PCE as

$$\hat{a}(\theta) = \sum_{i=0}^{P-1} a_i \psi_i, \ \hat{b}(\theta) = \sum_{j=0}^{P-1} b_j \psi_j \ \text{and} \ \hat{c}(\theta) = \sum_{k=0}^{P-1} c_k \psi_k \,, \tag{9.1}$$

where $\psi_\bullet(\boldsymbol{\xi}(\theta))$, $\boldsymbol{\xi}(\theta) = (\xi_1, \xi_2, ... \xi_M)$ are the M-dimensional polynomials[2] and the $\hat{\bullet}$ denotes the approximation of a RV.

9.2.1. Addition/Subtraction of PC-Variables

The basic operations subtraction and addition are straightforward. These operations are performed by adding (resp. subtracting) the corresponding terms of the PCE. With the RVs introduced in equation (9.1), the addition and subtraction of two RVs can be consequently written as

$$\hat{c}(\theta) = \hat{a}(\theta) \,\hat{\pm}\, \hat{b}(\theta) \,. \tag{9.2}$$

9.2.2. Galerkin Product (Multiplication of PC-Variables)

The multiplication of PC variables are not straightforward, because no direct solution exists. To be more specific, an assumption, such as

$$\hat{c}(\theta) = \hat{a}(\theta)\hat{b}(\theta) \,, \tag{9.3}$$

has to be made. This assumption is valid as long as the PCE of $\hat{a}(\theta)$ and $\hat{b}(\theta)$ is high enough for the representation of them. By use of equation (9.1), the multiplication

---

[2]In this work only HERMITE polynomials are used, because only normal distributed random variables are applied.

in equation (9.3) reads

$$\hat{c}(\theta) = \sum_{k=0}^{P-1} c_k \psi_k = \sum_{i=0}^{P-1} a_i \psi_i \sum_{j=0}^{P-1} b_j \psi_j \,. \tag{9.4}$$

For the calculation of the coefficients c_k a Galerkin approximation is applied to orthogonally project $\hat{c}$ onto the basis, spanned by the polynomials ψ_i and ψ_j. Therefore, equation $(9.4)_2$ has to be multiplied by ψ_k. Afterwards, taking the expectation on both sides with respect to the orthogonality property of the ψ's and rearranging the terms gives

$$\hat{c}_k = \sum_{i=0}^{P-1} \sum_{j=0}^{P-1} d_{ijk} a_i b_j \quad \text{with} \quad d_{ijk} \equiv \frac{\langle \psi_i \psi_j \psi_k \rangle}{\langle \psi_k^2 \rangle}, \quad \forall \, k \in 0, ... \, P-1. \tag{9.5}$$

The tensor d_{ijk} is a multiplication tensor similar to c_{ijk}, cf. equation (8.65). Two properties of d_{ijk}, which are useful for the realization in the computer code, are listed below:

1. d_{ijk} is only a function of the $\psi_\bullet$'s and needs to be calculated only once during the entire calculation process and can be saved for the recurring access.

2. d_{ijk} is sparse and can therefore be efficiently saved as sparse-cell-array.

As a shorthand notation, the Galerkin product of two approximated RVs $\hat{a}(\theta)$ and $\hat{b}(\theta)$ are prospectively written as $\hat{a}(\theta) \,\widehat{*}\, \hat{b}(\theta)$, thus

$$\hat{c}(\theta) = \hat{a}(\theta) \,\widehat{*}\, \hat{b}(\theta)\,. \tag{9.6}$$

The product of three PC variables can be realized in analogy to the presented procedure for two RVs. In general, the triple product of three approximated RVs $\hat{a}(\theta)$, $\hat{b}(\theta)$ and $\hat{c}(\theta)$ is given by

$$\hat{e}_l = \sum_{i=0}^{P-1} \sum_{j=0}^{P-1} \sum_{k=0}^{P-1} D_{ijkl} a_i b_j c_k \quad \text{with} \quad D_{ijkl} \equiv \frac{\langle \psi_i \psi_j \psi_k \psi_l \rangle}{\langle \psi_l^2 \rangle}, \quad \forall \, l \in 0, ... \, P-1, \tag{9.7}$$

where D_{ijkl} is a fourth-order multiplication tensor. The properties of D_{ijkl} are similar to those of the 3rd-order tensor d_{ijk}. However, note that this tensor becomes extremely large as the basis P of the stochastic space increases. In order to circumvent this problem, the triple product in equation (9.7) is approximated by

$$\hat{e}(\theta) = \widehat{abc} \approx \hat{a}(\theta) \,\widehat{*}\, (\hat{b}(\theta) \,\widehat{*}\, \hat{c}(\theta)) = \widehat{abc}\,, \tag{9.8}$$

where first a Galerkin product (9.6) is applied to determine $\hat{b}(\theta) \,\widehat{*}\, \hat{c}(\theta) = \widehat{bc}$, whose result is subsequently multiplied by $\hat{a}(\theta)$. This strategy is used when a Galerkin product of more than two RVs has to be evaluated.

9.2.3. Galerkin Division (Division of PC-Variables)

The division of two PC-expanded random variables is defined by

$$\hat{a}(\theta) = \frac{\hat{c}(\theta)}{\hat{b}(\theta)}, \tag{9.9}$$

with the unknown coefficients $\hat{b}(\theta)$ and $\hat{c}(\theta)$. This equation can be reformulated to get $\widehat{ab} = \hat{c}$, where this set of linear equations can be expressed as

$$\begin{pmatrix} \sum_{j=0}^{\bar{P}} d_{0j0}b_j & \cdots & \sum_{j=0}^{\bar{P}} d_{0j\bar{P}}b_j \\ \vdots & \ddots & \vdots \\ \sum_{j=0}^{\bar{P}} d_{\bar{P}j0}b_j & \cdots & \sum_{j=0}^{\bar{P}} d_{\bar{P}j\bar{P}}b_j \end{pmatrix} \begin{pmatrix} a_0 \\ \vdots \\ a_{\bar{P}} \end{pmatrix} = \begin{pmatrix} c_0 \\ \vdots \\ c_{\bar{P}} \end{pmatrix}, \tag{9.10}$$

with the relation $\bar{P} := P - 1$. To determine the unknown coefficients of $\hat{a}(\theta)$, the sparse-structure of the linear system can be efficiently solved with the generalized minimum residual method (GMRES)[3].

For the division of two RVs $\hat{b}(\theta)$, $\hat{c}(\theta)$, the shorthand notation

$$\hat{a}(\theta) = \hat{c}(\theta) \,\widehat{\div}\, \hat{b}(\theta), \tag{9.11}$$

is introduced.

9.2.4. Galerkin Inversion

The determination of an inverse linear system of equations is the last algebraic operation on RVs, which should be presented in this section. Let $\hat{a}$ be the approximation of the random variable a with known expansion. For the calculation of the stochastic inverse $\hat{a}^{-1}(\boldsymbol{\xi})$, the expansion coefficients a_k has to be determined as follows:

$$\hat{a}^{-1}(\boldsymbol{\xi}) = \frac{1}{\hat{a}(\boldsymbol{\xi})} = \left(\sum_{k=0}^{P-1} a_k \psi_k(\boldsymbol{\xi}) \right)^{-1}, \tag{9.12}$$

such that

$$\hat{a}^{-1}(\boldsymbol{\xi})\, \hat{a}(\boldsymbol{\xi}) = 1, \quad \text{a.s.}, \tag{9.13}$$

where a.s. is the abbreviation for **a**lmost **s**urely. Using the previous notation, the formulation projected via the Galerkin method corresponds to

$$\hat{a}^{-1} \,\widehat{*}\, \hat{a} = \psi_0, \tag{9.14}$$

---

[3]GMRES is a built-in function in Matlab.

with the usual definition $\psi_0 \equiv 1$. The use of the multiplication formula (9.6) leads to the following linear system of equations:

$$
\begin{pmatrix}
\sum_{j=0}^{\bar{P}} d_{0j0} a_j & \cdots & \sum_{j=0}^{\bar{P}} d_{0j\bar{P}} a_j \\
\vdots & \ddots & \vdots \\
\sum_{j=0}^{\bar{P}} d_{\bar{P}j0} a_j & \cdots & \sum_{j=0}^{\bar{P}} d_{\bar{P}j\bar{P}} a_j
\end{pmatrix}
\begin{pmatrix}
a_0^{-1} \\
\vdots \\
a_{\bar{P}-1}
\end{pmatrix}
=
\begin{pmatrix}
1 \\
\vdots \\
0
\end{pmatrix} ,
\tag{9.15}
$$

with the abbreviation $\bar{P} := P - 1$.

9.3. Regression Method

The regression method is based on a least-square minimization of the difference between the exact solution and the approximated solution using the polynomial chaos expansion. This section gives a compact summary of this method, presented among others by Sudret et al. [2003]; Berveiller et al. [2004, 2005]; Sudret et al. [2006]. For a detailed theoretical background the reader is referred to these works as well as the citations therein.

Preliminary Remarks

Let X be a random variable with prescribed Gaussian[4] PDF, which is approximated by the Hermite series as follows:

$$
\hat{X} = \sum_{i=0}^{P-1} a_i \psi_i(\boldsymbol{\xi}) ,
\tag{9.16}
$$

where $\{a_i,\ i = 0, \dots P - 1\}$ is a set of coefficients to be evaluated, ψ_i is the i-th Hermite polynomial and $\boldsymbol{\xi}$ is a standard normal vector. Such an expansion can be transformed into the standard normal space $X \to \boldsymbol{\xi} : F_X(X) = \Phi(\boldsymbol{\xi})$ by

$$
X(\boldsymbol{\xi}) = F_X^{-1}(\Phi(\boldsymbol{\xi})) ,
\tag{9.17}
$$

where $F_X(\cdot)$ is the CDF of the random variable $X(\boldsymbol{\xi})$ and $\Phi(\boldsymbol{\xi})$ defines the standard normal CDF of $\boldsymbol{\xi}$.

As pointed out at the beginning of this section, the aim of the regression method is to minimize the difference of the input variable X and its truncated approximation $\hat{X}$. Let $\{\boldsymbol{\xi}^1, \dots \boldsymbol{\xi}^n\}$ be a set of n outcomes of the standard normal vector $\boldsymbol{\xi}$, which leads to a set of n outcomes of the random variable X^j and the approximated variable $\hat{X}^j$, $j = 1, \dots n$ of equation (9.17). Consequently, the least squares method for finding the minimum of $X - \hat{X}$, with respect to the coefficients a_i, $i = 0, \dots P - 1$, reads

$$
\Delta X = \sum_{j=1}^{n} \left[X^j - \hat{X}^j \right]^2 .
\tag{9.18}
$$

---

[4]The Gaussian distribution is not the only possible choice, although it is exclusively used in this work. Alternative distributions and their corresponding polynomials are presented in subsection 7.2.3.

Substituting the expressions (9.16) and (9.17) into equation (9.18) leads to

$$\Delta X = \sum_{j=1}^{n} \left[F_X^{-1}(\Phi(\boldsymbol{\xi}^j)) - \sum_{i=0}^{P-1} a_i \psi_i(\boldsymbol{\xi}^j) \right]^2, \qquad (9.19)$$

which can be also written as a linear system of equations as follows:

$$\begin{pmatrix} \sum_{j=1}^{n} \psi_0(\boldsymbol{\xi}^j)\psi_0(\boldsymbol{\xi}^j) & \cdots & \sum_{j=1}^{n} \psi_0(\boldsymbol{\xi}^j)\psi_{\bar{P}}(\boldsymbol{\xi}^j) \\ \vdots & \ddots & \vdots \\ \sum_{j=1}^{n} \psi_{\bar{P}}(\boldsymbol{\xi}^j)\psi_0(\boldsymbol{\xi}^j) & \cdots & \sum_{j=1}^{n} \psi_{\bar{P}}(\boldsymbol{\xi}^j)\psi_{\bar{P}}(\boldsymbol{\xi}^j) \end{pmatrix} \begin{pmatrix} a_0 \\ \vdots \\ a_{\bar{P}} \end{pmatrix} = \begin{pmatrix} \sum_{j=1}^{n} X^j \psi_0(\boldsymbol{\xi}^j) \\ \vdots \\ \sum_{j=1}^{n} X^j \psi_{\bar{P}}(\boldsymbol{\xi}^j) \end{pmatrix}, \qquad (9.20)$$

with $\bar{P} := P - 1$, where the expansion coefficients $a_0, \ldots a_{P-1}$ can be determined. However, it should be remarked that the $P \times P$ matrix on the left hand side may be evaluated only once during the simulation procedure. This means, that it can be evaluated in a pre-processing step and stored in the workspace, such as the multiplication tensors c_{ijk} and d_{ijk}. To ensure that the method is not undefined, the number of points n, i.e. the number of outcomes n, should not be smaller than the basis P of the PCE.

9.4. Plasticity in a Stochastic Context

The stochastic discretization of the elastic-plastic problem is defined in any finite dimensional subspace $\mathcal{S}^P \subset \mathcal{S}$, where $\mathcal{S}^P = \mathcal{L}^2(\Theta, \mathcal{F}, \mathcal{P})$ is a reasonable choice. The subspace $\mathcal{S}^P$ is spanned by the polynomial chaos basis as already defined in (8.41) and repeated here for convenience:

$$\mathcal{S}^P = \text{span}\{\psi_j(\theta), \ j = 0, \ldots P - 1\}. \qquad (9.21)$$

Here, ψ_j form a set of orthogonal multidimensional Hermite Polynomials in the M independent Gaussian random variables $\boldsymbol{\xi} = \{\xi_1, \ldots \xi_M\}$. As already discussed in chapter 7, the Hermite polynomials are a suitable choice when using Gaussian random variables. However, Gaussian variables and Hermite polynomials are not the only possible combination. Instead, the use of other kinds of random variables, such as Gamma, Beta or Uniform distributed ones, with their corresponding polynomials (Laguerre, Jacobi and Legendre) is also possible. This methodology is referred to as *generalized* polynomial chaos or Wiener-*Askey* polynomial chaos, as already briefly discussed in section 7.2.3.

The deterministic discretization and the stochastic discretization of the elastic-plastic problem are similar to this one described in the linear SSFEM, cf. section 8.2. After the discretization, the displacements, strains and stresses within an element are

obtained as follows:

$$\hat{\mathbf{u}}(\mathbf{x}, \theta) := \sum_{i=1}^{n_n} \sum_{j=0}^{P-1} \hat{\mathbf{u}}_i^j(\theta) \, \mathbf{H} \, \psi_j(\theta) \,, \tag{9.22}$$

$$\hat{\boldsymbol{\epsilon}}(\mathbf{x}, \theta) := \sum_{i=1}^{n_{GP}} \sum_{j=0}^{P-1} \hat{\boldsymbol{\epsilon}}_i^j(\mathbf{x}, \theta) \, \psi_j(\theta) \,, \tag{9.23}$$

$$\hat{\boldsymbol{\sigma}}(\mathbf{x}, \theta) := \sum_{i=1}^{n_{GP}} \sum_{j=0}^{P-1} \hat{\boldsymbol{\sigma}}_i^j(\mathbf{x}, \theta) \, \psi_j(\theta) \,, \tag{9.24}$$

where n_n is the number of nodes per element, n_{GP} is the number of integration points per element and $\mathbf{H}$ denotes the matrix that contains the shape functions. All parameters, such as the stresses, strains, displacements and the internal variables are determined by applying the polynomial chaos algebra. The subsequent computation will be done similar to a deterministic FE analysis. More precisely, the unknown variables are determined locally in each integration point via the Newton-Raphson method, as illustrated in Algorithm 3. Afterwards, the statistics of the system response, such as the mean value and the standard deviation of the variable of interest are evaluated as described in section 8.4.

The basic steps of the proposed algorithm above are similar to the classical (deterministic) Newton-Raphson algorithm, where particular attention is paid to the calculation of the stochastic consistent tangent $\mathbb{D}^{ep}$, as discussed throughout this chapter.

9.5. Implementation of Stochastic Plasticity

The steps outlined in this section are similar to those presented in the deterministic elastic-plastic analysis, discussed in section 3.4. Due to the material fluctuations, the elasticity tensor $\mathbb{C}$ now becomes uncertain and will be denoted as $\mathbb{D}(\mathbf{x})$. This also applies to the yield stress σ_y, which is denoted by $\sigma_y(\mathbf{x}, \theta)$ in the stochastic context. For the hardening parameters, $\mathbb{H}_{iso}(\mathbf{x})$ and $\mathbb{H}_{kin}(\mathbf{x})$ are used to distinguish the deterministic case from the stochastic one. These random material parameters are modelled as independent Gaussian random fields via the KLE and defined over the probability space $(\Theta, \mathcal{F}, \mathcal{P})$. The random parameters make the analysis more complex, but the key steps are the same as in the deterministic elastic-plastic formulation, which will be later outlined in this section.

First of all, two notational remarks should be given:

1. To make use of a compact notation, the spatial dependence indicated by $\mathbf{x}$ will be omitted in this sequel.

2. All parameters in this section are discretized in a deterministic and in a stochastic manner, whereas the stochastic discretization as well as their approximation is indicated by $\hat{\bullet}$, e.g., the stochastic deviatoric strain tensor $\hat{\boldsymbol{\epsilon}}(\theta)$.

At the beginning of the stochastic formulation, the governing equations, from the deterministic analysis, cf. section 3.4, are summarized below. Note that all parameters that occur in the formulation are random variables and therefore are identified with $\bullet(\theta)$.

Algorithm 3 Newton-Raphson Scheme in a Stochastic Context

1: **for** each time (load) step t = 1 : t_{end} **do**
2:     Initialization for $n = 0$
3:     $^{t+\Delta t}\mathcal{U}_0 = {}^t\mathcal{U}, \quad {}^{t+\Delta t}\mathcal{K}_0 = {}^t\mathcal{K}, \quad {}^{t+\Delta t}\mathcal{F}_0 = {}^t\mathcal{F}$
4:     Iteration $n = n + 1$
5:     **for** each integration point n_{GP}, $i = 1 : n_{GP}$ **do**
6:         Update the approximated random strains $\boldsymbol{\epsilon}(\theta)$
7:         $^{t+\Delta t}\boldsymbol{\epsilon}_n(\theta)(\mathbf{x}_i) = \mathbf{B}_i \,{}^{t+\Delta t}\mathbf{u}_n(\theta)$
8:         Calculate the terms of the stochastic consistent tangent via the PCA, cf. section 9.2 and by the regression method, see section 9.3
9:         Update the approximated internal random variables $\alpha(\theta)$ and $\boldsymbol{\beta}(\theta)$
10:        $^{t+\Delta t}\alpha_n(\theta) = \alpha_{n-1}(\theta) + \Delta\lambda(\theta)\sqrt{\frac{2}{3}}$, cf. equation (9.33)
11:        $^{t+\Delta t}\boldsymbol{\beta}_n(\theta) = \boldsymbol{\beta}_{n-1}(\theta) + \Delta\lambda(\theta)\frac{2}{3}\,\mathbb{H}_{\text{kin}}\,\mathbf{n}_n(\theta)$, see equation (9.34)
12:        Update the approximated random stresses $\boldsymbol{\sigma}(\theta)$ according to equation (9.46)
13:        Compute the stochastic consistent tangent $\mathbb{D}^{\text{ep}}(\mathbf{x}_i, \theta)$, see Algorithm 4
14:        Assemble the stochastic element stiffness matrix $\mathbf{k}^e(\theta)$
15:        $\mathbf{k}^e(\theta) = \sum_{i=1}^{n_{GP}} \mathbf{B}_i^{\text{T}}\, \mathbb{D}^{\text{ep}}(\mathbf{x}_i, \theta)\, \mathbf{B}_i\, w_i \det J_i$
16:        Compute the stochastic internal element forces
17:        $\mathbf{f}^{e\,\text{int}}(\theta) := \sum_{i=1}^{n_{GP}} \mathbf{B}_i^{\text{T}}(\mathbf{x}_i)^{t+\Delta t}\boldsymbol{\sigma}_n(\theta)(\mathbf{x}_i)\, w_i \det J_i$
18:     **end for**
19:     Assemble the stochastic global stiffness matrix $\mathcal{K}_{n-1}$ and solve for $\Delta\mathcal{U}_n$
20:     $^{t+\Delta t}\mathcal{K}_{n-1}^\theta \Delta\mathcal{U}_n = \mathcal{R}_{n-1} \quad \text{with} \quad \mathcal{R}_{n-1} := {}^{t+\Delta t}\lambda\mathcal{F}^{\text{ext}} - {}^{t+\Delta t}\mathcal{F}_{n-1}^{\text{int}}$
21:     Update the displacements
22:     $^{t+\Delta t}\mathcal{U}_n = {}^{t+\Delta t}\mathcal{U}_{n-1} + \Delta\mathcal{U}_n$
23:     Check for convergence criterion
24:     **if** $\frac{\|\Delta\mathcal{U}_n\|}{\|{}^{t+\Delta t}\mathcal{U}_n\|} \leq \epsilon_{\text{D}}$ **then**
25:        $^{t+\Delta t}\bullet := {}^{t+\Delta t}\bullet_n$
26:     **else**
27:        go to 4
28:     **end if**
29: **end for**

- The additive decomposition of the *stochastic* strain tensor, where only the deviatoric parts, labelled by $\tilde{\bullet}$, are considered, i.e.

$$\tilde{\boldsymbol{\epsilon}}(\theta) = \tilde{\boldsymbol{\epsilon}}^{\text{el}}(\theta) + \tilde{\boldsymbol{\epsilon}}^{\text{pl}}(\theta) , \qquad\qquad \mathcal{P}_\theta - \text{a.s. , (9.25)}$$

- The split of the *stochastic* stresses into a *stochastic* deviatoric part $\mathbf{s}(\theta)$ and a *stochastic* hydrostatic part $p(\theta)$ reads

$$\mathbf{s}(\theta) = 2\,\mu(\theta)\,\tilde{\boldsymbol{\epsilon}}^{\text{el}}(\theta) = 2\mu(\theta)\left(\tilde{\boldsymbol{\epsilon}}(\theta) - \tilde{\boldsymbol{\epsilon}}^{\text{pl}}(\theta)\right) , \qquad \mathcal{P}_\theta - \text{a.s. , (9.26)}$$

$$p(\theta) = \mathbb{K}\,\text{tr}\,(\boldsymbol{\epsilon}^{\text{el}}(\theta)) , \qquad\qquad\qquad \mathcal{P}_\theta - \text{a.s. , (9.27)}$$

with the *stochastic* shear modulus $\mu(\theta)$ and the *stochastic* bulk modulus $\mathbb{K}$.

- The *stochastic* VON MISES yield condition ($\mathcal{P}_\theta$ − a.s.) is given by

$$f(\boldsymbol{\eta}(\theta), \alpha(\theta)) = \|\boldsymbol{\eta}(\theta)\| - \sqrt{\frac{2}{3}}(\sigma_y(\theta) + \mathbb{H}_{\mathrm{iso}}\alpha(\theta)) \leq 0\,, \tag{9.28}$$

  where $\boldsymbol{\eta}(\theta) = \mathbf{s}(\boldsymbol{\sigma}(\theta)) - \boldsymbol{\beta}(\theta)$ denotes the *stochastic* back-stress tensor and $\sigma_y(\theta)$ is the *stochastic* yield stress.

- The associative *stochastic* evolution equations, for the *stochastic* plastic strain and the *stochastic* internal variables, are

$$\dot{\boldsymbol{\epsilon}}^{\mathrm{pl}}(\theta) = \dot{\lambda}(\theta)\frac{\partial f(\theta)}{\partial \mathbf{s}(\theta)}\,, \qquad\qquad\qquad \mathcal{P}_\theta - \text{a.s. }, \quad (9.29)$$

$$\dot{\alpha}(\theta) = \sqrt{\frac{2}{3}}\dot{\lambda}(\theta)\,, \qquad\qquad\qquad\qquad \mathcal{P}_\theta - \text{a.s. }, \quad (9.30)$$

$$\dot{\boldsymbol{\beta}}(\theta) = -\frac{2}{3}\mathbb{H}_{\mathrm{kin}}\dot{\lambda}(\theta)\frac{\partial f(\theta)}{\partial \mathbf{s}(\theta)}\,, \qquad\qquad \mathcal{P}_\theta - \text{a.s. }. \quad (9.31)$$

After applying the implicit Euler rule to discretize the *stochastic* evolution equations, they can be reformulated as

$$\tilde{\boldsymbol{\epsilon}}^{\mathrm{pl}}_{n+1}(\theta) = \tilde{\boldsymbol{\epsilon}}^{\mathrm{pl}}_n(\theta) + \Delta\lambda(\theta)\mathbf{n}_{n+1}(\theta)\,, \qquad\qquad \mathcal{P}_\theta - \text{a.s.}, \quad (9.32)$$

$$\alpha_{n+1}(\theta) = \alpha_n(\theta) + \sqrt{\frac{2}{3}}\Delta\lambda(\theta)\,, \qquad\qquad \mathcal{P}_\theta - \text{a.s.}, \quad (9.33)$$

$$\boldsymbol{\beta}_{n+1}(\theta) = \boldsymbol{\beta}_n(\theta) + \frac{2}{3}\mathbb{H}_{\mathrm{kin}}\Delta\lambda(\theta)\mathbf{n}_{n+1}(\theta)\,, \qquad \mathcal{P}_\theta - \text{a.s.}, \quad (9.34)$$

where $\Delta\lambda(\theta) = \lambda(\theta) - \lambda_n(\theta)$. Using equation (9.26), the *stochastic* deviatoric stresses at the time-step t_{n+1}, are calculated as

$$\mathbf{s}_{n+1}(\theta) = 2\mu(\theta)\left(\tilde{\boldsymbol{\epsilon}}_{n+1}(\theta) - \tilde{\boldsymbol{\epsilon}}^{\mathrm{pl}}_{n+1}(\theta)\right)\,, \qquad\qquad \mathcal{P}_\theta - \text{a.s.}. \quad (9.35)$$

After substituting equation (9.34) into equation (9.35), the stochastic deviatoric stress becomes

$$\mathbf{s}_{n+1}(\theta) = 2\mu(\theta)\left(\tilde{\boldsymbol{\epsilon}}_{n+1}(\theta) - \tilde{\boldsymbol{\epsilon}}^{\mathrm{pl}}_n(\theta)\right) - 2\mu(\theta)\,\Delta\lambda(\theta)\mathbf{n}_{n+1}(\theta)\,, \quad \mathcal{P}_\theta - \text{a.s.} \quad (9.36)$$

9.5.1. Stochastic Closest Point Projection (SCPP)

The formulation of the stochastic predictor-corrector method, for the stochastic constitutive equations is in principle similar to the standard procedure, which was described in section 3.4. First, the *stochastic elastic-predictor* is presented, then followed by the *stochastic corrector* step. Here, particular emphasis is placed on the PCA and the regression method, which are applied for the evaluation of the corresponding equations. It should be remarked that from now on only the approximated random variables, characterized by $\hat{\bullet}$, are considered.
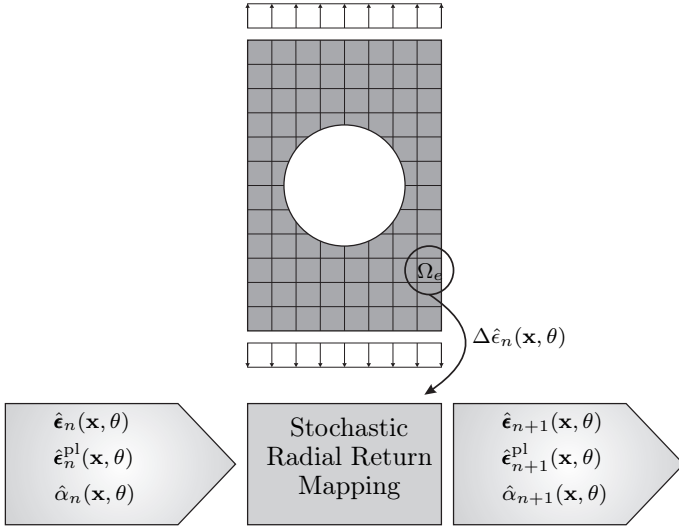
Figure 9.1.: Schematic illustration of the stochastic elastic-plastic radial return mapping algorithm.

Stochastic Elastic Predictor

In the stochastic elastic-predictor, the variables are assumed as fixed. This assumption results in the stochastic *trial* state and the corresponding set of equations is given by

$$\begin{cases} \hat{\mathbf{s}}_{n+1}^{\text{trial}}(\theta) &= 2\hat{\mu}(\theta)\,\widehat{\ast}\,\left(\hat{\boldsymbol{\epsilon}}_{n+1}^{\text{trial}}(\theta)\widehat{-}\hat{\boldsymbol{\epsilon}}_{n}^{\text{pl}}(\theta)\right), \\ \hat{\boldsymbol{\eta}}_{n+1}^{\text{trial}}(\theta) &= \hat{\mathbf{s}}_{n+1}^{\text{trial}}(\theta)\widehat{-}\hat{\boldsymbol{\beta}}_{n}(\theta), \\ \hat{\alpha}_{n+1}^{\text{trial}}(\theta) &= \hat{\alpha}_{n}(\theta), \end{cases} \tag{9.37}$$

with $\mathcal{P}_{\theta} = 1$. The set of stochastic plastic variables $\{\hat{\boldsymbol{\epsilon}}_{n}^{\text{pl}}(\theta), \hat{\alpha}_{n}(\theta), \hat{\boldsymbol{\beta}}_{n}(\theta)\}$ is known from the last time step at t_n. Because the stochastic elastic strain $\Delta\hat{\boldsymbol{\epsilon}}_n(\theta)$ was computed from the solution of the stochastic weak form, the stochastic *trial* parts in equation (9.37) can be computed directly, see Figure 9.1 for an illustration of this procedure.

The check of the stochastic yield condition (for $\mathcal{P}_{\theta} = 1$) is given in terms of the stochastic *trial* variables as follows:

$$\hat{f}_{n+1}^{\text{trial}}(\hat{\boldsymbol{\eta}}_{n+1}^{\text{trial}}(\theta), \hat{\alpha}_{n+1}^{\text{trial}}(\theta)) = \underbrace{\|\hat{\boldsymbol{\eta}}_{n+1}^{\text{trial}}(\theta)\|}_{\substack{\text{Regression} \\ \text{Method}}} \widehat{-}\sqrt{\frac{2}{3}}\left(\hat{\boldsymbol{\sigma}}_y(\theta)\widehat{+}\widehat{\mathbb{H}}_{iso}\,\widehat{\ast}\,\hat{\alpha}_n(\theta)\right) \leq 0, \tag{9.38}$$

where the norm of the back-stress tensor is evaluated with the regression method. From now on, all norms in this section are calculated with the regression method

even though it is not explicitly mentioned. If the stochastic deviatoric stress $\hat{\mathbf{s}}_{n+1}^{\text{trial}}(\theta)$ fulfils the yield condition within the time interval $[t_n,\, t_{n+1}] \subset [0,\, T]$, i.e. $\hat{f}_{n+1}^{\text{trial}}(\hat{\boldsymbol{\eta}}_{n+1}^{\text{trial}}(\theta), \hat{\alpha}_{n+1}^{\text{trial}}(\theta)) \leq 0$, the material behaviour is purely elastic and the set of the stochastic constitutive variables are updated as follows:

$$
\begin{cases}
\hat{\mathbf{s}}_{n+1}(\theta) & = \hat{\mathbf{s}}_{n+1}^{\text{trial}}(\theta)\,, & \mathcal{P}_\theta - \text{a.s.} \\
\hat{\boldsymbol{\epsilon}}_{n+1}^{\text{pl}}(\theta) & = \hat{\boldsymbol{\epsilon}}_n^{\text{pl}}(\theta)\,, & \mathcal{P}_\theta - \text{a.s.} \\
\hat{\boldsymbol{\beta}}_{n+1}(\theta) & = \hat{\boldsymbol{\beta}}_n(\theta)\,, & \mathcal{P}_\theta - \text{a.s.} \\
\hat{\alpha}_{n+1}(\theta) & = \hat{\alpha}_n(\theta), & \mathcal{P}_\theta - \text{a.s.} \ .
\end{cases}
\tag{9.39}
$$

Otherwise, the material shows an elastic-plastic behaviour within this time-step and the *trial* quantities have to be updated by the *stochastic radial-return* mapping procedure, which is outlined below.

Stochastic Corrector

In this case, the solution for the stochastic plastic multiplier $\Delta\hat{\lambda}(\theta)$ and its direction $\hat{\mathbf{n}}_{n+1}(\theta)$ have to be determined for the stochastic deviatoric stress $\hat{\mathbf{s}}_{n+1}(\theta)$, given in equation (9.36).

From the relation (a detailed derivation is given in section 3.4)

$$
\hat{\boldsymbol{\eta}}_{n+1}^{\text{trial}}(\theta) = \hat{\boldsymbol{\eta}}_{n+1}(\theta) \mathbin{\widehat{*}} \left[1 \mathbin{\widehat{+}} \left(\frac{2}{3}\widehat{\mathbb{H}}_{\text{kin}} + 2\hat{\mu}(\theta) \right) \mathbin{\widehat{*}} \underbrace{\frac{\Delta\hat{\lambda}(\theta)}{\|\hat{\boldsymbol{\eta}}_{n+1}(\theta)\|}}_{\widehat{\mathbb{F}}} \right]\,, \quad \text{with} \tag{9.40}
$$

$$
\widehat{\mathbb{F}} = \Delta\hat{\lambda}(\theta) \mathbin{\widehat{\div}} \|\hat{\boldsymbol{\eta}}_{n+1}(\theta)\|\,,
$$

it can be understood that the stochastic *trial* and the updated stochastic deviatoric parts of the relative stresses are co-linear. This implies that

$$
\begin{aligned}
\hat{\mathbf{n}}_{n+1}^{\text{trial}}(\theta) &= \frac{\hat{\boldsymbol{\eta}}_{n+1}^{\text{trial}}(\theta)}{\|\hat{\boldsymbol{\eta}}_{n+1}^{\text{trial}}(\theta)\|} = \hat{\mathbf{n}}_{n+1}(\theta) \\
&= \hat{\boldsymbol{\eta}}_{n+1}^{\text{trial}}(\theta) \mathbin{\widehat{\div}} \|\hat{\boldsymbol{\eta}}_{n+1}^{\text{trial}}(\theta)\|\,,
\end{aligned}
\tag{9.41}
$$

namely the stochastic flow vectors at the stochastic *trial* and updated states are coincide. After some algebra applied on equation (9.40)[5], the following relation is obtained

$$
\|\hat{\boldsymbol{\eta}}_{n+1}(\theta)\| = \|\hat{\boldsymbol{\eta}}_{n+1}^{\text{trial}}(\theta)\| \mathbin{\widehat{-}} \left(2\hat{\mu}(\theta) \mathbin{\widehat{+}} \frac{2}{3}\widehat{\mathbb{H}}_{\text{kin}} \right) \mathbin{\widehat{*}} \Delta\hat{\lambda}(\theta)\,, \qquad \mathcal{P}_\theta - \text{a.s.} \tag{9.42}
$$

---

[5] See section 3.4 for details.

Inserting this relation into the stochastic yield condition (9.28) gives

$$\hat{f}_{n+1}(\theta) = \|\hat{\boldsymbol{\eta}}_{n+1}^{\mathrm{trial}}(\theta)\| \widehat{-} \left(2\hat{\mu}(\theta)\widehat{+}\frac{2}{3}\widehat{\mathbb{H}}_{\mathrm{kin}}\right) \widehat{*} \Delta\hat{\lambda}(\theta)$$
$$\widehat{-}\sqrt{\frac{2}{3}}\left[\hat{\sigma}_y(\theta)\widehat{+}\widehat{\mathbb{H}}_{\mathrm{iso}}\widehat{*}\left(\hat{\alpha}_n(\theta)\widehat{+}\sqrt{\frac{2}{3}}\Delta\hat{\lambda}(\theta)\right)\right] = 0\,, \quad \mathcal{P}_\theta - \mathrm{a.s.}\,, \tag{9.43}$$

which has to be fulfilled at the current time increment t_{n+1}. The stochastic plastic multiplier $\Delta\hat{\lambda}(\theta)$ can be calculated in a closed form by rearranging the foregoing equation, i.e.

$$\Delta\hat{\lambda}(\theta) = \frac{\hat{f}_{n+1}^{\mathrm{trial}}(\theta)}{2\hat{\mu}(\theta)\widehat{*}\left(1\widehat{+}\frac{\widehat{\mathbb{H}}_{\mathrm{iso}}\widehat{+}\widehat{\mathbb{H}}_{\mathrm{kin}}}{3\hat{\mu}(\theta)}\right)} \tag{9.44}$$
$$= \hat{f}_{n+1}^{\mathrm{trial}}(\theta)\widehat{\div}\left[2\hat{\mu}(\theta)\widehat{*}\left(1\widehat{+}\left(\widehat{\mathbb{H}}_{\mathrm{iso}}\widehat{+}\widehat{\mathbb{H}}_{\mathrm{kin}}\right)\widehat{\div}3\hat{\mu}(\theta)\right)\right]\,, \quad \mathcal{P}_\theta - \mathrm{a.s.} \tag{9.45}$$

with $\hat{f}_{n+1}^{\mathrm{trial}}(\theta) = \|\hat{\boldsymbol{\eta}}_{n+1}^{\mathrm{trial}}(\theta)\|\widehat{-}\sqrt{\frac{2}{3}}(\hat{\sigma}_y(\theta)\widehat{+}\widehat{\mathbb{H}}_{\mathrm{iso}}\widehat{*}\hat{\alpha}_n(\theta))$. With the computed increment of the stochastic plastic multiplier, the stochastic stresses, stochastic plastic strains and the stochastic internal variables in equations (9.32) to (9.34) can be calculated. The actual stochastic stress at t_{n+1} are determined by

$$\hat{\boldsymbol{\sigma}}_{n+1}(\theta) = \widehat{\mathbb{K}}\operatorname{tr}\left(\hat{\boldsymbol{\epsilon}}(\theta)\right)\widehat{+}2\hat{\mu}(\theta)\widehat{*}\left(\hat{\boldsymbol{\epsilon}}_{n+1}(\theta)\widehat{-}\hat{\boldsymbol{\epsilon}}_n^{\mathrm{pl}}(\theta)\right)\widehat{-}2\hat{\mu}(\theta)\widehat{*}\Delta\hat{\lambda}(\theta)\widehat{*}\hat{\mathbf{n}}_{n+1}^{\mathrm{trial}}(\theta)\,, \tag{9.46}$$

for $\mathcal{P}_\theta = 1$. From the stochastic stress at t_{n+1}, the stochastic consistent elastic-plastic tangent modulus (for $\mathcal{P}_\theta = 1$) is computed by

$$\widehat{\mathbb{D}}_{n+1}^{\mathrm{ep}} = \frac{\partial\hat{\boldsymbol{\sigma}}_{n+1}(\theta)}{\partial\hat{\boldsymbol{\epsilon}}_{n+1}(\theta)}\,, \tag{9.47}$$
$$= \partial\hat{\boldsymbol{\sigma}}_{n+1}(\theta)\widehat{\div}\partial\hat{\boldsymbol{\epsilon}}_{n+1}(\theta)\,,$$
$$= \widehat{\mathbb{D}}_{n+1}^{\mathrm{el}}\widehat{-}2\hat{\mu}(\theta)\widehat{*}\hat{\mathbf{n}}_{n+1}^{\mathrm{trial}}(\theta)\widehat{\otimes}\frac{\partial\Delta\hat{\lambda}(\theta)}{\partial\hat{\boldsymbol{\epsilon}}_{n+1}(\theta)}\widehat{-}2\hat{\mu}(\theta)\widehat{*}\Delta\hat{\lambda}(\theta)\frac{\partial\hat{\mathbf{n}}_{n+1}^{\mathrm{trial}}(\theta)}{\partial\hat{\boldsymbol{\epsilon}}_{n+1}(\theta)}\,, \tag{9.48}$$

with

$$\frac{\partial\Delta\hat{\lambda}(\theta)}{\partial\hat{\boldsymbol{\epsilon}}_{n+1}(\theta)} = \partial\Delta\hat{\lambda}(\theta)\widehat{\div}\partial\hat{\boldsymbol{\epsilon}}_{n+1}(\theta) \quad \mathrm{and}\,,$$
$$\frac{\partial\hat{\mathbf{n}}_{n+1}^{\mathrm{trial}}(\theta)}{\partial\hat{\boldsymbol{\epsilon}}_{n+1}(\theta)} = \partial\hat{\mathbf{n}}_{n+1}^{\mathrm{trial}}(\theta)\widehat{\div}\partial\hat{\boldsymbol{\epsilon}}_{n+1}(\theta)\,.$$

After some algebraic calculation (see section 3.4, respectively, Appendix C), the algorithmic stochastic consistent tangent modulus reads

$$\widehat{\mathbb{D}}_{n+1}^{\mathrm{ep}} = \widehat{\mathbb{K}}\,\hat{\mathbf{1}}\widehat{\otimes}\hat{\mathbf{1}} + 2\hat{\mu}(\theta)\widehat{*}\widehat{\mathbb{A}}_{n+1}\left(\hat{\mathbb{I}} - \frac{1}{3}\hat{\mathbf{1}}\widehat{\otimes}\hat{\mathbf{1}}\right)$$
$$- 2\hat{\mu}(\theta)\widehat{*}\widehat{\mathbb{B}}_{n+1}\hat{\mathbf{n}}_{n+1}^{\mathrm{trial}}(\theta)\widehat{\otimes}\hat{\mathbf{n}}_{n+1}^{\mathrm{trial}}(\theta)\,. \tag{9.49}$$

Here, $\widehat{\mathbb{A}}_{n+1}$ is given by

$$
\begin{aligned}
\widehat{\mathbb{A}}_{n+1} &= \hat{1} \,\widehat{-}\, \frac{2\hat{\mu}(\theta)\,\widehat{*}\,\Delta\hat{\lambda}}{\|\hat{\boldsymbol{\eta}}_{n+1}^{\text{trial}}\|} \\
&= \hat{1} \,\widehat{-}\, 2\hat{\mu}(\theta)\,\widehat{*}\,\Delta\hat{\lambda}\,\widehat{\div}\,\|\hat{\boldsymbol{\eta}}_{n+1}^{\text{trial}}\|,
\end{aligned}
\tag{9.50}
$$

and $\widehat{\mathbb{B}}_{n+1}$ is defined as

$$
\begin{aligned}
\widehat{\mathbb{B}}_{n+1} &= \left(\hat{1}\,\widehat{+}\,\frac{\widehat{\mathbb{H}}_{\text{kin}}\,\widehat{+}\,\widehat{\mathbb{H}}_{\text{iso}}}{3\hat{\mu}(\theta)}\right)^{-1}\,\widehat{-}\,\frac{2\hat{\mu}(\theta)\,\widehat{*}\,\Delta\hat{\lambda}(\theta)}{\|\hat{\boldsymbol{\eta}}_{n+1}^{\text{trial}}(\theta)\|}, \\
&= \left(\hat{1}\,\widehat{+}\,\left(\widehat{\mathbb{H}}_{\text{kin}}\,\widehat{+}\,\widehat{\mathbb{H}}_{\text{iso}}\right)\,\widehat{\div}\,3\hat{\mu}(\theta)\right)^{-1}\,\widehat{-}\,2\hat{\mu}(\theta)\,\widehat{*}\,\Delta\hat{\lambda}(\theta)\,\widehat{\div}\,\|\hat{\boldsymbol{\eta}}_{n+1}^{\text{trial}}(\theta)\|.
\end{aligned}
\tag{9.51}
$$

From the previous equations it is obvious that the PCA makes the evaluation of the stochastic consistent elastic-plastic tangent matrix $\widehat{\mathbb{D}}^{\text{ep}}$ more complex than the standard deterministic counterpart. The complete procedure for the calculation of $\widehat{\mathbb{D}}^{\text{ep}}$ is summarized in Algorithm 4. Moreover, the key steps of the preceding algorithm of the stochastic radial-return mapping are summarized in Tab. 9.1.

Table 9.1.: Stochastic Radial-Return Mapping.

1. Computation of the stochastic trial elastic stress

$$\hat{\tilde{\boldsymbol{\epsilon}}}_{n+1}(\theta) = \hat{\boldsymbol{\epsilon}}_{n+1}(\theta) \widehat{-} \frac{1}{3}\,\mathrm{tr}(\hat{\boldsymbol{\epsilon}}(\theta))\hat{\mathbf{1}}\,,$$

$$\hat{\mathbf{s}}_{n+1}^{\mathrm{trial}}(\theta) = 2\hat{\mu}(\theta)\,\widehat{*}\,\left(\hat{\tilde{\boldsymbol{\epsilon}}}_{n+1}(\theta)\widehat{-}\hat{\tilde{\boldsymbol{\epsilon}}}_{n}^{\mathrm{pl}}(\theta)\right)\,, \tag{9.52}$$

$$\hat{\boldsymbol{\eta}}_{n+1}^{\mathrm{trial}}(\theta) = \hat{\mathbf{s}}_{n+1}^{\mathrm{trial}}(\theta)\widehat{-}\hat{\boldsymbol{\beta}}_{n}(\theta)\,.$$

2. Check the stochastic yield condition

$$\hat{f}_{n+1}^{\mathrm{trial}}(\hat{\boldsymbol{\eta}}_{n+1}^{\mathrm{trial}}(\theta),\hat{\alpha}_{n+1}^{\mathrm{trial}}(\theta)) = \|\hat{\boldsymbol{\eta}}_{n+1}^{\mathrm{trial}}(\theta)\|\widehat{-}\widehat{\mathbb{J}}\,, \tag{9.53}$$

where $\widehat{\mathbb{J}} = \sqrt{\frac{2}{3}}\left(\hat{\sigma}_y(\theta)\widehat{+}\widehat{\mathbb{H}}_{\mathrm{iso}}\,\widehat{*}\,\hat{\alpha}_n(\theta)\right)$.
IF $\hat{f}_{n+1}^{\mathrm{trial}}(\hat{\boldsymbol{\eta}}_{n+1}^{\mathrm{trial}}(\theta),\hat{\alpha}_{n+1}^{\mathrm{trial}}(\theta)) \leq 0$ THEN
  set $\hat{\bullet}_{n+1}(\theta) = \hat{\bullet}_{n+1}^{\mathrm{trial}}(\theta)$ and EXIT
ENDIF

3. Computation of $\hat{\mathbf{n}}_{n+1}^{\mathrm{trial}}(\theta)$ and evaluation of the stochastic multiplier $\Delta\hat{\lambda}(\theta)$

$$\hat{\mathbf{n}}_{n+1}^{\mathrm{trial}}(\theta) = \frac{\hat{\boldsymbol{\eta}}_{n+1}^{\mathrm{trial}}(\theta)}{\|\hat{\boldsymbol{\eta}}_{n+1}^{\mathrm{trial}}(\theta)\|} = \hat{\boldsymbol{\eta}}_{n+1}^{\mathrm{trial}}(\theta)\,\widehat{\div}\,\|\hat{\boldsymbol{\eta}}_{n+1}^{\mathrm{trial}}\|\,,$$

$$\hat{\alpha}_{n+1}(\theta) = \hat{\alpha}_n(\theta)\widehat{+}\sqrt{\frac{2}{3}}\Delta\hat{\lambda}(\theta)\,. \tag{9.54}$$

4. Update the stochastic plastic strain, stochastic back-stress and the stochastic stress

$$\hat{\tilde{\boldsymbol{\epsilon}}}_{n+1}^{\mathrm{pl}}(\theta) = \hat{\tilde{\boldsymbol{\epsilon}}}_{n}^{\mathrm{pl}}(\theta)\widehat{+}\Delta\hat{\lambda}(\theta)\,\widehat{*}\,\hat{\mathbf{n}}_{n+1}^{\mathrm{trial}}(\theta)\,,$$

$$\hat{\boldsymbol{\beta}}_{n+1}(\theta) = \hat{\boldsymbol{\beta}}_{n}(\theta)\widehat{+}\frac{2}{3}\widehat{\mathbb{H}}_{\mathrm{iso}}\,\widehat{*}\,\Delta\hat{\lambda}(\theta)\,\widehat{*}\,\hat{\mathbf{n}}_{n+1}^{\mathrm{trial}}(\theta)\,, \tag{9.55}$$

$$\hat{\boldsymbol{\sigma}}_{n+1}(\theta) = \widehat{\mathbb{K}}\,\widehat{*}\,\mathrm{tr}\,\hat{\boldsymbol{\epsilon}}(\theta)\widehat{+}\widehat{\mathbb{L}}_1\widehat{-}\widehat{\mathbb{L}}_2\,,$$

where $\widehat{\mathbb{L}}_1 = 2\hat{\mu}\,\widehat{*}\,\left(\hat{\tilde{\boldsymbol{\epsilon}}}_{n+1}(\theta)\widehat{-}\hat{\tilde{\boldsymbol{\epsilon}}}_{n}^{\mathrm{pl}}(\theta)\right)$ and $\widehat{\mathbb{L}}_2 = 2\hat{\mu}\,\widehat{*}\,\Delta\hat{\lambda}(\theta)\,\widehat{*}\,\hat{\mathbf{n}}_{n+1}^{\mathrm{trial}}(\theta)$.

5. Computation of the stochastic consistent elastic-plastic tangent moduli (see Algorithm 4)

$$\widehat{\mathbb{D}}_{n+1}^{\mathrm{ep}} = \frac{\partial\hat{\boldsymbol{\sigma}}_{n+1}(\theta)}{\partial\hat{\boldsymbol{\epsilon}}_{n+1}(\theta)} = \partial\hat{\boldsymbol{\sigma}}_{n+1}(\theta)\,\widehat{\div}\,\partial\hat{\boldsymbol{\epsilon}}_{n+1}(\theta)$$

$$= \widehat{\mathbb{K}}\,\widehat{*}\,\hat{\mathbf{1}}\widehat{\otimes}\hat{\mathbf{1}}\widehat{+}2\hat{\mu}(\theta)\,\widehat{*}\,\widehat{\mathbb{A}}_{n+1}\,\widehat{*}\,\left(\hat{\mathbb{I}}\widehat{-}\frac{1}{3}\hat{\mathbf{1}}\widehat{\otimes}\hat{\mathbf{1}}\right) \tag{9.56}$$

$$\widehat{-}2\hat{\mu}(\theta)\,\widehat{*}\,\widehat{\mathbb{B}}_{n+1}\,\widehat{*}\,\hat{\mathbf{n}}_{n+1}^{\mathrm{trial}}(\theta)\widehat{\otimes}\hat{\mathbf{n}}_{n+1}^{\mathrm{trial}}(\theta)\,,$$

with $\widehat{\mathbb{A}}_{n+1}$ given in equation (9.50) and $\widehat{\mathbb{B}}_{n+1}$ defined in equation (9.51).

9.5.2. Computation of the Consistent Stochastic Tangent Modulus

As already stated in the last subsection, the computation of the consistent stochastic tangent modulus $\widehat{\mathbb{D}}^{\mathrm{ep}}$ is not as simple as in the deterministic case. Due to the RVs, it is necessary to apply the PCA to determine $\widehat{\mathbb{D}}^{\mathrm{ep}}$. For easier algebraic operations, the specific calculation steps should be split into compact parts, for instance, if more than two RVs have to be multiplied by each other. The following algorithm illustrates the individual steps of the computation of $\widehat{\mathbb{D}}^{\mathrm{ep}}$. The stochastic consistent elastic-plastic

---

Algorithm 4 Consistent Stochastic Tangent Modulus $\widehat{\mathbb{D}}^{\mathrm{ep}}$

Require: $\hat{\mu}(\theta)$, $\hat{\boldsymbol{\eta}}(\theta)$, $\hat{f}(\hat{\boldsymbol{\eta}}(\theta), \hat{\alpha}(\theta))$, $\widehat{\mathbb{H}}_{\mathrm{iso}}$, $\widehat{\mathbb{H}}_{\mathrm{kin}}$

1: Evaluation of the stochastic plastic multiplier $\Delta\hat{\lambda}(\theta)$, cf. equation (9.45)

2: $\quad \Delta\hat{\lambda} = \hat{f}(\theta) \,\widehat{\div}\, \left[2\hat{\mu}(\theta) \,\widehat{*}\, \left(\hat{1} \,\widehat{+}\, \left(\widehat{\mathbb{H}}_{\mathrm{iso}} \,\widehat{+}\, \widehat{\mathbb{H}}_{\mathrm{kin}} \right) \,\widehat{\div}\, 3\hat{\mu}(\theta) \right) \right]$

3: Determination of the stochastic normal $\hat{\mathbf{n}}(\theta)$, see equation (9.41)

4: $\quad \hat{\mathbf{n}}(\theta) = \hat{\boldsymbol{\eta}}(\theta) \,\widehat{\div}\, \|\hat{\boldsymbol{\eta}}(\theta)\|$

5: Calculation of $\widehat{\mathbb{A}}$, cf. equation (9.50)

6: $\quad \widehat{\mathbb{X}}_1 = \hat{\mu}(\theta) \,\widehat{*}\, \Delta\hat{\lambda}$

7: $\quad \widehat{\mathbb{X}}_2 = 2\widehat{\mathbb{X}}_1$

8: $\quad \widehat{\mathbb{X}}_3 = \widehat{\mathbb{X}}_2 \,\widehat{\div}\, \|\hat{\boldsymbol{\eta}}\|$

9: $\quad \widehat{\mathbb{A}} = \hat{1} \,\widehat{-}\, \widehat{\mathbb{X}}_3$

10: Computation of $\widehat{\mathbb{B}}$, see equation (9.51)

11: $\quad \widehat{\mathbb{Y}} = \left(\widehat{\mathbb{H}}_{\mathrm{kin}} \,\widehat{+}\, \widehat{\mathbb{H}}_{\mathrm{iso}} \right) \,\widehat{\div}\, 3\hat{\mu}(\theta)$

12: $\quad \widehat{\mathbb{B}} = \left(\hat{1} \,\widehat{+}\, \widehat{\mathbb{Y}} \right)^{-1} \,\widehat{-}\, \widehat{\mathbb{X}}_3$

13: Calculation of the stochastic consistent tangent modulus as given in equation (9.49)

14: $\quad \widehat{\mathbb{D}}^{\mathrm{ep}} = \widehat{\mathbb{K}} \,\hat{\mathbf{1}} \,\widehat{\otimes}\, \hat{\mathbf{1}} \,\widehat{+}\, 2\hat{\mu}(\theta) \,\widehat{*}\, \widehat{\mathbb{A}} \left(\hat{\mathbb{I}} \,\widehat{-}\, \frac{1}{3}\hat{\mathbf{1}} \,\widehat{\otimes}\, \hat{\mathbf{1}} \right) \,\widehat{-}\, 2\hat{\mu}(\theta) \,\widehat{*}\, \widehat{\mathbb{B}} \,\hat{\mathbf{n}}(\theta) \,\widehat{\otimes}\, \hat{\mathbf{n}}(\theta)$

---

tangent matrix $\widehat{\mathbb{D}}^{\mathrm{ep}}$ consists of a number of block submatrices, which represent the PCE coordinates of the stochastic stresses $\boldsymbol{\sigma}(\theta)$ with respect to PCE coordinates of the stochastic strains $\boldsymbol{\epsilon}(\theta)$, which are matrices with a size of $P \times 6$.

9.5.3. Stochastic Stiffness Matrix

The computation of the element stochastic stiffness matrix $\mathbf{k}^e(\theta)$ is almost identical to the procedure in the deterministic analysis. The difference is, that the numerical integration at each Gaussian point has to be performed for all polynomial chaos expanded coordinates, i.e P times. The subsequent assembling process for the stochastic global stiffness matrix $\mathbf{K}(\theta)$ and the corresponding global block matrix $\boldsymbol{\mathcal{K}}$ is similar to the procedure presented for the linear SSFEM in section 8.2. Due to the structure of the RVs, which are represented by the PCE, the multiplication tensor d_{ijk} has to be used instead of c_{ijk}. This results in the following form of the equilibrium equation:

$$\boldsymbol{\mathcal{K}}\Delta\boldsymbol{\mathcal{U}} = \boldsymbol{\mathcal{F}}^{\mathrm{ext}} - \boldsymbol{\mathcal{F}}^{\mathrm{int}}, \tag{9.57}$$

where $\boldsymbol{\mathcal{K}}$ is the block matrix containing all stochastic global stiffness matrices. The size of $\boldsymbol{\mathcal{K}}$ is $(P \cdot n_{\mathrm{dof}}) \times (P \cdot n_{\mathrm{dof}})$. The (unknown) stochastic block vector $\Delta\boldsymbol{\mathcal{U}}$ contains
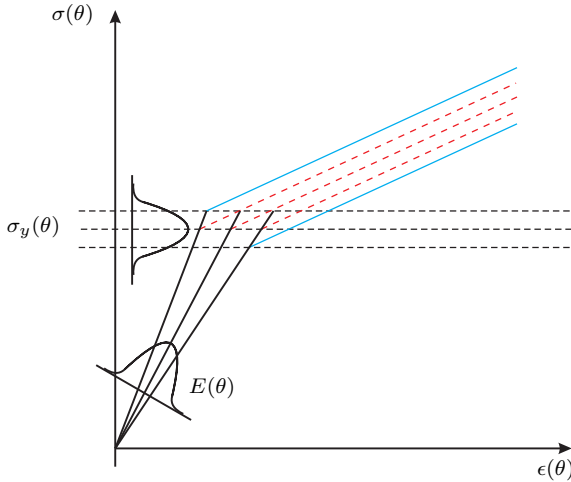
Figure 9.2.: Random yielding stress and its influence on the system response (inspired by Anders [2000]).

all global displacement vectors and $\mathcal{F}^{\text{ext}} - \mathcal{F}^{\text{int}}$ is referred to as the block form of the stochastic residual vector, where all vectors have a size of $(P \cdot n_{\text{dof}}) \times 1$. Here, the index $\bullet_{\text{dof}}$ denotes the degrees of freedom of the discretized FE system. The system of linear equations (9.57) is similar to the one in the deterministic case, given in equation (3.30) and the calculation can be done in the same way as for the deterministic formulation, see section 3.3.

9.6. Probabilistic Yielding

The evaluation of the yielding function $f(\theta)$ might be difficult if the yield stress σ_y is random. For convenience reasons, in this work, only the (via PC approximated) first coefficient $\hat{f}_0(\theta)$ of the stochastic yield surface $\hat{f}(\theta)$ is evaluated. However, to capture the whole randomness of the system response it is necessary to apply a stochastic approach for the evaluation of the uncertain yield surface. A schematic illustration, of the influence of a (stochastic) yield stress, is shown in Fig. 9.2, where the two following scenarios can be deduced:

1. The assumption that σ_y is deterministic, illustrated by the dashed lines.

2. The consideration of $\sigma_y(\theta)$ as a random variable, characterized by the straight lines.

When applying a sampling approach, such as the MCS, the stochastic yield stress makes no difficulty and the determination of the system response is quite simple, because the random variable is fixed, i.e. it is deterministic in each sample run. However, the application of the GALERKIN-type approach, developed in this chapter, could be complicated, because the yield function $f(\theta)$ is approximated by their polynomial chaos coefficients and no explicit value is known during the simulation process. With

regard to the presented methods of Anders [2000]; Sett [2007]; Arnst and R.Ghanem [2012] and Rosić [2013], different approaches has been applied to characterize the randomness of the yield stress, where Anders [2000] also used a purely elastic assumption. The other authors applied different formulations to take into account the stochastic yielding behaviour. Sett [2007] used weighted probabilities for the elastic and the elastic-plastic behaviour in his PhD thesis. These probabilities are then utilized in the proposed Fokker-Planck Kolmogorov approach to represent the material behaviour. These weights are based on the known CDF of the yield stress σ_y and assigned to the associated advection and the diffusion coefficients of the applied Fokker-Planck Kolmogorov equation. Arnst and R.Ghanem [2012] used a sampling based approach to approximate the stochastic yielding function. Through the finite number of sampling points n_p, the yield function $f(\theta)$ is approximated and thus almost surely not satisfied. However, with a sufficiently high number of sample points, the approximation can be quite accurate. Nevertheless, it should be mentioned that the number of sampling points n_p grows drastically with the stochastic dimension, which in turn also results in a drastic increasing computation time. The third approach has been presented by Rosić [2013], where it is checked if higher order moments of the yield stress (approximated via PC) $\hat{\boldsymbol{\sigma}}_y(\theta)$ are lager than the corresponding moments of the approximated von Mises stress $\hat{\boldsymbol{\sigma}}_{\mathrm{vM}}(\theta)$.

As being mentioned at the beginning of this subsection, a stochastic approach for the yield surface should be taken into account in the future., where the proposed approach by Rosić [2013] seems to be a reasonable start point for future research.

9.7. Numerical Verification

The following two subsections are dedicated to the verification of the proposed stochastic elastic-plastic approach by two numerical examples. It should be emphasized that both examples are defined in a three-dimensional space where four material parameters are assumed to be random and are represented by random fields. This stands in contrary to the methods presented in section 9.1 where only two-dimensional examples are considered and the number of random variables is limited to three. The numerical examples in this section are chosen in such a way that the KLE is evaluated analytically in the subsection 9.7.1) and numerically in the subsection 9.7.2).

In the case of the non-linear SSFEM, the estimates of the quantities of interest, namely the first two statistical moments, are evaluated by the post-processing discussed in section 8.4. When applying the coupled the SPRM-MCS or the LHS, the statistics are evaluated as presented in chapter 4.

The material properties, characterised by the KLE as well as the SPRM, are assumed to be statistically independent. All material parameters are assumed to be normal distributed, which is a reasonable choice for engineering problems, as already discussed in section 8.5. The accuracy of the approximated random fields depends on various parameters. For example, applying the KLE these are: the correlation length c and the number of dimensions M. Besides the accuracy of the random field, the subsequent approximation (or the accuracy of the approximation) of the system response depends on the order p and the resulting basis P of the polynomial chaos expansion. On the other hand, applying the coupled SPRM-MCS, the accuracy of the random field depends on the sample method used for the random phase angle (standard MCS, LHS, Sobol') and the correlation length c, while the approximation of the system response also depends on the number of samples n_{SPRM}. It should be noted that in

this section no detailed parameter studies are carried out with regard to the optimal choice of the model parameters or an optimal size of the FE mesh.

9.7.1. Four-Point Bending Beam

In the first example, a four-point bending test of a beam with the domain $\mathcal{D} = 2\,\text{cm} \times 50\,\text{cm} \times 2\,\text{cm}$ is considered. The dimensions and loads together with the FE model of the beam are shown in Fig. 9.3 (**a**). The discretized FE model, illustrated in Fig. 9.3 (**b**), consists of 400 FE elements with 2295 degrees of freedom. The displacements within the elements are approximated with linear shape functions. As

(a) Dimensions of the beam

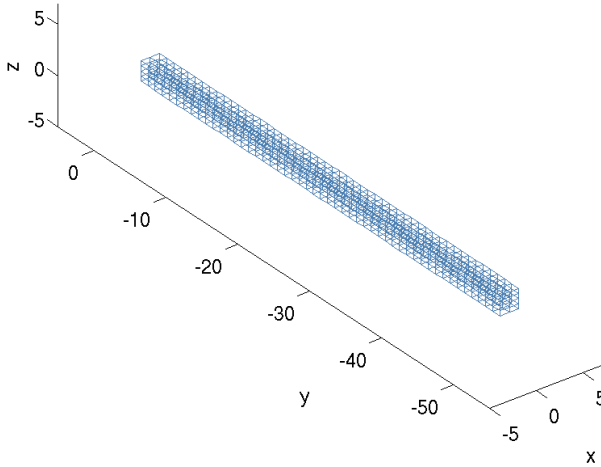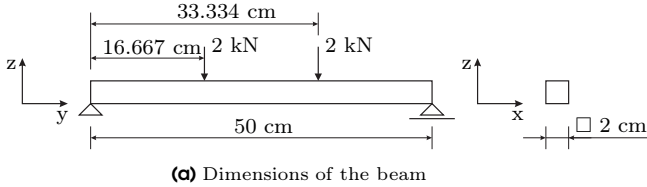**(b)** 3D view of the FE model of the beam

Figure 9.3.: Beam for the four-point bending test example.

stochastic material parameters the Young's modulus $E(\theta)$, yield stress $\sigma_y(\theta)$, isotropic hardening $\mathbb{H}_{\text{iso}}$ and the kinematic hardening $\mathbb{H}_{\text{kin}}$ are chosen. The type of distribution, mean and standard deviation are reported in Tab. 9.2.

Table 9.2.: Random material parameters for the four-point bending beam.

Material Parameter	Distribution	Mean μ	Standard Deviation σ
$E(\theta)$	Gaussian	21.000 kN/cm^2	10%
$\sigma_y(\theta)$	Gaussian	23.5 kN/cm^2	10%
$\mathbb{H}_{\mathrm{iso}}$	Gaussian	100 kN/cm^2	10%
$\mathbb{H}_{\mathrm{kin}}$	Gaussian	100 kN/cm^2	10%

The material parameters are spatially discretized with the KLE and SPRM. For the characterization of material parameters by the KLE, the covariance function defined in equation (6.30) is used, whereas the Fredholm integral in equation (6.20) can be solved analytically due to the simple geometry of the beam. When applying the SPRM, the random field $H_S(\cdot)$ is discretized ($H_S \longrightarrow \hat{H}_S$) n-times by using equation (6.104), where the power spectral density function $S_{\hat{H}_S \hat{H}_S}$ defined in equation (6.127) is utilized.

In terms of the proposed non-linear SSFEM, the resulting polynomial basis P of the PCE consists of the dimension M of the KLE and the polynomial order p of PC. Any random variable, such as the system response at an arbitrary node, can be approximated by

$$\mathbf{u}(\theta) = \sum_{i=0}^{P-1} u_i \psi_i \, . \tag{9.58}$$

Here u_i are deterministic coefficients and ψ_i are Hermite polynomials. The approximation of the system response $\mathbf{u}(\theta)$ has been done by using the polynomial chaos order $p = 2$. The representation of the material parameters by the KLE has been realized by applying various dimensions M and correlation lengths where the correlation length is assumed to be isotropic in all directions. All parameters for the generation of a random field by the KLE are summarized in Tab. 9.3, where the sub-dimension M' defines the dimension of each material parameter. For example, let the dimension assumed to be $M = 8$ with four random parameters. Then, the resulting sub-dimension is $M' = 2$, see also subsection 8.5.3.

Table 9.3.: Input parameters for the spatial characterization of the material parameters when applying the KLE.

Dimension M	Sub-Dimension M'	Order p	Correlation Length c in cm
8	2	2	10
12	3	2	5
16	4	2	5

In the case of the SPRM as spatial discretization technique and a MCS (coupled SPRM-MCS) as sample method, the system response $\mathbf{u}(\theta)$ of an arbitrary node is evaluated according to the following expression:

$$\mathbf{u}(\theta) = \hat{\mathbf{u}} = \frac{1}{n} \sum_{i=1}^{n} \mathbf{u}_i \, , \tag{9.59}$$

where the sample size is $n = n_{\mathrm{SPRM}} = 5000$, $\mathbf{u}_i$ is the i-th solution of the system response and $\hat{\mathbf{u}}$ is the sample mean of an arbitrary node. In this approach a correlation length of $c = 1$ cm is used. When applying the LHS, the response statistics are evaluated in the same manner as for the coupled SPRM-MCS with a sample size of $n_{\mathrm{LHS}} = 10000$. Both methods, the coupled SPRM-MCS and the LHS are used as reference solutions where the obtained results are compared with those obtained from the developed method.

The quantity of interest is the VON MISES (vM) stress σ_{vM}, where the approximation of the mean value, denoted in this chapter by $\mathbb{E}[\sigma_{\mathrm{vM}}]$ and the standard deviation $\sigma(\sigma_{\mathrm{vM}})$ are investigated.

Discussion of the Results

The results for the proposed non-linear SSFEM are shown in Fig. 9.4. They have been obtained by using the finite element mesh shown in Fig. 9.3 (**b**) and the polynomial bases $P = 45$ ($M = 8$, $p = 2$), $P = 91$ ($M = 12$, $p = 2$) and $P = 153$ ($M = 16$, $p = 2$). The reference solutions obtained by the coupled SPRM-MCS and the LHS are plotted in Figs. 9.5 and 9.6.

The computed results of the non-linear SSFEM show a good agreement of the mean value of the vM stress with the coupled SPRM-MCS as well as with a LHS. Besides the values of the mean stresses, the spatial distributions of the mean values of the characteristic stresses are comparable as well. However, these results do not reflect the quality of the obtained results. Future work may address this issue by applying a higher number of dimensions M, order p and different correlation lengths c.

The standard deviation of the non-linear SSFEM using a polynomial basis of $P = 45$ is noticeably higher in comparison with those obtained from the reference solutions. This may be attributed to the relatively large correlation length of $c = 10$ cm and the small dimension of $M = 8$. The standard deviation for the polynomial basis $P = 91$ and $P = 153$ shows the expected deceasing value where, due to the higher dimension M, differences of spatial distribution are clearly visible. Besides of the higher dimension is the smaller correlation length an indicator for these spatial characteristics. The highest effect of the influence of the correlation length is observed in the coupled SPRM-MCS model, where the small standard deviation results from the relatively small correlation length of $c = 1$ cm. All results, which are characterized by random fields, show significant influences of the standard deviation outside the stress zones, whereas the LHS show almost exclusively influences of the standard deviation within the stress zone. This phenomena may be attributed to the spatial characteristics of the material parameters, represented by random fields.

With regard to the KLE, a direct correlation exists between the dimension M of the KLE and the correlation length c. To be more specific, an increasing dimension M combined with a decreasing correlation length c represents the standard deviation more accurately. This is consistent with the observations in subsection 6.3.2 and section 8.6, where it has been noted that a small correlation length is closely related to a slower decay of the eigenvalues. This means, that a higher sub-dimension M' and a smaller correlation length c captures the characteristics of the random field more accurately than a smaller M' combined with a higher c. Moreover, the polynomial order p is another parameter which has an influence on the accuracy of the approximation of the system response, but the non-linearities in this example are small and the applied polynomial order of $p = 2$ seems to be sufficient. However, parameter

(a) $\mathbb{E}[\sigma_{\mathrm{vM}}]$ in kN/cm^2 with $M = 8$ and $p = 2$

(b) $\sigma(\sigma_{\mathrm{vM}})$ in kN/cm^2 with $M = 8$ and $p = 2$

(c) $\mathbb{E}[\sigma_{\mathrm{vM}}]$ in kN/cm^2 using $M = 12$ and $p = 2$

(d) $\sigma(\sigma_{\mathrm{vM}})$ in kN/cm^2 using $M = 12$ and $p = 2$

(e) $\mathbb{E}[\sigma_{\mathrm{vM}}]$ in kN/cm^2 applying $M = 16$ and $p = 2$

(f) $\sigma(\sigma_{\mathrm{vM}})$ in kN/cm^2 applying $M = 16$ and $p = 2$

Figure 9.4.: Left: Mean value $\mathbb{E}[\sigma_{\mathrm{vM}}]$ of the von Mises stress. Right: Standard deviation $\sigma(\sigma_{\mathrm{vM}})$ of the von Mises stress applying the non-linear SSFEM.

(a) $\mathbb{E}[\sigma_{vM}]$ in kN/cm^2 using the SPRM-MCS **(b)** $\sigma(\sigma_{vM})$ in kN/cm^2 using the SPRM-MCS

Figure 9.5.: Left: Mean value $\mathbb{E}_{\sigma_{vM}}$ of the vM stress. Right: Standard deviation $\sigma_{\sigma_{vM}}$ of the vM stress. The results are obtained utilizing the coupled SPRM-MCS.

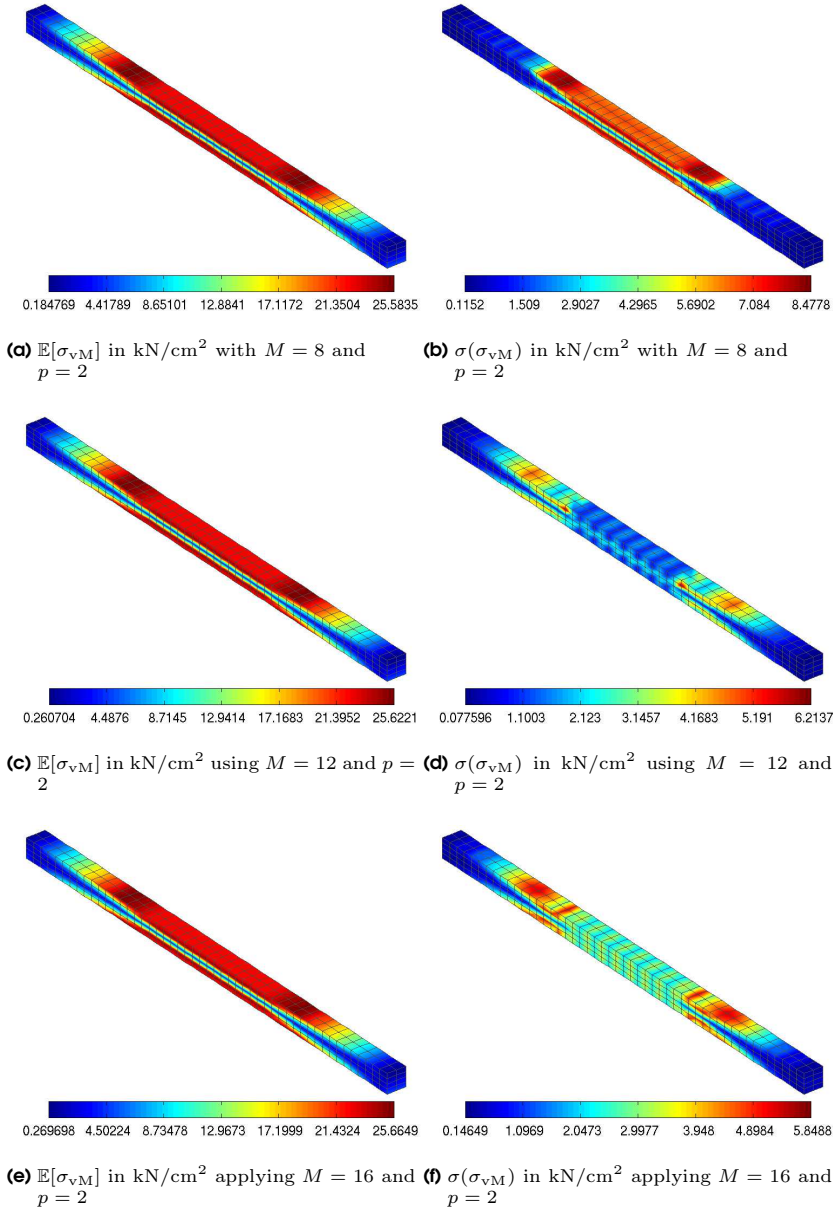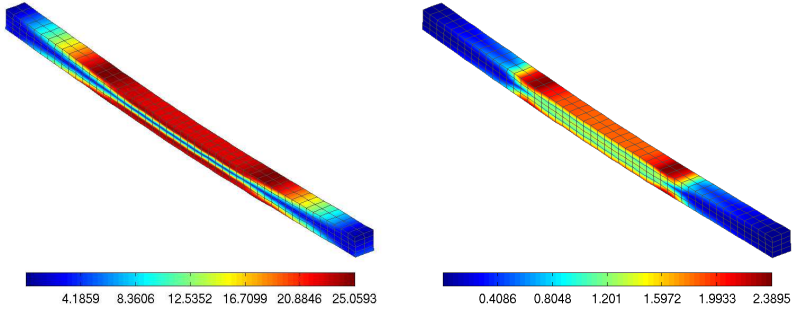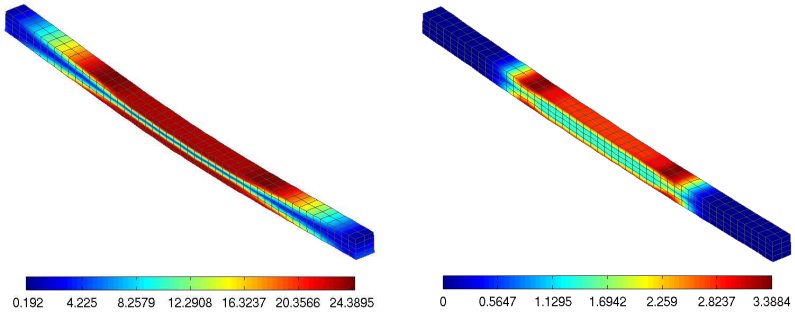**(a)** $\mathbb{E}[\sigma_{vM}]$ in kN/cm^2 using the LHS **(b)** $\sigma(\sigma_{vM})$ in kN/cm^2 using the LHS

Figure 9.6.: Left: Mean value $\mathbb{E}[\sigma_{vM}]$ of the vM stress. Right: Standard deviation $\sigma(\sigma_{vM})$ of the vM stress. The results are obtained using the LHS.

studies with various M and p as well as c should be subject in future research in the context of non-linear analysis. Special emphasis should be taken on effective numerical strategies for handling the rapidly growing basis P by an appropriate choice of M and p, where a reference to efficient approximation methods was already given in subsection 8.2.4.

Another remark should be given on the applied linear shape functions where the polynomial degree could be too small, especially when a large number of KLE dimensions is applied to characterize the material fluctuations. This means, that a large dimension M results in high frequencies of the small eigenvalues, which can lead to noticeable inaccuracies since small eigenvalues might not be mapped with linear shape functions good enough. Also here, additional investigations, with higher order shape functions, should be taken into account in future work.

In general, the investigation in this example shows that the developed approach approximates the first two statistical moments of the vM stress quiet well compared with those obtained from the coupled SPRM-MCS and LHS. In addition, the method, despite the relatively large standard deviation of 10% per each material parameter, is numerically robust.

In engineering structures, for example, bridges the structural safety parameter is an important value. For the analysis of the structural safety the knowledge of the maximal stress is necessary and the identification of these values (areas where the maximal stress occurs) is important, because these regions of the structure may failed first. Therefore, in Figs. 9.7 to 9.9 the areas are highlighted where the stress exceeds a predetermined stress limit. The values of the vM stress limits are chosen with respect to the value of the yield stress σ_y, i.e., $\mathcal{P}(\mathbb{E}[\sigma_{\mathrm{vM}}]) < 20.5\,\mathrm{kN/cm}^2$ and $\mathcal{P}(\mathbb{E}[\sigma_{\mathrm{vM}}]) < 23.5\,\mathrm{kN/cm}^2$. The blue elements mark the regions where the yield stress is exceeded and the red ones are the elements that are within the permissible yield stress. The stress limits obtained from the non-linear SSFEM (shown in Fig. 9.7) are comparable to those obtained from the SPRM-MCS and LHS, which are displayed in Figs. 9.8 and 9.9.

(a) $\mathcal{P}(\mathbb{E}[\sigma_{\mathrm{vM}}]) < 20.5$ kN/cm² applying $M = 8$ and $p = 2$

(b) $\mathcal{P}(\mathbb{E}[\sigma_{\mathrm{vM}}]) < 23.5$ kN/cm² applying $M = 8$ and $p = 2$

(c) $\mathcal{P}(\mathbb{E}[\sigma_{\mathrm{vM}}]) < 20.5$ kN/cm² for $M = 12$ and $p = 2$

(d) $\mathcal{P}(\mathbb{E}[\sigma_{\mathrm{vM}}]) < 23.5$ kN/cm² for $M = 12$ and $p = 2$

(e) $\mathcal{P}(\mathbb{E}[\sigma_{\mathrm{vM}}]) < 20.5$ kN/cm² using $M = 16$ and $p = 2$

(f) $\mathcal{P}(\mathbb{E}[\sigma_{\mathrm{vM}}]) < 23.5$ kN/cm² for $M = 16$ and $p = 2$
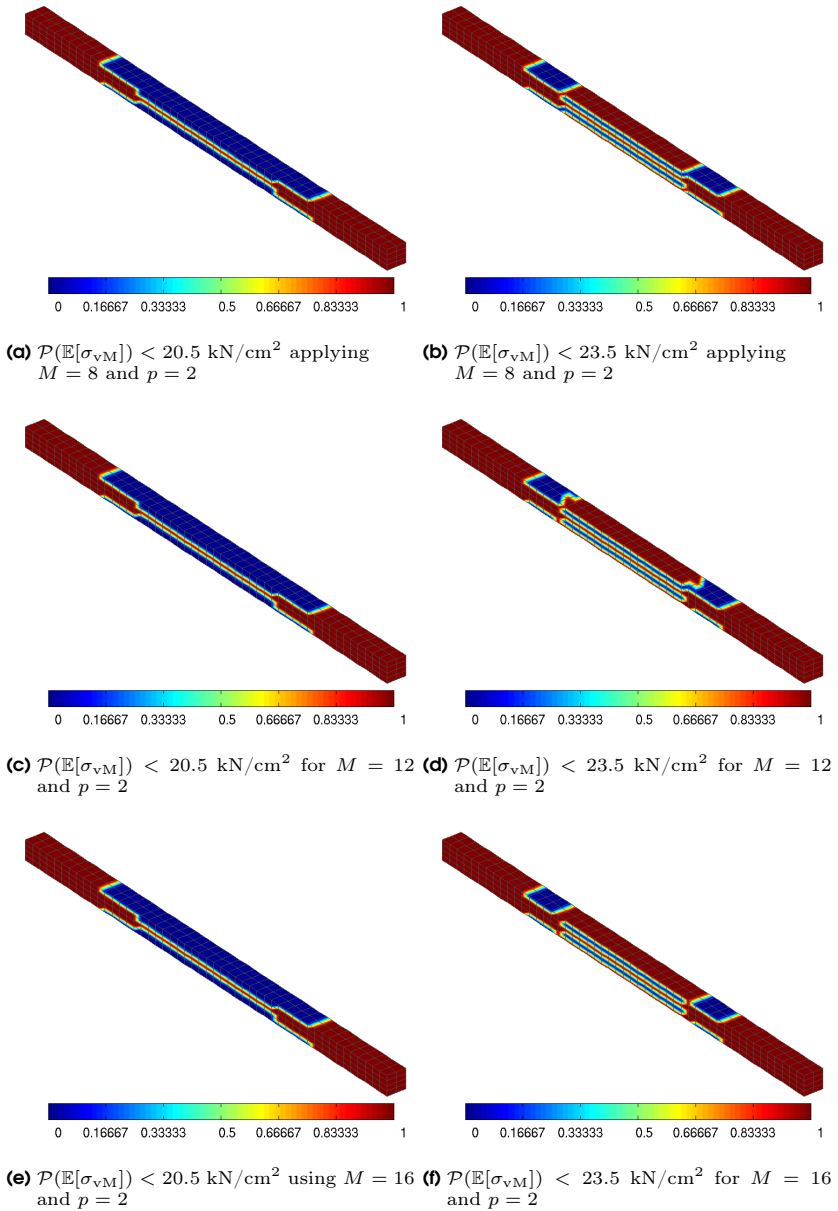
Figure 9.7.: Limits of the mean value of the von Mises stress $\mathbb{E}_{\sigma_{\mathrm{vM}}}$ in the case of the non-linear SSFEM.

(a) $\mathcal{P}(\mathbb{E}[\sigma_{vM}]) < 20.5 \text{ kN/cm}^2$

(b) $\mathcal{P}(\mathbb{E}[\sigma_{vM}]) < 23.5 \text{ kN/cm}^2$

Figure 9.8.: Limits of the mean value of the von Mises stress $\mathbb{E}_{\sigma_{vM}}$ utilizing the coupled SPRM-MCS.

(a) $\mathcal{P}(\mathbb{E}[\sigma_{vM}]) < 20.5 \text{ kN/cm}^2$
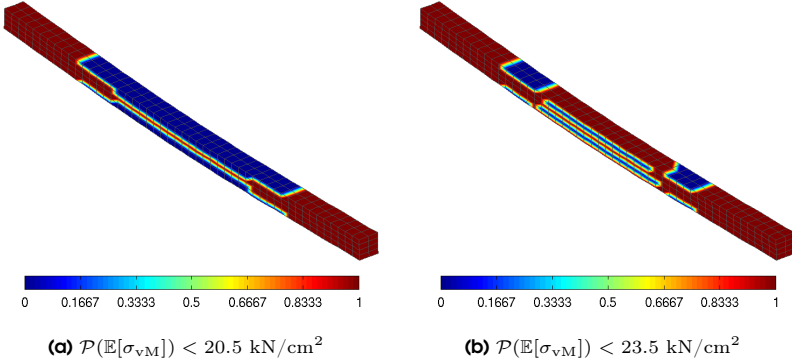
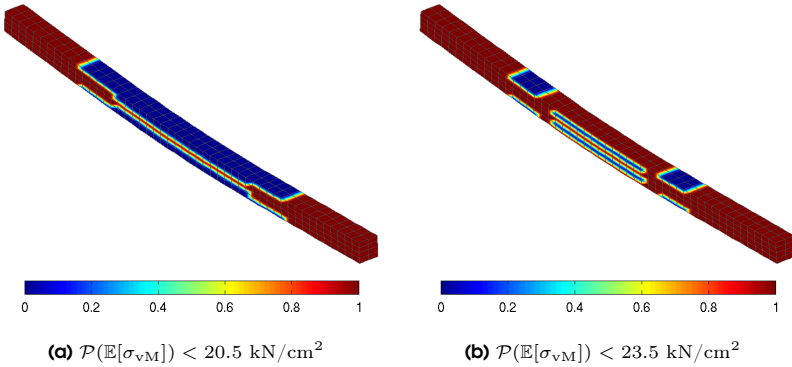**(b)** $\mathcal{P}(\mathbb{E}[\sigma_{vM}]) < 23.5 \text{ kN/cm}^2$

Figure 9.9.: Limits of the mean value of the von Mises stress $\mathbb{E}_{\sigma_{vM}}$ using the LHS.

9.7.2. Three-Dimensional Plate with a Hole

In the second example, a plate with a hole at the centre and the size $\mathcal{D} = 10\,\text{cm} \times 10\,\text{cm} \times 1\,\text{cm}$ is investigated. The dimensions and loads together with the FE model of the plate are shown in Fig. 9.10 (**a**). The discretized FE model, illustrated in Figs. 9.10 (**b**) and (**c**), consists of 140 elements with 1008 degrees of freedom. The displacements within the elements are approximated with linear shape functions. As stochastic material parameters the Young's modulus $E(\theta)$, yield stress $\sigma_y(\theta)$, isotropic hardening $\mathbb{H}_{\text{iso}}$ and the kinematic hardening $\mathbb{H}_{\text{kin}}$ are chosen. The type of distribution, mean and standard deviation are reported in Tab. 9.4. The material parameters

Table 9.4.: Random material parameters for the plate with a hole.

| Material Parameter	Distribution	Mean μ	Standard Deviation σ
$E(\theta)$	Gaussian	21.000 kN/cm^2	10%
$\sigma_y(\theta)$	Gaussian	23.5 kN/cm^2	10%
$\mathbb{H}_{\text{iso}}$	Gaussian	100 kN/cm^2	10%
$\mathbb{H}_{\text{kin}}$	Gaussian	100 kN/cm^2	10%

are spatially discretized with the KLE and the SPRM. The characterization of the material parameters, by the KLE, is done using the covariance function defined in equation (6.30), whereas (due to the geometry) the Fredholm integral has to be solved numerically. The applied covariance function is similar to the one used in the first example and has been defined in equation (6.30). When applying the SPRM, the random field $H_S(\cdot)$ is discretized ($H_S \longrightarrow \hat{H}_S$) n-times by using equation (6.104), where the power spectral density function $S_{\hat{H}_S \hat{H}_S}$, defined in equation (6.127), is applied.

In terms of the developed non-linear SSFEM, the resulting polynomial basis P of the PCE consists of the dimension M of the KLE and the polynomial order p of PC. Any random variable, such as the system response at an arbitrary node, can be approximated by the expression defined in equation (9.58). The approximation of the system response $\mathbf{u}(\theta)$, at an arbitrary node, is done by using the polynomial chaos orders $p = 2$ and $p = 3$. The material parameters are characterized by various dimensions M and correlation lengths c, where c is assumed to be isotropic in all directions. All parameters for the generation of a random field, applying the KLE, are summarized in Tab. 9.5, where the sub-dimension M' defines the dimension of each material parameter as already explained in the previous example.

Table 9.5.: Input parameters for the spatial characterization of the material parameters when applying the KLE.

Dimension M	Sub-Dimension M'	Order p	Correlation Length c in cm
8	2	2	10
8	2	3	10
12	3	2	5
16	4	2	5

In case of the SPRM as spatial discretization technique and a MCS as sample method,

(a) Dimensions of the plate.
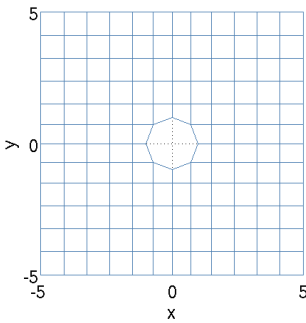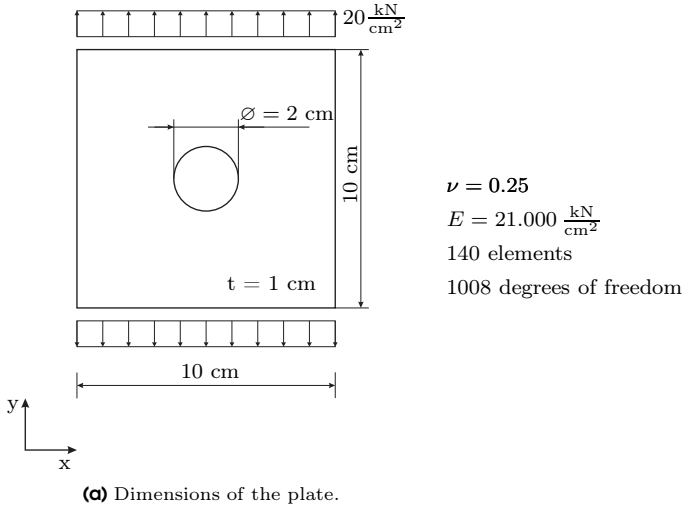
(b) FE model of the plate.
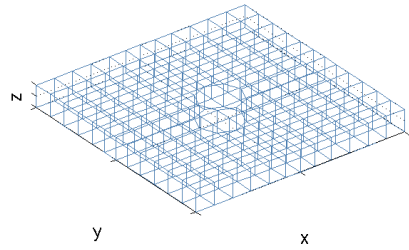
(c) 3D view of the discretized plate.

Figure 9.10.: Elastic-plastic example of the plate with a hole at the center.

the system response $\mathbf{u}(\theta)$ of an arbitrary node is evaluated according to equation (9.59). As in the first example, a sample size of $n_{\text{SPRM}} = 5000$ is used when applying the coupled SPRM-MCS. In this approach a correlation length of $c = 1$ cm is used. In case of a LHS, the response statistics are computed in the same manner as in the coupled SPRM-MCS, with a sample size of $n_{\text{LHS}} = 10000$. Both methods, the coupled SPRM-MCS and the LHS, are used as reference solutions where the obtained results are compared with those obtained from the proposed non-linear SSFEM approach.

The quantity of interest is the von Mises (vM) stress σ_{vM} where the approximation of the mean value $\mathbb{E}[\sigma_{\text{vM}}]$ and the standard deviation $\sigma(\sigma_{\text{vM}})$ are investigated.

Discussion of the Results

The resulting mean of the vM stresses and the standard deviation for the non-linear SSFEM are shown in Figs. 9.11 and 9.12. The reference solutions of the coupled SPRM-MCS and LHS are displayed in Fig. 9.13. Comparing these figures, it can be clearly seen that the mean value of the vM stress is quite similar. From the contour plots of the developed approach in Fig 9.11 it is obvious that the vM stresses are identical. This implies that the spatial variability of the material properties, in terms of the dimension M of the KLE, has a larger influence on the system response than the order p of the PCE. On the other hand, the approximated mean values in Fig. 9.11 are nearly identical to those one displayed in Fig. 9.12, where, in addition to larger dimensions M ($M = 12$ and $M = 16$), the correlation length has been reduced to $c = 5$ cm. Form this result it may be deduced that the correlation length c has no remarkable influence on the approximation of the mean value of the vM stress.

In contrast, it appears that the proposed approach underestimates the standard deviation in comparison to the reference solutions. A declining trend is observable when comparing the standard deviations in Figs. 9.11 and 9.12. Furthermore, the distribution of the standard deviations in these figures show some asymmetric areas, which may be attributed to the numerical solution of the Fredholm integral. To be more specific, from the results in 9.11 it is quite obvious that the applied dimension M of the KLE is to small to approximate the Fredholm integral satisfactory. The results in Fig. 9.12 show that, with increasing M, the approximation of random field is much more accurate. With regard to the obtained results of the standard deviation suggests that the dimension of M must be chosen large enough, especially when the random field is realized in a numerical manner. However, currently no statement can be made with regard to the influence of the spatial variability when expanding the dimension M of the KLE. In addition, further possibilities for an inaccurate approximation of the random field is the relatively coarse discretization of the plate and the resulting interpolation errors. In this context more investigations are needed and should be done in future work. Moreover, the results indicate that the system response is not that sensitive to the order p of the polynomial chaos when comparing the results for $p = 2$ with those obtained for $p = 3$. Under this loading conditions and the resulting small non-linearities, it seems that a polynomial order of $p = 2$ is sufficient to get a satisfactory accuracy of the system response.

A further observation is the relatively small spatial variability of the standard deviation of a LHS in comparison to the coupled SPRM-MCS and to the developed non-linear approach. This can be understood by the fact that the spatial variability of the coupled SPRM-MCS and the non-linear SSFEM has a larger influence on the system behaviour than a set of random variables as applied in a LHS. Basically, it can

be concluded that the non-linear SSFEM and the coupled SPRM-MCS underestimate the standard deviation of the LHS, which is consistent with that of the example in section 8.6.

As already in the previous example of the four-point bending beam the areas with the maximal vM stresses are evaluated. Therefore, in Figs. 9.14 to 9.16 theses regions are shown where the predetermined stress limit exceeded. The values of the vM stress limits are also set here to $\mathcal{P}(\mathbb{E}[\sigma_{vM}]) < 20.5\,\text{kN/cm}^2$ and $\mathcal{P}(\mathbb{E}[\sigma_{vM}]) < 23.5\,\text{kN/cm}^2$. The blue elements show the areas where the yield stress is exceeded and the red ones are the elements which are within the permissible yield stress. The trends of the stress distribution are quiet similar for all methods. The stress limits obtained from the non-linear SSFEM shown in Figs. 9.14 and 9.15 and those obtained from SPRM-MCS and LHS are displayed in Fig. 9.16. The identical stress distributions in Figs. 9.14 and 9.15 follows from the nearly identical mean values of the vM stresses, cf. Figs. 9.11 and 9.12. In contrast, it appears that the non-linear SSFEM and the coupled SPRM-MCS overestimate the stress region compared to those one obtained from a LHS, which is likewise obvious when the computed vM stresses are compared, cf. Figs. 9.11 to 9.13.

(a) $\mathbb{E}[\sigma_{\mathrm{vM}}]$ in kN/cm^2 using $M = 8$ and $p = 2$

(b) $\sigma(\sigma_{\mathrm{vM}})$ in kN/cm^2 using $M = 8$ and $p = 2$

(c) $\mathbb{E}[\sigma_{\mathrm{vM}}]$ in kN/cm^2 applying $M = 8$ and $p = 3$

(d) $\sigma(\sigma_{\mathrm{vM}})$ in kN/cm^2 with $M = 8$ and $p = 3$

Figure 9.11.: Left: Mean value $\mathbb{E}[\sigma_{\mathrm{vM}}]$ of the von Mises stress. Right: Standard deviation $\sigma(\sigma_{\mathrm{vM}})$ of the von Mises stress utilizing the non-linear SSFEM and the bases $P = 45$ and $P = 165$.

(a) $\mathbb{E}[\sigma_{\mathrm{vM}}]$ in kN/cm² applying $M = 12$ and $p = 2$

(b) $\sigma(\sigma_{\mathrm{vM}})$ in kN/cm² using $M = 12$ and $p = 2$

(c) $\mathbb{E}[\sigma_{\mathrm{vM}}]$ in kN/cm² using $M = 16$ and $p = 2$

(d) $\sigma(\sigma_{\mathrm{vM}})$ in kN/cm² using $M = 16$ and $p = 2$
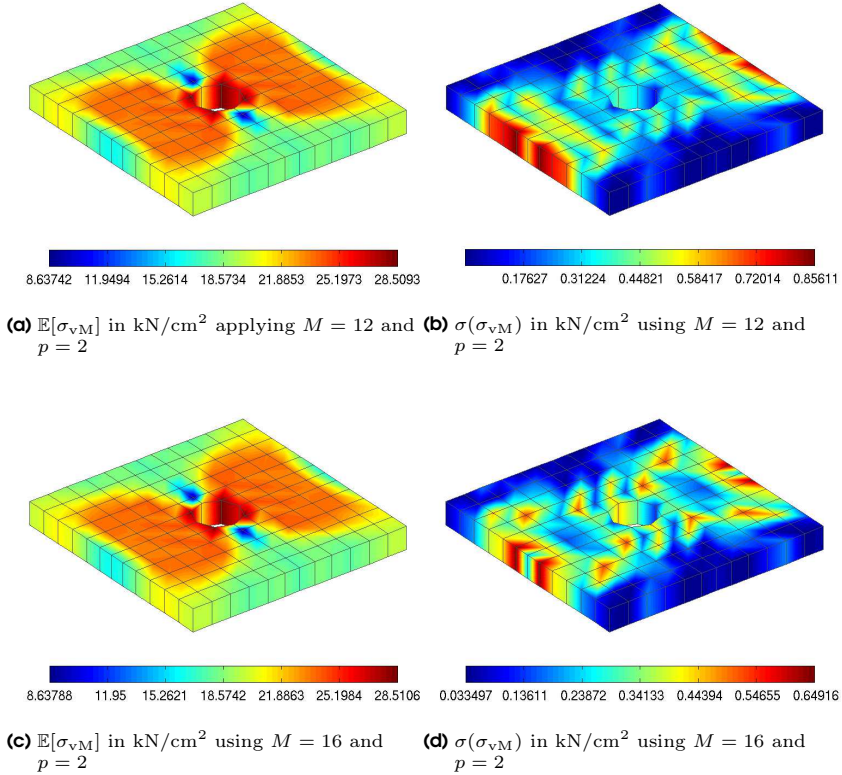
Figure 9.12.: Left: Mean value $\mathbb{E}[\sigma_{\mathrm{vM}}]$ of the von Mises stress. Right: Standard deviation $\sigma(\sigma_{\mathrm{vM}})$ of the von Mises stress using the non-linear SSFEM and the bases $P = 91$ and $P = 153$.

(a) $\mathbb{E}[\sigma_{\mathrm{vM}}]$ in kN/cm^2 using the SPRM-MCS **(b)** $\sigma(\sigma_{\mathrm{vM}})$ in kN/cm^2 with the SPRM-MCS

(c) $\mathbb{E}[\sigma_{\mathrm{vM}}]$ in kN/cm^2 applying the LHS **(d)** $\sigma(\sigma_{\mathrm{vM}})$ in kN/cm^2 with a LHS
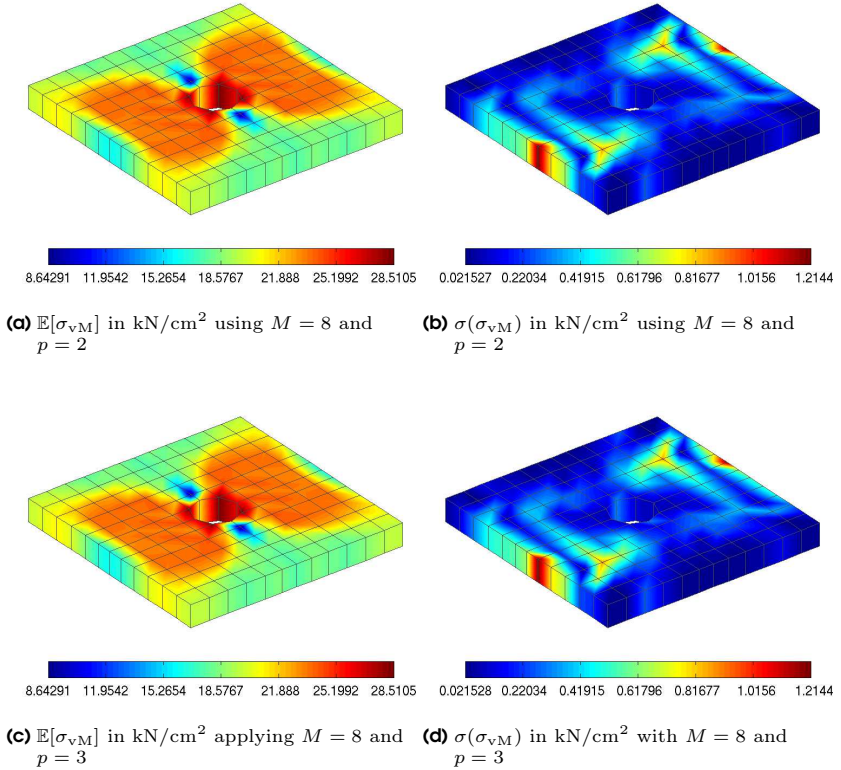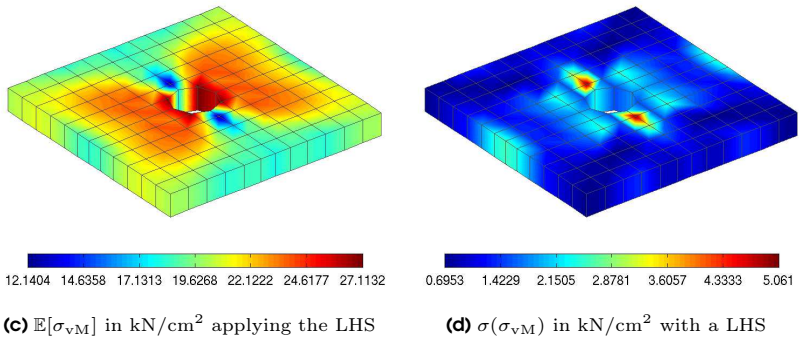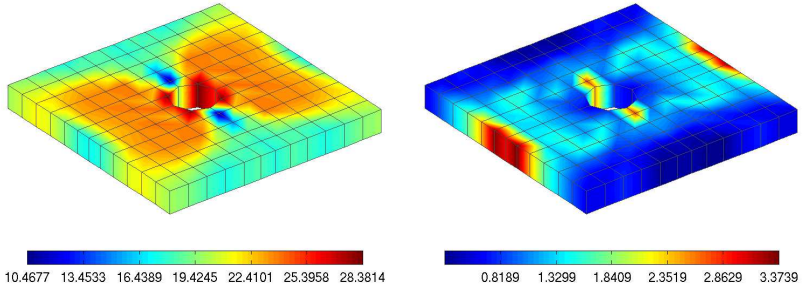
Figure 9.13.: Left: Mean value $\mathbb{E}[\sigma_{\mathrm{vM}}]$ of the vM stress. Right: Standard deviation $\sigma(\sigma_{\mathrm{vM}})$ of the vM stress utilizing the SPRM-MCS (**a**) and (**b**) as well as a LHS (**c**) and (**d**).

(a) $\mathcal{P}(\mathbb{E}[\sigma_{\mathrm{vM}}]) < 20.5$ kN/cm^2 with $M = 8$ and $p = 2$

(b) $\mathcal{P}(\mathbb{E}[\sigma_{\mathrm{vM}}]) < 23.5$ kN/cm^2 with $M = 8$ and $p = 2$

(c) $\mathcal{P}(\mathbb{E}[\sigma_{\mathrm{vM}}]) < 20.5$ kN/cm^2 for $M = 8$ and $p = 3$

(d) $\mathcal{P}(\mathbb{E}[\sigma_{\mathrm{vM}}]) < 23.5$ kN/cm^2 for $M = 8$ and $p = 3$
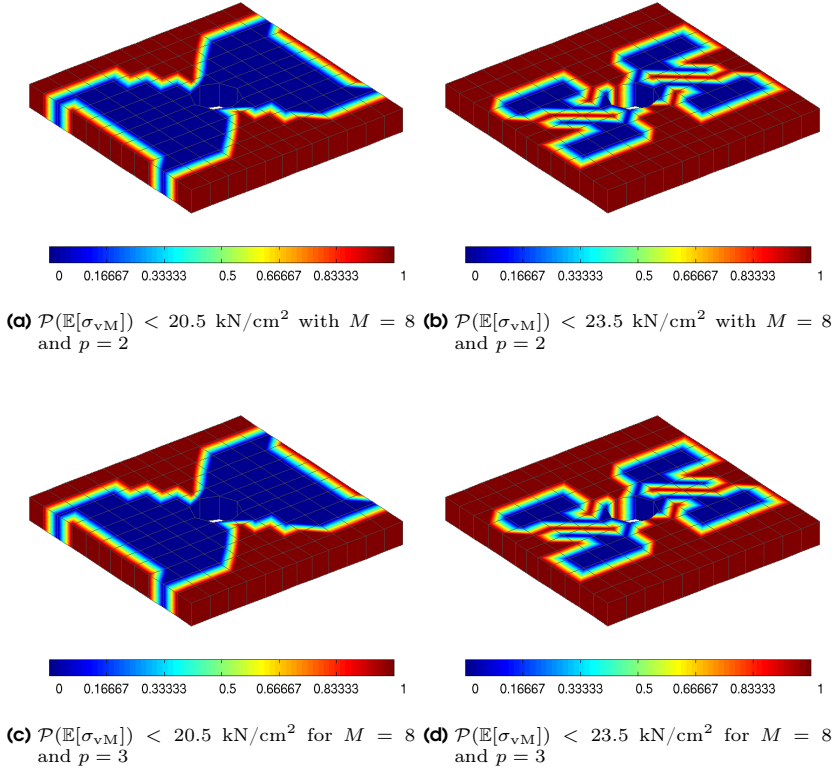
Figure 9.14.: Limits of the mean value of the VON MISES stress $\mathbb{E}[\sigma_{\mathrm{vM}}]$ utilizing the non-linear SSFEM.

(a) $\mathcal{P}(\mathbb{E}[\sigma_{vM}]) < 20.5$ kN/cm^2 utilizing $M = 12$ and $p = 2$

(b) $\mathcal{P}(\mathbb{E}[\sigma_{vM}]) < 23.5$ kN/cm^2 utilizing $M = 12$ and $p = 2$

(c) $\mathcal{P}(\mathbb{E}[\sigma_{vM}]) < 20.5$ kN/cm^2 applying $M = 16$ and $p = 2$

(d) $\mathcal{P}(\mathbb{E}[\sigma_{vM}]) < 23.5$ kN/cm^2 applying $M = 16$ and $p = 2$
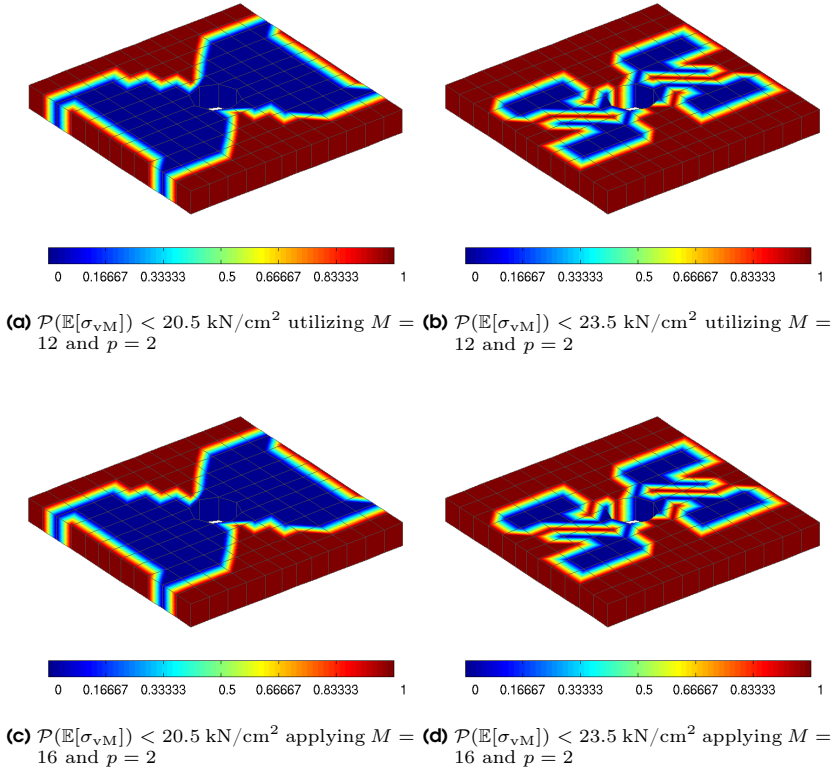
Figure 9.15.: Limits of the mean value of the von Mises stress $\mathbb{E}[\sigma_{vM}]$ utilizing the non-linear SSFEM.

(a) $\mathbb{E}[\sigma_{\mathrm{vM}}] < 20.5 \text{ kN/cm}^2$

(b) $\mathbb{E}[\sigma_{\mathrm{vM}}] < 23.5 \text{ kN/cm}^2$

(c) $\mathbb{E}[\sigma_{\mathrm{vM}}] < 20.5 \text{ kN/cm}^2$

(d) $\mathbb{E}[\sigma_{\mathrm{vM}}] < 23.5 \text{ kN/cm}^2$

Figure 9.16.: Limits of the mean value of the von Mises stress $\mathbb{E}[\sigma_{\mathrm{vM}}]$ for SPRM-MCS (**a**) and (**b**) as well as a LHS (**c**) and (**d**).
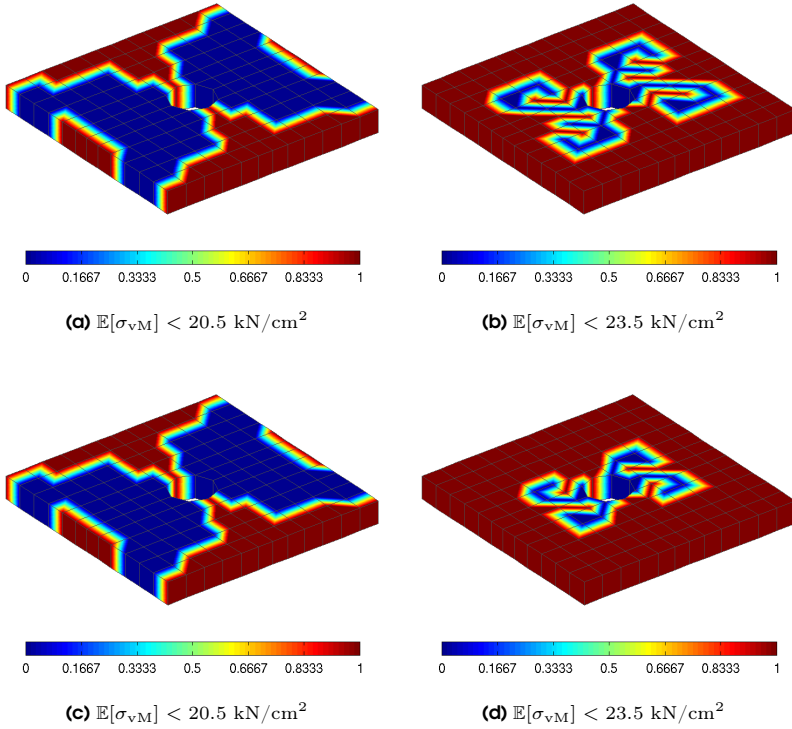
9.8. Summary and Concluding Remarks

The aim of this chapter was the development of an approach to capture stochastic material properties in an elastic-plastic finite element simulation. The developed formulation relies on the classical theory of deterministic J_2 plasticity, which has been extended for the computation of stochastic elastic-plastic material behaviour. The proposed formulation is an intrusive approach, where the KLE is used for the characterization of the random material parameters and the PCE is utilized for the approximation of the system response. The regression method, which was applied for the calculation of the norm of the stochastic back-stress tensor $\hat{\boldsymbol{\eta}}(\theta)$ in the stochastic radial return mapping scheme. An alternative for the computation of the norm is the PCA, which was applied in Rosić [2013]. However, in this work the regression method was preferred, because it needs to be evaluated only once and for all during the simulation process. This has the attractiveness that it can be realized in a pre-processing step. The results of the regression method are comparable with those obtained with PCA assuming that the number of samples[6] is large enough. In this work, the sample size of the regression method is set to $n_{\mathrm{col}} = 100000$. In case of the coupled SPRM-MCS method, a sample size of $n_{\mathrm{SPRM}} = 5000$ is used and for the LHS a sample size of $n_{\mathrm{LHS}} = 10000$ is applied.

As already known from the linear SSFEM, presented in chapter 8, the necessarily high polynomial basis P for the accurate approximation of the system response is the major difficulty. This aspect has to be taken into account especially in non-linear analysis, because for the accurate approximation of the system response, a relatively high basis P is necessary. With this respect, two remarks should be given with regard to the polynomial dimension P and an accordingly accurate approximation. The first refers to the dimension M of the KLE, which should be chose with respect to the material properties. More precisely, if the material properties have high fluctuations, a larger M should be set, while for small fluctuations few dimensions M are sufficient. The second remark relates to the polynomial order p. A higher order should be used if a strongly non-linear system response is expected, while a lower polynomial order p seems to be sufficient if it is expected that the system response has less non-linearities.

The numerical examples in this chapter are performed with a relatively small polynomial basis P. The results allow the assumption that the basis P is not large enough to make final assessment of the accuracy of the approximated system response. However, by applying a dimension of $M = 12$ and a polynomial order of $p = 4$ leads to a polynomial basis $P = 495$. Attempt to apply this basis on the numerical examples shows that a result cannot be obtained in a reasonable time. Nonetheless, the numerical results show that the developed method approximates the first two moments of the vM stresses quite well comparing with the non-intrusive coupled SPRM-MCS and LHS. The highest basis applied in the examples was $P = 165$. Nevertheless, to make additional statements about the influence of the parameters M of the KLE, order p of PC and the correlation length c further investigations are necessary in the future.

The statistics of the material parameters for the numerical examples have been chosen, because such material data is rare. For some materials various parameters are reported in Lemaitre and Chaboche [1990] or Shackelford [2000]. However, no statistical informations, such as the probability distribution or standard deviation of the

---

[6]The sample size is dependent of the mechanical problem. This means, whether it is elastic, non-linear with small deformations or non-linear with large deformations, the sample size needs to be accordingly adjusted. The number of samples n_{col} should be large if a large (non-linear) system response is expected, which also applies to the order p of PC.

material parameters are listed there. In engineering applications, this information is of special interest for the evaluation of the structural system. One possibility to identify the statistics of the material parameters could be the Bayesian theorem. It determines the probability of the occurrence of an event of B under the condition that an event A has occurred already. An application could be that the material parameters from a known system response are determined. Some more details about this approach will be given in the outlook of the next chapter.

All investigations in the presented examples have been performed with a fixed FE mesh. Besides, the investigation of the stochastic convergence $\mathcal{S}^P \to \mathcal{S}$ by increasing P, the deterministic convergence $\mathcal{V}^h \to \mathcal{V}$, by applying a finer FE discretization should be also investigated in further studies, where particular attention should be placed on a local mesh refinement.

10. Summary and Outlook

The application of stochastic finite element methods has been rapidly developed in the last decade. Various techniques such as *sampling based methods*, *perturbation methods*, *moment equations* (FOKKER-PLANCK), *operator methods* (e.g., the weighted integral method) or GALERKIN methods (intrusive/non-intrusive) were continuously developed. The aim of this thesis was the formulation of a new GALERKIN-based method for the computation of non-linear equations applying random material parameters with regard on J_2 elastic-plastic material behaviour. As reference solutions, the coupled SPRM-MCS method and the LHS are applied, where the results of the developed approach are verified with. The presented non-linear approach is tested on two numerical examples with a subsequent discussion of the results.

10.1. Summary

The present thesis addresses to the simulation of elastic-plastic material behaviour where it is assumed that the probability distributions of the input parameters are a priori known. The classical well-known J_2 elastio-plasticity, with small deformations, is used as basis formulation. The deterministic formulation has been subsequently extended to capture random fluctuations of the material parameters. The random material parameters are characterized by random fields for which the KARHUNEN-LOÈVE Expansion and the Spectral Representation Method are utilized. The former method has been applied with the polynomial chaos, which is well known as Spectral Stochastic Finite Element Method. The widespread linear approach of this method has been extended to a novel non-linear spectral stochastic finite element method (non-linear SSFEM). The latter method has been coupled with the Monte Carlo Sampling, referred to as coupled SPRM-MCS, to get a reference solution in order to compare the results with those obtained from the developed approach.

In the proposed non-linear SSFEM formulation, the stochastic elastic-plastic problem is projected in a GALERKIN manner, similar to the one in the classical finite element formulation, onto the polynomial basis P of the discretized space. The stochastic closest point projection has been realized in a combined algebraic-sampling manner to compute the relevant quantities in the stochastic radial return scheme. This is achieved by applying the polynomial chaos algebra and the regression method. The numerical realization of this novel formulation is straightforward. The developed approach seems to be quite effective and robust but it requires a reformulation of the existing program code (intrusive formulation). Due to the deterministic character of the coupled SPRM-MCS as well as the LHS, the computer code for the non-linear calculation needs no reformulation and can be treated in a black-box manner (non-intrusive formulation).

The presented studies show that the developed method approximates the first two moments of the vM stress quite well comparing with the coupled SPRM-MCS as well as with LHS. However, to make further statements about the influence of the parameters, such as the dimension M of the KLE, order p of PC or the correlation length c, further investigations are necessary.

A further emphasis of this work was to identify the characteristics of the employed methods that makes it more attractive than the other. The developed non-linear approach is an intrusive method that represents the random quantity with a set of coefficients in a suitable basis and this basis contains the complete statistics. Here, only one computer run is necessary to receive the stochastic system response. However, the implementation in a computer code is cumbersome, because the deterministic code needs a reformulation to handle the expansion coefficients and the corresponding coupled system of equations. In contrast, the applied coupled SPRM-MCS and the LHS are non-intrusive methods, which allow the analyst to compute the coefficients by a series of runs of the mechanical model at hand. Such methods may be launched in a fully parallel computational environment. The post-processing of the results is straight forward and the implementation, compared to the intrusive method, is relative simple, because the existing computer code needs no reformulation.

With respect to the computational cost and accuracy, it is difficult to say whether the developed non-linear SSFEM, the coupled SPRM-MCS or the standard MCS is the best method for applications. In view of industrial practice, Augustin et al. [2008] remarks that the use of the SSFEM is the only reasonable method, because the standard methods are unfeasible with respect to the computational costs. This observation has also been done in the investigations in this work, where the non-linear SSFEM leads to accurate results in less computation time. However, as mentioned several times in this thesis, the computation time depends strongly on the number of stochastic random input parameters and the properties of the problem under consideration. Furthermore, the SSFEM (no matter if linear or non-linear) is only applicable when there is an access to the computer code, because of the necessary reformulation of the code.

In view of the applied methods in this thesis, the method should be used in case where the most information about the stochastic parameters is available. Such information could be:

- How many random input parameters are there in the system?
- Which distribution does the input parameters have?
- Is there any information regarding the correlation length of the interesting parameters?
- Is a covariance function available?

From this listing the following conclusion may be drawn. The standard MCS should be preferred if nothing but the probability distributions of the input parameters are known. Furthermore, the MCS should be the first choice if there are a lot of random input parameters (high dimension) in the system. Moreover, due to its simple handling and convergence properties, the MCS method is a reasonable reference solution. On the other hand, if the number of random input parameters is moderate and information on the correlation length and the covariance function is available, the presented non-linear SSFEM seems to be the better choice, because the computation of the system response is less time consuming.

10.2. Outlook

As verified in the numerical examples, the developed non-linear SSFEM works well and leads to an accurate approximation of the system response. However, a few points are

identified, which can be further improved to get a (hopefully) more accurate solution within less calculation time. The following paragraphs are dealing with some points and ideas are given to eliminate these weaknesses where possible.

As pointed out in subsections 6.3.2 and 6.3.3, the computational costs for the numerical solution of the eigenvalue problem increase drastically with increasing degrees of freedom of the FE system. When a coarse mesh is used the error of the numerical eigenvalue solution grows with increasing eigenvalue and no accurate solution can be expected. To achieve a possible improvement here, two opportunities will be shown. An option could be a local mesh refinement where only those regions are refined which are of particular interest. These are the areas where high strains, stresses or displacements are expected. Moreover, the calculation of the eigenvalues is a very time consuming process and the application of effective eigenvalue solvers is reasonable. In this regard, Le Maître and Knio [2010] propose the application of multi-pole expansions. This area seems to be of particular interest of further research.

To increase the effectiveness of the random field representation using the spectral representation method seems to be less complicated, because with rather simple methods a notable improvement of the computational time and approximation quality can be reached. Examples could be the application of a more precise sampling method for the evaluation of the random phase angle than a standard Latin Hypercube sampling. Some investigations with different sampling techniques has been already done in section 6.4. Moreover, the computation of the random fields as well as the system response can be realized in a completely parallel code, which is time efficient.

In this thesis GAUSSIAN distributions with corresponding Hermite polynomials are exclusively used. However, the random input parameters are consistently non-GAUSSIAN distributed. To include various distributions beyond the normal and log-normal distribution, the generalized polynomial chaos or Askey-scheme is a reasonable possibility. A brief introduction to this subject has been given in subsection 7.2.3. Besides this generalization, further research could go in the direction of generalization in terms of non-orthogonal polynomials or the numerical construction of unknown polynomials. For example, if no distribution for the characterization of the system response is available.

Further Research Subjects

The discussion in this section up to this point has involved possible improvements/extensions with respect to the applied methods in this thesis. In this paragraph some related topics are discussed, which goes beyond the present work. This includes the following topics:

- Random geometry, random excitations, non-linear hardening or other plasticity models, such as the DRUCKER PRAGER model and

- the parameter estimation via the BAYESIAN theorem.

Throughout this thesis it has been exclusively assumed that the *geometry* and the *external forces* of the structural systems are deterministic. However, in practice it is almost impossible to accurately characterize neither the geometry of the structural system nor the forces (e.g., seismic excitations, waves, wind, snow) acting on the structural system. An approach for the characterization of the random domain has been proposed by Xiu and Tartakovsky [2006]. The idea of *random excitations/loads* goes back a long way, see, e.g., Rackwitz and Flessler [1978], and is still not fully

reflected in structural systems. Indeed, deterministic excitations is a widespread and often reasonable assumption. In some engineering systems the external forces are not sufficiently well characterized by deterministic assumptions, such as wave or snow loads. To generalize the proposed non-linear SSFEM stochastic loading conditions may be taken into account.

For the sake of simplicity, the J_2 flow theory with *linear hardening* parameters has been used in this thesis. This formulation is widely utilized for the representation of the material behaviour of steel. A field where stochastic modelling of material behaviour has long been used is geological engineering, e.g., Sett [2007]. For the modelling of geotechnical materials, plasticity models such as the Cam Clay model are applied to represent the material behaviour. In general, the developed approach in this thesis is applicable to such models and the first step could be the computational realization of the combined VON MISES DRUCKER PRAGER material model, which has been proposed by Lutz [2011]. The advantage of this formulation is the smooth transition between the VON MISES and the DRUCKER PRAGER model, which makes the computational realization less complicated. Furthermore, the extension to mixed non-linear hardening[1] is a further issue. Some investigations with random material properties in the context of non-linear isotropic hardening can be found in the PhD thesis of Jablonski [2014].

For the computation of a stochastic structural system, for example, the set of equations in (8.36), knowledge of the system parameters, such as the material properties is necessary. A very important information is the probability distribution of the respective input parameter. However, in many cases less parameter information is available, because

- the measurement of the parameters is too expensive and/or
- it is impossible to measure the parameters.

To quantify unknown parameters, different methods are available and some of them are already listed in subsection 5.1. Beyond this methods, the BAYESIAN theorem should be briefly presented here. For further informations to the BAYESIAN theorem the reader is referred to Sivia and J.Skilling [2006] or Christensen et al. [2011] and with special emphasis to civil engineering to Scheiwiller [1999].

The BAYESIAN theorem is used for the calculation of an event A given that some event B has already occurred, which is denoted by $\mathcal{P}(A|B)$. The mathematical definition of the (simplest) BAYESIAN theorem is,

$$\mathcal{P}(A|B) = \frac{\mathcal{P}(A)\mathcal{P}(B|A)}{\mathcal{P}(B)} \ , \tag{10.1}$$

where $\mathcal{P}(A|B)$ is the posteriori probability, $\mathcal{P}(A)$ the prior probability, $\mathcal{P}(B|A)$ the likelihood and $\mathcal{P}(B)$ is a norming constant. The interpretation of this equation is as follows:

Due to the existing knowledge of A an initial estimate for $\mathcal{P}(A)$ is given. This estimate corresponds to the so-called prior probability or more general of the prior information. With new insights (event B) the estimate of the probability of occurrence of A changed and the prior information is updated. The quotient $\mathcal{P}(B|A)/\mathcal{P}(B)$ shows how to perform the update. The updated conditional probability $\mathcal{P}(A|B)$ includes the whole available information on the occurrence of A and is called posteriori probability.

---

[1] The theory of mixed non-linear hardening can be found, e.g., in Neto et al. [2008].

A method to evaluate the posteriori probability is the Bayesian inference. Marzouk et al. [2007] presents an approach which represents the random variables with the polynomial chaos expansion. The author comes to the conclusion that the proposed approach provides a reduction of the computational time in comparison when using a direct sampling approach. This seems to be a research area of particular interest, especially when the parameter information is rare or the numerical approximation of the forward problem[2] seems to be very time consuming and consequently very costly. A typical example for this method could be the determination of the input parameters when the system response of the structural system is known, such as the system response of a offshore wind turbine.

---

[2]In a forward problem a class of possible descriptions of a system exists and a forward operator maps each of these descriptions onto a probability measure for the characteristic values.

A. Additional Mathematical Background

This chapter contains miscellaneous mathematical topics, such as some derivations, mathematical calculation rules and additional definitions, which are applied in the context of this thesis. The references, where the theoretical information has been taken from are indicated accordingly.

A.1. Derivation of the Variance between two Random Variables

Let $\mathrm{Var}(X+Y)$ be the variance of the two random variables $X, Y \in (\Theta, \mathcal{F}, \mathcal{P})$, which is derived as follows:

$$
\begin{aligned}
\mathrm{Var}(X + Y) &= \mathbb{E}\left[((X+Y) - \mathbb{E}[X+Y])^2\right] \\
&= \mathbb{E}\left[((X+Y) - (\mathbb{E}[X] + \mathbb{E}[Y]))^2\right] \\
&= \mathbb{E}\left[((X - \mathbb{E}[X]) + (Y - \mathbb{E}[Y]))^2\right] \\
&= \mathbb{E}\left[(X - \mathbb{E}[X])^2 + (Y - \mathbb{E}[Y])^2 + 2(X - \mathbb{E}[X])(Y - \mathbb{E}[Y])\right] \quad \text{(A.1)} \\
&= \mathbb{E}\left[(X - \mathbb{E}[X])^2\right] + \mathbb{E}\left[(Y - \mathbb{E}[Y])^2\right] \\
&\quad + 2\,\mathbb{E}\left[(X - \mathbb{E}[X])(Y - \mathbb{E}[Y])\right] \\
&= \mathrm{Var}(X) + \mathrm{Var}(Y) + 2\,\mathbb{E}\left[(X - \mathbb{E}[X])(Y - \mathbb{E}[Y])\right] .
\end{aligned}
$$

A.2. Derivation of the Covariance between two Random Variables

Let $\mathrm{Cov}(X+Y)$ be the covariance of the two random variables $X, Y \in (\Theta, \mathcal{F}, \mathcal{P})$, which is be derived as described below:

$$
\begin{aligned}
\mathrm{Cov}(X, Y) &= \mathbb{E}\left[(X - \mathbb{E}[X])(Y - \mathbb{E}[Y])\right] \\
&= \mathbb{E}\left[XY - \mathbb{E}[X]Y - X\mathbb{E}[Y] + \mathbb{E}[X]\mathbb{E}[Y]\right] \\
&= \mathbb{E}[XY] - \mathbb{E}[X]\mathbb{E}[Y] - \mathbb{E}[X]\mathbb{E}[Y] + \mathbb{E}[X]\mathbb{E}[Y] \\
&= \mathbb{E}[XY] - \mathbb{E}[X]\mathbb{E}[Y] .
\end{aligned}
\quad \text{(A.2)}
$$

A.3. Binomial Coefficient

The *Binomial Coefficient*, in a mathematical context, is a family of integers, which occur as coefficients in the binomial theorem. The following explanation has been taken from Bronshtein et al. [2007].

The definition is for non-negative integers n and k (read *n choose k*) and is defined

as

$$\binom{n}{k} = \frac{n!}{(n-k)!k!}\,, \qquad 0 \le k \le n\,. \tag{A.3}$$

Here, n is the product of the positive integers from 1 to n

$$n! = 1 \cdot 2 \cdot 3 \cdot \ldots \cdot n\,,$$

called n *factorial*. By definition is $0! = 1$ as well as

$$\binom{n}{0} = 1\,, \quad \binom{n}{1} = n\,, \quad \binom{n}{n} = 1\,.$$

A.4. Chebyshev Inequality

The Chebyshev Inequality furnishes a bound on the probability of how much the RV X can deviate from its expected value. If X has the expected value μ_X and the standard deviation σ_X, then for arbitrarily $\lambda > 0$ the Chebyshev inequality reads

$$\mathcal{P}(|X - \mu_X| \ge \lambda\sigma) \le \frac{1}{\lambda^2}\,. \tag{A.4}$$

Whereas this inequality is only useful for $\lambda > 1$, because when $\lambda < 1$ the right-hand side becomes greater one what makes the inequality meaningless. In general, the Chebyshev inequality is only a weak bound compared to what might be possible if there informations about the associated probability distribution are available.

A.5. Central Limit Theorem

The *Cental Limit Theorem* (CLT) is one of the most useful theorems in the probability theory. It states that a random sample set $\{X_1, X_2, \ldots X_n\}$ with mean equal zero and finite variances $\sigma_1^2, \sigma_2^2, \ldots \sigma_n^2$ tends to the standard normal distribution[1]. This statement is defined by

$$Z = \frac{\hat{\mu} - \mu}{\sigma/\sqrt{n}}\,, \tag{A.5}$$

where $\hat{\mu}$ is the sample mean, μ and σ are the mean and the standard deviation of the population and n is the sample size. From this equation it is obvious that the sampling result for $\hat{\mu}$ depends on the sample size n. Montgomery and Runger [1994] distinguishes between the following two ranges of n.

- If $n \ge 30$:
  The normal distribution will be satisfactory regardless of the shape of the population.

- If $n < 30$:
  The CLT will work if the distribution of the population is not strongly non-normal.

---

[1]Provided that the individual variances σ_j^2, $j = 1, \ldots n$ are small compared to $\sum_{i=1}^{n} \sigma_i^2$.

A.6. Law of Large Numbers

The *Law of Large Numbers* (LLN) is the theoretical basis for estimating μ from measurements. When an experimenter takes the sample mean $\hat{\mu}$ of n measurements, it is relying on the LLN in order to use $\hat{\mu}$ as an estimate of the unknown theoretical expectation μ. A distinction is made between the *weak* and the *strong* law. The weak law obtains convergence in probability, while the strong law leads to convergence with probability $p - 1$, $p \in [0, 1]$, whereas $p - 1$ is a further expression for almost surely (a.s.). In the following both laws are briefly presented. For a detailed treatment the reader is referred to the standard textbooks on probability theory, e.g., by Loève [1977] or Papoulis [1991].

Weak Law of Large Numbers

Let $\{X_1, \dots X_n\}$ be a set of random variables with (unknown) mean μ_X and also (unknown) standard deviation σ_X. In such a case the sample mean $\hat{\mu}$,

$$\hat{\mu} = \frac{1}{n} \sum_{i=1}^{n} X_i \,, \tag{A.6}$$

has to be considered, which is an estimate of μ_X. By use of the Chebyshev Inequality (A.4) and for every $\lambda \in (0, \infty)$ follows

$$\mathcal{P}\left(\left| \frac{1}{n} \sum_{i=1}^{n} X_i - \mu_X \right| \geq \lambda \right) \leq \frac{1}{\lambda^2} \, \text{Var}\left(\frac{1}{n} \sum_{i=1}^{n} X_i \right) \,, \tag{A.7}$$

$$= \frac{1}{\lambda^2} \frac{1}{n^2} \sum_{i=1}^{n} \text{Var}\left(X_i \right), \tag{A.8}$$

$$= \frac{\sigma^2}{\lambda^2 n} \to 0 \,, \tag{A.9}$$

and finally for $n \to \infty$ it reads

$$\frac{1}{n} \sum_{i=1}^{n} X_i \to \mu \,. \tag{A.10}$$

Strong Law of Large Numbers

Specifying the weak law of large numbers by the formulation of the $p - 1$ convergence of

$$\frac{1}{n} \sum_{i=1}^{n} X_i \,, \tag{A.11}$$

with $n \to \infty$ against the mean μ_X leads to the *Strong Law of Large Numbers*.

Let $\{X_k\}$, $k \in \mathbb{N}$ be a set of independent identically distributed (i.i.d.) random

variables with mean μ_X and standard deviation σ_X, which leads to

$$\hat{\mu}_k = \frac{1}{n} \sum_{k=1}^{n} X_k \rightarrow \mu_X \,, \qquad \text{a.s.} \,, \tag{A.12}$$

for $n \rightarrow \infty$.

A.7. Hilbert Spaces

As first discussed in chapter 3, the mathematical description of the Finite Element Method is based on a variation formulation of elliptical (in static mechanical systems) differential equations. This variational problem has a solution in the so-called Sobolev space. From a numerical point of view, one carries out the solution of the differential equations in a weak form, defined in a finite dimensional subspace. For linear differential equations it is suitable to use Hilbert Spaces as solution spaces. In this section the basic properties of Hilbert spaces are summarized. For further informations of the mathematics of the FEM, the reader is referred to the textbooks by Braess [1992] or Oden and Reddy [2011]. A more (general) mathematical background can be found, for example, in Bronshtein et al. [2007]; Dobrowolski [2010]; Werner [2011]; Alt [2012]. Hilbert spaces are Banach[2] spaces, which are additionally allow the mathematical structure of a scalar product.

Definition Normed Spaces

If every vector $\mathbf{x}$ of a real vector field (space) $\mathcal{V}$ is assigned with a real number $\|\mathbf{x}\|$ so that $\mathbf{x}, \mathbf{y} \in \mathcal{V}$ and $\alpha \in \mathbb{R}$ the following properties apply:

$$\|\mathbf{x}\| \geq 0 \qquad \text{and} \qquad \|\mathbf{x}\| = 0 \Longrightarrow \mathbf{x} = \mathbf{0} \,, \tag{A.13}$$

$$\|\alpha \cdot \mathbf{x}\| = |\alpha| \cdot \|\mathbf{x}\| \,, \tag{A.14}$$

$$\|\mathbf{x} + \mathbf{y}\| \leq \|\mathbf{x}\| + \|\mathbf{y}\| \,, \tag{A.15}$$

where $\| \bullet \|$ denotes the norm on $\mathcal{V}$ and $(\mathcal{V}, \| \bullet \|)$ is a normed space.

Definition pre-Hilbert Spaces

Let $\mathbf{x}, \mathbf{y}$ be two vectors of a real vector space $\mathcal{V}$ where a real number $\langle \mathbf{x}, \mathbf{y} \rangle$ is assigned, so that $\forall \, \mathbf{x}, \mathbf{y}, \mathbf{z} \in \mathcal{V}$ and $\alpha \in \mathbb{R}$ the following properties apply:

$$\langle \mathbf{x}, \mathbf{x} \rangle \geq 0 \qquad \text{and} \qquad \langle \mathbf{x}, \mathbf{x} \rangle = 0 \Longrightarrow \mathbf{x} = \mathbf{0} \,, \tag{A.16}$$

$$\langle \mathbf{x}, \mathbf{y} \rangle = \langle \mathbf{y}, \mathbf{x} \rangle \,, \tag{A.17}$$

$$\langle \mathbf{x} + \alpha \cdot \mathbf{y}, \mathbf{z} \rangle = \langle \mathbf{x}, \mathbf{y} \rangle + \alpha \cdot \langle \mathbf{y}, \mathbf{z} \rangle \,, \tag{A.18}$$

where $\langle \bullet, \bullet \rangle$ is the scalar product on $\mathcal{V}$ and $(\mathcal{V}, \langle \bullet, \bullet \rangle)$ is a pre-Hilbert space. In general, a scalar product generates a norm according to

$$\|\mathbf{x}\| := \sqrt{\langle \mathbf{x}, \mathbf{x} \rangle} \,, \tag{A.19}$$

---

[2]For the mathematical theory of Banach spaces the reader is referred to the cited literature in this section.

where the frequently used Euclidean norm is given by

$$\|\mathbf{x}\|_2 := \sqrt[2]{|x_1|^2 + \cdots + |x_n|^2} \,. \tag{A.20}$$

Orthogonality

A further important property, which is frequently used in this thesis is the orthogonality property of two vectors. Let $\mathbf{x}$, $\mathbf{y}$ be two vectors of a Hilbert space $\mathcal{H}$, which are orthogonal to each other $(\mathbf{x} \perp \mathbf{y})$ if the scalar product $\langle \mathbf{x}, \mathbf{y} \rangle = 0$. Furthermore, holds the orthogonality for two subsets A, $B \subset \mathcal{H}$ $(A \perp B)$ if $\mathbf{x} \perp \mathbf{y}$, $\forall \mathbf{x} \in A$ and $\mathbf{y} \in B$. For a single element $x \in A$ the notation is $x \perp B$.

Moreover, the orthogonality can be also applied to *orthogonal* systems. Therefore let $\{\mathbf{x}_i\}$, $i = 1, 2, \ldots$ be a vector set of $\mathcal{H}$, which is orthogonal if it does not contain the zero vector and $\mathbf{x}_i \perp \mathbf{x}_j$, $i \neq j$ and $\langle \mathbf{x}_i, \mathbf{x}_j \rangle = \delta_{ij}$, where δ_{ij} denotes the Kronecker delta.

B. Classical Probability Density Functions

In this Appendix, various probability distributions are briefly presented. These probability density functions (PDFs) are commonly used in the context of structural mechanics with random input parameters. The following explanations are referred basically to the textbooks by Haldar and Mahadevan [2000]; Bucher [2009] and to the doctoral thesis by Blatman [2009]. A claim to completeness is not applicable here and for further readings the reader is referenced to the standard textbooks of probability theory.

B.1. Gaussian Distribution

Due to its simplicity, the GAUSSIAN or *normal* distribution is probably the most commonly used distribution in engineering applications. Let X be a (normal) random variable. Then, the corresponding probability density function reads

$$f_X(x) = \frac{1}{\sqrt{2\pi\sigma_X^2}} \exp\left(-\frac{(x-\mu_X)^2}{2\sigma_X^2}\right),$$
(B.1)

where μ_X denotes the expected value of X and σ_X is the corresponding standard deviation. The corresponding cumulative density function $F_X(x)$ is defined by

$$F_X(x) = \int_{-\infty}^{x} f_X(x)\,\mathrm{d}x.$$
(B.2)

A GAUSSIAN random variable with expected value $\mu = 0$ and standard deviation $\sigma = 1$ is denoted as *standard normal variable*. The corresponding PDF (resp. CDF) is often given by

$$\Theta(x) = \frac{1}{\sqrt{2\pi}} \int_{-\infty}^{x} \exp\left(-\frac{t^2}{2}\right)\,\mathrm{d}t.$$
(B.3)

The values $\Theta(x)$ of the CDF on the interval [0,1] of the normal distribution are not solvable in closed form. However, tables are widely available or it can be calculated numerically. Higher moments as the second moment σ can be derived in terms of μ and σ. At this point, it will be waived, because the GAUSSIAN distribution is completely characterized by its first two moments. For the GAUSSIAN distribution, the third and fourth moment is:

$$\text{Third moment (skewness)}: s = 0,$$
(B.4)

$$\text{Fourth moment (kurtosis)}: \kappa = 3.$$
(B.5)

B.2. Log-Normal Distribution

A *log-normal* distribution is commonly used to characterize quantities which are always positive, such as material properties in engineering applications. In this context, the natural logarithm of the random variable X is used. Let X be a log-normal random variable, then the probability density function is given by

$$f_X(x) = \frac{1}{x\sqrt{2\pi}\sigma_L}\exp\left(-\frac{\left(\log\frac{x}{\mu_L}\right)^2}{2\sigma_L^2}\right), \qquad \text{for } x \geq 0. \tag{B.6}$$

Here, the subscript $\bullet_L$ refers to the corresponding parameters of the log-normal distribution. The corresponding CDF of a log-normal distribution reads

$$F_X(x) = \Theta\left(\frac{\log\frac{x}{\mu_L}}{\sigma_L}\right), \tag{B.7}$$

where Θ is already given in equation (B.3). The expected value μ and standard deviation σ is defined as follows:

$$\mu = \mu_L\exp\left(-\frac{\sigma_L^2}{2}\right) = \frac{\mu_L^2}{\sqrt{\mu_L^2 + \sigma_L^2}}, \tag{B.8}$$

$$\sigma = \sqrt{\ln\left(\frac{\sigma_L^2}{\mu_L^2} + 1\right)}. \tag{B.9}$$

B.3. Uniform Distribution

A *uniform* distribution can be used to represent a parameter when only its bounded domain of variation is known by two limits, (say) a and b. The PDF of an uniform random variable X is given by

$$f_X(x) = \frac{1}{b-a}, \qquad \text{for } x \in [a,b], 0 \text{ otherwise}, \tag{B.10}$$

with $b > a$. The corresponding CDF reads

$$F_X(x) = \frac{x-a}{b-a}, \qquad \text{for } x \in [a,b], 0 \text{ otherwise}. \tag{B.11}$$

The expected value μ_X and standard deviation σ_X is defined by

$$\mu_X = \frac{a+b}{2} \tag{B.12}$$

$$\sigma_X = \frac{b-a}{2\sqrt{3}}. \tag{B.13}$$

The skewness of the uniform distribution is $s = 0$ and the corresponding kurtosis is specified to $\kappa = 1.8$.

B.4. Gamma and Exponetial Distribution

The *Gamma* distribution is also useful to represent parameters with only positive values. A random variable X follows a Gamma distribution if its PDF is defined by

$$f_X(x) = \frac{1}{a^\nu \Gamma(\nu)} x^{\nu-1} \exp\left(-\frac{x}{a}\right), \qquad \text{for } x \geq 0. \tag{B.14}$$

Here, ν is a shape parameter, a is a scale parameter and $\Gamma(\cdot)$ denotes the complete Gamma function, which is defined by

$$\Gamma(\nu) = \int_0^\infty t^{\nu-1} e^{-t} \, dt, \qquad \text{for } \nu > 0. \tag{B.15}$$

The expected value is given by $\mu = \nu a$ and the standard deviation is defined by $\sigma = \sqrt{\nu} a$. For the case $\nu = 1$ equation (B.14) leads to the exponential density function

$$f_X(x) = \frac{1}{a} \exp\left(-\frac{x}{a}\right), \qquad \text{for } x \geq 0. \tag{B.16}$$

The skewness s of the Gamma distribution and kurtosis κ are specified by

$$s = \frac{2}{\sqrt{\nu}}, \tag{B.17}$$

and

$$\kappa = \frac{6}{\nu}. \tag{B.18}$$

B.5. Weibull Distribution

The Weibull or (Type III smallest) distribution is often used to represent material strengths and time to failure of mechanical structures. A random variable X follows a Weibull distribution if its PDF reads

$$f_X(x) = \frac{k}{\nu} \left(\frac{x}{\lambda}\right)^{k-1} \exp\left(-\left(\frac{x}{\lambda}\right)^k\right), \qquad \text{for } x \geq 0. \tag{B.19}$$

Here, the parameter $\lambda > 0$ denotes a scale parameter and the value of $k > 0$ influences the shape of the distribution. The corresponding CDF is defined as

$$F_X(x) = 1 - \exp\left(-\left(\frac{x}{\lambda}\right)^k\right), \qquad \text{for } x \geq 0. \tag{B.20}$$

The expected value μ and the standard deviation σ can be calculated under consideration of the distribution parameters λ and k as follows:

$$\mu = \lambda \Gamma\left(1 + \frac{1}{k}\right) \tag{B.21}$$

$$\sigma^2 = \lambda^2 \left(\Gamma\left(1 + \frac{2}{k}\right) - \Gamma^2\left(1 + \frac{1}{k}\right)\right), \tag{B.22}$$

where, $\Gamma(\cdot)$ is the Gamma function, cf. equation (B.15). The skewness s and the kurtosis of the Weibull distribution can be found, e.g., in the textbook by Rinne [2009].

C. Derivatives of the Elastic-Plastic Tangent Modulus

In this Appendix, the explicit derivatives of the elastic-plastic tangent modulus introduced in equation (3.51) are calculated.

Starting point is the partial derivative

$$\frac{\partial \Delta \lambda}{\partial \boldsymbol{\epsilon}_{n+1}}$$

which, when applying the chain rule, leads to

$$\frac{\partial \Delta \lambda}{\partial \boldsymbol{\epsilon}_{n+1}} = \underbrace{\frac{\partial \Delta \lambda}{\partial f_{n+1}^{\mathrm{trial}}}}_{a_1} \underbrace{\frac{\partial f_{n+1}^{\mathrm{trial}}}{\partial \boldsymbol{\eta}_{n+1}^{\mathrm{trial}}}}_{a_2} \underbrace{\frac{\partial \boldsymbol{\eta}_{n+1}^{\mathrm{trial}}}{\partial \boldsymbol{\epsilon}_{n+1}}}_{a_3}$$

$$a_1 = \left(2\mu \left(1 + \frac{\mathrm{H}_{\mathrm{iso}} + \mathrm{H}_{\mathrm{kin}}}{3\mu} \right) \right)^{-1}$$

$$a_2 = \frac{\partial \|\boldsymbol{\eta}_{n+1}^{\mathrm{trial}}\|}{\partial \boldsymbol{\eta}_{n+1}^{\mathrm{trial}}} = \frac{1}{2} \left(\sum_{i=1}^{n} \left(\boldsymbol{\eta}_{n+1,\,i}^{\mathrm{trial}} \right)^2 \right)^{-\frac{1}{2}} 2\,\boldsymbol{\eta}_{n+1,\,i}^{\mathrm{trial}} = \mathbf{n}_{n+1}^{\mathrm{trial}}$$

$$a_3 = 2\mu\,,$$

and finally

$$\frac{\partial \Delta \lambda}{\partial \boldsymbol{\epsilon}_{n+1}} = \left(1 + \frac{\mathrm{H}_{\mathrm{kin}} + \mathrm{H}_{\mathrm{iso}}}{3\mu} \right)^{-1} \mathbf{n}_{n+1}^{\mathrm{trial}}\,. \tag{C.1}$$

The explicit derivation of

$$\frac{\partial \mathbf{n}_{n+1}^{\mathrm{trial}}}{\partial \boldsymbol{\epsilon}_{n+1}}$$

is calculated by

$$\frac{\partial \mathbf{n}_{n+1}^{\mathrm{trial}}}{\partial \boldsymbol{\epsilon}_{n+1}} = \frac{\partial \mathbf{n}_{n+1}^{\mathrm{trial}}}{\partial \mathbf{s}_{n+1}} \frac{\partial \mathbf{s}_{n+1}}{\partial \boldsymbol{\epsilon}_{n+1}}$$

$$= \frac{2\mu}{\|\boldsymbol{\eta}_{n+1}^{\mathrm{trial}}\|} \left[\mathbb{I} - \mathbf{n}_{n+1}^{\mathrm{trial}} \otimes \mathbf{n}_{n+1}^{\mathrm{trial}} \right]\,, \tag{C.2}$$

with the derivative of a unit normal field

$$\frac{\partial \mathbf{n}}{\partial \mathbf{s}} = \frac{1}{\|\boldsymbol{\eta}\|} (\mathbb{I} - \mathbf{n} \otimes \mathbf{n})\,.$$

After substituting the derivatives (C.1), (C.2) and the explicit definition for the elasticity tensor $\mathbb{C}^{\mathrm{el}}$ into equation (3.51) results in the algorithmic consistent tangent

modulus for the J_2-elastic-plastic material, i.e.

$$\mathbb{C}^{\text{ep}}_{n+1} = K\mathbf{1} \otimes \mathbf{1} + 2\mu A_{n+1} \left(\mathbb{I} - \frac{1}{3}\mathbf{1} \otimes \mathbf{1} \right) - 2\mu B_{n+1}\mathbf{n}^{\text{trial}}_{n+1} \otimes \mathbf{n}^{\text{trial}}_{n+1} \,, \qquad \text{(C.3)}$$

where

$$A_{n+1} = 1 - \frac{2\mu\Delta\lambda}{\|\eta^{\text{trial}}_{n+1}\|} \,,$$

and

$$B_{n+1} = \left(1 + \frac{H_{\text{kin}} + H_{\text{iso}}}{3\mu} \right)^{-1} - \frac{2\mu\Delta\lambda}{\|\eta^{\text{trial}}_{n+1}\|} \,.$$

D. Additional Remarks on Random Fields

In the first two sections of this Appendix, some additional theoretical background to the theory of random fields is presented. In section D.3 some additional graphs of the SPRM are given. In detail, these are the evolution of the skewness and the kurtosis of the random phase angle plotted against the sample number applying a LHS and SOBOL' sequences.

D.1. Wiener-Khinchine Relations

In what follows is a compact summary of the theoretical explanations, which is taken from the textbook by Vanmarcke [2010]. Let $\hat{H}(\mathbf{x}) = \hat{H}(x_1, \dots x_n)$ be a discretized n-dimensional homogeneous random field, which is expressed as a sum of $2K$ independent random sinusoidal components as follows:

$$\hat{H}(\mathbf{x}) = \mu + \sum_{k=-K}^{K} \hat{H}_{\boldsymbol{k}}(\mathbf{x}) \,, \tag{D.1}$$

where μ is the mean of the random field and $\hat{H}_{\boldsymbol{k}}(\mathbf{x})$ is given by

$$\hat{H}_{\boldsymbol{k}}(\mathbf{x}) = A_{\boldsymbol{k}} \cos(\boldsymbol{\omega_k} \cdot \mathbf{x} + \Phi_{\boldsymbol{k}}) \,. \tag{D.2}$$

Here, $A_{\boldsymbol{k}}$ is the random amplitude and $\Phi_{\boldsymbol{k}}$ is the random phase angle of the component $\hat{H}_{\boldsymbol{k}}(\mathbf{x})$ associated with a point in the n-dimensional frequency domain. The cosine function depends on the inner product of the frequency $\boldsymbol{\omega_k} = \{\omega_{k_1}, \dots \omega_{k_n}\}$ and the vectors $\mathbf{x} = \{x_1, \dots x_n\}$

$$\boldsymbol{\omega_k} \cdot \mathbf{x} = \omega_{k_1} x_1 + \omega_{k_2} x_2 + \dots + \omega_{k_n} x_n \,, \tag{D.3}$$

where $\omega_{k_i} = \pm [\Delta \omega_i (2k_i - 1)/2] \,, \; k_i = 1, \dots, K_i$ denotes the i-th coordinate of a point in the n-dimensional frequency domain. Each elementary random function $\hat{H}_{\boldsymbol{k}}(\mathbf{x})$ has a mean equal to zero and a variance given by

$$\sigma_{\boldsymbol{k}} = \mathbb{E}[\hat{H}_{\boldsymbol{k}}(x)^2] = \mathbb{E}[A_{\boldsymbol{k}}^2] \, \mathbb{E}[\cos^2(\boldsymbol{\omega_k} \cdot \mathbf{x} + \Phi_{\boldsymbol{k}})] = \frac{1}{2} \mathbb{E}[A_{\boldsymbol{k}}^2] \,. \tag{D.4}$$

Here, the expectation $\mathbb{E}[\cos^2(\boldsymbol{\omega_k} \cdot \mathbf{x} + \Phi_{\boldsymbol{k}})]$ is defined with respect to the random phase angle $\Phi_{\boldsymbol{k}}$. The variance of $\hat{H}(\mathbf{x})$ is obtained by summing the spectral masses throughout the frequency domain, i.e.

$$\sigma^2 = \sum_{k=-K}^{K} \frac{1}{2} \mathbb{E}[A_{\boldsymbol{k}}^2] \tag{D.5}$$

$$\Rightarrow \int_{-\infty}^{\infty} S(\boldsymbol{\omega}) \, d\boldsymbol{\omega} \,, \tag{D.6}$$

where $S(\boldsymbol{\omega})$ denotes the multidimensional spectral density function and $d\boldsymbol{\omega} = d\omega_1 d\omega_2 \cdots d\omega_n$ represents an elementary region in the frequency domain. The covariance function is analogously formulated as

$$C(\boldsymbol{\tau}) = \sum_{k=-K}^{K} \frac{1}{2}\mathbb{E}[A_{\boldsymbol{k}}^2]\cos\boldsymbol{\omega_k} \cdot \boldsymbol{\tau} \,. \tag{D.7}$$

Substituting equation (D.6) into equation (D.7) and replacing the summation by an integration leads to the first relation of the Wiener-Khinchine transform pair

$$C(\boldsymbol{\tau}) = \int_{-\infty}^{\infty} S(\boldsymbol{\omega})\cos\boldsymbol{\omega_k} \cdot \boldsymbol{\tau} \, d\boldsymbol{\omega} = \int_{-\infty}^{\infty} S(\boldsymbol{\omega})e^{i\boldsymbol{\omega}\cdot\boldsymbol{\tau}} \, d\boldsymbol{\omega} \,, \tag{D.8}$$

where i denotes the imaginary unit. Performing a Fourier transformation of equation (D.8) leads to the n-dimensional spectral density function $S(\boldsymbol{\omega})$,

$$S(\boldsymbol{\omega}) = \frac{1}{(2\pi)^n} \int_{-\infty}^{\infty} C(\boldsymbol{\tau})\cos\boldsymbol{\omega_k} \cdot \boldsymbol{\tau} \, d\boldsymbol{\tau} = \frac{1}{(2\pi)^n} \int_{-\infty}^{\infty} C(\boldsymbol{\tau})e^{-i\boldsymbol{\omega}\cdot\boldsymbol{\tau}} \, d\boldsymbol{\tau} \,. \tag{D.9}$$

The last two equations are referred to as the Wiener-Khinchine transform pair (Khintchine [1934]), which states that the n-dimensional Fourier transform of the covariance function $C(\boldsymbol{\tau})$ is equal to the spectral density function $S(\boldsymbol{\omega})$. This means, that the covariance function can be transformed directly into the spectral density function and vice versa.

D.2. Additional Remarks on the Karhunen Loève Expansion

The following derivation is a compact summary of the explanations given in Ghanem and Spanos [2003]. First of all, the required equations, introduced in chapter 6, are repeated here for convenience. These are:

- The expansion of the random field $H(\mathbf{x}, \theta)$

$$\alpha(\mathbf{x}, \theta) = \sum_{i=0}^{\infty} \sqrt{\lambda_i} f_i(\mathbf{x})\xi_i(\theta) \,, \text{ and} \tag{D.10}$$

- the normalization condition

$$\int_{\mathcal{D}} f_i(\mathbf{x})f_j(\mathbf{x}) \, d\mathcal{D} = \delta_{ij} \,. \tag{D.11}$$

First, multiplying both sides of equation (D.10) by $\alpha(\mathbf{x_2}, \theta)$ and taking the expectation on both sides leads to

$$C(\mathbf{x_1}, \mathbf{x_2}) = \mathbb{E}[\alpha(\mathbf{x_1}, \theta)\alpha(\mathbf{x_2}, \theta)] = \sum_{i=0}^{\infty}\sum_{j=0}^{\infty} \sqrt{\lambda_i\lambda_j} f_i(\mathbf{x_1})f_j(\mathbf{x_2})\mathbb{E}[\xi_i(\theta)\xi_j(\theta)] \,. \tag{D.12}$$

Multiplying equation (D.12) by $f_k(\mathbf{x}_2)$, integrating over the domain $\mathcal{D}$ and applying the normalization condition (D.11) gives

$$
\int_{\mathcal{D}} C(\mathbf{x}_1, \mathbf{x}_2) f_k(\mathbf{x}_2) \, \mathrm{d}\mathcal{D}_{\mathbf{x}_2} = \sum_{i=0}^{\infty} \sum_{j=0}^{\infty} \sqrt{\lambda_i \lambda_j} f_i(\mathbf{x}_1) \delta_{jk} \mathbb{E}\left[\xi_i(\theta)\xi_j(\theta)\right]
$$
$$
= \sum_{i=0}^{\infty} \sqrt{\lambda_i \lambda_k} f_i(\mathbf{x}_1) \mathbb{E}\left[\xi_i(\theta)\xi_k(\theta)\right] .
$$

(D.13)

Subsequently multiplying both sides of equation (D.13) by $f_l(\mathbf{x}_1)$ and integrating over the domain $\mathcal{D}$ the equation results in

$$
\lambda_k \int_{\mathcal{D}} f_k(\mathbf{x}_1) f_l(\mathbf{x}_1) \, \mathrm{d}\mathcal{D}_{\mathbf{x}_1} = \sum_{i=0}^{\infty} \sqrt{\lambda_i \lambda_k} f_i(\mathbf{x}_1) f_l(\mathbf{x}_1) \mathbb{E}\left[\xi_i(\theta)\xi_k(\theta)\right]
$$
$$
\lambda_k \delta_{kl} = \sum_{i=0}^{\infty} \sqrt{\lambda_i \lambda_k} \delta_{il} \mathbb{E}\left[\xi_i(\theta)\xi_k(\theta)\right]
$$
$$
= \sqrt{\lambda_k \lambda_l} \mathbb{E}\left[\xi_k(\theta)\xi_l(\theta)\right] ,
$$

(D.14)

where the relation $\int_{\mathcal{D}} = C(\mathbf{x}_1, \mathbf{x}_2) f_k(\mathbf{x}_2) = \lambda_k f_k(\mathbf{x}_1)$ is applied. Equation (D.14)$_3$ can be rearranged, and the normalized condition

$$
\delta_{kl} = \mathbb{E}\left[\xi_k(\theta)\xi_l(\theta)\right] ,
$$

(D.15)

is finally obtained.

D.3. Additional Results on the Spectral Representation Method

Figure D.1.: Result for $\hat{s}_{\hat{H}_S}$ (left) and $\hat{\kappa}_{\hat{H}_S}$ (right) used LHS with $n = 100$ samples.

Figure D.2.: Result for $\hat{s}_{\hat{H}_S}$ (left) and $\hat{\kappa}_{\hat{H}_S}$ (right) used a Sobol' sequence with $n = 100$ samples.

Figure D.3.: Result for $\hat{s}_{\hat{H}_S}$ (left) and $\hat{\kappa}_{\hat{H}_S}$ (right) used the LHS with $n = 250$ samples.

Figure D.4.: Result for $\hat{s}_{\hat{H}_S}$ (left) and $\hat{\kappa}_{\hat{H}_S}$ (right) used a Sobol' sequence with $n = 250$ samples.

Figure D.5.: Result for $\hat{s}_{\hat{H}_S}$ (left) and $\hat{\kappa}_{\hat{H}_S}$ (right) used the LHS with $n = 500$ samples.

Figure D.6.: Result for $\hat{s}_{\hat{H}_S}$ (left) and $\hat{\kappa}_{\hat{H}_S}$ (right) used a Sobol' sequence with $n = 500$ samples.
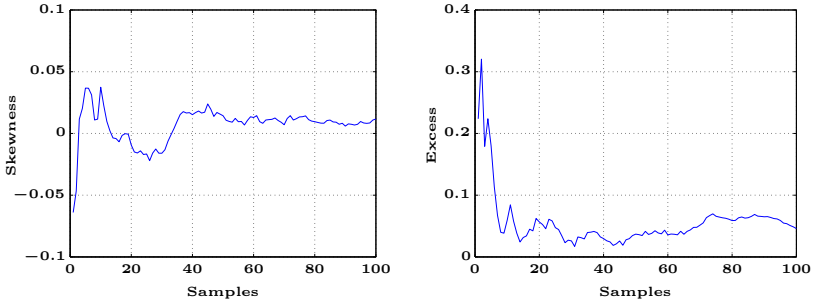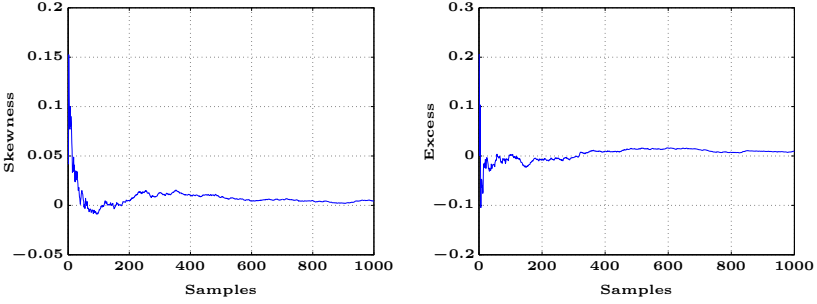
Figure D.7.: Result for $\hat{s}_{\hat{H}_S}$ (left) and $\hat{\kappa}_{\hat{H}_S}$ (right) used the LHS with $n = 1000$ samples.
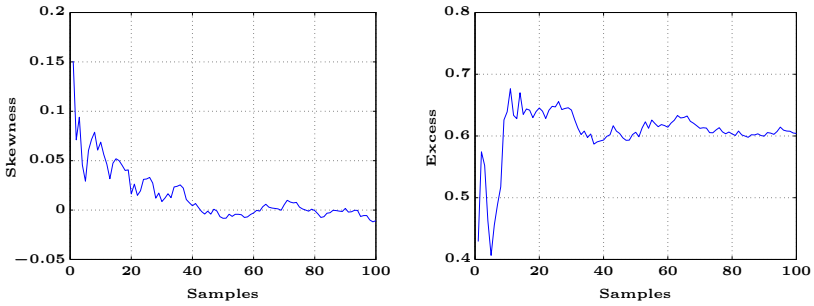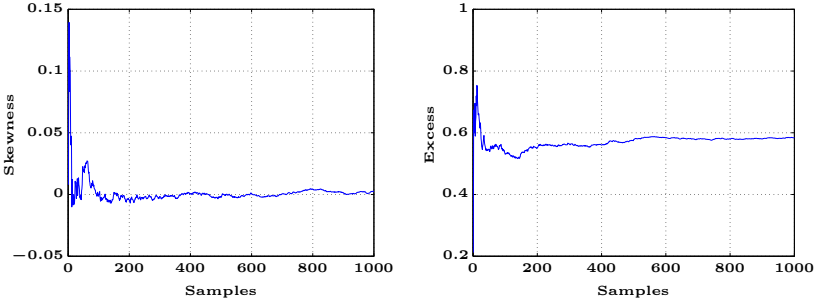

Figure D.8.: Result for $\hat{s}_{\hat{H}_S}$ (left) and $\hat{\kappa}_{\hat{H}_S}$ (right) used a Sobol' sequence with $n = 1000$ samples.
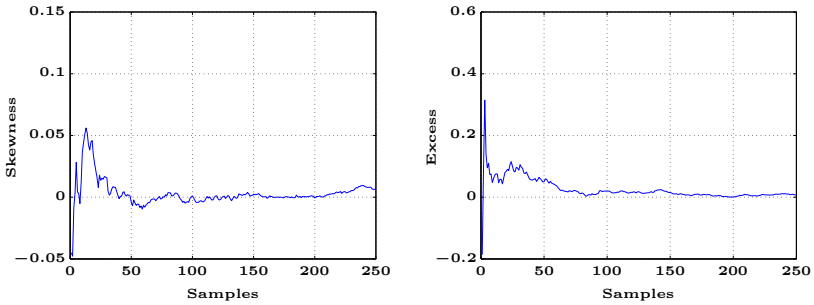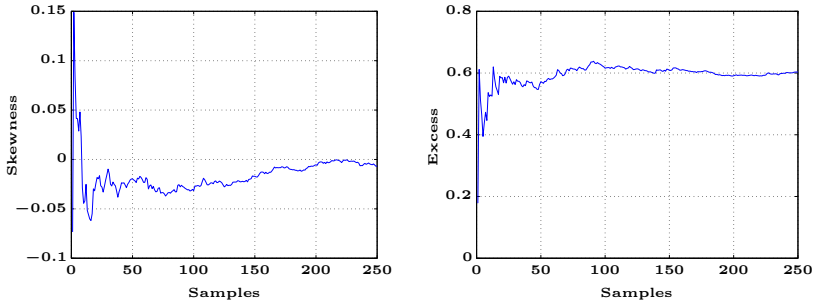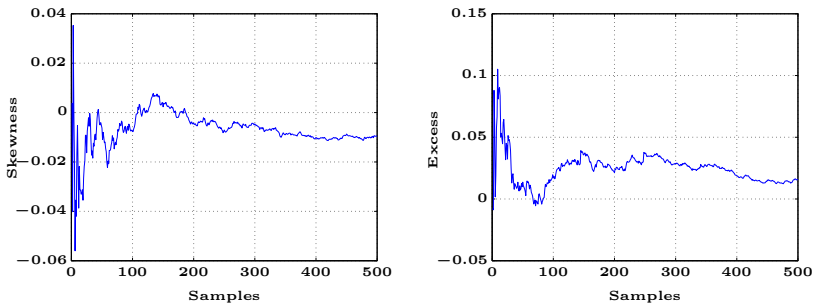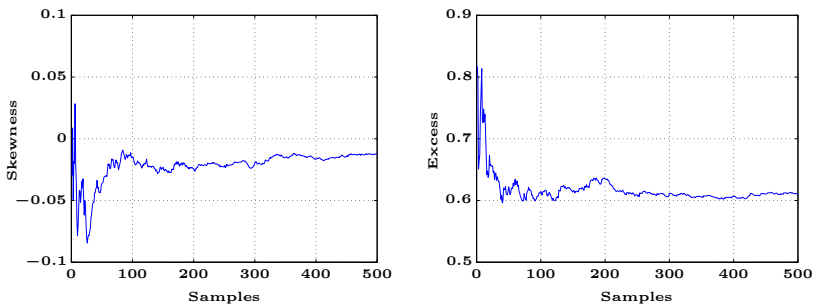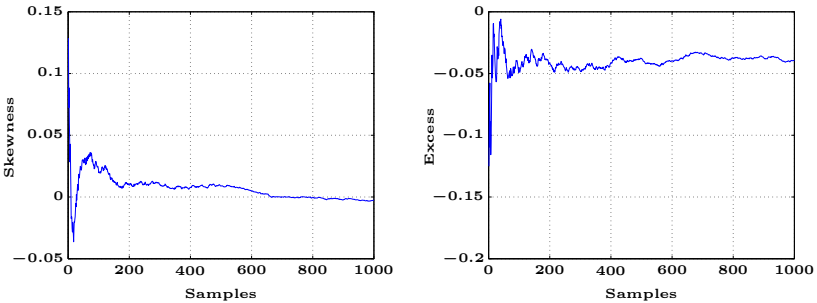

Figure D.9.: Result for $\hat{s}_{\hat{H}_S}$ (left) and $\hat{\kappa}_{\hat{H}_S}$ (right) used the standard MCS with $n = 1000$ samples.

Symbols

Abbreviations

a.s.	Almost surely
$\text{Cov}(\cdot, \cdot)$	Covariance of $(\cdot, \cdot)$
CDF	Cumulative density function
CLT	Central limit theorem
det	Determinant
dim	Dimension
FE	Finite element
FEM	Finite element method
FPK	Fokker-Planck-Kolmogorov
i.i.d	Idependent identically distributed
KLE	Karhunen-Loève expansion
LHS	Latin Hypercube Sampling
LLN	Law of large numbers
MCS	Monte Carlo Sampling
PC	Polynomial chaos
PCA	Polynomial chaos algebra
PCE	Polynomial chaos expansion
PDF	Probability density function
QMC	Quasi Monte Carlo
RV	Random variable
SPRM	Spectral representation method
SCPP	Stochastic closest point projection
$\text{Var}(\bullet)$	Variance of $\bullet$
vM	Von Mises

Greek Symbols

$\boldsymbol{\alpha}$	Set of internal variables (Chap. 2); Set of multi-indices $\boldsymbol{\alpha} = \{\alpha_1, \dots \alpha_p\}$ (Chap. 7 to 9)
$\boldsymbol{\epsilon}$	Linear stress tensor
$\boldsymbol{\epsilon}^{\text{el}}$	Elastic part of the linear stress tensor
$\boldsymbol{\epsilon}^{\text{pl}}$	Plastic part of the linear stress tensor
$\hat{\Gamma}$	Space of polynomials in $\{\xi(\theta)\}_{i=1}^{\infty}$
Γ_p	Polynomial chaos of order p
$\tilde{\Gamma}$	Space spanned by Γ
Γ	Total production of entropy (Chap. 2)

ϵ_M	Residual of the numerical solution of KLE
ϵ_λ	Relative error of the eigenvalue λ
$\tilde{\boldsymbol{\epsilon}}^\bullet$	Deviatoric part of the stress tensor with respect to $\bullet$
$\dot{\epsilon}^{\text{pl}}$	Plastic strain rate
$\boldsymbol{\eta}$	Back-stress tensor (Chap. 2)
$\eta_c,\ \eta$	Specific entropy in the current and reference configuration
Θ	Absolute temperature (Chap. 2); Sample space
θ	Outcome $\theta \in \Theta$
κ_X	Kurtosis (fourth moment) of X
κ_{X_e}	Excess of X
$\kappa_{\bullet u}$	Upper cut-off wave numbers with respect to the coordinate $\bullet$ (Chap. 6)
$\dot{\lambda}$	Plastic multiplier
λ_i	i-th Eigenvalue of KLE
μ	Shear modulus
$\hat{\mu}$	Sample mean
μ_X	Mean value of X
ν	Poisson's ratio
ξ	Uncorrelated Gaussian random variable
ρ_0	Density in the reference configuration
ρ	Density in the current configuration
ρ_{XY}	Correlation between X and Y
$\boldsymbol{\sigma}$	Cauchy stress tensor
σ_y	Yield stress
$\sigma_y(\mathbf{x}, \theta)$	Random yield stress
σ_X	Standard deviation of X
$\hat{\sigma}_X$	Standard deviation of the sample of X
Σ	Covariance matrix
Φ	Motion of the body $\mathcal{B}$
$\Phi_{n_\bullet}$	Random phase angle with respect to the sample value $n_\bullet$
$\phi_{n_\bullet}$	Realization of the random phase angle with respect to the sample number $n_\bullet$
χ	Mapping of the body $\mathcal{B}$
ψ	Free energy function (Chap. 2)
$\psi(\cdot)$	Functional/Polynomial
$\Psi(\boldsymbol{\sigma}, \mathbf{A})$	Flow potential (Chap. 2)
$\partial\Omega$	Boundary of the domain
Ω_0	Reference configuration
Ω	Current configuration

$\omega(\mathbf{x})$	Weighting function

Latin Symbols

$\mathbf{A}$, $\mathbf{a}$	Acceleration field in the reference and current configuration; Thermodynamical force
$\mathcal{B}$	Material (continuum) body
$\mathcal{B}^h$	Discretized continuum body
$\mathbf{B}$	$\mathbf{B}$-matrix
$\mathbf{b}$	Body force
$\mathrm{C}_{xx}(\cdot,\cdot)$	Autocovariance function
$\mathbf{C}$	Right Cauchy-Green tensor strain tensor
$\mathbb{C}$	Fourth-order material tensor
$C_{\bullet D}$	Covariance function with respect to the dimension $\bullet$
$c_\bullet$	Correlation length with respect to the coordinate $\bullet$
$\mathbf{d}$	Deformation rate tensor
$\mathcal{D}_{\mathrm{el}}$	Elastic domain
D^{pl}	Plastic dissipation function
$\mathbb{D}(\mathbf{x})$	Stochastic elasticity tensor
$\mathbf{E}$, $\mathbf{e}$	Orthogonal base system in the reference and current configuration
$\mathcal{E}(t)$	Thermal energy
e_{c}	Specific internal energy
$\mathbf{E}$	Green-Lagrange strain tensor
$\mathbf{e}$	Euler-Almansi strain tensor
E	Young's modulus
$E(\mathbf{x},\theta)$	Random Young's modulus
E	Event
$\mathbb{E}(\bullet)$	First moment (mean) of $\bullet$
$\mathcal{F}$	σ-Algebra
$\boldsymbol{\mathcal{F}}$	Block vector of the stochastic force field
$\mathbf{F}(\theta)$	Stochastic force field
$\mathbf{F}(\cdot,t)$	Deformation gradient
f	Deterministic yield function
$f(\theta)$	Stochastic yield function
f_X	Probability density function of X
F_X	Cumulative distribution function of X
f_{XY}	Joint probability density function of X and Y
F_{XY}	Joint cumulative probability distribution of X and Y
$f_{Y|x}(y)$	Conditional probability of Y given $X = x$
$\mathbf{f}^{e\,\mathrm{int}}$	Internal force of element e
$\mathbf{f}^{e\,\mathrm{ext}}$	External force of element e

$\mathbf{F}^{\text{int}}$	Global internal force
$\mathbf{F}^{\text{ext}}$	Global external force
f_i	i-th Eigenfunction of KLE
$\mathfrak{h}$	One-dimensional Hermite polynomial
$H(\cdot)$	Random field
$H_S(\cdot)$	Random field realized with SPRM
$\hat{H}(\cdot)$	Discretized random field
$\hat{H}_S(\cdot)$	Discretized random field realized with SPRM
H_{iso}	Isotropic hardening modulus
H_{kin}	Kinematic hardening modulus
$\mathbb{H}_{\text{iso}}(\mathbf{x}, \theta)$	Random isotropic hardening
$\mathbb{H}_{\text{kin}}(\mathbf{x}, \theta)$	Random kinematic hardening
$\mathbf{H}(\boldsymbol{\eta})$	Vector of the shape functions
$\mathbf{H}(\boldsymbol{\sigma}, \mathbf{A})$	Hardening variables
$\mathbf{h}$	Cauchy entropy flux
$\mathcal{L}^2$	Hilbert space
$\mathbf{1}$	Second-order identity tensor
$\mathbb{I}$	Fourth-order identity tensor
J	Jacobian matrix
$\mathbf{J}$	Angular momentum
J_2	Second invariant of the deviatoric stresses
$\mathbf{K}(\theta)$	Stochastic global stiffness matrix
$\mathcal{K}$	Block matrix consisting all stochastic global stiffness matrices
$\mathcal{K}(t)$	Kinetic energy
$\mathbf{k}^e$	Element stiffness matrix
$\mathbf{K}$	Global stiffness matrix
K	Bulk modulus
$\mathbb{K}$	Stochastic bulk modulus
$\mathfrak{l}(\theta)$	Log-normal random variable
$\mathbf{L}$	Impulse
$L_{\bullet_0}$	Period with respect to the coordinate $\bullet$ (Chap. 6)
M	Dimension of KLE
M'	Sub-Dimension of KLE
m	Mass
$\mathbf{M}$	External moments
$\mathbf{N}, \mathbf{n}$	Normal vector in the reference and current configuration
$\mathbf{N}(\boldsymbol{\sigma}, \mathbf{A})$	Flow vector
N_I	I-th Shape function
O	Origin of the coordinate system
P	Material point

$\mathcal{P}_{\mathrm{ext}}(t)$	External mechanical power
$\mathcal{P}_{\mathrm{int}}(t)$	Internal mechanical work
$\mathbf{P}$	1. Piola-Kirchhoff stress tensor
$\mathcal{P}(\cdot)$	Probability of an event E·
P	Polynomial chaos basis
p	Order of the polynomials of the Polynomial Chaos
$\mathcal{Q}(t)$	Thermal power
$\mathbf{q}$	Cauchy heat flux
q_n	Normal heat flux
$\mathbb{R}^3$	Euclidean space
$\mathcal{R}$	Residuum of the Newton-Raphson method
r	Heat source
$\mathcal{S}$	Hilbert space $\mathcal{L}^2(\Theta, \mathcal{F}, \mathcal{P})$
$\mathcal{S}^P$	Subspace of $\mathcal{S}$ spanned by the polynomial basis P
$S(\omega)$	Spectral density
$\mathcal{S}(t)$	Entropy
$\mathbf{S}$	2. Piola-Kirchhoff stress tensor
$\mathbf{s}$	Deviatoric stresses
s_X	Skewness (third moment) of X
$\mathbf{t}$	Chauchy vector
$\bar{\mathbf{t}}$	Traction boundary conditions
t_0	Initial time
$\mathbf{t}$	Surface load
$\mathbf{U}(\theta)$	Stochastic displacement field
$\boldsymbol{\mathcal{U}}$	Block vector of the stochastic displacement field
$\bar{\mathbf{u}}$	Displacement boundary conditions
$\mathbf{U}$, $\mathbf{u}$	Displacement field in the reference and current configuration
$\mathbf{V}$, $\mathbf{v}$	Velocity field in the reference and current configuration
$\mathcal{V}$	Deterministic space for the random solution
$\mathcal{V}^h$	Subspace of $\mathcal{V}$
∂W	Virtual work
X	Random variable
x	Value of a random variable X
$\boldsymbol{X}$	Random vector
$X(t)$	Stochastic process
$\mathcal{Y}$	Set of yield surfaces

Operators

$\mathcal{V} \otimes \mathcal{S}$	Tensor product space
$\langle \cdot, \cdot \rangle$	Inner product
Div, div	Divergenz in the reference and in the current configuration
Grad, grad	Gradient in the reference and in the current configuration
$\times$	Cross product
$\cdot$	Scalar product
:	Dual scalar product
$\otimes$	Tensor product
∂	Partial differential operator
$\boldsymbol{\delta}_\bullet$	(Vector-valued) Variation of $\bullet$
$\boldsymbol{\delta}_\bullet(\theta)$	(Vector-valued) stochastic Variation of $\bullet$
$\Delta \bullet$	Increment of $\bullet$
$\frac{\mathrm{d}}{\mathrm{d}t}(\bullet), \dot{\bullet}$	Time derivative of $\bullet$
$\bullet^{\mathrm{T}}$	Transpose of vector or matrix $\bullet$
sin, cos	Sine, cosine
$\| \bullet \|$	Norm of $\bullet$
$*$	Appropriate product operation (Chap. 2)
δ_{ij}	Kronecker delta
Π	Product operator
$\pm$	Addition/Subtraction of random variables
$\widehat{\pm}$	Projection of $\pm$ onto the Polynomial basis
$*$	Multiplication of random variables (Chap. 9)
$\widehat{*}$	Projection of $*$ onto the Polynomial basis
$\div$	Division of random variables
$\widehat{\div}$	Projection of $\div$ onto the Polynomial basis
sign	Sign function
$\delta(\bullet_1 - \bullet_2)$	Delta function
$\widehat{\bullet}(\theta)$	Approximation of the random variable $\bullet(\theta)$ (Chap. 9)
$\mathrm{tr}(\bullet)$	Trace of $\bullet$
$\cup$	Assembly process (Chaps. 3 and 8)

References

Adler, R. and Taylor, J. (2007). *Random Fields and Geometry*. Springer.

Alt, H. W. (2012). *Lineare Funktionalanalysis*. Springer, 6th edition.

Altenbach, H. (2012). *Kontinuumsmechanik. Einführung in die materialunabhängigen und materialabhängigen Gleichungen*. Springer-Verlag, 2 nd edition.

Anders, M. and Hori, M. (1999). Stochastic Finite Element Method For Elasto-Plastic Body. *International Journal for Numerical Methods in Engineering*, 46:1897–1916.

Anders, M. and Hori, M. (2001). Three-dimensional stochastic finite element method for elasto-plastic bodies. *International Journal for Numerical Methods in engineering*, 51:449–478.

Anders, M. S. (2000). *Application of Stochastic Finite Element Method to Non-Linear Elasto-Plastic Problems*. PhD thesis, University of Tokyo.

Anderson, T. W. (1958). *An introduction to multivariate statistical analysis*. Wiley.

Arnst, M. and R.Ghanem (2012). A variational-inequality approach to stochastic boundary value problems with inequality constraints and its application to contact and elastoplasticity. *International Journal for Numerical Methods in Engineering*, 89:1665–1690.

Augusti, G., Baratta, A., and Casciati, F. (1984). *Probabilistic methods in structural engineering*. Chapman and Hall.

Augustin, F., Gilg, A., Paffrath, M., Rentrop, P., and Wever, U. (2008). Polynomial chaos for the approximation of uncertainties: Chances and limits. *European Journal of Applied Mathematics*, 19:149–190.

Babuška, I. and Chatzipantelidis, P. (2002). On solving elliptic stochastic partial differential equations. *Computer Methods in Applied Mechanics and Engineering*, 191:4093–4122.

Babuška, I., Tempone, R., and Zouraris, G. (2004). Galerkin Finite Element Approximations of Stochastic Elliptic Partial Differential Equations. *SIAM Journal on Numerical Analysis*, 42:800–825.

Bathe, K.-J. (2002). *Finite-Elemente-Methoden*. Springer-Verlag.

Berveiller, M., Sudret, B., and Lemaire, M. (2004). Presentation of two methods for computing the response coefficients in stochastic finite element analysis. In *Proc. 9th ASCE specialty Conference on Probabilistic Mechanics and Structural Reliability, Albuquerque, USA*.

Berveiller, M., Sudret, B., and Lemaire, M. (2005). Non linear non intrusive stochastic element method - Application to a fracture mechanics problem. Technical report, Electricité de France, R&D Division.

Besson, J., Cailletaud, G., Chaboche, J.-L., Forest, S., and Blétry, M. (2010). *Nonlinear Mechanics of Materials*. Springer.

Betten, J. (2001). *Kontinuumsmechanik. Elastisches und inelastisches Verhalten isotroper und anisotroper Stoffe.* Springer-Verlag, 2. edition.

Blatman, G. (2009). *Adaptive sparse polynomial chaos expansions for uncertainty propagation and sensitivity analysis.* PhD thesis, Université Blaise Pascal, Clermont-Ferrand, France.

Blatman, G. and Sudret, B. (2008). Sparse polynomial chaos expansions and adaptive stochastic finite elements using a regression approach. *Comptes Rendus Mécanique*, 336:518–523.

Bocchini, P. and Deodatis, G. (2008). Critical review and latest developments of a class of simulation algorithms for strongly non-Gaussian random fields. *Probabilistic Engineering Mechanics*, 23:393–407.

Braess, D. (1992). *Finite Elemente. Theorie, schnelle Löser und Anwendungen in der Elastizitätstheorie.* Springer.

Bratley, P. and Fox, B. L. (1988). Algorithm 659: Implementing Sobol's quasirandom sequence generator. *ACM Transactions on Mathematical Software*, 17:88–100.

Bronshtein, I. N., Semendyayev, K. A., Musiol, G., and Muehlig, H. (2007). *Handbook of Mathematics*. Springer-Verlag, 5th edition.

Bucher, C. (2009). *Computational analysis of randomness in structural mechanics.* CRC Press/Taylor & Francis.

Burhenne, S., Jacob, D., and Henze, G. P. (2011). Sampling based on Sobol' sequences for Monte Carlo techniques applied to building simulations. In *Proceedings of Building Simulation 2011*.

Caflisch, R. E. (1998). Monte Carlo and quasi-Monte Carlo methods. *Acta Numerica*, 7:1–49.

Cai, G. Q. and Lin, Y. K. (1996). Generation of non-Gaussian stationary stochastic processes. *Physical Review E*, 54:299–303.

Cameron, R. H. and Martin, W. T. (1947). The Orthogonal Development of Non-Linear Functionals in Series of Fourier-Hermite Functionals. *Annals of Mathematics*, 48:385–392.

Chadwick, P. (1999). *Continuum Mechanics.* Dover Publications, INC.

Chakraborty, S. and Bhattacharyya, B. (2002). An efficient 3D stochastic finite element method. *International Journal of Solids and Structures*, 39:2465–2475.

Chen, N.-Z. and Soares, C. G. (2008). Spectral stochastic finite element analysis for laminated composite plates. *Computer Methods in Applied Mechanics and Engineering*, 197:4830–4839.

Chen, W.-F. and Han, D.-J. (2007). *Plasticity for Structural Engineers.* J. Ross Publishing.

Choi, S.-K., Grandhi, R. V., and Canfield, R. A. (2007). *Reliability-based Structural Design.* Springer-Verlag.

Christakos, G. (1992). *Random Field Models in Earth Sciences.* Academic Press, Inc.

Christensen, R., Johnson, W., Branscum, A., and E. Hanson, T. (2011). *Bayesian Ideas and Data Analysis. An Introduction for Scientists and Statisticians.* Taylor and Francis Group.

Christian, J. (2004). Geotechnical Engineering Reliability: How Well Do We Know What We Are Doing? *Journal of Geotechnical and Geoenvironmental Engineering*, 130:985–1003.

Chung, D. B., Gutiérrez, M. A., Graham-Brady, L. L., and Lingen, F.-J. (2005). Efficient numerical strategies for spectral stochastic finite element models. *International Journal for Numerical Methods in Engineering*, 64:1334–1349.

Contreras, H. (1980). The stochastic finite-element method. *Computers & Structures*, 12:341–348.

Crisfield, M. (1991). *Non-Linear Finite Element Analysis of Solids and Structures*. John Wiley & Sons.

de Boer, R. (1982). *Vektor- und Tensorrechnung für Ingenieure*. Springer Verlag.

de Borst, R., Crisfield, M. A., J.C. Remmers, J., and Verhoosel, C. V. (2012). *Non-linear finite element analysis of solids and structures*. John Wiley & Sons Ltd, 2 edition.

de Lima, B. S. and Ebecken, N. F. (2000). A comparison of models for uncertainty analysis by the finite element method. *Finite Elements in Analysis and Design*, 34:211–232.

Deb, M. K., Babuska, I. M., and Oden, J. T. (2001). Solution of stochastic partial differential equations using Galerkin finite element techniques. *Computer Methods in Applied Mechanics and Engineering*, 190:6359–6372.

Debusschere, B. J., Najm, H. N., Pébay, P. P., Knio, O. M., Ghanem, R. G., and Maître, O. P. L. (2005). Numerical Challenges in the Use of Polynomial Chaos Representations for Stochastic Processes. *SIAM Journal on Scientific Computing*, 26:698–719.

Deodatis, G. (1990). Bounds on Response Variability of Stochastic Finite Element Systems. *Journal of Engineering Mechanics*, 116:565–585.

Deodatis, G. (1991). Weighted Integral Method. I: Stochastic Stiffness Matrix. *Journal of Engineering Mechanics*, 117:1851–1864.

Deodatis, G. (1996a). Non-stationary stochastic vector processes: seismic ground motion applications. *Probabilistic Engineering Mechanics*, 11:149–167.

Deodatis, G. (1996b). Simulation of Ergodic Multivariate Stochastic Processes. *Journal of Engineering Mechanics*, 122:778–787.

Deodatis, G. (1997). Simulation of stochastic processes and fields to model loading and material uncertainties. In *Probabilistic Methods for Structural Design*. kluwer Academic Publishers.

Deodatis, G. and Micaletti, R. C. (2001). Simulation of Highly Skewed Non–Gaussian Stochastic Processes. *Journal of Engineering Mechanics*, 127:1284–1295.

Deodatis, G. and Shinozuka, M. (1989). Simulation of Seismic Ground Motion Using Stochastic Waves. *Journal of Engineering Mechanics*, 115:2723–2737.

Deodatis, G. and Shinozuka, M. (1991). Weighted Integral Method. II: Response Variability and Reliability. *Journal of Engineering Mechanics*, 117:1865–1877.

Ditlevsen, O. and Madsen, H. (2007). *Structural Reliability Methods*. http://od-website.dk/books/OD-HOM-StrucRelMeth-Ed2.3.7.pdf, 2.3.7 internet edition.

Dobrowolski, M. (2010). *Angewandte Funktionsanalysis.* Springer.

Espig, M., Hackbusch, W., Litvinenko, A., Matthies, H. G., and Wähnert, P. (2014). Efficient low-rank approximation of the stochastic Galerkin matrix in tensor formats. *Computers & Mathematics with Applications*, 67(4):818–829.

Eveleigh, L. J. (1996). Fourier transform and signal manipulation. In *Data Handling in Science and Technology*, volume 18, chapter 1, pages 1–24. Elsevier.

Field Jr., R. and Grigoriu, M. (2004). On the accuracy of the polynomial chaos approximation. *Probabilistic Engineering Mechanics*, 19:65–80.

Field Jr., R. and Grigoriu, M. (2007). Model Selection in Applied Science and Engineering: A Decision-Theoretic Approach. *Journal of Engineering Mechanics*, 133:780–791.

Fishman, G. S. (1996). *Monte Carlo. Concepts, Algorithms, and Applications.* Springer-Verlag.

Florian, A. (1992). An efficient sampling scheme: Updated Latin Hypercube Sampling. *Probabilistic Engineering Mechanics*, 7:123–130.

Fox, B. L. (1999). *Strategies for Quasi-Monte Carlo.* Kluwer Academic Publishers.

Frauenfelder, P., Schwab, C., and Todor, R. A. (2005). Finite elements for elliptic problems with stochastic coefficients. *Computer methods in applied mechanics and engineering*, 194:205–228.

Funaro, D. (1992). *Polynomial Approximation of Differential Equations.* Springer.

Gardiner, C. (2009). *Handbook of Stochastic Methods for Physics, Chemistry and the Natural Sciences.* Springer-Verlag.

Gautschi, W. (2004). *Orthogonal Polynomials. Computation and Approximation.* Oxford University Press.

Geistefeldt, J. (2003). *Stochastische Finite-Element-Methoden mit Anwendung auf aerolastische Tragsysteme.* PhD thesis, Institut für Statik, Technische Universität Braunschweig.

Ghanem, R. (1999). Stochastic Finite Elements with Multiple Random Non-Gaussian Properties. *Journal of Engineering Mechanics*, 125:26–40.

Ghanem, R. and Dham, S. (1998). Stochastic Finite Element Analysis for Multiphase Flow in Heterogeneous Porous Media. *Transport in Porous Media*, 32:239–262.

Ghanem, R. and Spanos, P. (1989). Polynomial Chaos in Stochastic Finite Elements. *Journal of Applied Mechanics*, 57:197–202.

Ghanem, R. and Spanos, P. (2003). *Stochastic Finite Elements: A Spectral Approach.* Dover Publications, INC . Revised edition of the originally work, by Springer-Verlag, in 1991.

Ghanem, R. G. and Kruger, R. M. (1996). Numerical solution of spectral stochastic finite element systems. *Computer Methods in Applied Mechanics and Engineering*, 129:289–303.

Goodman, L. A. (1960). On the Exact Variance of Products. *Journal of the American Statistical Association*, 55:708–713.

Grigoriu, M. (1993). On the spectral representation method in simulation. *Probabilistic Engineering Mechanics*, 8:75–90.

Grigoriu, M. (2000a). A spectral representation based model for Monte Carlo simulation. *Probabilistic Engineering Mechanics*, 15:365–370.

Grigoriu, M. (2000b). Non-Gaussian models for stochastic mechanics. *Probabilistic Engineering Mechanics*, 15:15–23.

Gurtin, M. E. (1981). *An Introduction to Continuum Mechanics*. Academic Press, INC.

Gutiérrez, M. A. and Krenk, S. (2004). *Stochastic Finite Element Methods. Encyclopedia of Computational Mechanics*, chapter 20, pages 657–681. John Wiley & Sons, Ltd.

Haldar, A. and Mahadevan, S. (2000). *Reliability Assessment using Stochastic Finite Element Analysis*. John Wiley & Sons.

Halton, J. (1960). On the efficiency of certain quasi-random sequences of points in evaluating multi-dimensional integrals. *Numererische Mathematik*, 2:84–90.

Hanss, M. (2005). *Applied Fuzzy Arithmetic. An Introduction with Engineering Applications*. Springer.

Haupt, P. (2000). *Continuum Mechanics and Theory of Materials*. Springer-Verlag.

Helton, J. and Davis, F. (2003). Latin hypercube sampling and the propagation of uncertainty in analyses of complex systems. *Reliability Engineering & System Safety*, 81:23–69.

Helton, J. C., Johnson, J. D., Oberkampf, W., and Sallaberry, C. (2008). Representation of Analysis Results Involving Aleatory and Epistemic Uncertainty. Technical report, Sandia National Laboratories.

Hill, R. (1948). A Variational Principle of Maximum Plastic Work in Classical Plasticity. *The Quarterly Journal of Mechanics and Applied Mathematics*, 1:18–28.

Hill, R. (1950). *The Mathematical Theory of Plasticity*. Oxford University Press.

Holzapfel, G. A. (2000). *Nonlinear Solid Mechanics*. John Wiley & Sons Ltd.

Horstemeyer, M. F. and Bammann, D. J. (2010). Historical review of internal state variable theory for inelasticity. *International Journal of Plasticity*, 26:1310–1334.

Huang, S. P., Quek, S. T., and Phoon, K. K. (2001). Convergence study of the truncated Karhunen–Loève expansion for simulation of stochastic processes. *International Journal for Numerical Methods in Engineering*, 52:1029–1043.

Hughes, T. J. R. (2000). *The Finite Element Method: Linear Static and Dynamic Finite Element Analysis*. Dover Pubn Inc.

Ibrahimbegovic, A. (2006). *Nonlinear Solid Mechanics. Theoretical Formulations and Finite Element Solution Methods*. Springer.

Iman, R. L. and Conover, W. (1980). Small sample sensitivity analysis techniques for computer models.with an application to risk assessment. *Communications in Statistics - Theory and Methods*, 9:1749–1842.

Iman, R. L. and Conover, W. J. (1982). A distribution-free approach to inducing rank correlation among input variables. *Communications in statistics. Simulation and computation*, 11:311–334.

Itskov, M. (2009). *Tensor Algebra and Tensor Analysis for Engineers. With Applications to Continuum Mechanics*. Springer, second edition edition.

Jablonski, P. (2014). *Numerische Simulation probabilistischer Schädigungsmodelle mit der Stochastischen Finite Elemente Methode*. PhD thesis, Institut für Baumechanik und numerische Mechanik, Leibniz Universität Hannover. In Print.

Jeremić, B. and Sett, K. (2009). On probabilistic yielding of materials. *Communications in numerical Methods in Engineering*, 25:291–300.

Jeremić, B., Sett, K., and Kavvas, M. L. (2007). Probabilistic elasto-plasticity: formulation in 1D. *Acta Geotechnica*, 2:197–210.

Kavvas, M. L. (2003). Nonlinear Hydrologic Processes: Conservation Equations for Determining Their Means and Probability Distributions. *Journal of Hydrologic Engieneering*, 8:44–53.

Keese, A. (2004). *Numerical Solution of systems with Stochastic Uncertainties - A General Purpose Framework for Stochastic Finite Elements*. PhD thesis, Technische Universität Braunschweig.

Khintchine, A. (1934). Korrelationstheorie der stationären stochastischen Prozesse. *Mathematische Annalen*, 109:604–615.

Kiureghian, A. D. and Ditlevsen, O. (2009). Aleatory or epistemic? Does it matter? *Structural Safety*, 31:105–112.

Kiureghian, A. D. and Ke, J.-B. (1988). The stochastic finite element method in structural reliability. *Probabilistic Engineering Mechanics*, 3:83–91.

Kleiber, M. and Hien, T. (1992). *The Stochastic Finite Element Element Method. Basic Perturbation Technique and Computer Implementation*. John Wiley & Sons.

Kojic, M. and Bathe, K.-J. (2005). *Inelastic Analysis of Solids and Structures*. Springer-Verlag.

Kriegesmann, B. (2012). *Probabilistic Design of Thin-Walled Fiber Composite Structures*. PhD thesis, Gottfried Wilhelm Leibniz Universität Hannover.

Lawrence, M. (1989). An Introduction to Reliability Methods. In *Computational Mechanics of Probabilistic and Reliability Analysis*. Elmepress International.

Lawrence, M. A. (1987). Basis Random Variables in Finite Element Analysis. *International Journal for Numerical Methods in Engineering*, 24:1849–1863.

Le Maître, O. P. and Knio, O. M. (2010). *Spectral Methods for Uncertainty Quantification*. Springer.

L'Ecuyer, P. and Lemieux, C. (2005). *Recent Advances in Randomized Quasi-Monte Carlo Methods. Modeling Uncertainty. An Examination of Stochastic Theory, Methods, and Applications*, chapter 20, pages 419–474. Springer Science + Business Media, Inc.

Lemaitre, J. and Chaboche, J.-L. (1990). *Mechanics of solid materials*. Cambridge University Press.

Lemieux, C. (2009). *Monte Carlo and Quasi-Monte Carlo Sampling*. Spinger.

Li, C. and Der Kiureghian, A. (1993). Optimal Discretization of Random Fields. *Journal of Engineering Mechanics*, 119:1136–1154.

Li, R. and Ghanem, R. (1998). Adaptive Polynomial Chaos Expansions Applied to Statistics of Extremes in Nonlinear Random Vibration. *Journal of Computational Physics*, 13:125–136.

Liu, W. K., Belytschko, T., and Mani, A. (1986a). Probabilistic finite elements for nonlinear structural dynamics. *Computer Methods in Applied Mechanics and Engineering*, 56:61–81.

Liu, W. K., Belytschko, T., and Mani, A. (1986b). Random field finite elements. *International Journal for Numerical Methods in Engineering*, 23:1831–1845.

Liu, W. K., Mani, A., and Belytschko, T. (1987). Finite element methods in probabilistic mechanics. *Probabilistic Engineering Mechanics*, 2:201–213.

Loève, M. (1977). *Probability Theory I.* Springer-Verlag, 4th edition edition.

Lubliner, J. (2008). *Plasticity Theory.* Dover Publications.

Lutz, A. (2011). *Ein integrales Modellierungskonzept zur numerischen Simulation der Osseointegration und Langzeitstabilität von Endoprothesen.* PhD thesis, Gottfried Wilhelm Leibniz Universität Hannover.

Marzouk, Y. M., Najm, H. N., and Rahn, L. A. (2007). Stochastic spectral methods for efficient Bayesian solution of inverse problems. *Journal of Computational Physics*, 224:560–586.

Matheron, G. (1989). *Estimating and choosing: An essay on probability in practice.* Springer-Verlag.

Matoušek, J. (1998). On the L_2-discrepancy for anchored boxes. *Journal of Complexity*, 14:527–556.

Matthies, H. G., Brenner, C. E., Bucher, C. G., and Soares, C. G. (1997). Uncertainties in probabilistic numerical analysis of structures and solids - Stochastic finite elements. *Structural Safety*, 19:283–336.

Matthies, H. G. and Bucher, C. (1999). Finite elements for stochastic media problems. *Computer Methods in Applied Mechanics and Engineering*, 168:3–17.

Mckay, M. D., Beckman, R. J., and Conover, W. J. (1979). A Comparison of Three Methods for Selecting Values of Input Variables in the Analysis of Output from a Computer Code. *Technometrics*, 21:239–245.

Mises, R. v. (1913). Mechanik der festen Körper im plastisch-deformablen Zustand. *Nachrichten von der Gesellschaft der Wissenschaften zu Göttingen, Mathematisch-Physikalische Klasse*, 1913:582–592.

Moens, D. and Vandepitte, D. (2005). A survey of non-probabilistic uncertainty treatment in finite element analysis. *Computer Methods in Applied Mechanics and Engineering*, 194:1527–1555.

Montgomery, D. C. and Runger, G. C. (1994). *Applied Statistics and Probability for Engineers.* John Wiley & Sons, Inc.

Morokoff, W. J. (1998). Generating Quasi-Random Paths for Stochastic Processes. *SIAM Review*, 40:765–788.

Morokoff, W. J. and Caflisch, R. E. (1993). A quasi-Monte Carlo approach to particle simulation of the heat equation. *SIAM Journal on Numerical Analysis*, 30:1558–1573.

Morokoff, W. J. and Caflisch, R. E. (1994). Quasi-Random Sequences and Their Discrepancies. *SIAM Journal on Scientific Computing*, 15:1251–1279.

Morokoff, W. J. and Caflisch, R. E. (1995). Quasi-Monte Carlo Integration. *Journal of Computational Physics*, 122:218–230.

Najm, H. N. (2009). Uncertainty Quantification and Polynomial Chaos Techniques in Computational Fluid Dynamics. *Annual Review of Fluid Mechanics*, 41:35–52.

Neto, E. d. S., Perić, D., and Owen, D. (2008). *Computational Methods for Plasticity: Theory and Applications*. John Wiley & Sons Ltd.

Niederreiter, H. (1988). Low-discrepancy and low-dispersion sequences. *Journal of Number Theory*, 30:51–70.

Niederreiter, H. (1992). *Random number generation and quasi-Monte Carlo methods*. Society for Industrial and Applied Mathematics.

Nouy, A. (2009). Recent Developments in Spectral Stochastic Methods for the Numerical Solution of Stochastic Partial Differential Equations. *Archives of Computational Methods in Engineering*, 16:251–285.

Oberkampf, W. L., DeLand, S. M., Rutherford, B. M., Diegert, K. V., and Alvin, K. F. (2002a). Error and uncertainty in modeling and simulation. *Reliability Engineering & System Safety*, 75:333–357.

Oberkampf, W. L., Trucano, T. G., and Hirsch, C. (2002b). Verification, validation and predictive capability in computational engineering and physics. In *Hopkins University*.

Oden, J., Belytschko, T., Babuska, I., and Hughes, T. (2003). Research directions in computational mechanics. *Computer Methods in Applied Mechanics and Engineering*, 192:913–922.

Oden, J. T. and Reddy, J. N. (2011). *An Introduction to the Mathematical Theory of Finite Elements*. Dover Publications.

Owen, A. B. (1994). Randomly Permuted (t,m,s)-Nets and (t,s)-Sequences. Technical report, Department of Statistics. Stanford University.

Papadrakakis, M. and Kotsopulos, A. (1999). Parallel solution methods for stochastic finite element analysis using Monte Carlo simulation. *Computer Methods in Applied Mechanics and Engineering*, 168:305–320.

Papoulis, A. (1991). *Probability, Random Variables and Stochastic Processes*. McGraw-Hill, Inc., third edition edition.

Phoon, K., Huang, H., and Quek, S. (2004). Comparison between Karhunen–Loève and wavelet expansions for simulation of Gaussian processes. *Computers & Structures*, 82:985–991.

Phoon, K., Huang, S., and Quek, S. (2002a). Implementation of Karhunen–Loève expansion for simulation using a wavelet-Galerkin scheme. *Probabilistic Engineering Mechanics*, 17:293–303.

Phoon, K., Huang, S., and Quek, S. (2002b). Simulation of second-order processes using Karhunen–Loeve expansion. *Computers & Structures*, 80:1049–1060.

Poles, S. and Lovison, A. (2009). A polynomial chaos approach to robust multiobjective optimization. In *Hybrid and robust approaches to multiobjective optimization, Schloss Dagstuhl—Leibniz-Zentrum fuer Informatik, Germany, Dagstuhl, Germany, Dagstuhl seminar proceedings*.

Popescu, R., Deodatis, G., and Prevost, J. (1998). Simulation of homogeneous non-Gaussian stochastic vector fields. *Probabilistic Engineering Mechanics*, 13:1–13.

Rackwitz, R. and Flessler, B. (1978). Structural reliability under combined random load sequences. *Computers & Structures*, 9:489–494.

Ramadan, O. and Novak, M. (1993). Simulation of Spatially Incoherent Random Ground Motions. *Journal of Engineering Mechanics*, 119:997–1016.

Rinne, H. (2009). *The Weibull Distribution*. Chapman & Hall/CRC.

Rosić, B. (2013). *Variational Formulations and Functional Approximation Algorithms in Stochastic Plasticity of Materials*. PhD thesis, Technische Universität Braunschweig.

Rosić, B. and Matthies, H. (2008). Computational Approaches to Inelastic Media with Uncertain Parameters. *Journal of Serbian Society for Computational Mechanics*, 2:28–43.

Rosić, B., Matthies, H., and Živković, M. (2010). Mathematical Formulation and Numerical Simulation of Stochastic Elastoplastic Behaviour. ECCM European Conference on Computational Mechanics, Paris.

Rosić, B. V. and Matthies, H. G. (2012). Stochastic Plasticity - A Variational Inequality Formulation and Functional Approximation Approach. The Linear Case. Technical report, Technical University Braunschweig, Institute of Scientific Computing.

Rösler, J., Harders, H., and Bäker, M. (2008). *Mechanisches Verhalten der Werkstoffe*. Vieweg+Teubner Verlag, 3rd edition.

Rubinstein, R. Y. and Kroese, D. P. (2008). *Simulation and the Monte Carlo method*. Wiley, 2. ed. edition.

Sachdeva, S. K., Nair, P. B., and Keane, A. J. (2006). Comparative study of projection schemes for stochastic finite element analysis. *Computer Methods in Applied Mechanics and Engineering*, 195:2371–2392.

Sakamoto, S. and Ghanem, R. (2002). Simulation of multi-dimensional non-Gaussian non-stationary random fields. *Probabilistic Engineering Mechanics*, 17:167–176.

Schade, H. and Neemann, K. (2009). *Tensoranalysis*. de Gruyter.

Scheiwiller, A. (1999). Informationsverknüpfung im Bauwesen. Eine Anwendung der Bayes'schen Methode auf die Ingenieurproblematik. Technical report, ETH Zürich, Institut für Baustatik und Konstruktion.

Schenk, C. A. and Schuëller, G. I. (2005). *Uncertainty Assemssment of Large Element Systems*. Springer-Verlag.

Schmidt, G. (2013). Simulation von linear-elastischem Materialverhalten durch eine Kombinierung von Karhunen-Loève und dem Polynomial Chaos. Bachelorarbeit, Leibniz Universität Hannover.

Schoutens, W. (2000). *Stochastic Processes and Orthogonal Polynomials*. Springer-Verlag.

Schuëller, G. (1997). A State-of-the-Art Report on Computational Stochastic Mechanics. *Probabilistic Engineering Mechanics*, 12:197–321.

Schwab, C. and Todor, R. A. (2006). Karhunen-Loève Approximation of Random Fields by Generalized Fast Multipole Methods. Technical report, Seminar für Angewandte Mathematik. Eidgenössische Technische Hochschule Zürich.

Sett, K. (2007). *Probabilistic Elasto-Plasticity and Its Application in Finite Element Simulations of Stochastic Elastic-Plastic Boundary Value Problems*. PhD thesis, University of California.

Sett, K. and Jeremić, B. (2010). Probabilistic Yielding and Cyclic Behavior of Geomaterials. *Int. J. Numer. Anal. Meth. Geomech.*, 34:1541–1559.

Sett, K., Jeremić, B., and Kavvas, M. L. (2007a). Probabilistic elasto-plasticity: solution and verification in 1D. *Acta Geotechnica*, 2:211–220.

Sett, K., Jeremić, B., and Kavvas, M. L. (2007b). The role of nonlinear hardening/softening in probabilistic elasto-plasticity. *International Journal for Numerical and Analytical Methods in Geomechanics*, 31:953–975.

Sett, K., Jeremić, B., and Kavvas, M. L. (2011). Stochastic elastic-plastic finite elements. *Computer Methods in Applied Mechanics and Engineering*, 200:997–1007.

Shabana, A. A. (2008). *Computational Continuum Mechanics*. Cambridge University Press.

Shackelford, J. F. (2000). *Introduction to materials science for engineers*. Prentice-Hall, Inc., Fifth edition.

Shi, Y. and Deodatis, G. (2004). A novel approach for the simulation of non-Gaussian fields: Application in Estimating Wire Strengths From Experimental Data. In *Proceedings of the 9th Joint Special Conference on Structural Safety and Reliability*.

Shinozuka, M. and Deodatis, G. (1988). Response Variability of stochastic finite element systems. *Journal of Engineering Mechanics*, 114:499–519.

Shinozuka, M. and Deodatis, G. (1991). Simulation of stochastic processes by spectral representation. *Applied Mechanics Reviews*, 44:191–204.

Shinozuka, M. and Deodatis, G. (1996). Simulation of Multi-Dimensional Gaussian Stochastic Fields by Spectral Representation. *Applied Mechanics Reviews*, 29-53:29.

Shinozuka, M. and Jan, C.-M. (1972). Digital Simulation of Random Processes and its Applications. *Journal of Sound and Vibration*, 25:111–128.

Shinozuka, M. and Lenoe, E. (1976). A probabilistic model for spatial distribution of material properties. *Engineering Fracture Mechanics*, 8:217–227.

Simo, J. and Hughes, T. (1998). *Computational Inelasticity*. Springer.

Sivia, D. and J.Skilling (2006). *Data Analysis. A Bayesian Tutorial*. Oxford University Press, second edition.

Sobol', I. (1967). On the distribution of points in a cube and the approximate evaluation of integrals. *USSR Computational Mathematics and Mathematical Physics*, 7:86–112.

Sobol', I. M. (1994). *A primer for the Monte Carlo method*. CRC Press, Inc.

Spanos, P. and Ghanem, R. (1989). Stochastic Finite Element Expansion for Random Media. *Journal of Engineering Mechanics*, 115:1035–1053.

Springer, M. D. (1979). *The Algebra of Random Variables*. John Wiley & Sons.

Stark, H. and Woods, J. W. (1986). *Probability, random processes, and estimation theory for engineers*. Prentice-Hall.

Stefanou, G. (2011). Response variability of cylindrical shells with stochastic non-Gaussian material and geometric properties. *Engineering Structures*, 33:2621–2627.

Stefanou, G. and Papadrakakis, M. (2004). Stochastic finite element analysis of shells with combined random material and geometric properties. *Computer Methods in Applied Mechanics and Engineering*, 193:139–160.

Stefanou, G. and Papadrakakis, M. (2007). Assessment of spectral representation and Karhunen–Loève expansion methods for the simulation of Gaussian stochastic fields. *Computer Methods in Applied Mechanics and Engineering*, 196:2465–2477.

Stein, M. (1987). Large Sample Properties of Simulations Using Latin Hypercube Sampling. *Technometrics*, 29:143–151.

Stoer, J. and Bulirsch, R. (2002). *Introduction to numerical analysis*. Springer.

Sudret, B. (2007). *Uncertainty propagation and sensitivity analysis in mechanical models Contributions to structural reliability and stochastic spectral methods*. Habilitation thesis, Université Blaise Pascal.

Sudret, B., Berveiller, M., and Lemaire, M. (2003). Application of a Stochastic Finite Element Procedure to Reliability Analysis. Technical report, Electricité de France, R&D Division, Site des Renardieres and Institute Francais de Mecanique Avancee, LaRAMA, Campus des Cezeaux.

Sudret, B., Berveiller, M., and Lemaire, M. (2006). A stochastic finite element procedure for moment and reliability analysis. *European Journal of Computational Mechanics*, 15:825–866.

Sudret, B. and der Kiureghian, A. (2000). Stochastic Finite Element Methods and Reliability. A State-of-the-Art Report. Technical Report UCB/SEMM-2000/08, Department of Civil & Environmental Engineering University of California, Berkeley.

Sundararajan, C., editor (1995). *Probabilistic Structural Mechanics Handbook*. Chapman & Hall.

Tabachnick, B. G. and Fidell, L. S. (2013). *Using Multivariate Statistics*. Pearson, 6th edition.

Takada, T. (1990a). Weighted integral method in multi-dimensional stochastic finite element analysis. *Probabilistic Engineering Mechanics*, 5:158–166.

Takada, T. (1990b). Weighted integral method in stochastic finite element analysis. *Probabilistic Engineering Mechanics*, 5:146–156.

van Kampen, N. G. (2007). *Stochastic Processes in Physics and Chemistry*. Elsevier B.V.

Vanmarcke, E. (2010). *Random Fileds. Analysis and Synthesis*. World Scientific Publishing Co. Pte. Ltd.

Vanmarcke, E. and Grigoriu, M. (1983). Stochastic Finite Element Analysis of Simple Beams. *Journal of Engineering Mechanics*, 109:1203–1214.

Vanmarcke, E., Shinozuka, M., Nakagiri, S., Schuëller, G., and Grigoriu, M. (1986). Random fields and stochastic finite elements. *Structural Safety*, 3:143–166.

Wand, M. and Jones, M. (1995). *Kernel Smoothing*. Chapman & Hill.

Werner, D. (2011). *Funktionalanalysis*. Springer.

Wiener, N. (1938). The Homogeneous Chaos. *American Journal of Mathematics*, 60:897–936.

Wriggers, P. (2008). *Nonlinear Finite Element Methods*. Springer-Verlag.

Xiu, D. (2009). Fast Numerical Methods for Stochastic Computations: A Review. *Communications in Computational Physics*, 5:242–272.

Xiu, D. (2010). *Numerical Methods for Stochastic Computations. A Spectral Method Approach*. Princeton University Press.

Xiu, D. and Karniadakis, G. E. (2002). The Wiener–Askey Polynomial Chaos for Stochastic Differential Equations. *SIAM Journal on Scientific Computing*, 24:619–644.

Xiu, D. and Karniadakis, G. E. (2003). Modeling uncertainty in flow simulations via generalized polynomial chaos. *Journal of Computational Physics*, 187:137–167.

Xiu, D. and Tartakovsky, D. M. (2006). Numerical methods for differential equations in random domains. *SIAM Journal on Scientific Computing*, 28:1167–1185.

Yamazaki, F. and Shinozuka, M. (1988). Digital Generation of non-Gaussian Stochastic Fields. *Journal of Engineering Mechanics*, 114:1183–1197.

Yamazaki, F., Shinozuka, M., and Dasgupta, G. (1988). Neumann Expansion for Stochastic Finite Element Analysis. *Journal of Engineering Mechanics*, 114:1335–1354.

Zhang, J. and Ellingwood, B. (1994). Orthogonal Series Expansions of Random Fields in Reliability Analysis. *Journal of Engineering Mechanics*, 120:2660–2677.

Zhu, W., Ren, Y., and Wu, W. (1992). Stochastic FEM Based on Local Averages of Random Vector Fields. *Journal of Engineering Mechanics*, 118:496–511.

Zienkiewicz, O. C. and Taylor, R. L. (2000). *The Finte Element Method. Volume 1: The Basis*, volume Fifth edition. Butterworth-Heinemann.

Curriculum vitae

Personal Information

Sebastian Fink

Born on March 7th, 1982 in Hildesheim, Germany

School Education

08/1988–06/1992	Grundschule Haste
08/1992–07/1994	Orientierungsstufe Bad Nenndorf
09/1994–07/1998	Kooperative Gesamtschule Barsinghausen

Professional Training

08/1998–01/2002	Professional training as industrial mechanic, Standortverwaltung Nienburg. **Degree**: Craft certificate as industrial mechanic
02/2002–07/2002	Working as industrial mechanic, Standortverwaltung Nienburg.

Social Work

08/2002–05/2003	Civilian service, Deutsches Rotes Kreuz, Springe

School Education

08/2003–07/2004	Fachoberschule Technik, Hannover

University Education

09/2004–10/2008	Diploma studies in the field: Computational Mechanics in Mechanical Engineering. **Degree**: Dipl.-Ing (FH)

Professional Experience

11/2008–03/2014	Research Assistant at Institute of Mechanics and Computational Mechanics, Leibniz Universität Hannover, Germany

Research and seminar reports

Institut für Baumechanik und Numerische Mechanik
Gottfried Wilhelm Leibniz Universität Hannover

Reports that have been published so far:

S 73/1   Seminar über Thermodynamik und Kontinuumsmechanik, Hannover 1973

F 75/1   "Die Spannungsberechnung im Rahmen der Finite–Element–Methode",
R. Ahmad, Dissertation, April 1975

F 76/1   "Zur Theorie und Anwendung der Stoffgleichungen elastisch–plastisch–viskoser Werkstoffe",
H. Mentlein, Dissertation, April 1976

S 77/1   Seminar über lineare und geometrisch nichtlineare Schalentheorie einschließlich Stabilitätstheorie, Hannover 1977

F 77/2   "Beitrag zur Berechnung von Gründungsplatten mit Hilfe der Finite–Element–Methode",
H. Meyer, Dissertation, Juli 1977

F 77/3   "Zur Berechnung der Eigenfrequenzen und Eigenschwingungsformen räumlich vorgekrümmter und vorverwundener Stäbe",
J. Möhlenkamp, Dissertation, Dezember 1977

F 77/4   "Zur Theorie und Berechnung geometrisch und physikalisch nichtlinearer Kontinua mit Anwendung der Methode der finiten Elemente",
J. Paulun, Dissertation, Dezember 1977

S 78/1   2. Seminar über Thermodynamik und Kontinuumsmechanik,
Hannover 1978

F 79/1   "Theoretische und numerische Behandlung geometrisch nichtlinearer viskoplastischer Kontinua",
K.–D. Klee, Dissertation, Februar 1979

F 79/2   "Zur Konstruierbarkeit von Variationsfunktionalen für nichtlineare Probleme der Kontinuumsmechanik",
J. Siefer, Dissertation, Oktober 1979

F 80/1   "Theoretische und numerische Behandlung gerader Stäbe mit endlichen Drehungen",
M. Kessel, Dissertation, Februar 1980

F 81/1   "Zur Berechnung von Kontakt– und Stoßproblemen elastischer Körper mit Hilfe der Finite–Element–Methode",
P. Wriggers, Dissertation, Januar 1981

F 81/2   "Stoffgleichungen für Steinsalze unter mechanischer und thermischer Beanspruchung",
J. Olschewski, E. Stein, W. Wagner, D. Wetjen, geänderte Fassung eines Zwischenberichtes zum BMFT–Forschungsvorhaben KWA 1608/5

F 82/1   "Konvergenz und Fehlerabschätzung bei der Methode der Finiten Elemente",
R. Rohrbach, E. Stein, Abschlußbericht eines VW–Forschungsvorhabens, Februar 1982

F 82/2   "Alternative Spannungsberechnung in Finite–Element–Verschiebungsmodellen",
C. Klöhn, Dissertation, November 1982

F 83/1   Seminar über nichtlineare Stabtheorie, Hannover 1983

F 83/2   "Beiträge zur nichtlinearen Theorie und inkrementellen Finite–Element– Berechnung dünner elastischer Schalen",
A. Berg, Dissertation, Juli 1983

F 83/3   "Elastoplastische Plattenbiegung bei kleinen Verzerrungen und großen Drehungen",
J. Paulun, Habilitation, September 1983

F 83/4   "Geometrisch nichtlineare FE–Berechnung von Faltwerken mit plastisch / viskoplastischem Deformationsverhalten",
M. Krog, Dissertation, Dezember 1983

F 85/1   Verleihung der Ehrendoktorwürde des Fachbereichs Bauingenieur– und Vermessungswesen der Universität Hannover an die Herren Prof. Dr. Drs. h.c. J.H. Argyris, Dr.–Ing. H.Wittmeyer

F 85/2   "Eine geometrisch nichtlineare Theorie schubelastischer Schalen mit Anwendung auf Finite–Element–Berechnungen von Durchschlag– und Kontaktproblemen",
W. Wagner, Dissertation, März 1985

F 85/3   "Geometrisch/physikalisch nichtlineare Probleme — Struktur und Algorithmen — ",
GAMM–Seminar im Februar 1985 in Hannover

F 87/1   "Finite–Elemente–Berechnungen ebener Stabtragwerke mit Fließgelenken und großen Verschiebungen",
R.Kahn, Dissertation, Oktober 1987

F 88/1   "Theorie und Numerik schubelastischer Schalen mit endlichen Drehungen unter Verwendung der Biot–Spannungen",
F. Gruttmann, Dissertation, Juni 1988

F 88/2   "Optimale Formgebung von Stabtragwerken mit Nichtlinearitäten in der Zielfunktion und in den Restriktionen unter Verwendung der Finite-Element-Methode",
V. Berkhahn, Dissertation, Oktober 1988

F 88/3   "Beiträge zur Theorie und Numerik großer plastischer und kleiner elastischer Deformationen mit Schädigungseinfluß",
R. Lammering, Dissertation, November 1988

F 88/4   "Konsistente Linearisierungen in der Kontinuumsmechanik und ihrer Anwendung auf die Finite–Elemente–Methode",
P. Wriggers, Habilitation, November 1988

F 88/5   "Mathematische Formulierung und numerische Methoden für Kontaktprobleme auf der Grundlage von Extremalprinzipien",
D. Bischoff, Habilitation, Dezember 1988

F 88/6   "Zur numerischen Behandlung thermomechanischer Prozesse",
C. Miehe, Dissertation, Dezember 1988

F 89/1   "Zur Stabilität und Konvergenz gemischter finiter Elemente in der linearen Elastizitätstheorie",
R. Rolfes, Dissertation, Juni 1989

F 89/2   "Traglastberechnungen von Faltwerken mit elastoplastischen Deformationen",
K.-H. Lambertz, Dissertation, Oktober 1989

F 89/3   "Transientes Kriechen und Kriechbruch im Steinsalz",
U. Heemann, Dissertation, November 1989

F 89/4   "Materialgesetze zum Verhalten von Betonkonstruktionen bei harten Stößen",
E. Stein, P. Wriggers, T. Vu Van & T. Wedemeier, Dezember 1989

F 89/5   "Lineare Konstruktion und Anwendungen von Begleitmatrizen",
C. Carstensen, Dissertation, Dezember 1989

F 90/1   "Zur Berechnung prismatischer Stahlbetonbalken mit verschiedenen Querschnittsformen für allgemeine Beanspruchungen",
H. N. Lucero–Cimas, Dissertation, April 1990

F 90/2   "Zur Behandlung von Stoß- Kontaktproblemen mit Reibung unter Verwendung der Finite–Element–Methode",
T. Vu Van, Dissertation, Juni 1990

F 90/3   "Netzadaption und Mehrgitterverfahren für die numerische Behandlung von Faltwerken",
L. Plank, Dissertation, September 1990

F 90/4   "Beiträge zur Theorie und Numerik finiter inelastischer Deformationen",
N. Müller–Hoeppe, Dissertation, Oktober 1990

F 90/5   "Beiträge zur Theorie und Numerik von Materialien mit innerer Reibung am Beispiel des Werkstoffes Beton", T. Wedemeier, Dissertation, Oktober 1990

F 91/1   "Zur Behandlung von Stabilitätsproblemen der Elastostatik mit der Methode der Finiten Elemente", W. Wagner, Habilitation, April 1991

F 91/2   "Mehrgitterverfahren und Netzadaption für lineare und nichtlineare statische Finite–Elemente–Berechnungen von Flächentragwerken", W. Rust, Dissertation, Oktober 1991

F 91/3   "Finite Elemente Formulierungen im Trefftzschen Sinne für dreidimensionale anisotrop–elastische Faserverbundstrukturen", K. Peters, Dissertation, Dezember 1991

F 92/1   "Einspielen und dessen numerische Behandlung von Flächentragwerken aus ideal plastischem bzw. kinematisch verfestigendem Material", G. Zhang, Dissertation, Februar 1992

F 92/2   "Strukturoptimierung stabilitätsgefährdeter Systeme mittels analytischer Gradientenermittlung", A. Becker, Dissertation, April 1992

F 92/3   "Duale Methoden für nichtlineare Optimierungsprobleme in der Strukturmechanik", R. Mahnken, Dissertation, April 1992

F 93/1   "Kanonische Modelle multiplikativer Elasto–Plastizität. Thermodynamische Formulierung und numerische Implementation", C. Miehe, Habilitation, Dezember 1993

F 93/2   "Theorie und Numerik zur Berechnung und Optimierung von Strukturen aus isotropen, hyperelastischen Materialien", F.–J. Barthold, Dissertation, Dezember 1993

F 94/1   "Adaptive Verfeinerung von Finite-Element-Netzen für Stabilitätsprobleme von Flächentragwerken", E. Stein, B. Seifert, W. Rust, Forschungsbericht, Oktober 1994

F 95/1   "Adaptive Verfahren für die Formoptimierung von Flächentragwerken unter Berücksichtigung der CAD–FEM–Kopplung", A. Falk, Dissertation, Juni 1995

F 96/1   "Theorie und Numerik dünnwandiger Faserverbundstrukturen", F. Gruttmann, Habilitation, Januar 1996

F 96/2   "Zur Theorie und Numerik finiter elastoplastischer Deformationen von Schalenstrukturen", B. Seifert, Dissertation, März 1996

F 96/3   "Theoretische und algorithmische Konzepte zur phänomenologischen Beschreibung anisotropen Materialverhaltens", J. Schröder, Dissertation, März 1996

F 96/4   "Statische und dynamische Berechnungen von Schalen endlicher elastischer Deformationen mit gemischten finiten Elementen", P. Betsch, Dissertation, März 1996

F 96/5   "Kopplung von Finiten Elementen und Randelementen für ebene Elastoplastizität mit Implementierung auf Parallelrechnern", M. Kreienmeyer, Dissertation, März 1996

F 96/6   "Theorie und Numerik dimensions- und modelladaptiver Finite-Elemente-Methoden von Flächentragwerken", S. Ohnimus, Dissertation, Juni 1996

F 96/7   "Adaptive Finite Elemente Methoden für MIMD-Parallelrechner zur Behandlung von Strukturproblemen mit Anwendung auf Stabilitätsprobleme", O. Klaas, Dissertation, Juli 1996

F 96/8   "Institutsbericht 1971–1996 aus Anlaß des 25-jährigen Dienstjubiläums von Prof. Dr.-Ing. Dr.-Ing. E.h. Dr. h.c. mult. Erwin Stein, Dezember 1996

F 97/1   "Modellierung und Numerik duktiler kristalliner Werkstoffe", P. Steinmann, Habilitation, August 1997

F 97/2   "Formoptimierung in der Strukturdynamik",
L. Meyer, Dissertation, September 1997

F 97/3   "Modellbildung und Numerik für Versagensprozesse in Gründungen von Caisonwellen-brechern",
M. Lengnick, Dissertation, November 1997

F 98/1   "Adaptive gemischte finite Elemente in der nichtlinearen Elastostatik und deren Kopplung mit Randelementen",
U. Brink, Dissertation, Februar 1998

F 98/2   "Theoretische und numerische Aspekte zur Parameteridentifikation und Modellierung bei metallischen Werkstoffen",
R. Mahnken, Habilitation, Juli 1998

F 98/3   "Lokalisierung und Stabilität der Deformation wassergesättigter bindiger und granularer Böden",
J. M. Panesso, Dissertation, August 1998

F 98/4   "Theoretische und numerische Methoden in der angewandten Mechanik mit Praxisbeispielen",
R. Mahnken (Hrsg.), Festschrift anlässlich der Emeritierung von Prof. Dr.–Ing. Dr.–Ing. E.h. h.c. mult. Erwin Stein, November 1998

F 99/1   "Eine h-adaptive Finite–Element–Methode für elasto–plastische Schalenprobleme in unilateralem Kontakt",
C.-S. Han, Dissertation, Juli 1999

F 00/1   "Ein diskontinuierliches Finite–Element–Modell für Lokalisierungsversagen in metallischen und granularen Materialien",
C. Leppin, Dissertation, März 2000

F 00/2   "Untersuchungen von Strömungen in zeitlich veränderlichen Gebieten mit der Methode der Finiten Elemente",
H. Braess, Dissertation, März 2000

F 00/3   "Theoretische und algorithmische Beiträge zur Berechnung von Faserverbundschalen",
J. Tessmer, Dissertation, März 2000

F 00/4   "Theorie und Finite-Element-Methode für die Schädigungsbeschreibung in Beton und Stahlbeton",
D. Tikhomirov, Dissertation, August 2000

F 01/1   "A C1 - continuous formulation for finite deformation contact",
L. Krstulovic-Opara, Dissertation, Januar 2001

F 01/2   "Strain Localisation Analysis for Fully and Partially Saturated Geomaterials",
H. Zhang, Dissertation, Januar 2001

F 01/3   "Meso-makromechanische Modellierung von Faserverbundwerkstoffen mit Schädigung",
C. Döbert, Dissertation, April 2001

F 01/4   "Thermomechanische Modellierung gummiartiger Polymerstrukturen",
S. Reese, Habilitation, April 2001

F 01/5   "Thermomechanisches Verhalten von Gummimaterialien während der Vulkanisation – Theorie und Numerik –",
M. André, Dissertation, April 2001

F 01/6   "Adaptive FEM für elastoplastische Deformationen – Algorithmen und Visualisierung",
M. Schmidt, Dissertation, Juni 2001

F 01/7   "Verteilte Algorithmen für h-, p- und d-adaptive Berechnungen in der nichtlinearen Strukturmechanik ",
R. Niekamp, Dissertation, Juni 2001

F 01/8   "Theorie und Numerik zur Berechnung und Optimierung von Strukturen mit elastoplastischen Deformationen",
K. Wiechmann, Dissertation, Juli 2001

F 01/9   "Direct Computation of Instability Points with Inequality Contraints using the Finite Element Method",
H. Tschöpe, Dissertation, September 2001

F 01/10   "Theorie und Numerik residualer Fehlerschätzer für die Finite-Elemente-Methode unter Verwendung äquilibrierter Randspannungen",
S. Ohnimus, Habilitation, September 2001

F 02/1   "Adaptive Algorithmen für thermo-mechanisch gekoppelte Kontaktprobleme",
A. Rieger, Dissertation, August 2002

F 02/2   "Consistent coupling of shell- and beam-models for thermo-elastic problems",
K. Chavan, Dissertation, September 2002

F 03/1   "Error-controlled adaptive finite element methods in large strain hyperelasticity and fracture mechanics",
M. Rüter, Dissertation, Mai 2003

F 03/2   "Formulierung und Simulation der Kontaktvorgänge in der Baugrund-Tragwerks-Interaktion",
A. Haraldsson, Dissertation, Juni 2003

F 03/3   "Concepts for Nonlinear Orthotropic Material Modeling with Applications to Membrane Structures",
T. Raible, Dissertation, Juni 2003

F 04/1   "On Single- and Multi-Material arbitrary Lagrangian-Eulerian Approaches with Application to Micromechanical Problems at Finite Deformations",
D. Freßmann, Dissertation, Oktober 2004

F 04/2   "Computational Homogenization of Microheterogeneous Materials at Finite Strains Including Damage",
S. Löhnert, Dissertation, Oktober 2004

F 05/1   "Numerical Micro-Meso Modeling of Mechanosensation driven Osteonal Remodeling in Cortical Bone",
C. Lenz, Dissertation, Juli 2005

F 05/2   "Mortar Type Methods Applied to Nonlinear Contact Mechanics",
K.A. Fischer, Dissertation, Juli 2005

F 05/3   "Models, Algorithms and Software Concepts for Contact and Fragmentation in Computational Solid Mechanics",
C. Hahn, Dissertation, November 2005

F 06/1   "Computational Homogenization of Concrete",
S. Moftah, Dissertation, Januar 2006

F 06/2   "Reduction Methods in Finite Element Analysis of Nonlinear Structural Dynamics",
H. Spiess, Dissertation, Februar 2006

F 06/3   "Theoretische und algorithmische Konzepte zur Beschreibung des beanspruchungsadaptiven Knochenwachstums",
B. Ebbecke, Dissertation, März 2006

F 06/4   "Experimentelle Untersuchungen an elastomeren Werkstoffen",
M. Dämgen, Dissertation, Dezember 2006

F 07/1   "Numerische Konzepte zur Behandlung inelastischer Effekte beim reibungsbehafteten Rollkontakt",
M. Ziefle, Dissertation, Februar 2007

F 07/2   "Begleitbuch zur Leibniz-Ausstellung",
Hrsg: E. Stein, P. Wriggers, 2007

F 07/3   "Modellierung und Simulation der hochfrequenten Dynamik rollender Reifen",
M. Brinkmeier, Dissertation, Juni 2007

F 07/4   "Computational Homogenization of micro-structural Damage due to Frost in Hardened Cement Paste",
M. Hain, Dissertation, Juli 2007

F 07/5   "Elektromechanisch gekoppelte Kontaktmodellierung auf Mikroebene",
T. Helmich, Dissertation, August 2007

F 07/6   "Dreidimensionales Diskrete Elemente Modell für Superellipsoide",
C. Lillie, Dissertation, Oktober 2007

F 07/7   "Adaptive Methods for Continuous and Discontinuous Damage Modeling in Fracturing Solids",
S.H. Reese, Dissertation, Oktober 2007

F 08/1   "Student Projects of Micromechanics",
Hrsg: U. Nackenhorst, August 2008

F 09/1   "Theory and Computation of Mono- and Poly- crystalline Cyclic Martensitic Phase Transformations",
G. Sagar, Dissertation, August 2009

F 09/2   "Student projects of Micromechanics",
D. Balzani and U. Nackenhorst, Course Volume, October 2009

F 09/3   "Multiscale Coupling based on the Quasicontinuum Framework, with Application to Contact Problems",
W. Shan, Dissertation, November 2009

F 10/1   "A Multiscale Computational Approach for Microcrack Evolution in Cortical Bone and Related Mechanical Stimulation of Bone Cells",
D. Kardas, Dissertation, September 2010

F 11/1   "Ein integrales Modellierungskonzept zur numerischen Simulation der Osseointegration und Langzeitstabilität von Endoprothesen",
A. Lutz, Dissertation, Oktober 2011

F 12/1   "Ein physikalisch motiviertes Reifen-Fahrbahnmodell für die Gesamtfahrzeugsimulation",
R. Chiarello, Dissertation, Februar 2012

F 13/1   "Thermomechanical Analysis of Tire Rubber Compounds in Rolling Contact',
A. Suwannachit, Dissertation, September 2012

F 13/2   "Towards a Finite Element Model for Fluid Flow in Human Hip Joint",
K. Fietz, Dissertation, September 2013

F 14/1   "Micro-Mechanically Based Damage Analysis of Ultra High Performance Fibre Reinforced Concrete Structures with Uncertainties",
A. Hürkamp, Dissertation, Dezember 2013

F 14/2   "Numerical Solution of High-Dimensional Fokker-Planck Equations with Discontinuous Galerkin Methods",
F. Loerke, Dissertation, Dezember 2013

F 14/3   "Numerische Simulation probabilistischer Schädigungsmodelle mit der Stochastischen Finite Elemente Methode",
P.-P Jablonski, Dissertation, September 2014

F 15/1   "On a Finite Element Approach for the Solution of a Mechanically Stimulated Biomechanical Fracture Healing Model",
A. Sapotnick, Dissertation, Februar 2015